THE WILD GOOSE ASSOCIATION

PROCEEDINGS OF THE
ELEVENTH ANNUAL TECHNICAL SYMPOSIUM
13-15 OCTOBER 1982
WASHINGTON, D.C.

★ ★ ★ ★ ★

PUBLISHED BY
THE WILD GOOSE ASSOCIATION
P.O.BOX 556
BEDFORD, MASSACHUSETTS 01730

THE WILD GOOSE ASSOCIATION

The Wild Goose Association (WGA) is a professional organization of individuals and organizations having an interest in loran (long range navigation). It is named after the magestic birds that navigate thousands of miles with unerring accuracy. The WGA was organized in 1972 and its membership now includes hundreds of professional engineers, program managers, scientists and operational personnel from all segments of government, industry, and the user community throughout the world, working for the advancement of loran.

CONVENTION COMMITTEE

D.A. Carter .... Chairman
Cdr. J. Weseman .... Guest Speakers
R. Schellhase .... Administration
Cdr. D. Amos .... Technical Program
L.D. Higginbotham .... Hospitality

BOARD OF DIRECTORS 1981-82

B. Ambroseno .... President
W. Dean .... Vice President
C. Andren .... Secretary
L. Fehlner .... Treasurer

R. Abraczinskas
J. Beukers
J. Culbertson
G. Haroules
L. Higginbotham
J. Illgen
V. Johnson
C. Kirlin
E. McGann
B. Uttam
J. Van Etten
V. Weihe

BOARD OF DIRECTORS 1982-83

C.S. Andren .... President
E.L. McGann .... Vice President
L.F. Fehlner .... Secretary
D.A. Carter .... Treasurer

J. Alexander
B. Ambroseno
J. Beukers
J. Culbertson
W. Dean
L. Higginbotham
J. Illgen
V. Johnson
J. Van Etten
V. Weihe

TABLE OF CONTENTS

THE AUTHORS

BIOGRAPHIC SKETCHES

ROBERT M. BOWLES

Mr. Bowles is employed by the U. S. Geological Survey at Woods Hole, Massachusetts. He received his Bachelor of Science degree in Geology from the University of New Hampshire in 1961. From 1963 to 1978, he was project geophysicist on world wide gravity surveys for the U. S. Naval Oceanographic Office. For the past four years, he has been project chief for Navigation/Gravity Operations and Development with the U. S. Geological Survey, Branch of Atlantic Marine Geology.

GARY LYNN GRAHAM

Mr. Graham received his Bachelor of Science degree in Agriculture and is in the process of completing a Master of Science degree in Wildlife and Fisheries Science at Texas A&M University. He is presently an Associate Marine Fisheries Specialist coordinating marine fisheries programs on commercial and recreational vessels. Special efforts have been directed toward utilization of LORAN Radionavigational Systems and the cataloging of related coordinates of fishing obstructions in the Western Gulf of Texas. Included in his publications are LORAN related subjects which include: "Conversion of LORAN Coordinates," 1978 Radionavigational Journal; "Hangs of the Northwestern Gulf," and "Coordinate Conversion on the Demise of LORAN A."

ROGER W. HASSARD, CDR, USCG

CDR Hassard graduated from the U. S. Coast Guard Academy in 1963. He received the MSEE Degree from the Naval Postgraduate School in 1969 and the MSBA Degree from Boston University in 1982. His indoctrination into Loran-C was by a four and one half year tour (1970 - 1974) in the Systems Development Branch of the Electronics Engineering Division at Coast Guard Headquarters. During this period he was project manager for development of some early shipboard guidance/area-navigation systems and for low-cost Loran-C receivers. He is currently (since 1980) Chief of the Loran Division of Coast Guard Activities Europe, responsible for operation of the European chains. CDR Hassard last appeared before the Wild Goose Association at the 1976 symposium to present a paper entitled "The Globtic Sun Incident" for which he was awarded the Association's 1976 Paper Award. He is a charter member of the Wild Goose Association.

BARRY J. IRWIN

Mr. Irwin is employed by the U. S. Geological Survey at Woods Hole, Massachusetts, currently doing LORAN-ASF research for offshore acoustical surveying. As a member of the navigation and gravity group from 1976 to present, he has been responsible for the navigational support of geophysical cruises along the East Coast and Gulf of Mexico as well as operation of sea gravity meters. His previous experience was with the U. S. Naval Oceanographic Office, Gravity Division, where he worked with gravimeters, LORAN-C, and Transit Satellite. He is a graduate of Cornell University with a Bachelor of Science degree in Marine Ecology, 1967.

LARRY D. KING

Mr. King received his B. S. degree in Aerospace Engineering from the University of Florida in 1973. He has been a member of the staff of Systems Control Technology Inc., since 1978. He is presently Program Manager on a Loran-C flight test program to be conducted in the State of Alaska. In addition, he is also program manager on a Terminal Instrument Procedures (TERPS) data collection effort being conducted at the FAA's Technical Center in Atlantic City, New Jersey. He is an active member of American Institute of Aeronautics and Astronautics and a member of Radio Technical Commission for Aeronautics (RTCA) Special Committee. Mr. King's publications include: "Airborne Radar Approach Flight Test Evaluating Various Track Orientation Techniques," "3D LORAN-C Navigator Documentation," and co-author "Airborne Radar Approach Flight Test Experiment."

THOMAS A. KING, JR.

Mr. King presently a member of Bowditch Navigation Systems' senior technical staff, sailed in various deck officer capacities in the U. S. Merchant Marine following graduation from the United States Merchant Marine Academy. Past experience includes marine simulation with respect to research and training, shipboard computers and productivity.

EDWIN D. MCCONKEY

Mr. McConkey received his B. S. degree in Electrical Engineering and Mathematics from the University of Michigan in 1963, and received his B. S. in Electrical Engineering in 1964. He continued graduate studies in Automatic and Optimal Control Systems in partial fulfillment or Ph.D. requirements. His professional experience as systems engineer in navigation includes the Institute of Science and Technology at the University of Michigan, Polhemus Navigation Sciences, Inc., and his current position as Senior Engineer at the Champlain Technology Industries Division of Systems Control, Inc. (Vt). Recently he has been program manager or project engineer for several programs concerned with the use of area navigation in civil avaiation. These programs include the Microwave Landing System and LORAN-C. Mr McConkey is a member of TAU BETA PI and ETA KAPPA NU, and he is a registered professional engineer in the State of Florida.

JAMES R. MCCULLOUGH

Mr McCullough is a Research Specialist with the Woods Hole Oceanographic Institution. He received his undergraduate Degree in Electrical Engineering from Yale University in 1959, and did graduate work in astronomy at the University of Texas. He taught physics at Pomfret School and worked as a radar computer systems analyst with Lincoln Laboratory. Since joining WHOI in 1967, he has headed their flow-meter development program. For the past two years, he has been working with offshore applications and calibration of LORAN-C in conjunction with the U. S. Geological Survey.

KRISHNAN NATARAJAN

Mr. Natarajan was born in Bangalore, India, on May 2, 1958. He received the S.B. and S.M. degrees in aeronautical engineering from MIT in 1979 and 1981 respectively. During the course of his studies at MIT, he conducted research into the use of Loran-C by general aviation aircraft. Since 1981 he has been with JAYCOR, Woburn, MA, as a systems engineer involved with processing Loran data and development of a semi-empirical method for Loran calibration/prediction. His current interests include control and estimation, radio-navigation systems, and microprocessor-based systems.

JOHN NICHOLAS NEWMAN

Mr "Nick" Newman is a Professor of Naval Architecture in the Department of Ocean Engineering at MIT. Prior to joining the MIT Faculty in 1967 he was employed by the David Taylor Naval Ship Research and Development Center in Carderock. His field of specialization is hydrodynamics, with applications to ships and offshore structures. He is the author of numerous papers and one textbook on marine hydrodynamics. In addition to the WGA he is a member of the Society of Naval Architects and Marine Engineers, the American Association for the Advancement of Science, the Royal Institution of Naval Architects, and the Institute of Navigation. He was educated at MIT and Cambridge University, and has spent sabbatical leaves at universities in Australia and Norway. Professor Newman is an avid sailor. He has enjoyed the benefits of Loran-C on his 38' sloop for the past four years, particularly during a transatlantic cruise to Scotland and Norway in 1981.

WILLIAM F. O'HALLORAN

Mr. O'Halloran received his S.B., S.M., and Engineers Degree in electrical engineering from the Massachusetts Institute of Technology in 1964, 1965, and 1966, respectively. He is now the director of Jaycor's Systems Engineering Division located in Woburn, MA. Mr. O'Halloran has extensive experience in modern estimation and control systems, with particular emphasis on navigation system applications. Numerous projects in Loran-C include the St. Mary's River Loran grid calibration, Loran-C grid calibration and error modeling for the U. S. Navy, test data analysis for the Navy's AN/BRN-5 Loran-C receiver, and a Loran-C monitor system for the FAA. He is a contributing author to the book, "Applied Optimal Estimation," and is a member of the Wild Goose Association, ION and IEEE.

CARTER P. PFAELZER

Mr. Pfaelzer received his M. S. degree from M.I.T. in June 1982. For the past six years he has been associated with M.I.T. as a Fellow at the Center for Advanced Engineering Studies, and more recently as a graduate student in the department of Aeronautics and Astronautics. He is also president of his own company, and co-founder and past president of Intronics, Inc. Prior to this he worked for Raytheon Co. as a manager of a micro-electronics R & D laboratory, as well as being chairman of their commercial patent committee. Mr Pfaelzer is a graduate of Harvard University, and a member of IEE, AIP/APS, the New York Academy of Sciences, and an associate member of Sigma XI.

FREDERICK H. RAAB, Ph.D

Dr. Raab is a consultant in power amplifiers, radio navigation, and communications. He received B.S., M.S., and Ph.D degrees in electrical engineering from Iowa State University in 1968, 1970, and 1972, respectively. He is coauthor of "Solid State Radio Engineering," has authored or coauthored over 30 technical papers, and holds two patents. Since starting Green Mountain Radio Research in 1980, Dr. Raab has been involved in RF design, target transfer using GPS and JTIDS, adaptive noise cancellation, and proximity warning. From 1975 to 1980, he was with Polhemus Navigation Sciences, Inc. and was involved with terrestrial use of Loran-C, trapped-miner location systems, and special-purpose position-finding systems. From 1971 to 1975 he was with Cincinnati Electronics and was involved in using OMEGA and GPS for search and rescue. He is a senior member of the IEEE and a member of CASI, WGA, IOA, HKN and Sigma XI.

GERALD F. SAGE

Mr. Sage is President of Navigation Technology Inc. He provides consulting services for the analysis, design and test of radio navigation systems. His more than twenty years of experience in the navigation and communications field include the design of user equipment for Loran-C, Omega, Transit, and GPS systems. He has designed multisensor navigation systems using Kalman filtering and suboptimal filters. These equipments have been designed for Military, civil aviation, and civil marine users. Mr. Sage received the BSEE from the University of Michigan and completed graduate studies for the MSEE at the University of Maryland.

DAVID C. SCULL

Mr. Scull received his B.S. in Geology and Mineralogy from Pennsylvania State University and his M.S. Degree in Systems Management from the University of Southern California. As an employee of Naval Oceanographic Office (NAVOCEANO) from 1960 to 1972 he was involved in various geodetic investigations leading to an interest in electronic positioning methods. During this time he was appointed as Chief of NAVOCEANO's Electronic Systems Branch and was responsible for LORAN, Navigational Satellite and Omega projects directed at providing navigational data and information. At present, Mr Scull is the Radionavigation and Communications Program Manager within the Research and Special Programs Administration (RSPA) of the Department of Transportation. Mr Scull is a member of the Wild Goose Association, the International Omega Association and recently served as Eastern Regional Vice President of the Institute of Navigation.

ROBERT E. VOIGT, CAPT, USAF

Captain Voigt, (B. S., Mechanical Engineering, USAF Academy; M. S., Systems Management, USAF Institute of Technology) is assigned to the Air Traffic Control Systems Directorate of Electronics Systems Division (AFSC) and functions as Chief, Tactical LORAN Operating Location, Eglin AFB, FL. He has served as a Program Manager in the Fighter-Attack System Program Office and as Commander, Base Investigation Detachment, AF Office of Special Investigation, Norton AFB, CA. Capt Voigt is a graduate of Squadron Officer's School and Air Command and Staff College.

ROBERT S. WESTER, CAPT, USAF

Captain Wester, (B.A., Engineering Electronics, Park College, MO) is assigned to the Air Traffic Control Systems Directorate of Electronics Systems Division (AFSC) and functions as Lab Director, Tactical LORAN Operating Location, Eglin AFB, FL. He has served as an Airborne Navigation Systems Engineer and as Officer in Charge of the Instrumentation and and Support Section, 6585th Test Group, Holloman AFB, NM.

SESSION I

TECHNOLOGY

SPREAD-SPECTRUM LORAN (LORAN-E)

Frederick H. Raab, Ph.D., Consultant
Green Mountain Radio Research Company
240 Staniford Road
Burlington, Vermont 05401

ABSTRACT

A new Loran signal based upon spread-spectrum modulation is presented. This signal uses pseudonoise modulation of a 100-kHz carrier with sequenced transmissions from each station. Performance equivalent to that of the Loran-C signal is achieved with only 1/1000 of the radiated power. The cost savings for both installation and operation of 1-kW rather than 1-MW transmitters are obvious. Narrowband retransmission (relay) can be accomplished without preprocessing for accurate, low-cost automatic-vehicle-monitoring and vessle-traffic-control systems. This is especially significant, since retransmitted OMEGA does not yield comparable accuracy and retransmitted NAVSTAR/GPS requires either a large banddwidth or preprocessing. The Loran-E signal can be transmitted simultaneously with the current signal to allow a gradual phase-in period. The advantages of the new spread-spectrum signal should help to maintain Loran's place in the future mix of radio-navigation systems.

1. INTRODUCTION

The present Loran-C/D signal (Fig. 1) was designed in the 1950s to meet four key requirements:

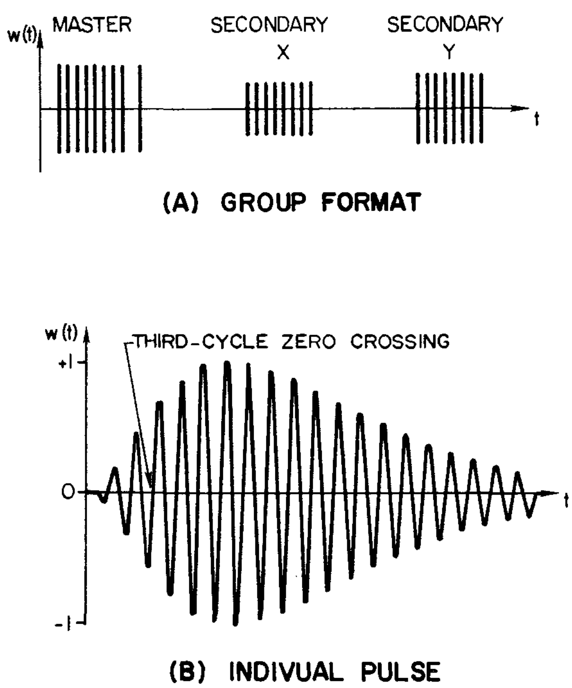

Figure 1. Loran-C signal.

- Visual acquisition of the signal from a particular transmitter (Fig. 1a),
- Visual identification (Fig. 1b) of the tracking point (third-cycle zero crossing),
- Rejection of skywave interference, and
- Not more than one percent of the power outside of the 90 - 110 kHz band.

In the last twenty-five years, there have been several technological developments that would impact the design of the signal if it were done today:

- Modern receivers acquire signals automatically, eliminating the need for visual-acquisition capability.
- Spread-spectrum modulation has used many navigation and communications systems (e.g., GPS, JTIDS, Sydelis).
- Microprocessors are common-place in navigation and communication receivers, both for tracking and coordinate conversion.

The proposed "Loran-E" waveform (Section 3) has the following general characteristics:

- 100-kHz carrier frequency
- 10-kb/s pseudonoise (PN) biphase modulation
- Time-sequenced transmissions by each station.

The use of a unique code by each station allows both identification and rejection of unwanted signals from other chains. Code tracking rejects skywave signals and unambiguously identifies the zero crossing to be tracked. The accuracy of Loran-C is maintained.

The proposed signal would update Loran from a 1950's technology to a 1980's technology. The advantages of the new signal include:

- Reduction of the average power, hence lower operating costs,
- Reduction of the peak power, hence lower installation costs,
- Increased portability for tactical and survey use,
- Less complicated and less expensive receivers, and
- Narrowband retransmission *without* processing.

Spread-spectrum loran is not an altogether new concept; similar techniques were used in the Multi-User Tactical Navigation System ("Loran-F"), which was tested circa 1960 [1]. However, given today's technol-

This paper was presented at the Eleventh Annual Wild Goose Association Convention, Washington, D.C., October 11 - 13, 1982.

ogy, the advantages of Loran-E are quite significant, and could therefore affect the future "mix" of U. S. radio-navigation systems. Furthermore, Loran-C and Loran-E can be transmitted simultaneously to allow a gradual phase-in period. It is therefore time to reconsider the future Loran signal format.

This paper presents a preliminary analysis of the capabilities and requirements of a Loran-E system. First, the power and efficiency of Loran-C and -D are evaluated. The characteristics and advantages of the Loran-E signal are then determined.

2. POWER COMPARISONS

The operational characteristics and requirements of Loran-C are well established. For preliminary-evaluation purposes, it is therefore sufficient to compare Loran-E to Loran-C. This section determines the peak, average, and effective power of Loran-C/D signals.

Loran-C/D Signal

The Loran-C/D pulse waveform [2,3] is described by

$$w(t) = e(t) \sin \omega_c t = A\ t^2 \exp(-at) \sin(\omega_c t)\ , \quad (1)$$

where time t is in *seconds*, A is an amplitude constant,

$$a = (2/65)/10^{-6} = 3.077 \cdot 10^4\ , \quad (2)$$

and

$$\omega_c = 2\pi f_c = 2\pi \cdot 10^5\ . \quad (3)$$

Setting the derivative of the envelope $e(t)$ equal to zero yields

$$t_{ma} = 2/a = 65\ \mu s \quad (4)$$

for the occurance of maximum pulse amplitude. For unity peak amplitude,

$$1 = e_{max} = e(65 \cdot 10^{-6}) = 65^2 \exp(-2)\ A \cdot 10^{-12}\ , \quad (5)$$

hence

$$A = 1.749 \cdot 10^9\ . \quad (6)$$

Most Loran-C receivers tracking the third-cycle zero crossing, for which the normalized envelope is

$$e(30\mu s) = 0.625\ . \quad (7)$$

For short-range Loran-D systems that track the sixth-cycle zero crossing,

$$e(60\mu s) = 0.994\ . \quad (8)$$

which is 0.05 dB below the peak amplitude. The tracking-point envelopes are 4.05 dB and 0.05 dB, respectively, below the peak pulse amplitude.

Energy in Loran-C/D Pulse

The energy in a single Loran-C/D pulse of unity peak amplitude is

$$E_{LP} = \int_0^\infty w^2(t)\ dt \cong \int_0^\infty e^2(t)\ dt \cdot \frac{1}{2\pi} \int_0^{2\pi} \sin^2\theta\ d\theta\ . \quad (9)$$

The simplification of (9) into two separate integrals is based upon the envelope being approximately constant over any single cycle of the carrier.

The first integral can be evaluated from the relationship [4]

$$\int_0^\infty x^n \exp(-kx)\ dx = n!/k^{n+1}\ , \quad (10)$$

which implies

$$\int_0^\infty e^2(t)\ dt = A^2\ 4!/(2a)^5 \cong 8.318 \cdot 10^{-5}\ . \quad (11)$$

Evaluation of the second integral produces

$$(1/2\pi) \int_0^{2\pi} \sin^2 \theta\ d\theta = (1/2)\ . \quad (12)$$

Equations (11) and (12) can now be combined to yield

$$E_{LP} = 4.159 \cdot 10^{-5}\ . \quad (13)$$

Average Power in Loran-C/D Signal

The average power in a Loran-C/D signal is obtained by multiplying the single-pulse energy E_{LP} by the number of pulses per second. The number of pulses per second is the product of the group rate (inverse GRI, $10 \leq f_G \leq 20$ Hz) and the number N_P of pulses per transmission, thus

$$P_{L,AVG} = N_P\ f_G\ E_{LP}\ . \quad (14)$$

For Loran-C, $N_P = 8$, hence $3.327 \cdot 10^{-3} \leq P_{L,AVG} \leq 6.654 \cdot 10^{-3}$. For Loran-D, $N_P = 16$, and $6.654 \cdot 10^{-3} \leq P_{L,AVG} \leq 1.331 \cdot 10^{-2}$.

Effective Power in Loran-C/D Signal

Only one zero crossing of the Loran-C/D pulse is used for time-of-arrival measurements. The third-cycle zero crossing is used in most long-range Loran-C systems for three reasons:

- Subsequent zero crossing are corrupted by skywaves and have markedly poorer accuracy,
- The rate of change (envelope) is greater than that of previous zero crossings, and
- Only the third-cycle zero crossing is accurately timed at most transmitters.

Since the difference in the times of arrival of the skywave and groundwave signals is greater at shorter distances, short-range Loran-C/D systems can use a later zero crossing (fourth, fifth, or sixth), which has a larger signal envelope.

Since only one zero crossing of the Loran-C/D pulse is actually used, a single-cycle pulse (Fig. 2) would provide equivalent time-of-arrival-measurement accuracy. For equivalent accuracy, the rates of change (hence envelopes) at the zero crossing must be equal.

If the envelope of the single-cycle pulse is A_{SP}, the energy in one such pulse is

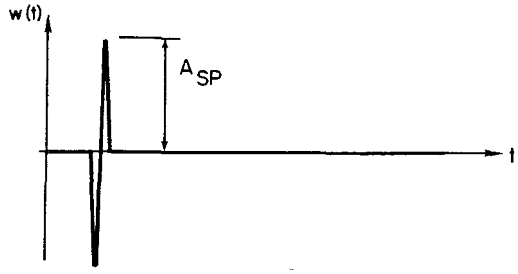

Figure 2. Single-cycle pulse.

$$E_{SP} = \int_0^{1/f_c} A_{SP}^2 \sin^2\omega_c t \, dt = \frac{A_{SP}^2}{2f_c} . \qquad (15)$$

The average transmitted power is the energy E_{SP} in a single pulse multiplied by the number of pulses per second. If Loran-C/D format and group rates were used,

$$P_{SP,AVG} = N_P \, f_G \, E_{SP} . \qquad (16)$$

Efficiency of Loran-C/D Signal

The *efficiency* of Loran-C/D signal may be defined as the ratio of the effective transmitted power to the actual transmitted power. From (14) and (16),

$$\eta = P_{SP,AVG}/P_{L,AVG} = E_{SP}/E_{LP}$$

$$= (A_{SP}^2/2 \cdot 10^5)/(4.159 \cdot 10^{-5}) = 0.120 \, e^2(t_{ZC}) , \qquad (17)$$

where t_{ZC} is the time of the tracked zero crossing.

For a Loran-C system using the third-cycle zero crossing, (17) gives an efficiency of only 4.7 percent. Equivalently, 95.3 percent of the transmitted power is wasted, and average transmitted power could be reduced by 13.2 dB (a factor of 21.3) if a single-cycle pulse signal were used. For Loran-D with tracking at the sixth-cycle zero crossing, η = 11.9 percent, and a 9.2 dB reduction in average transmitted power could be achieved.

Equivalent Continuous Signal

Assume, for the moment, that skywave interference can be rejected and cycle identification can be accomplished. Equivalent time-difference measurement accuracy can then be obtained by transmitting a CW signal whose average power is equal to that of a single-cycle pulse. The required power is

$$P_{CW} = P_{SP,AVG} = N_P \, f_G \, E_{SP} = N_P \, f_G \, A_{SP}^2/2f_c$$

$$= (N_P \, f_G/f_c) \, P_{SP,PEP} = \xi \, P_{SP,PEP} . \qquad (18)$$

The quantity ξ is simply the ratio of the number of pulses transmitted per second to the number of carrier cycles (single-cycle pulses) per second. For Loran-C, N_P = 8 and $0.0008 < \xi < 0.0016$, depending upon the GRI (f_G). For Loran-D, N_P = 16, and $0.0016 < \xi < 0.0032$.

Time-Sequenced Signal

To allow reception of distant signals when the receiver is in close proximty to a Loran-E transmitter, it is necessary to time-sequence the transmissions from nearby transmitters. While time sequencing does not affect the average power required, it does necessitate greater peak power. The increase required over that of the equivalent continuous signal is inversely proportional to the fraction of time during which a given station transmitts. Thus a transmission format with five time slots implies a factor of five (7 dB) increase in the peak power (Table 1).

Nonetheless, the use of a Loran-E signal instead of a Loran-C signal allows kilowatt rather than megawatt transmitter power. These projections are consistant with the 100 to 350 W radiated power of Decca transmitters [5]. The implications for antenna size, installation cost, operational cost, and transportability (tactical/survey systems) are obvious.

3. WAVEFORM

Stable groundwave propagation requires a carrier frequency in the 100-kHz range. However, simple CW signals can provide neither the required cycle identification nor the skywave rejection necessary for accu-

FMT	N_P	f_G	TRACK CYCLE	SINGLE-PULSE PEAK POWER	LORAN AVG POWER	SINGLE-PULSE AVG POWER CW POWER	η	REDUCTION, AVG POWER		REDUCTION, PEAK POWER 100% DUTY		REDUCTION, PEAK POWER 20% DUTY	
								FACTOR	dB	FACTOR	dB	FACTOR	dB
C	8	10	3	0.625	$3.327 \cdot 10^{-3}$	$1.563 \cdot 10^{-4}$	0.0470	21.3	13.3	6400	38.1	1280	31.1
		20	3	0.625	$6.654 \cdot 10^{-3}$	$3.125 \cdot 10^{-4}$	0.0470	21.3	13.3	3200	35.1	640	28.1
D	16	10	6	0.994	$6.654 \cdot 10^{-3}$	$7.904 \cdot 10^{-4}$	0.1188	8.4	9.2	1265	31.0	253	24.0
		20	6	0.994	$1.331 \cdot 10^{-3}$	$1.581 \cdot 10^{-4}$	0.1188	8.4	9.2	633	28.0	127	21.0

Note: Loran-C/D peak power normalized to 1.0.

Table 1. Equivalent power requirements.

rate low-frequency radio navigation.

The Loran-E signal (Fig. 3a) is therefore a 100-kHz carrier biphase-modulated by a pseudorandom binary sequence (code). This spread-spectrum technique [6] is also known as *pseudonoise* (PN) modulation. The code chipping (bit) rate is in the order of 10 to 30 kb/s and code chip transitions are synchronized with carrier zero crossings. Transmissions are time-sequenced (Fig. 3b) to prevent allow reception when the receiver is relatively close to a transmitter.

Spread-Spectrum Fundamentals

The use of pseudonoise modulation in the Loran-E signal accomplishes four key functions:

- Transmitter identification,
- Rejection of signals from other transmitters,
- Unambiguous cycle identification, and
- Skywave rejection.

Before proceeding to the detailed discussion, it will be useful to review some fundamental characteristics of spread-spectrum modulation. More detailed discussions can be found elsewhere [6].

PN codes are generated by linear feedback shift-register generators (LFSRGs). The input to the LFSRG is a modulo-2 sum of selected registers in the LFSRG. Code generators generally be implemented in a single logic chip.

Certain sets of feedback taps produce sequences of the maximum possible length $L = 2^N-1$. Such *maximal-length* sequences [7] have very desirable auto- and cross-correlation properties. Their autocorrelation function is L for perfect alignment and -1 for misalignment of one chip or more. The cross correlation of two different maximal-length sequences varies between +1 and -1 for all alignments.

Biphase modulation is implemented by shifting the carrier phase by 180° whenever the LFSRG produces a 1. PN-modulated signals are received by correlation with a locally generated replica of the PN code (Section 4). The low cross-correlation with other sequences allows separation of simultaneously transmitted signals. The sharp autocorrelation function allows precise tracking of time of arrival.

Transmitter Identification

Each transmitter is assigned a unique code sequence and transmits continuously. Because of the low cross correlation between different sequences, only the signals from the selected transmitter are detected by the receiver. Selection of a particular sequence for the receiver code generator therefore both selects a particular transmitter and rejects signals from other transmitters.

Dynamic Range

The cross-correlation product of different spread-spectrum sequences is low, but not zero. The rejection of an undesired PN-modulated signal is directly proportional to the length of the PN codes. For a 10 kb/s chipping rate and a 1-s sequence duration, the effects of the undesired signal are reduced 40 dB by code correlation.

Placement of a Loran-E receiver in the vicinity of a Loran-E transmitter in general produces considerable "dynamic range" in the amplitudes of the received signals. Since the dynamic range can exceed the rejection achievable by code correlation alone, continuous transmissions are in general undesirable.

The preferred general-purpose signal format therefore has a set of four or five time slots. Each transmitter transmitts continuously within its assigned time slot. Time slots are assigned geographically to ensure that transmitters that are used together do not transmit simultaneously.

Since transmissions are not continuous, the peak power must be greater than that of the equivalent CW signal discussed earlier. The penalty for a five-time-slot pattern is only 10 log 5 = 7 dB. In spite of this penalty, the peak power of a five-slot Loran-E system is still only 1/640 (or less) of that of an equivalent Loran-C system (e.g., 1.7-kW instead of 1-MW).

Cycle Identification

Reception of spread-spectrum signals requires the receiver to adjust the timing of its code generator to match that of the received signal. The timing of the code generator therefore corresponds to signal time of arrival. This measurement of time of arrival should be sufficiently accurate to identify the tracking cycle of the 100-kHz carrier.

The code repitition rate determines the range ambiguity inherent in the time-of-arrival measurements.

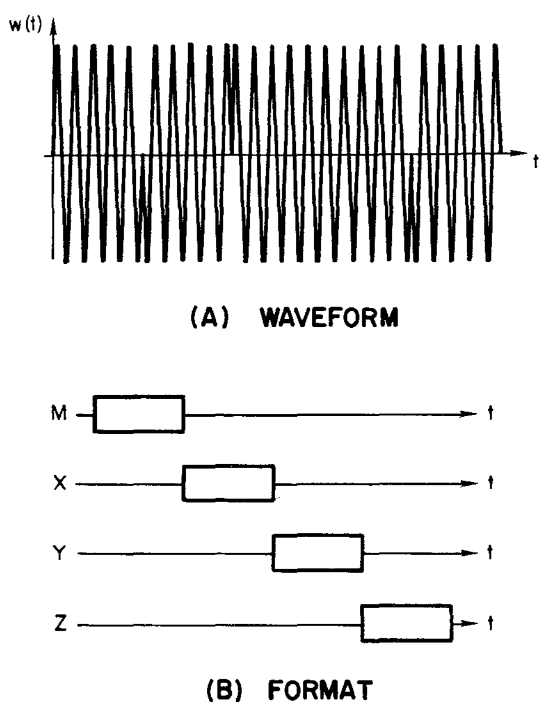

Figure 3. Loran-E signal.

For example, a code of length 1023 with a chipping rate of 10 kb/s repeats at a 10.23-Hz rate, producing a range ambiguity of 29.3 Mm (18222 mi). It is apparent that range ambiguities are not a problem.

Skywave Rejection

The sharp autocorrelation function of PN code sequences provides automatic rejection of multipath (skywave) signals. Figure 4 presents an example of a receiver correlation function for a groundwave and one skywave signal. Since the skywave is always delayed with respect to the groundwave, the receiver simply locks onto the first correlation peak. As long as the delay is greater than the time occupied by one code chip, the skywave signal contributes negligibly to the correlator output and is thereby completely rejected.

The use of third-cycle zero crossings in long-range Loran-C systems is based upon a minimum groundwave-skywave time-of-arrival difference of 20 μs. Positive rejection of skywave signals is therefore guaranteed by a code chipping rate of 33 kb/s. For short-range systems, the groundwave-skywave time difference is greater and a lower chipping rate is possible.

Additional skywave rejection is provided by the simultaneous use of code-lock and phase-lock techniques in the receiver. The autocorrelation function of the PN-modulated Loran-E signal is shown in Fig. 5. It is apparent that a skywave signal with less than a one-chip delay can produce a positive, negative, or zero contribution to the correlator output, depending upon the relative phasing of its carrier to that in the receiver.

The rms jitter in the time of arrival of a skywave signal can be several microseconds. It is therefore probable that the average contribution of the skywave signal to the correlator output will be considerably less than its peak contribution. It should therefore be possible to use a lower chipping rate (e.g., 10 kb/s) that is more consistant with the 90 - 110 kHz frequency allocation.

Spectrum

The power spectrum of a Loran-E signal with a 10 kb/s chipping rate is shown in Fig. 6. Integration of

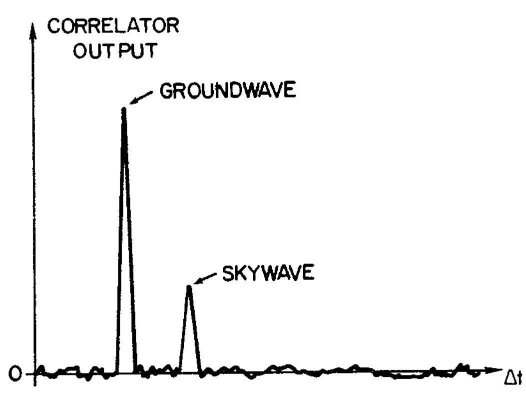

Figure 4. Groundwave and skywave responses.

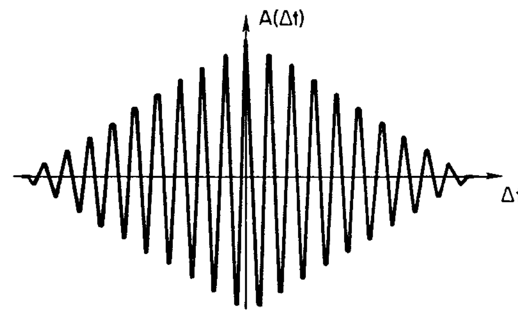

Figure 5. Combined code-and-phase autocorrelation function.

this sin x/x function shows [6, Fig. 2.8] that 90 percent of the transmitted power is in the 90 - 110 kHz band. The out-of-band "splatter" is 10 percent of the total transmitted power, which is roughly only 5 percent of that of a comparable Loran-C station. Since 99 percent of the power transmitted by a Loran-C station is contained in the 90 - 110 kHz band, its out-of-band emissions are roughly twice (3 dB greater than) those of a comparable Loran-E station. It therefore seems that simple biphase PN modulation should be acceptable.

Since Loran-E is not a pulse transmission, the CCIR requirement (99 percent of the power between 90 and 110 kHz) should not be applicable. However, even if this requirement is imposed, the Loran-E signal can be modified to meet it.

Data Transmission

Data can be transmitted on a Loran-E signal by sequence-inversion keying; e.g., the data bits reverse the code chips. Data can include error messages ("blink codes"), transmitter locations, service schedules, differential corrections, etc. Data rates would be in the order of 10 to 100 b/s.

Compatible Transmissions

Since the Loran-E signal appears to be a low-level noise to other receivers, simultaneous operation of Loran-E and Loran-C is possible during a transition period. Similarly, the presence of Loran-C pulses should not disrupt Loran-E reception, since received signals are hard-limited and the two signals have a very low cross correlation product. Figure 7 illustrates a transition signal format.

4. HARDWARE

This section gives a brief description of the

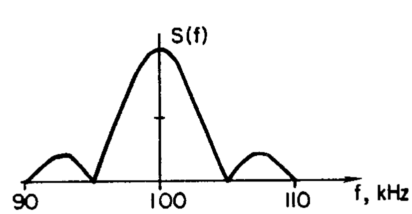

Figure 6. Spectrum of signal with 10 kb/s PN biphase modulation.

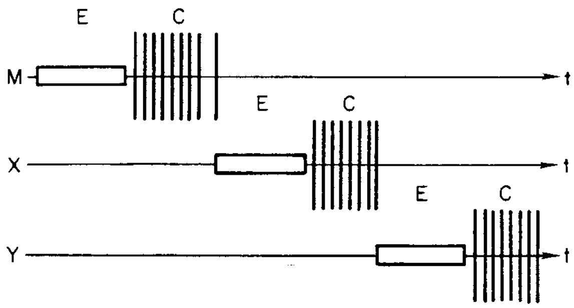

Figure 7. Loran-C/E transition format.

principal functions of the Loran-E transmitter and receiver.

Transmitter Block Diagram

A simplified block diagram of a Loran-E transmitter is shown in Fig. 8. The 100-kHz carrier frequency, the code chipping rate (e.g., 10 kHz), and the time slot (e.g., 0.2 Hz) are obtained by frequency division of the output of the same stable oscillator. Not shown are circuits that assure synchronization with other Loran-E transmitters.

The code-generator output modulates the carrier through a digital mixer that reverses carrier polarity for a "1" code bit. The biphase-modulated signal is then amplified and coupled to the antenna. Since the modulated carrier has constant amplitude, a relatiely simple and efficient (90%) class-D power amplifier can be used.

Receiver Block Diagram

Figure 9 shows a simplified block diagram of a single-channel Loran-E receiver. Received signals are preamplified and bandpass filtered, as in a Loran-C receiver. However, since the Loran-E signal has a constant envelope, the received signal is hard limited. This greatly reduces the effects of impulsive noise (due to lightning) and Loran-C pulses.

The received signal is then mixed with a locally generated code. When the locally generated code matches and is aligned with the code of the received signal, a 100-kHz CW signal is produced at the output of the mixer. The mixer output is then mixed separately with 100 kHz sine and cosine waves, integrated, and sampled to obtain its "I" and "Q" components.

Approximate code timing is acquired by slewing the code generator until a CW signal appears at the output of the first mixer. Code tracking is then accomplished by dithering the code generator back and forth about the tracking point. Carrier phase lock is then accomplished using the "I" and "Q" signals.

5. ADVANTAGES

This section summarizes the potential advantages of Loran-E over Loran-C and other radio navigation systems.

Accuracy

Loran-E will have the same high accuracy demonstrated by Loran-C.

Coverage

Low-frequency radio navigation systems such as Loran-C, D, and E provide navigation capability at all altitudes. Consequently, they are useable by terrestrial, maritime, and airborne users. Signal availability makes Loran preferable to VOR/DME for use by general aviation, especially at low altitudes [8]. Furthermore, Loran may provide better terrestrial coverage in valleys than is possible from a satellite system.

Location

There may be an advantage to land-based transmitters located in the user country.

Average Power

The average transmitted power can be reduced by a factor of 20. The impact upon a $60,000/year electricity cost (for one transmitter) is obvious.

Peak Power

The peak transmitted power can be reduced by a factor of 640 or more. If 1 kW radiated power is required instead of 1 MW, the cost of both the transmitter and the antenna are greatly reduced.

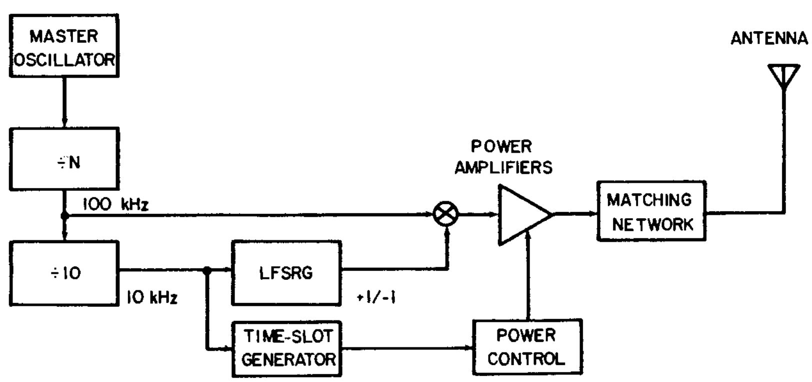

Figure 8. Simplified transmitter block diagram.

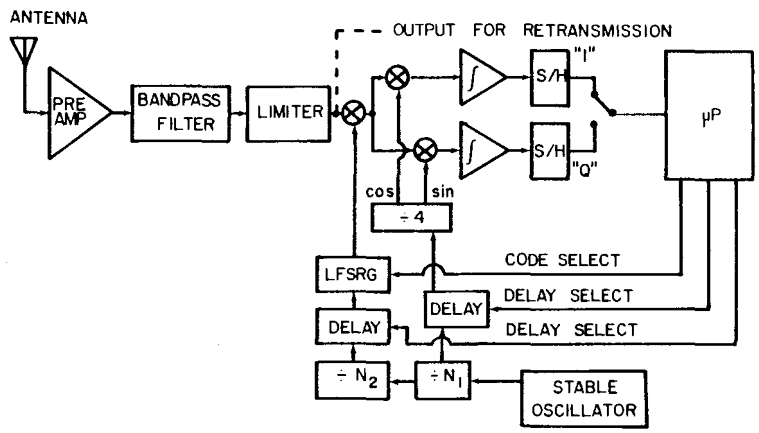

Figure 9. Simplified receiver block diagram.

Receiver

The spread-spectrum Loran-E signal is more easily acquired automatically by a receiver than is the Loran-C/D pulse signal. Receiver architecture is less complex, resulting in lower cost. Lower receiver cost is a very significant advantage, since it would make the system preferable to VOR/DME for general-aviation use.

Group/Phase Velocity

Variations in ground conductivity that *increase* phase velocity *decrease* group (envelope) velocity of propagation. The use of the difference in the times of arrival (ECD) to correct for some propagation uncertainties has been proposed. However, Loran-C envelopes and envelope measurements are not accurate enough to be useful. Since code-tracking accuracy can approach phase measurement accuracy, Loran-E may enable exploitation of group/phase-velocity effects. This would result in increased accuracy without calibration or differential corrections.

Retransmission

The location of a vehicle can be determined at a remote location by retransmission (relay) of radio-navigation signals [9]. At present, only OMEGA signals can be retransmitted in the narrow-bandwidth of a land-mobile communications channel without signifiant preprocessing. Limiting of the Loran-C/D signal to a reasonable dynamic range distorts or destroys envelope information. The bandwidth of NAVSTAR/GPS signals are clearly too large (e.g., 2 MHz for the C/A signal) for narrowband retransmission [10]. Consequently, both Loran-C/D and NAVSTAR/GPS signals must be processed to extract timing measurements prior to relay through a narrowband channel.

In contrast, received Loran-E signals can be hard-limited and retransmitted in a 20-kHz bandwidth. Since hard limiting will be used in most Loran-E receivers, no degradation of information occurs. Since negligible processing occurs in the retransmitter, the retransmitter can be quite inexpensive. Such a technique should therefore have significant potential in many terrestrial applications such as automatic vehicle monitoring.

CW Interference

Power-line carrier communications and other CW signals in the 90 - 110 kHz band can disrupt terrestrial reception of Loran-C. The spread-spectrum receiver should provide greater rejection of interference from these signals.

Tactical/Survey Applications

The reduced peak and average power requirements are of considerable importance in tactical and survey applications. Reduction of the required radiated power allows operation with a smaller antenna, which is more easily transported, erected, and replaced.

6. CONCLUSIONS AND RECOMMENDATIONS

The basic concepts for a spread-spectrum Loran system (Loran-E) have been presented. The preliminary analysis presented here suggests numerous potential benefits, including a considerable reduction in power requirements and retransmission without preprocessing. The benefits gained by conversion to the spread-spectrum format could be significant enough to ensure Loran's place in the future mix of radio navigation systems. A more thorough study of this concept is therefore recommended.

7. REFERENCES

1. R. L. Frank, "History of Loran-C," *Navigation*, vol. 29, no. 1, pp. 1 - 33, Spring 1982.

2. "Specification of the transmitted Loran-C signal," Report COMDTINST M16562.4, U.S. Coast Guard, Washington, DC, July 1981.

3. S. F. Appleyard, *Marine Electronic Navigation*, London: Routledge and Kegan Paul, 1980.

4. C. D. Hodgman, Editor, *Standard Mathematical Tables*, Twelfth Edition, Cleveland, Ohio: Chemical Rubber Publishing Company, 1962.

5. E. B. Blood, "Navigation requirements for the U.S. coastal confluence region," *Navigation*, vol. 20, no. 1, pp. 68 - 76, Spring 1973.

6. R. C. Dixon, *Spread Spectrum Systems*, New York: Wiley, 1976.

7. W. W. Peterson, *Error Correcting Codes*, New York: Wiley, 1961.

8. L. Rzonca, "Loran-C RNAV in mountainous areas," *Proceedings of the Institute of Navigation Thirty-Seventh Annual Meeting*, Atlantic City, NJ, pp. 129 - 140, June 9-11, 1981.

9. F. H. Raab, "Search and rescue using navaid re-transmissions," *Proceedings of the Institute of Navigation Natural Marine Meeting*, Linthicum Heights, MD, pp. 25 - 34, October 31 - November 1, 1977.

10. F. H. Raab et. al., "An application of the global positioning system to search and rescue and remote tracking," *Navigation*, vol. 24, no. 3, pp. 216 - 228, Fall 1977.

DESIGN OF A DUAL RATE, MASTER INDEPENDENT, DIRECT RANGE LORAN-C RECEIVER

BY

Gerald F. Sage
Jesse Pipkin

Navigation Technology Inc.
2327 Double "O" Mine Trail
Cool, California 95614
(916) 885-1089

ABSTRACT

An increase in the coverage area of a Loran-C receiver can be achieved by simultaneously tracking signals from two Loran-C chains. To obtain the maximum advantages of the dual chain operation, a secondary must be able to be tracked without receiving the master. Further gains in coverage and accuracy with single or dual chain operation are provided by operation in a direct range mode. Dual chain operation also gives automatic operation as the receiver passes from the coverage area of one chain to another.

A modular hardware and software design approach is taken. The hardware consists of two subassemblies plus the analog circuits and their digital controls. Four automatic notch filters and envelope-to-cycle discrepancy compensation are included. The digital receiver assembly provides all of the hardware including a microprocessor for signal processing. For single chain, time difference operation these two assemblies make up a complete Loran-C receiver including coordinate conversion and navigation. For dual chain master independent operation more processing power is required. The microprocessor on the digital receiver assembly uses a different program and outputs time of arrivals from two chains. These outputs are passed to a second processor assembly which provides the coordinate conversion and naivgation. When direct range operation is desired an oven-controlled, crystal oscillator is included in the processor assembly. A Kalman filter is used to derive position and velocity based on the Loran time of arrivals.

The design approach described provides a Loran-C receiver with premium performance and operational characteristics. At the same time the modular design gives a family of receivers that has a range of performance and cost.

INTRODUCTION

The equipment design that has been undertaken by Navigation Technology Inc., is directed towards the development of a Loran component. The Loran component is a Loran receiver implemented as a subsystem to be included in another product by a manufacturer. In the last five years the focus of Loran has passed from telling the user where he is in Loran numbers to providing more and more navigation information. The use of the Loran component allows the application specialists to concentrate on the application problem without developing the system to extract the very low level Loran signals from the noise and converting them to position.

A combination of techniques have been implemented to: improve the reliability of navigation with station outage, extend the coverage area, make operation more automatic, and provide performance improvement. The techniques not normally implemented in present day Loran receivers are: dual rate operation, master independence and direct range coordinate conversion. Implementation of these techniques is primarly in the system software. A limited amount of additional hardware is used for the dual chain operation. The superior system characteristics are achieved at a very modest increase in cost.

When operating in many areas, more than two secondaries can be received. If one of the secondaries used for position fixing has a signal outage, the system can still perform a position fix using alternate secondaries. In conventional TD implementations the loss of the master makes the chain useless. By mechanizing the receiver and the position fixing process to operate without a master, operation can still be achieved with a master outage.

With proper calibration and a moderately good system oscillator, a pseudo direct range system can function for a limited time with only two stations received or in a base line extension area. The oscillator frequency offset and phase are estimated when three stations are received or when two stations are received at a fixed known location. After the oscillator is calibrated the system can continue to compute position based on the signals from two stations until the unknown oscillator drift becomes large. In addition, when three signals are received the variation due to noise on the position fix is smaller than in an equivalent TD mechanization.

In some areas where inadequate stations from a single chain are received, a position fix can be made by supplementing the signals with a signal from another chain. The coverage area between chains can be increased by using these techniques. When the receiver is moving from the coverage of one chain to another the transition will be continuous without a loss of operation while the receiver acquires the new chain stations.

HARDWARE

The Loran hardware is divided into two parts, the digital or processor portion and the analog or RF portion. The user interface has usually been part of the digital portion and its burdens have subtracted from the responsiveness of the Loran itself. As the user interface became more and more complex (meaning more useful), this interface became the dominant part of the Loran itself and precious little opportunity to improve Loran performance was left over. A change in application, such as downsizing, often requires a redesign of the entire system rather than just the user interface which is the application. The Loran component changes this by stepping back from the user interface, concentrating on doing the Loran function, and communicating with the user by placing an interface inbetween. This interface could be as simple as a single chip microcomputer directly handling a keyboard and display or it can be a system of which the Loran component is truly a component.

The parts count of the Loran component consists of a fairly low number of IC's, mostly inexpensive, in the digital portion and a large number of very inexpensive parts such as resistors and capacitors and a few not so low cost ones such as the tuning veractors in the analog portion. When expanding from single chain to dual chain capability, only separate timing and signal interface portions are required. This is the only part of the system that needs to do two things at exactly the same time. The programming becomes more complex and the processor load for two chains reaches 70-80% of the processing time, which leaves little time for the high performance programs that allow direct ranging, partial solutions from two chains, and master independence. Thus, a second processor is required for the mathematics. The partitioning is functional: one processor is tracking all the Loran signals, one processor is calculating the position, and neither is saturated.

SOFTWARE

To use a local reference that is not perfect for direct range the local oscillator phase and frequency must be estimated. To obtain the local oscillator phase and rate, operation is required for the estimation of these parameters under one of the following conditions:

a) Reception of three stations continuously to solve for three unknowns, latitude, longitude and time at an unknown location or during motion; or

b) Reception of two stations at a known location with no movement.

After the local oscillator frequency and phase are computed two station operation is available for some period of time depending on what the accuracy requirements are and how good the local oscillator is.

The Loran chain reference time is controlled to coincide with universal time. The control is not exact and a difference of several microseconds usually exists. A drift rate of the order of a microsecond per month exists with occasional instantaneous resets of several microsecond that occurring every few months.

When estimating local time and time rate using a single chain, the chain offsets and rates are combined in these estimates giving the difference phase and phase rates. When opeating dual rate the difference time and rates are different for the two chains. For most situations the rates between the chains are low and the frequency of the offset is entirely that of the local crystal oscillator.

Separate estimates of the difference between local time and each chain time must be kept because the difference will have a significant effect on naivgation accuracy.

If a time correction occurs during operation the time differences are not affected since all stations in the chain are adjusted at once. However, in the direct range mode, a temporary navigation error will be seen if operating with three stations, and a permanent error will be observed if operating with two stations. If a critical operation would be disrupted by the adjustment, a check with time and frequency notices will give advance warning of the adjustment.

The method used for selecting the modes of operation is now described. A table of position dependent data is kept. Included in the table are the two best GRI's received at that locatiön. Also included are the best selection of stations for each GRI as well as alternate selections in case the stations in the primary selection are not received.

When the primary GRI is received with enough stations to provide an adequate position fix, it is used to update a six state variable Kalman filter. While this is a pseudo direct range solution, it is not overdetermined and will give the same position as a hyperbolic solution but with less variation. The repeatability of Loran is retained by insuring that the same stations are selected, when possible at this location.

If the second choice of GRI is received, all available stations are used to compute the time offset between the primary and secondary GRI's. This value is refined and retained until it is needed for dual chain operation.

If the primary GRI can not provide an adequate position fix but the second GRI can, a similar procedure is used. The second GRI is used for position fixing and the offset to the primary GRI is computed.

When neither GRI can provide an adequate position fix the system can be in either a position fixing or a calibration mode. When in a position fixing mode, stations from both chains are used to update the position, velocity and oscillator parameters. Any offset between the times of the two chains that have been previously computed is applied to the appropriate chain data.

In the calibration mode, the exact position is inputted and the receiver is not moving. Data from both chains is used to compute the oscillator parameters and the offset between the chains. The calabrated oscillator can then be used for position fixing.

POSITION FIXING

To take full advantage of the measurements of time of arrivals, the position fix process must estimate the local clock parameters as well as the position and velocity components. A Kalman filter is used to estimate:

North Position
East Position
North Velocity
East Velocity
Local Oscillator Phase
Local Oscillator Frequency

This implementation allows estimates of clock parameters to be made with three stations when appropriate geometry is available. After the oscillator's parameters have been estimated, operation can continue for a limited time with two stations or in poor geometry.

The state variables that are estimated in the navigation solution are:

X1	Latitude
X2	Longitude
X3	North Velocity
X4	East Velocity
X5	Local Time
X6	Frequency Offset

The position and velocity components are the desired navigation outputs. The unknown local time must be estimated for direct range operation. When a crystal oscillator is used for maintaining the local time reference, the frequency offset is computed.

The model of the systems used for formulating the filter is

$$\begin{vmatrix} X1 \\ X2 \\ X3 \\ X4 \\ X5 \\ X6 \end{vmatrix} = \begin{vmatrix} 1 & 0 & T & 0 & 0 & 0 \\ 0 & 1 & 0 & T & 0 & 0 \\ 0 & 0 & 1 & 0 & 0 & 0 \\ 0 & 0 & 0 & 1 & 0 & 0 \\ 0 & 0 & 0 & 0 & 1 & T \\ 0 & 0 & 0 & 0 & 0 & 1 \end{vmatrix} * \begin{vmatrix} X1 \\ X2 \\ X3 \\ X4 \\ X5 \\ X6 \end{vmatrix}$$

The measurements are the time of arrivals from the Loran stations. The measurement matrix will be.

H = L*cos(Bn),L*sin(Bn), 0,0,1,0

where L relates microseconds to distance and Bn is the bearing angle to the station

ESTIMATION OF OFFSET

The position estimated from the position fixing is the best available position. The oscillator phase and frequency relative to the position fixing chain time is computed by the six-state variable filter. The offset to the second chain time is the expected station time of arrival minus any known additional secondary phase factor difference. The quantity left over is the chain offset. These values for all secondaries are combined and filtered to provide the estimate of offset. A one state variable Kalman filter is used.

CALIBRATION MODE

In the calibration mode the receiver is not moving. The variables estimated are the primary GRI time, the oscillator frequency offset and the offset to the second GRI.

The state variables are

T	Time of Primary GRI
F	Oscillator Offset
OFF	Time Offset to Second GRI

The transition matrix is

$$\begin{vmatrix} 1 & T & 0 \\ 0 & 1 & 0 \\ 0 & 0 & 1 \end{vmatrix}$$

The system driving function covariance matrix is

$$\begin{vmatrix} 0 & 0 & 0 \\ 0 & Q2 & 0 \\ 0 & 0 & 0 \end{vmatrix}$$

The measurement matrix for the primary state GRI is

$$H = [1 \quad 0 \quad 0]$$

The measurement matrix for the secondary GRI is

$$H = [0 \quad 0 \quad 1]$$

GEOGRAPHICAL ACCURACY

To achieve the full potential of the Loran system, the lines of position are adjusted by adding the additional secondary phase factor to correspond, as well as possible, to their theoretical geographic position. The additional secondary phase factors are derived from a combination of theoretical and measured corrections. Over the coastal confluence zone of Loran coverage and the Great Lakes, the position error due to inaccuracies is attempted to be held at .25 miles RMS. Over land accuracies of similar magnitude have been achieved.

Because of the wide range of conditions of the propagation paths and the goemetry over which these accuracy figures are derived, it is not possible to correctly extend these figures to other modes of operation. However, some observations can be made. In the master independent mode using three secondaries and a hyperbolic solution, the master path for all secondaries is the same. The correct ASF correction can be found by subtracting the corrections for the master dependent LOP's.

In making a position fix using three secondaries an error in the same range as a master and two secondaries would be expected.

For direct range operation the ASF for each LOP is applied to the corresponding secondary. The correction due to the master is included in the computed clock times. As the vehicle moves the new corrections are applied and the oscillator time is recomputed. If the oscillator time can not be recomputed, as when only two secondaries from a chain are received, the change in the ASF due to the master will increase errors, and the change in ASF should not be applied.

CONCLUSION:

The increased performance derived from a dual rate, master independent, direct range Loran-C receiver can be obtained at a very modest increase in hardware cost. The implementation in a Loran component allows the advantages of these techniques to be enjoyed in many applications without a separate development for each application.

THE ROLE OF THE BOWDITCH NAVIGATOR AND LORAN C IN THE PROMOTION OF EFFICIENT AND SAFE VESSEL OPERATIONS

Thomas A. King, Jr.
Bowditch Navigation Systems
40 Pleasant Street
Portsmouth, New Hampshire 03801

ABSTRACT

The advances made in electronic navigation systems during the past decade have been significant. Presently, a navigator can choose among numerous navigation receivers the one best suited to his ship's needs, both in terms of the operating areas covered and the degree of position accuracy provided by a given system. Refinement of the Loran C system has produced accurate position data that is continually available for vessel positioning throughout the United States coastal confluence and port areas. And Loran C coverage is becoming available through more areas of the world. But electronic navigation receivers provide, at best, only data which must be transferred to a chart for a meaningful display of the vessel's position. The Bowditch Navigator MK-I, an automatic visual positioning aid (AVPA), provides the navigator with a chart display continuously indicating the vessel's position. The MK-I optimizes Loran C fixes and automates the process of transferring the position fixing data onto the chart. The AVPA system gives the operator a representation of position he can instantly assimilate resulting in safer and more efficient navigation.

BACKGROUND

Past navigation practices have required time-consuming data gathering, evaluation and calculations followed by the transfer of that data to the nautical chart for a meaningful position display. Once a position is finally plotted, it is for all practical purposes where the vessel <u>was</u>; not where it <u>is</u>.

The Bowditch Navigator MK-I, an automatic visual positioning aid (AVPA), automates this task and significantly lessens the conning officer's burden of position fixing, leaving him time to concentrate on traffic, communications and his obligations under the rules of the road. Additionally, the Bowditch Navigator provides a means to cross check traditional navigational and piloting practices, reducing the chances of undetected human error. However, this automation is most accurate with an electronic navigation system such as Loran C providing the basic position data.

Over the past decade, there has been a significant growth in the areas of offshore petroleum and mineral exploration and production, vessel size, traffic density and subsequent traffic lane configuration schemes. Correspondingly, there has also been an increased awareness and concern for the environment and the losses of life, cargo and vessel caused by vessel groundings, rammings and collisions. The passage of the Port and Tanker Safety Act of 1978 is one demonstration of this growing industry-wide concern.

The events of several successive winters have demonstrated the need for an automatic precision Loran C positioning system which has both port and coastal capabilities. The Atlantic and Gulf coasts of the United States alone were the scene for numerous vessel casualties like the loss of the Argo Merchant.

Vessel movement came to a virtual standstill in Northern ports as ice submerged and removed floating navigational aids. Prolonged periods of fog closed ports such as Galveston for days on end. The end result: increased shipper costs and underutilized port facilities.

Sudden weather disturbances degrade radar performance while at the same time obscuring visual ranges and markers. The Sunshine Skyway Bridge tragedy is one memorable result of such circumstances.

Planned reductions of the number of floating navigational aids and the accepted tendencies for vessel operations to continue in even the most restricted visibilities without adequate vessel positioning information may very well set the stage for future marine casualties, many of which can now be avoided.

Let's take a moment and look at the conning officer. His ability to successfully perform the job is dependent on a number of factors; training, experience and available information, to mention a few. Like all of us, he uses all of his senses to perform his job. His visual perception is the most important sense. To complement his efforts and support his perception, technology has contributed such aids as radar, ARPA and the numerous electronic radio navigation positioning systems.

Radars and ARPAs present meaningful but incomplete pictures of the situation. Their performance can be significantly degraded in certain weather conditions. However, their information is very often subconsciously absorbed and utilized. They represent something almost tangible, that is, something that can be interpreted, digested and used in its present form, a picture. However, there remains a serious deficiency in current position information. While this same technology has provided very accurate position data, it has not presented it in a meaningful or assimilable form. For example, if you were told your position was Latitude 43' 04.56'N, Longitude 070' 45.47'W or TD1 13709.1, TD2 26016.2, you could no more satisfactorily determine your position than you could determine the relative position of surrounding ship traffic in a thick fog without radar. By itself, a numeric representation of position cannot be translated by the mind into a useful picture of the ship and its surroundings. So traditionally that numeric representation is plotted on a nautical chart to define these spatial relationships.

The primary objective in marine navigation is accurate vessel positioning. The frequency of positioning is dependent on the surrounding circumstances. Inland waters and port approach areas require continual positioning. The coastal confluence areas are most demanding. It is here that the watch officer makes the transition from a leisurely open sea watch to one which is highly demanding. Increased traffic density and irregular traffic patterns at times require his complete attention. Accurate positioning becomes very critical as the vessel moves into confined waters with shoals, obstructions and traffic schemes. Today's navigation procedures, while the results are more accurate and easier achieved, are much the same as they were 500 years ago. It still remains the navigator's responsibility to manually collect, evaluate and select from the numerous navigation sensors and instruments the data he needs to manually plot on the nautical chart to gain a meaningful display of position.

And where is this most important task performed today? Back in the chart room away from the conning station. The work load is further increased as port arrival and departure tasks are performed. Trade offs take place. Vessel positioning during certain periods of the voyage may take a back seat to collision avoidance or communications. Generally, all ends well but too often, it does not.

Ship owners and port managers must run a cost effective operation to remain viable, yet safety is a vital ingredient for any successful operation. The Bowditch Navigator, working with Loran C, provides the means to achieve safe and efficient vessel operations in all weathers.

THE BOWDITCH APPROACH TO ALL WEATHER PRECISE POSITIONING WITH LORAN C

The Bowditch approach to precise vessel positioning with Loran C calibrates the entire navigation system including the nautical chart to an appropriate charted reference point, e.g., intersection of channel ranges. The advantage of this approach is that the system is calibrated to the surrounding local geography. The calibration process involves the calculation of a system differential or offset. The system's differential is composed of the difference between the position's theoretical and actual time differences, receiver bias error, chart error, MK-I system error and grid bias errors. MK-I system calibration is a single key user-performed procedure. It very simply consists of re-initializing or re-entering the vessel's actual present position on the nautical chart via the cursor keys (Figure 1). The procedure can be performed at a dock prior to getting underway or at any time the vessel is making way. It should be pointed out that the calibration is local with no general rule of thumb to determine its effective range. However, the Bowditch Navigator can store a table of system differentials which are automatically applied at the appropriate geographic position as the vessel proceeds along its planned route. The result is continual precise vessel positioning as the vessel proceeds along its track. It should also be mentioned that the degree of position precision is dependent on the receiver's resolution. That is, a .1 microsecond receiver will not provide position accuracy to the same degree of precision as will a .01 microsecond receiver.

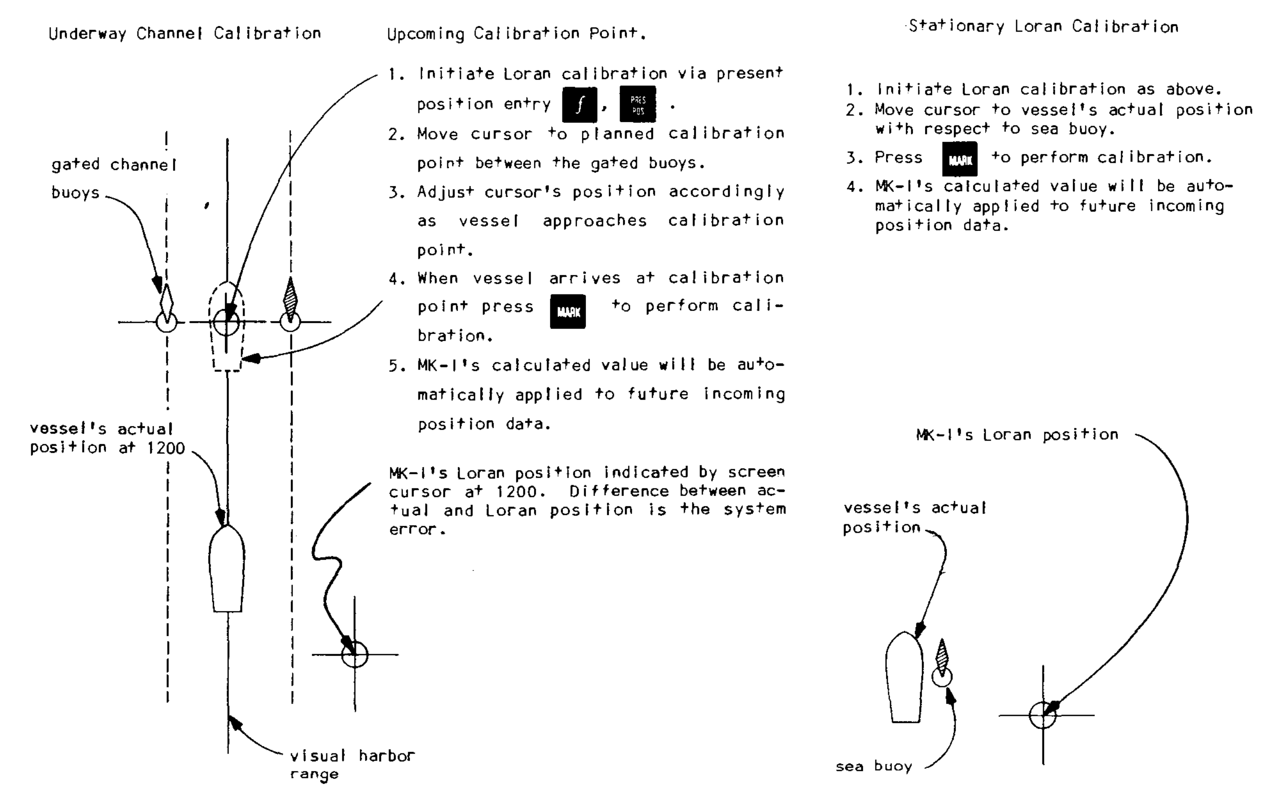

Precise Loran C positioning can also be achieved in instances where past MK-I system port calibration values are not available and Loran C time difference waypoints are available, such as those which have been published by the U.S. Coast Guard. These values are entered by their respective Latitude/Longitude positions.

One of the most significant attributes of the Bowditch system is that it does not require pre-programming for a specific operating area and it does not require outside support services. It can be used at any location around the world where a stable electronic navigation system provides coverage.

THE BOWDITCH NAVIGATOR MK-I

The Bowditch Navigator's primary feature is present position displayed automatically and continually on a familiar nautical chart. Why a nautical chart? Nautical charts are familiar to all who venture to sea. They include an enormous amount of information which is readily assimilable and necessary. Any display of present position which does not utilize the standard nautical chart, e.g., numeric position data, CRT channel outline displays, is incomplete. In addition to displaying present position, nautical charts are used for route planning. These same tasks can be performed with the Bowditch Navigator through its waypoint sailing and navigational hazard warning features. When an operating mode is selected, e.g., Loran, SatNav, Omega, Decca, D.R., the vessel's position will be updated by that mode's incoming data. When in the Loran mode, position updates will occur as frequently as every second. The MK-I's microprocessors continually evaluate and process all available Loran secondaries (TDs) considering such factors as GDOP (geometric dilution of position), SF and ASF corrections. When the satellite navigation mode is selected, position updates occur with each valid transit satellite pass. Between satellite passes, positions are updated by either dead reckoning or one of the alternate radio navigation system modes, e.g., Loran, Omega.

The development of the Bowditch Navigator MK-I required the development and application of technology in the areas of photography, optics, electronics and electromechanics.

The visual display of ship's position on the nautical chart is derived from an optical projection of a Bowditch Microchart onto the viewing screen of the MK-I. The Bowditch Microchart is a full color film transparency of a single standard NOAA or DMA nautical chart. The individual films are permanently mounted in durable cassettes for easy storage and retrieval. The specific Microchart for the appropriate coverage area and scale is selected just as a corresponding paper chart would be selected. The amount of Microchart area in immediate view is dependent on the loaded Microchart's scale. With a typical harbor chart loaded, approximately three square miles is immediately viewable. Other areas of the Microchart may be easily viewed by initiating the Microchart viewing feature. The smallest scale Microcharts will provide immediate viewing areas in excess of 1500 miles.

When a Microchart is loaded into the Bowditch Navigator, it is actually placed in the Microchart transport mechanism which is under control of the MK-I's computer. The transport mechanism is responsible for precisely positioning the Microchart in the optical system. As the Microchart is positioned in the optic system, the vessel's present position is displayed on the front screen at the screen cursor.

CONCLUSION

Loran C is a proven electronic navigation system which has the inherent characteristics of stability and position repeatability. Its precise positioning capabilities have been demonstrated and provide a basis for a precise knowledge of position. The Bowditch Navigator MK-I is the first Navaid to fully utilize Loran C's potential.

The MK-I's ability to provide and display meaningful, precise, all-weather positioning, without outside services, and in both inland and offshore waters around the world, makes the system truly cost effective. The implementation of such a standardized navigational system will have a positive and significant impact on the efficiency and safety of vessel operations, ultimately aiding in the prevention of vessel casualties.

SESSION II

POSITIONING I

A COMPARISON OF
METHODOLOGIES FOR AIRBORNE
LORAN GRID DATA GATHERING

Robert E. Voigt, Captain, USAF
Robert S. Wester, Captain, USAF
Eglin Air Force Base, Florida

ABSTRACT

The usefulness of loran in many applications is dependent upon the relative accuracy of the hyperbolic to geodetic conversion process. The non-homogeneous nature of the earth surface causes warpage of the loran signal and introduces a source of positional error. A model for the secondary phase correction term developed from known Time Difference/Latitude-Longitude pairs can offset effects of warpage. The three known methodologies for gathering airborne data over a large area are compared: radar/phototheodolites, RF-4C photo-mapping, and the Completely Integrated Reference Instrumentation System (CIRIS).

I. Introduction

The usefulness of loran in many applications is dependent upon the relative accuracy of the hyperbolic (loran time difference-TD) to geodetic (latitude/longitude) coordinate conversion process. Changes in the propagation medium over which the signal travels will disturb the smooth hyperbolic lines of position (LOP) in loran and will introduce a source of significant positional error during TD/Lat-Long conversion. This error is a result of the simple fact that the loran grid is not directly related to the geodetic grid. The difference between loran TDs measured with a receiver and TDs calculated using a homogeneous conductivity model is referred to as warpage. Loran warpage can be corrected during coordinate conversion by using an appropriate model for the secondary phase correction term.

In the AN/ARN-101 Digital Modular Avionics System (DMAS) used in F-4E and RF-4C aircraft the effect of loran warpage is corrected through a two part procedure. The first part operates as an off-line computer program called WARP and requires a data base of measured TDs and latitude/longitude pairs to generate a set of 15 coefficients for each loran station. These coefficients are used in the second part of the process to compute the secondary phase correction term each time the ARN-101 does a coordinate conversion. The warpage is corrected by using the coefficients to estimate an effective wave impedance for the secondary phase correction of each loran time of arrival (TOA). If the coefficients are not available, the ARN-101 system will automatically degrade to stored constants representings a sea water model.

Precision coordinate conversion by the ARN-101 in areas of warpage requires an accurate paired data base of measured TDs and geodetic position for input into the WARP program. This paper presents a comparison of the three known methodologies for gathering airborne loran grid data: radar/phototheodolites, RF-4C photo-resection, and the Completely Integrated Reference Instrumentation System (CIRIS). A general description of loran, the ARN-101, warpage, and CIRIS is provided before comparing the methodologies.

II. General Background Information

Loran

A loran position fix is determined by measuring the TOA of loran signals from three stations (Master, Slave A, Slave B). The two slave transmissions are initiated by the arrival of a master station signal at the slave stations and the loran fix is obtained by measuring the difference of the TOA at the receiver of the master and the slave signals. The TDs for each master/slave pair (TDA and TDB) describe an hyperbolic LOP for a constant TD and the intersection of the TDA and TDB LOPs describe a loran hyperbolic fix as shown in Figure 1.

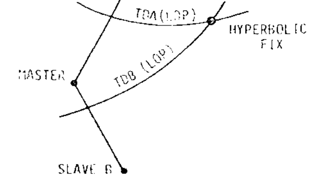

Fig 1. Hyperbolic Lines Of Position

In theory the hyperbolic grid described by the LOPs may be easily converted to a convenient geodetic grid, however, non-uniform conductivities of the terrain cause warpage. Since the loran TDs, measured at a given position, are a function of the RF transmission characteristics of the ground over which the signal must pass, a known position may be characterized in terms of an effective impedance relative to a loran transmitter site.

ARN-101 DMAS System Description

The ARN-101 is a navigation, weapon delivery, and sensor management system installed in the F-4 to provide all-weather navigation and weapon delivery capabilities to the aircraft. The ARN-101 employs fourteen Line Replacement Units (LRUs)which include a central digital computer, a signal data converter (for analog-to-digital and digital-to-analog conversions), a loran receiver, and a digital IMU. The navigation computer uses both inertial measurement and loran receiver inputs to provide an improved navigation function via software Kalman filtering. In each navigation mode, position information is available in three coordinate references: latitude/longitude, universal transverse mercator (UTM), and loran TDs. The system is designed to degrade through the following navigation modes as subsystems are lost:

1. Integrated loran/inertial (prime mode)
2. Loran with inertial velocity aiding
3. Loran with true airspeed (TAS) aiding
4. Inertial only
5. Loran only
6. Dead reckoning (TAS and heading)

In weapon delivery modes, navigation and steering functions are provided by the ARN-101 to allow accurate weapon deliveries. The weapon delivery modes aided by the ARN-101 are loran blind, sensor aided blind, and visual weapon deliveries. In both navigation and weapon delivery modes, the ARN-101 can direct sensors to destinations, targets, or offset points for navigation updates, and for sensor-aided weapons deliveries.

WARP Program

The warpage coefficient generation program (WARP) was developed by Lear Siegler, Inc. (LSI) as off-line support software for the loran navigation function of the ARN-101 and models the effective impedance for a predetermined coverage area via a least-squares fit regression model. The WARP program was developed to model the secondary phase effects and generate the warpage coefficients for a fourth order polynomial used by the ARN-101. WARP was assembled by combining several theoretical methodologies which characterize low frequency wave propagation over varying terrain conditions. It uses mathematical routines to fit observed data (TD/Lat-Long pairs) to an impedance surface model, and performs statistical analyses of the modeling process. The current version of program WARP is a composite of original LSI methodology and several new routines designed to enhance program execution and provide expected position error estimates over portions of the loran hyperbolic grid. The program has been coded in ANSI standard FORTRAN-66 and implemented on the CDC-6600 and CYBER-176 computer systems.

The area for which a given set of warpage correction coefficients is valid represents a relatively small portion of the total loran triad coverage area. This area is known as the prime area for WARP and is defined as that area of interest for which accurate TD versus geodetic position data has been collected.

The prime area is defined by the geodetic positions (latitude and longitude) of its southwest and northeast corners (Figure 2). The uniform distribution of data points within the prime area is very important. Ideally, when the prime area is divided into square cells which are 5 nautical miles (nm) by 5 nm in size, each cell should contain a minimum of at least one data point. This distribution insures that the prime area will be accurately modeled. More data points per cell in the prime area will generally result in a more accurate model. Program WARP calculates an average constant impedance value for the four areas outside the prime area.

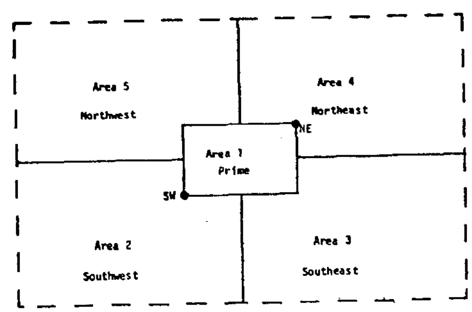

Fig 2. Program WARP Area Definitions

CIRIS System Description

The CIRIS system was initially designed to provide a highly accurate, realtime, position velocity, and attitude reference for flight tests of inertial navigation, guidance, and radar systems. This airborne automated system was configured to be carried aboard both cargo and fighter test-bed aircraft as well as used in a mobile testing van. Utilizing ground-based transponders positioned in a triangular pattern along the flight path of the aircraft, the CIRIS system provides a mobile positional reference capability which can be deployed worldwide. Position accuracy to 13ft in three axes and velocity accuracy to 0.1 feet/sec in three axes provide the Air Force with a valuable airborne test facility for use in development and verification of navigation systems.

III. Data Gathering Methodology

The loran warpage data base consists of loran TDs and corresponding geodetic latitude-longitude positions. The accuracy of the final conversion process in the ARN-101 is directly related to the accuracy of this measured data base. Three methods for gathering airborne loran grid data acceptable for input to the WARP program have been demonstrated at Eglin AFB, FL (EAFB).

The Southeast U.S. Loran-C chain or Gulf-Coast Chain (see Figure 3 for chain specifications) was initially modeled in May 79 using unique EAFB radar/phototheodolite test resources and an ARN-101 modified F-4E. Later that year the data collection process was repeated and the validity of an RF-4C photo-resection procedure was established . This procedure has been adopted as the standard USAF methodology and has been used to map warpage in portions of Korea, Europe and Nevada. The feasibility of using CIRIS for loran grid data gathering was demonstrated in Dec 81 at EAFB in support of a grid prediction development effort by Jaycor. Each of these procedures are unique and offer technical, cost, and schedule advantages or disadvantages.

Radar/Phototheodolite Procedure

The reconfiguration of the East Coast Loran C chain and the activation of the Gulf Coast chain in 1979 established a requirement to model the loran warpage for the EAFB range complex in support of on-going AN/ARN-101 developmental flight testing. Loran TD and aircraft positioning data were gathered during F-4E missions which were flown throughout the prime coverage area (PCA) on mosaic flight profiles (see Figure 4). Continuous AN/AFP-16 radar using beacon tracking provided accurate time-space-position information (TSPI) of the aircraft. Additional accuracy was provided by a network of phototheodolites. The radar was used to monitor aircraft position on the desired profile and was the primary source of TSPI when phototheodolite coverage was not available. The radar data are accurate to within ±35 feet in position and ±10 feet per second in velocity. Normally, three phototheodolites were used to yield a position accuracy of ±3 feet. Using successive positions to determine velocity, the phototheodolites were accurate to within ±1 foot per second.

The data gathered from the radar coverage and phototheodolite coverage were merged in the following manner. First, the bias in the radar coverage was estimated from the phototheodolite data and removed; then the radar data were combined. The data of the radar closest to the aircraft were weighed more heavily than those of the second radar. The resulting merged data were accurate to under 100 feet throughout the primary coverage area.

The F-4E aircraft used in the data collection were specially instrumented to record and time tag loran positioning data. This instrumentation data was merged with the dual radar/phototheodolite space positioning data to provide paired Lat/Longs and TDs as required by the WARP program.

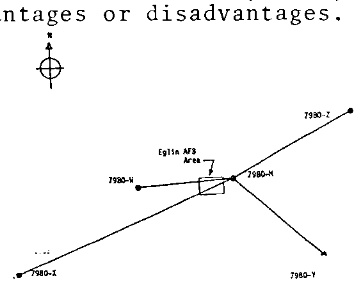

Station	Latitude & Longitude	Station Function	Coding Delay & Baseline Length	Radiated Peak Power
Malone, Florida	30-59-39.74N 85-10-09.31W	Master	- - -	800 kw
Grangeville, Louisiana	30-43-31.02N 90-49-43.60W	W Secondary	11,000µs 1809.54µs	800 kw
Raymondville, Texas	26-31-55.01N 97-50-00.09W	X Secondary	23,000µs 4443.38µs	400 kw
Jupiter, Florida	27-01-58.49N 80-06-53.52W	Y Secondary	43,000µs 2201.88µs	275 kw
Carolina Beach, N. Carolina	34-03-46.04N 77-54-46.75W	Z Secondary	59,000µs 2542.74µs	550 kw

Fig 3. SE U.S. LORAN-C Chain Configuration

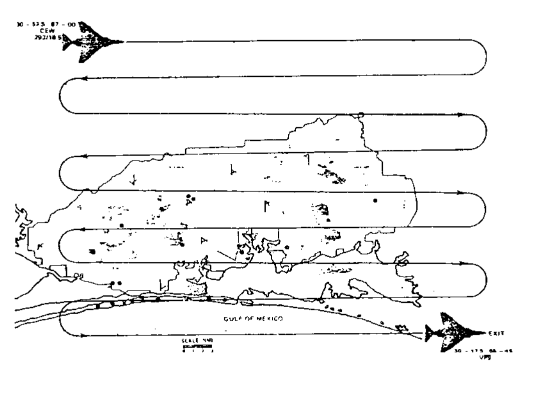

Fig 4. Gulf Coast Modeling Flight Profile

Data points were selected which minimized the aircraft positioning errors, normally less than 100 feet, and which satisfied the 5nm distribution desired by WARP.

This procedure could be completed in less than 2 months and would cost approximately $16K for the EAFB PCA as indicated in Figure 5. The cost for a 10,000 nm^2PCA, if radar coverage was available, would increase to approximately $76K and would take 2 mos to accomplish. The overriding disadvantage of this procedure is that accurate radar coverage over the entire PCA must be available. For this reason, even though cost and schedule criteria are excellent, the procedure is unsatisfactory for operational use.

RF-4C Photo-Resection Procedure

RF-4C photo-mapping aircraft equipped with the ARN-101 were selected for operational loran grid data collection due to their unique capability to accurately record position and loran data worldwide. RF-4C aircraft are tasked to fly a 5nm wide mosaic profile over the PCA (Figure 4) and at 4-6 second intervals the KS-87 camera photographs the present position of the aircraft. The loran TDs for that point are printed on each frame of film via the AN/ASQ-154 Data Display Set which has a predicted 200 feet accuracy. The processed film is forwarded to the Defense Mapping Agency (DMA) to determine the aircraft latitude/longitude via photo-resection of RF-4C photographs. This process is extremely time-consuming (3-6 months) and requires an extensive data base of known geographic locations which is not always available, especially in potential war zones.

The development of warpage coefficients using this procedure for a standard 10,000 nm^2 PCA (3-4 times EAFB coverage) would require 6-12 months and would cost approximately $131K (See Figure 5). It should also be noted that the photo gathering capability of the RF-4C is highly weather dependent and collected data could be determined to be unuseable several months into the resectioning process. The schedule for this method of data gathering is therefore extremely optimistic.

	RADAR/PHOTOTHODOLITES ($900\ nm^2/10{,}000\ nm^2$)	RF-4C PHOTO-MAPPING ($10{,}000\ nm^2$)	CIRIS ($10{,}000\ nm^2$)
COST			
AIRCRAFT	$10K / $50K	$50K (5 missions)	$50K (5 missions)
COMPUTER SUPPORT	$1K	$1K	$1K
DMA SUPPORT		$80K	
CIRIS SUPPORT			$25K
RANGE SUPPORT	$5K / $25K		
TOTALS	$16K / $76K	$131K	$76K
SCHEDULE			
AIRCRAFT	1 mo / 2 mos	2 mos	2 mos
DMA PHOTO RESECTION		6 mos	
CIRIS DATA REDUCTION			1 day
WARP (RUN AND VERIFY)	1 mo	1 mo	1 mo
TOTALS	2 mos/ 3 mos	9 mos	3 mos

Fig 5. Cost and Schedule Comparisons

CIRIS

The CIRIS system, when utilized in a loran data gathering application, consisted of the following units installed in a SUU-16 gun pod shell:

1. Hewlett Packard HP21MXE host computer to control measurement devices, process data, produce and record position and velocity reference data.

2. Litton LN15 inertial navigation system for attitude, position, and velocity comparison data.

3. Sperry air data computer for computing barometric altitude, airspeed, and wind.

4. Cubic Corp. radio-range/range-rate/interrogator system (RRS) to calculate position and velocity data.

5. Time code generator for data time reference.

6. Magnetic tape cartridge data recorder.

The CIRIS pod is mounted on the centerline station of an RF-4C (or F-4E) ARN-101 modified aircraft. There are no physical modifications required to the aircraft. The pod mates with the Class V Pave Tack centerline harness and utilizes Pave Tack electrical and signal connectors. A minor modification was made to the ARN-101 software to display statistical performance indicators on the Pave Tack video. This allows the Weapon System Operator (WSO) to monitor CIRIS, loran, and ARN-101 airborne status. The CIRIS pod is completely automated and requires no crewmember interface.

CIRIS accuracies are directly dependent upon the RRS measurements. The RRS includes ground based transponders in addition to the airborne equipment carried in the pod. The transponders are rugged, transportable, self-contained units capable of sustained operation at a remote surveyed site. A minimum of three transponders are necessary at any time in flight for precision accuracy and a total of 7-8 are required for a 10,000 nm^2 PCA at 20K mission altitude. The transponders are deployed at first order surveyed points in a triangular pattern separated by a distance which will provide total grid coverage with the greatest positional accuracy (see Figure 6). The airborne interrogator and HP21MXE uses the line-of-sight range and range rate to each transponder to compute a position and velocity estimate using a time-phased triangulation scheme which is the key to the CIRIS accuracies. The signal, in traveling to the transponder and returning, experiences a delay in place that is proportional to the slant range distance traveled. Range rate is measured by determining the doppler frequency shift of the signal exchanged

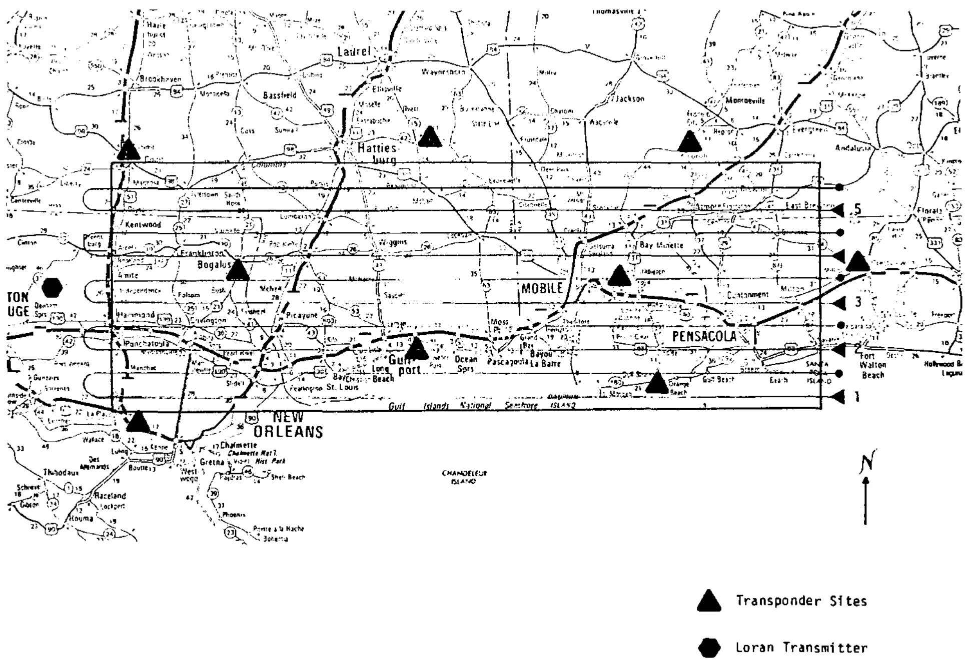

Fig 6. CIRIS Coverage of EAFB PCA

during interrogator-transponder interaction.

The CIRIS system offers an all weather data collection capability with minimal (2-3 hrs) data reduction turn-around. It is dependent only upon the positioning of transponders. One engineer and four technicians are normally required to support and maintain the system during a deployment. In the EAFB CIRIS data gathering effort, five missions were planned to fly the entire coverage area as indicated in Figure 6. Eight missions were actually flown, six of which were considered successful. Two missions were lost due to mechanical failures and one mission was flown to gather data omitted during earlier missions.

Data for a 10,000 nm^2 PCA could be collected in 2 mos at an estimated cost of \$76K. Detailed cost and schedule information is provided in Figure 5. The primary disadvantage with CIRIS in this role is availability. CIRIS resources and manning are currently inadequate to support numerous development efforts and are therefore only able to support operational requirements on a workload permitting basis.

IV. Summary

Although three methodologies for gathering airborne latitude/longitude-TD pairs have been used, only RF-4C photo-mapping appears to be able to support the operational ARN-101 fleet. The CIRIS system offers obvious cost and schedule advantages, however, the non-availability of the system for operational support will essentially rule out this approach.

References

1. AD-TR-81-4, AN/ARN-101 and Pave Tack Interoperability Test (U), CONFIDENTIAL.

2. ESD-TR-81-116(I), Gary Brown, et al, Loran Warpage Coefficient Generation Program (Program WARP) User's Manual, Mar 81.

3. ESD-TR-81-116(III), Capt Michael A. Marchand, et al., Loran Warpage Coefficients Generation Program (WARP). Feb 81.

4. Howard, Joe. "Loran Warpage Data Base Requirements", Bedford, MA, Undated.

COORDINATE CONVERSION BASED ON A SIMPLIFIED RAZIN ALGORITHM

J. Nicholas Newman
Department of Ocean Engineering
Massachusetts Institute of Technology
Cambridge, Massachusetts 02139

ABSTRACT

A simplified algorithm is described for direct coordinate conversion, from a pair of Loran time differences to the latitude and longitude of the receiver. This algorithm is based on the approach of Razin, with simplifications which facilitate its use without significantly degrading the accuracy. The associated constants for each Loran-C chain are tabulated, and sample calculations for each chain are presented to verify the method.

INTRODUCTION

The process of coordinate conversion from a pair of Loran-C time differences (TD's) is a routine task which can be performed internally by several Loran receivers, or on a programmable hand calculator. In either case it is desirable to seek an efficient algorithm which minimizes the storage requirements of the device, and time for execution. In the context of marine navigation it is desirable to preserve a degree of precision commensurate with the inherent accuracy of the TD's.

The mathematical relations between TD's and geodetic coordinates (latitude and longitude) are most straightforward for the inverse problem. There the coordinates are known and TD's are determined, in terms of the differences in geodesics corresponding to the relevant propagation paths. The same equations can be used in an iterative manner for the problem of coordinate conversion, assuming an approximate position and proceeding iteratively to compute the corresponding TD's and their gradients until a suitable degree of convergence is achieved. However this approach is time-consuming, and requires an initial specification of the assumed position.

Razin's algorithm [1] permits a direct conversion from a pair of TD's to latitude and longitude, and is particularly efficient for routine use. The principal complication is the determination of various auxiliary constants which depend on the geometry of the Loran chain. However these constants are essentially independent of the position of the receiver, and can be precomputed for a particular combination of master and secondary stations, and stored for subsequent routine use. Explicit formulae for determining these constants are given by Fell [2].

This paper presents a tabulation of the auxiliary constants in Razin's algorithm, for the principal Loran-C chains, and also describes certain simplifications of the algorithm to facilitate its use for routine coordinate conversion. Test results are included for each Loran-C chain.

APPROACH

In the process of coordinate conversion it is desirable to maintain a degree of precision commensurate with the inherent accuracy of the TD's, say $\pm 0.1\ \mu s$. To achieve this objective, three corrections must be accounted for:

1) Spheroidal earth correction

2) Secondary phase correction (SF)

3) Additional secondary phase correction (ASF)

The first two corrections can be made theoretically, but the ASF correction generally must be based on local calibrations. Uncertainties in the ASF correction are the dominant error limiting the overall accuracy of coordinate conversion.

In Razin's algorithm the spheroidal correction is made by mapping the spheroid onto an osculating sphere which has the same total radius of curvature at a prescribed tangent point. The accuracy of this approximation decreases with increasing distance from the tangent point, but the error from this source is usually negligible if the tangent point is located centrally in the Loran chain. For convenience, the constants tabulated below are based on a tangent point at the master station.

Secondary phase corrections depend on the relevant propagation distances, and hence on the unknown position of the receiver. This difficulty is overcome in the original Razin algorithm by first determining an approximate position without SF corrections, followed by a second iteration which includes the SF corrections. This iterative approach practically doubles the computing time required.

In the simplified algorithm a linear approximation is utilized for the SF correction, in the form

$$SF = T\left[\frac{1}{0.9994} - 1\right] - 0.2, \qquad (1)$$

where T is the propagation distance in μs. The error in this approximation is less than ±0.1 μs for propagation distances greater than 75 km, as illustrated in Figure 1. The principal advantage of this linear SF correction is that it can be incorporated in the Razin algorithm without performing a second iteration.

In summary, the two fundamental simplifications outlined here are to use a common tangent point for the spheroidal correction, and to use a linear approximation for the SF correction. The first simplification enables the auxiliary constants to be tabulated in advance for a given chain, and reduces the total number of constants which must be stored. The SF correction obviates the need for a second iteration and reduces the time required for coordinate conversion. The cumulative error from these two simplifications usually is less than or comparable with the inherent 0.1 μs tolerance. In any event, the errors resulting from these simplifications can be incorporated in the (much larger) ASF corrections, provided the calibration to determine the ASF corrections is performed with the same algorithm.

Some additional simplifications of the Razin algorithm can be achieved simply by rationalization of the constants and equations from their original form in Reference 1. The final result of this simplification is shown in Figure 2, and in a slightly different form in Reference 3. The latter reference also describes an auxiliary algorithm suitable for determining the ASF corrections at a calibration point.

In Figure 2, TD_i denotes the two observed time differences, and DT_i are the coding delays for the corresponding secondary stations. The remaining parameters which are not otherwise identified correspond to those in Reference 1, but with some changes in notation and normalization as shown in Table 1. These parameters are explained briefly below.

The parameter $R/\tilde{V}$ is the ratio of the radius of curvature divided by the (reduced) velocity of propagation, in units of microseconds per degree. The reduction factor 0.9994 is included to account for the linear portion of the secondary-phase correction. The parameter θ_{Mi} denotes the arclength in degrees between the master (M) and each secondary station, and K is the included spherical angle between two such arcs. The "universal" constants C_{01}, C_{02}, C_{03} depend only on the coordinates of the tangent point at the master station. The remaining nine constants C_{ij} depend on the coordinates of the master and both secondary stations. The latter constants, and the parameter K, must be determined separately for each possible combination of two secondary stations in a chain.

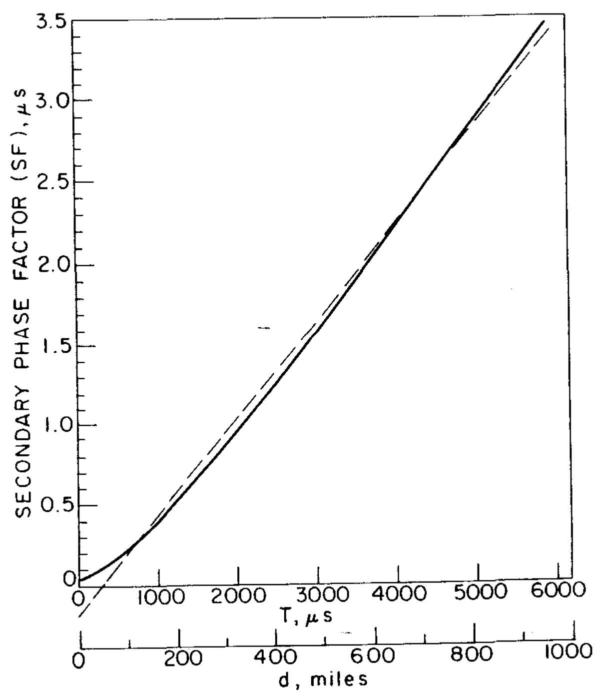

Figure 1. Comparison of the linear approximation (1) (dashed line) with the more exact secondary-phase correction (3) (solid line). (From Reference 3.)

Auxiliary Constants

The constants which appear in Table 1 have been computed in the manner outlined by Fell [2], using an HP-41C programmable hand calculator with 10 significant figures of internal accuracy. The results, which are tabulated in Table 2, are based on the WGS-72 spheroid (a=6378.135km, b=6356.7505km), and a propagation velocity v=0.2996916km/μs after correction for the index of refraction. Additional inputs are the coordinates of each Loran chain, which are based on the Chain Data Tables in the WGA Radionavigation Journal and on USCG Notices to Mariners.

Referring to Table 2, the first column of data for each chain is a listing of the latitude (LAi) and longitude (LOi) of the master and each secondary, in degrees, minutes, seconds and hundredths of seconds with a decimal point separating the degrees and minutes. Each secondary is labelled numerically, in order of increasing coding delay time and in the same order as shown in the Chain Data Tables. All latitudes shown are in the northern hemisphere. Both east and west longitudes have been defined as positive for chains which lie entirely within the corresponding hemisphere. For chains which span the prime or 180° meridian west longitude is positive and east longitude is negative.

The second column in Table 2 lists the constants (beginning with R/$\bar{V}$ and ending with CØ3) which are universal for each chain. The remaining columns list separately the ten constants which differ for each combination of secondary stations, designated by the pair of numeric labels separated by a comma and located above the identifying symbols of each column.

The original constants defined by Razin [1] can be recovered from the data in Table 2, using the relations listed in Table 1. (The extra constant C_{14} in Reference 1 is simply the ratio a/b=1.0033606.) It should be noted that the spheroidal latitude ϕ utilized by Razin [1] and Fell [2] differs from the usual geodetic latitude L in accordance with the relation

$$\tan L = (a/b) \tan \phi \qquad (2)$$

This transformation is applied to the geodetic latitude of each Loran station before computing the constants in Table 2. Similarly, the inverse transformation to geodetic latitude must be made after using the original algorithm of Razin [1] if conventional geodetic coordinates are used for navigation. The latter transformation is included in the simplified algorithm shown in Figure 1, and the final result is the geodetic latitude L.

TEST RESULTS

To illustrate the use of the simplified algorithm, and test its accuracy, sample results are presented in Table 3 for each chain and combination of secondary stations. In each case an appropriate position has been assumed, defined by integer values of the (geodetic) latitude and longitude. The theoretical time differences at this position have been computed directly, using Lambert's solution for the spheroidal geodesic [3] and the SF correction

$$SF = \frac{1}{T}\begin{Bmatrix} 2.741282 \\ 129.04323 \end{Bmatrix} - \begin{Bmatrix} 0.011402 \\ 0.40758 \end{Bmatrix} + T\begin{Bmatrix} 0.00032774815 \\ 0.00064576813 \end{Bmatrix}, \; T \lesssim 537 \ \mu s \qquad (3)$$

These theoretical TD's are shown to two decimal places in Table 3, with appropriate identification numbers (TDi). Following each pair of TD's are the computed latitude and longitude in decimal degrees, as obtained from the simplified Razin algorithm with the constants in Table 2. The error in coordinate conversion can be determined in each case from the fractional part of the latitude and longitude.

As an example, the first entry in Table 3 shows theoretical TD's for the North Atlantic Chain, 7930-W and 7930-X, corresponding to an assumed position at 50°N, 30°W, and a resulting computed position of 50.0025°N, 30.0014°W. In this case, the error in coordinate conversion is .0025° in latitude, and .0014° in longitude, or 9 seconds and 5 seconds respectively. Expressed in distance, the computed position is in error by approximately 0.3km. This is the largest error shown in Table 3 for any chain. It results in part from the width of the North Atlantic Chain, with distances up to 2000 km from the tangent point to each of the secondaries and to the receiver. Improved accuracy will result in this situation if the tangent point is placed centrally between the master and secondary stations. However the principal cause of error in this particular example is poor geometry, with a crossing angle of 13° between the W and X secondary stations. In normal use this pair would not be used together.

The remaining test results in Table 3 are more accurate, with most errors in latitude and longitude less than .0005°, corresponding to errors in position less than 50 meters. Typically these errors are reduced when the geometry is favorable, and are consistent with the tolerance of 0.1 μs in time differences. Thus the simplified Razin algorithm

INPUT:

TD_1, TD_2

$$P_i = (TD_i - DT_i + 0.2)/(R/\tilde{V}) - \theta_{Mi}$$

$$b_i = \sin P_i/\sin \theta_{Mi}$$

$$a_i = \cos P_i/\sin \theta_{Mi} - \cot \theta_{Mi}$$

$$u = a_2 b_1 - a_1 b_2$$

$$v = a_1 \sin K$$

$$w = a_1 \cos K - a_2$$

$$c = \frac{uw \pm v\sqrt{v^2 + w^2 - u^2}}{v^2 + w^2}$$

$$\theta_{MS} = \tan^{-1}[a_1/(b_1 + c)] \quad (0 < \theta_{MS} < 180°)$$

$$\theta_{Si} = \theta_{MS} + P_i$$

$$X_j = C_{Mj} \cos \theta_{MS} + C_{1j} \cos \theta_{S1} + C_{2j} \cos \theta_{S2} + C_{0j}$$

$$(j = 1, 2, 3)$$

$$LON = \tan^{-1}(X_1/X_2)$$

$$LAT = \tan^{-1}\left\{X_3/\sqrt{X_1^2 + X_2^2}\right\}$$

Figure 2. Flow chart for simplified Razin algorithm. The plus sign is used in the expression for c unless the receiver is in a sector bounded by extensions of the arcs connecting the master and secondary stations.

presented here is generally compatible with the overall precision of Loran-C navigation.

SUMMARY AND CONCLUSIONS

This paper describes a simplified version of the Razin algorithm, and gives values of the auxiliary constants for existing Loran-C chains. This algorithm is computationally efficient, and the errors associated with its use are consistent with the inherent accuracy of observed time differences.

During summer sailing in the domains of the Loran-C chains 9960, 5930, 7930, and 7970 during the past four years, the author has used this method for coordinate conversion with programmable hand-calculators and a conventional Loran-C receiver. The practical results have been extremely satisfactory.

REFERENCES

1. S. Razin, "Explicit (noniterative) Loran solution," Journal of the Institute of Navigation, Vol. 14, No. 3, pp. 265-269, Fall 1967.
2. H. Fell, "Comments on Loran Conversion Algorithms," Journal of the Institute of Navigation, Vol. 22, No. 2, pp. 184-5, Summer 1975.
3. J. N. Newman, "Loran Navigation with a Hand Calculator," Proceedings of the New England Sailing Yacht Symposium, New London, Connecticut, January 1979, pp. 6-1 - 6-13, Society of Naval Architects and Marine Engineers.

TABLE 1
EXPLANATION OF CONSTANTS

Figure 1	Reference 1	Table 2
$R/\tilde{V}$	$r_c/.9994v$	R/V
θ_{Mi}	θ_{mi}	HMi
c_{01}	c_{10}	CØ1
c_{02}	c_{11}	CØ2
c_{03}	$c_{12}(c_{14})^2$	CØ3
K	K	K
c_{M1}	c_5	CM1
c_{11}	c_4	C11
c_{21}	c_6	C21
c_{M2}	c_2	CM2
c_{12}	c_1	C12
c_{22}	c_3	C22
c_{M3}	$c_8(c_{14})^2$	CM3
c_{13}	$c_7(c_{14})^2$	C13
c_{23}	$c_9(c_{14})^2$	C23

TABLE 2
CONSTANTS FOR SIMPLIFIED RAZIN ALGORITHM

RATE 4990		RATE 5930		RATE 5990		RATE 7960	
LAM	16.444395	LAM	46.482720	LAM	51.575878	LAM	63.194281
LOM	169.303120	LOM	67.553771	LOM	122.220224	LOM	142.483190
LA1	20.144916	LA1	41.151193	LA1	55.262085	LA1	57.262021
LO1	155.530970	LO1	69.583909	LO1	131.151965	LO1	152.221122
LA2	28.234177	LA2	46.463211	LA2	47.034799	LA2	55.262085
LO2	178.173020	LO2	53.102816	LO2	119.443953	LO2	131.151965
R/V	370.6300825	R/V	371.7468694	R/V	371.9689375	R/V	372.4148585
HM1	13.4157155	HM1	5.7354504	HM1	6.3011854	HM1	7.5310805
HM2	14.1741647	HM2	10.1014724	HM2	5.1821943	HM2	9.8045273
C01	-0.0010529	C01	-0.0037634	C01	-0.0043014	C01	-0.0054158
C02	-0.0029050	C02	0.0004057	C02	-0.0004217	C02	-0.0002427
C03	0.0005380	C03	0.0010005	C03	0.0006653	C03	0.0001842
1,2		1,2		1,2		1,2	
K	106.2252138	K	110.8447572	K	147.1040331	K	84.8906440
CM1	-1.8795466	CM1	-5.0903149	CM1	0.7877535	CM1	-3.4857234
C11	3.5551112	C11	6.8387882	C11	-4.5721238	C11	-1.7830103
C21	-1.4482802	C21	-1.0969568	C21	4.2947027	C21	5.6065737
CM2	-3.1807195	CM2	-9.3496889	CM2	32.4561275	CM2	6.9234360
C12	1.3824553	C12	3.8224662	C12	-15.7408070	C12	-7.0876561
C22	0.9224874	C22	5.8949444	C22	-17.2106027	C22	-0.2582741
CM3	-5.8254080	CM3	9.1600559	CM3	14.4372377	CM3	4.9813338
C13	2.3823499	C13	-7.3475088	C13	-3.5949470	C13	-2.3102823
C23	3.9173921	C23	-1.1329186	C23	-10.1123860	C23	-1.8179143

RATE 7930

				1,2		1,3		2,3	
LAM	59.591727	R/V	372.2928549	K	12.0118394	K	148.9385874	K	136.9267476
LOM	45.102747	HM1	10.9274319	CM1	6.0269455	CM1	3.7547087	CM1	0.5180708
LA1	64.542658	HM2	18.2752825	C11	-7.0638328	C11	-4.1502249	C11	-1.8954569
LO1	23.552175	HM3	14.0008156	C21	1.3306792	C21	0.6956864	C21	1.6866416
LA2	62.175968	C01	-0.0051061	CM2	8.1260427	CM2	-15.6773687	CM2	-8.5617768
LO2	7.042671	C02	0.0002971	C12	-21.3981937	C12	9.1240689	C12	4.1670703
LA3	46.463218	C03	0.0002989	C22	13.9398787	C22	7.2878447	C22	5.1092776
LO3	53.102816			CM3	-4.6543822	CM3	6.0408455	CM3	4.4587907
				C13	11.6854955	C13	-2.0286122	C13	-0.9264912
				C23	-6.2633954	C23	-3.2745373	C23	-2.7901626

TABLE 2 - continued

RATE 7990

				1,2		1,3		2,3	
LAM	38.522061	R/V	371.4033836	K	153.6138620	K	65.1599398	K	141.2261959
LOM	16.430596	HM1	4.7286374	CM1	-23.7005429	CM1	7.2469359	CM1	2.1783021
LA1	35.312088	HM2	8.8138711	C11	12.4742953	C11	-2.4432171	C11	1.9047829
LO1	12.312996	HM3	10.7695575	C21	11.6300030	C21	-4.6703332	C21	-3.9054176
LA2	40.582095	C01	-0.0029491	CM2	-15.9660319	CM2	-6.7410634	CM2	11.6906420
LO2	27.520152	C02	0.0015214	C12	13.3312565	C12	8.8845749	C12	-6.9265994
LA3	42.033649	C03	0.0004570	C22	3.4667254	C22	-1.3921546	C22	-4.1737126
LO3	3.121590			CM3	29.2160194	CM3	7.0635924	CM3	-13.1617034
				C13	-20.4271958	C13	-9.7491335	C13	7.6006272
				C23	-8.3248394	C23	3.3430579	C23	6.3952895

RATE 8970

				1,2		1,3		2,3	
LAM	39.510754	R/V	371.4451889	K	100.2856569	K	165.0775291	K	94.6368113
LOM	87.291214	HM1	9.0332384	CM1	-1.6374444	CM1	-11.4653647	CM1	6.2404101
LA1	30.593874	HM2	8.5134292	C11	3.7017497	C11	8.3198219	C11	-2.2796717
LO1	85.100930	HM3	10.1063374	C21	-1.2653743	C21	4.0789832	C21	-3.2696272
LA2	42.425060	C01	-0.0030473	CM2	-9.2061973	CM2	42.4134769	CM2	-3.4593612
LO2	76.493382	C02	0.0000668	C12	2.7003988	C12	-21.5553314	C12	5.9062657
LA3	48.364980	C03	0.0015217	C22	6.6461881	C22	-21.4242459	C22	-2.3851687
LO3	94.331850			CM3	4.0309640	CM3	13.1428670	CM3	-5.7652773
				C13	-4.6031865	C13	-8.8848071	C13	2.4344804
				C23	1.1731849	C23	-3.7818071	C23	4.0658351

RATE 9940

				1,2		1,3		2,3	
LAM	39.330662	R/V	371.4323460	K	99.1785204	K	146.3084021	K	114.5130823
LOM	118.495637	HM1	7.5307133	CM1	14.2591470	CM1	-8.1891556	CM1	-6.4614473
LA1	47.034799	HM2	2.9473545	C11	-5.0824048	C11	0.4237771	C11	-0.6585361
LO1	119.443953	HM3	5.2972135	C21	-8.5564321	C21	8.4807187	C21	7.8280098
LA2	38.465699	C01	-0.0030171	CM2	16.6382058	CM2	-29.8004300	CM2	19.3818756
LO2	122.294453	C02	-0.0007442	C12	0.6729749	C12	12.0635722	C12	-18.7464089
LA3	35.191818	C03	0.0013518	C22	-17.7006272	C22	17.5439995	C22	-1.0365279
LO3	114.481743			CM3	-3.8653197	CM3	-7.1925790	CM3	19.8752781
				C13	5.8231596	C13	6.6392790	C13	-10.3172292
				C23	-1.2682237	C23	1.2570015	C23	-8.9689335

RATE 9990

				1,2		1,3		2,3	
LAM	57.090988	R/V	372.1826256	K	117.3219797	K	171.7720060	K	70.9060144
LOM	170.145981	HM1	10.4128995	CM1	9.5373921	CM1	-28.9809133	CM1	-3.9266252
LA1	52.494505	HM2	8.2468129	C11	-6.1985995	C11	11.5345587	C11	-2.2011378
LO1	-173.105231	HM3	9.6465934	C21	-3.3840155	C21	17.9824455	C21	6.2857375
LA2	65.144012	C01	-0.0048295	CM2	-6.1221377	CM2	59.8940969	CM2	-6.4584755
LO2	166.531447	C02	-0.0005297	C12	-0.1548441	C12	-30.5475708	C12	5.8293877
LA3	57.262021	C03	0.0000910	C22	5.7998388	C22	-30.8199785	C22	0.1570208
LO3	152.221122			CM3	-3.7732464	CM3	42.7557284	CM3	-2.5066677
				C13	0.5831108	C13	-20.8380203	C13	3.9765158
				C23	4.0877908	C23	-21.7222628	C23	-0.5913080

TABLE 2 - continued

RATE 7970

LAM	62.175968	R/V	372.3782880
LOM	7.042671	HM1	10.8714334
LA1	68.380615	HM2	10.9185521
LO1	-14.274700	HM3	7.9079641
LA2	54.482980	HM4	8.6378010
LO2	-8.173633	C01	-0.0053226
LA3	64.542658	C02	0.0003358
LO3	23.552175	C03	0.0000417
LA4	70.545261		
LO4	8.435869		

	1,2	1,3	2,3	1,4	2,4	3,4
K	81.0162340	108.6206312	170.3631335	48.8362980	129.8525321	59.7843329
CM1	6.8757379	-1.6882818	-45.7304550	1.5192399	12.5755800	-4.1238497
C11	-3.6209269	-3.0314585	17.0876397	-7.0237384	-6.8583782	8.3883494
C21	-3.3226990	4.7679223	29.2879099	5.4980508	-5.8504682	-4.1748358
CM2	0.0851613	9.8721950	-49.5087566	6.2066122	5.4586255	6.5883802
C12	-3.4135896	-4.0872391	23.0388337	0.4751720	0.4639850	-0.5674910
C22	3.7972083	-5.4488216	27.6108595	-6.2832187	-5.5154654	-5.6288258
CM3	0.6448248	-3.9312995	30.0825230	-2.2173826	-2.5447280	-2.0503075
C13	2.0262206	2.3411990	-13.1968044	0.2079520	0.2030562	-0.2483541
C23	-1.7754611	2.5477061	-16.3891095	2.9378452	3.2738411	3.2242306

RATE 7980

LAM	30.593874	R/V	371.0828441
LOM	85.100930	HM1	4.8770765
LA1	30.433202	HM2	11.9744164
LO1	90.494360	HM3	5.9343242
LA2	26.315501	HM4	6.8527846
LO2	97.500009	C01	-0.0021969
LA3	27.015849	C02	0.0001785
LO3	80.065352	C03	0.0021125
LA4	34.034604		
LO4	77.544676		

	1,2	1,3	2,3	1,4	2,4	3,4
K	16.9564937	137.8385921	120.8820948	153.2450182	170.2015122	68.9163957
CM1	11.0570777	-14.2314671	-6.7387332	20.9894138	34.6969856	0.5847478
C11	-18.5216425	7.7983373	2.4992707	-10.7397517	-11.6414199	4.2609778
C21	8.4352282	7.3549546	5.1757577	-9.5022552	-22.6162743	-3.9972724
CM2	13.3510664	9.7447265	-0.5885424	14.7674934	31.8684056	-10.6883938
C12	-14.5081587	-10.7547283	-3.4467575	-13.3984015	-14.5232796	5.3157925
C22	1.2029281	1.0488728	4.0542147	-1.3550943	-17.7155183	5.5126595
CM3	-18.3938125	24.3453533	13.2913257	-35.1800595	-60.4842659	2.4869968
C13	32.9774690	-11.5048843	-3.6871732	19.8256042	21.4900855	-7.8657740
C23	-14.2560444	-12.4303168	-9.2153485	16.0593844	40.2678911	5.8971745

TABLE 2 - continued

RATE 9960

LAM	42.425060	R/V	371.5686802
LOM	76.493386	HM1	7.5286946
LA1	46.482720	HM2	5.3023251
LO1	67.553771	HM3	8.6710588
LA2	41.151193	HM4	8.5105943
LO2	69.583909	C01	-0.0033387
LA3	34.034604	C02	0.0003044
LO3	77.544676	C03	0.0013003
LA4	39.510754		
LO4	87.291214		

	1,2	1,3	2,3
K	49.5711924	131.9192424	82.3480505
CM1	1.9521836	-1.2153953	-2.1720626
C11	-6.9744937	-1.6178157	-1.7221081
C21	5.7019963	3.5755439	4.6554241
CM2	-10.4811933	-15.9816801	-10.0102611
C12	0.7963911	10.0982389	10.7492218
C22	9.9014913	6.2089162	-0.5315853
CM3	2.0161977	6.7464013	6.2781129
C13	7.2073049	-0.7919203	-0.8429714
C23	-8.5148952	-5.3394250	-4.8108240

	1,4	2,4	3,4
K	160.0843602	150.3444456	67.9963970
CM1	21.2899587	-21.1359989	-4.4667539
C11	-12.8160618	12.5098494	4.0921043
C21	-7.9565816	9.4996972	1.1494909
CM2	23.0987676	-7.8448407	4.3129658
C12	-9.3474660	9.1241283	2.9845991
C22	-13.8165688	-1.0847346	-7.1750040
CM3	-26.8612551	25.8750726	5.1548623
C13	15.9306254	-15.5499971	-5.0865689
C23	11.8817087	-9.8168007	0.5626754

RATE 9970

LAM	24.480410	R/V	370.8609516
LOM	141.192900	HM1	11.5516250
LA1	24.170770	HM2	18.0267880
LO1	153.585150	HM3	12.0348907
LA2	42.443700	HM4	15.4967044
LO2	143.430906	C01	-0.0016638
LA3	26.362499	C02	-0.0019652
LO3	128.085621	C03	0.0015730
LA4	9.324566		
LO4	138.095523		

	1,2	1,3	2,3
K	84.1904970	168.4703117	84.2798176
CM1	5.0647896	16.7644727	-1.7004334
C11	-3.7683282	-10.2852230	-1.3369308
C21	-0.8471024	-6.2578526	3.6185397
CM2	1.4947638	-13.2440158	-4.4023053
C12	-3.2847538	4.9249622	0.6401741
C22	1.0671448	7.8833853	3.1541871
CM3	-1.9530746	-42.9507808	-2.7727232
C13	-0.4565563	22.3797662	2.9090472
C23	2.9683930	21.9285940	0.4384085

	1,4	2,4	3,4
K	101.8630723	173.9464292	89.6666125
CM1	3.1599096	-45.8203476	-4.2518639
C11	-3.6272612	21.7815800	3.4092815
C21	0.9974106	26.6438694	1.5408004
CM2	3.8944533	-42.8604886	-3.1805818
C12	-3.4624642	20.7919796	3.2543880
C22	-1.2564968	23.2247689	-0.7377948
CM3	4.7219532	-8.1181240	2.7789715
C13	-0.9508793	5.7099979	0.8937364
C23	-3.4950985	3.2280697	-3.3526499

TABLE 3
TEST RESULTS

RATE 7930

TD1	15831.26	TD2	29430.01	LAT	50.0025	LON	30.0014
TD1	15831.26	TD3	49135.88	LAT	49.9998	LON	30.0005
TD2	29430.01	TD3	49135.88	LAT	50.0001	LON	30.0015

RATE 7990

TD1	13007.12	TD2	32279.05	LAT	29.9995	LON	24.9999
TD1	13834.59	TD3	50997.27	LAT	46.9994	LON	13.0000
TD2	33650.21	TD3	50997.27	LAT	46.9996	LON	13.0001

RATE 8970

TD1	17518.44	TD2	31485.52	LAT	45.0002	LON	85.0002
TD1	14904.98	TD3	49948.65	LAT	34.9998	LON	94.9998
TD2	31485.52	TD3	48503.41	LAT	45.0000	LON	85.0001

RATE 9940

TD1	13120.35	TD2	29008.91	LAT	45.0001	LON	113.0003
TD1	13120.35	TD3	43011.89	LAT	45.0002	LON	112.9998
TD2	27766.14	TD3	41769.16	LAT	33.9995	LON	121.0003

RATE 9990

TD1	16390.99	TD2	31947.03	LAT	62.0001	LON	177.9996
TD1	17669.03	TD3	46335.56	LAT	50.0008	LON	160.0002
TD2	34407.66	TD3	46335.56	LAT	49.9991	LON	160.0000

RATE 7970

TD1	14752.31	TD2	31674.07	LAT	65.0001	LON	-4.9998
TD1	17399.41	TD3	49002.57	LAT	65.9999	LON	13.0002
TD2	31200.34	TD3	50659.13	LAT	55.0002	LON	9.9997
TD1	14752.31	TD4	63894.58	LAT	65.0001	LON	-4.9998
TD2	31674.07	TD4	63894.58	LAT	65.0001	LON	-4.9998
TD3	49002.57	TD4	63457.42	LAT	66.0000	LON	13.0000

RATE 7980

TD1	12462.28	TD2	27905.77	LAT	25.0007	LON	89.0001
TD1	12462.28	TD3	45715.16	LAT	24.9996	LON	89.0002
TD2	27905.77	TD3	45715.16	LAT	25.0000	LON	88.9997
TD1	13121.64	TD4	62205.36	LAT	37.0002	LON	87.0001
TD2	30314.04	TD4	62205.36	LAT	36.9995	LON	86.9993
TD3	47185.84	TD4	62205.36	LAT	37.0004	LON	87.0004

RATE 9960

TD1	13768.21	TD2	25351.39	LAT	42.0002	LON	70.0001
TD1	15534.93	TD3	41563.46	LAT	36.9999	LON	74.0002
TD2	26660.96	TD3	41563.46	LAT	36.9998	LON	73.9999
TD1	16552.32	TD4	58499.82	LAT	42.0000	LON	80.0000
TD2	26660.96	TD4	58962.67	LAT	37.0001	LON	73.9998
TD3	44313.52	TD4	58499.82	LAT	41.9998	LON	79.9999

RATE 9970

TD1	14532.45	TD2	37185.33	LAT	32.0006	LON	149.9997
TD1	14532.45	TD3	62922.30	LAT	31.9980	LON	149.9991
TD2	41924.77	TD3	61552.78	LAT	26.0006	LON	138.0005
TD1	17418.31	TD4	84416.83	LAT	21.9995	LON	143.9994
TD2	41924.77	TD4	85626.07	LAT	26.0001	LON	137.9993
TD3	61552.78	TD4	85626.07	LAT	25.9991	LON	138.0001

RATE 4990

TD1	16129.72	TD2	35412.75	LAT	25.0000	LON	165.0006

RATE 5930

TD1	13597.15	TD2	30301.86	LAT	43.9999	LON	64.0002

RATE 5990

TD1	13776.83	TD2	29181.77	LAT	47.9997	LON	130.0003

RATE 7960

TD1	13374.70	TD2	28372.20	LAT	54.9998	LON	140.0001

LORAN-C LATITUDE-LONGITUDE CONVERSION AT SEA: PROGRAMMING CONSIDERATIONS

James R. McCullough
Woods Hole Oceanographic Institution
Woods Hole, Massachusetts 02543

Barry J. Irwin
U. S. Geological Survey
Woods Hole, Massachusetts 02543

Robert M. Bowles
U.S. Geological Survey
Woods Hole, Massachusetts 02543

ABSTRACT

To aid programmers of LORAN-C latitude-longitude conversion, we:

1. Provide reference to the literature.

2. Compare digital "processings-noise" for several arc-length methods.

3. Discuss some practical aspects of overland signal propagation (ASF) modeling for offshore navigation.

Comparisons are made of the precision of arc-length routines as computer precision is reduced. Overland propagation delays (ASF's) are discussed and illustrated with observations from offshore New England. Present practice of LORAN-C error budget modeling is then reviewed with the suggestion that additional terms be considered in future modeling. Finally, some detailed numeric examples are provided to help with new computer program checkout.

INTRODUCTION

LORAN-C is a pulsed, 100-kHz, ground-wave, hyperbolic navigation aid with extensive world coverage. Its accuracy is conservatively rated at 1/4 nautical mile (500 m) over a range of about 800 nautical miles. Repeatability (a measure of the resolution and stability of the LORAN observation) is more nearly 20-100 m. The accuracy with which latitude and longitude can be determined can approach this level via calibrated radio propagation models. Such model techniques are currently under study at the United States Coast Guard (USCG) and the Defense Mapping Agency/Hydrographic Topographic Center (DMA).

Until 1981, DMA LORAN error model coefficients and results were classified. Their declassification, together with the recent evolution of microprocessors, has generated renewed interest in LORAN calibration, particularly for harbor navigation and offshore survey applications. For offshore survey work in good LORAN coverage, an order of magnitude improvement in positional accuracy is feasible with no change in present equipment. Technically, the calibration process requires detailed error models and field calibration data. Practically, calibration requires organization, funding, and motivation.

But why calibrate LORAN when world coverage with the Navstar Global Positioning System (GPS) is nearly here? We propose to calibrate and pace. That is, to use GPS now to help calibrate and improve LORAN, and to use LORAN in the future to pace GPS.

This paper presents results of studies conducted by the U.S. Geological Survey at Woods Hole, Mass. In it, we evaluate several arc-length methods, discuss LORAN propagation model parameters, and compare present model predictions with offshore observations. We have included some details that were initially puzzling or not readily available during our learning process; we hope they will be of interest to others. Our intent is to provide a tutorial overview and entry to the literature for readers familiar with basic LORAN technology. Excellent LORAN primers, histories, and reviews include Bigelow (1965), Canadian Coast Guard Primer (1981), Grant (1973), Hefley (1972), U.S. Coast Guard Handbook (1980), and Weseman (1982b).

BACKGROUND

Overview

The LORAN latitude/longitude conversion process has three parts. It is necessary to find:

1) Arc-length (the distance between two points on the Earth ellipsoid);

2) Distance to time conversion (the radio travel-time for a given arc-length); and

3) Time Difference (TD) to latitude/longitude conversion (the latitude and longitude of a given TD pair having solved for items 1 and 2).

The last step is implemented as an iterative solution or in closed form (Collins, 1980; Fell, 1975; Razin, 1967: and Stuifbergen, 1980). Its somewhat involved processing details are well documented in the literature and are, therefore, not covered here. This paper discusses steps 1 and 2, with emphasis on the distance to time conversion which now represents the largest single error source in LORAN surveying.

Arc-length Methods

Numerous arc-length methods have been developed. Appendix A compares results calculated with the Sodano (1965), Collins (1980), Lambert (1942), and Thomas (1970) methods using different computer precision. The Sodano method is the least sensitive to reduced precision. Example code and test problems give distance, forward azimuth, backward azimuth and the RTCM SALT-model travel time. (RTCM in this paper stands for the now defunct Radio Technical Commission for Marine Services, a cooperative government and industrial advisory commission. The present RTCM or Radio Technical Commission for Maritime Services continues the earlier work without direct government affiliation).

The RTCM (1981) method is somewhat harder to program than the original Sodano (1965) method. With the latter, longitude (positive east) can be entered directly and the azimuths require no additional testing when returned with a four-quadrant tangent solution.

Length and Time

Given an arc-length, d, in meters, it is desired to find the LORAN travel-time, t, in microseconds. The technique used by DMA and the USCG is described in the section on propagation below. Their method is reduced to three terms called the primary-phase factor (PF), the secondary-phase factor (SF), and the additional secondary-phase factor (ASF). The total phase ϕ_T is:

$$\phi_T = PF + SF + ASF$$

and

$$t = \frac{\phi_T}{2\pi f} \times 10^6 \quad \mu sec$$

$$= 5\phi_T/\pi$$

where f = 100,000 Hz is the LORAN center-frequency, and t is the desired propagation time. The travel-time code can be programmed on a pocket calculator, such as the HP-41CV, (i.e. Newman, 1980; and Newman, in this Proceedings). The travel-time of the PF (t_{PF}) equals the arc-distance, d, divided by the mean speed, $\overline{C}$, of LORAN waves in homogenous air with no earth effects, i.e.,

$$t_{PF} = d/\overline{C}$$

where $\overline{C} = C_0/n$, C_0 equals the speed of light in free-space, and n is a nominal index of refraction of air. The travel time of the SF term (t_{SF}), is found from polynomial approximations of the nominal salt-water conditions tabulated in Johler et al. (1956). Finally, the travel time of the ASF term (t_{ASF}), is tabulated by DMA from detailed geographical, geological, theoretical, and observational data. Thus, the total travel-time, t, is:

$$t = t_{PF} + t_{SF} + t_{ASF}$$

The primary and secondary terms are fixed by definitions discussed below. The ASF term is usually relatively small and accounts for the additional travel-time due to planetary boundary conditions other than those of the standard salt-water model used in the SF calculation.

Other conditions related to LORAN chain timing, (weather effects, seasons, climate, pulse shape, skywave, noise, etc.), are generally not modeled by DMA but are partially compensated by active steering of the LORAN chain timing.

Fixed Coefficient Model (Present status)

The DMA LORAN propagation model, RTCM (1981), has a fixed structure with fixed coefficients. It provides a much needed community-wide standard of sufficient accuracy for most needs. It makes a one-time adjustment to local conditions at the time of calibration. Obviously, a simplified model with fixed coefficients cannot be optimal for all places and conditions.

The following constants have been selected by DMA and the USCG for use in their computations:

$C_o = 2.99792458 \times 10^8$	m/sec	Speed of light (IUGG-75)
$n = 1.000338$	-	Index of refraction
Sigma = 5.0	mho/m	Conductivity of seawater
$e_2 = 80$	esu	Permittivity of seawater
$h_1 = h_2 = 0$	m	Altitude of transmitter/receiver
Alpha = .75	-	Index of refraction profile factor
$f = 100{,}000$	Hz	LORAN center frequency
$a = 6378135$	m	Earth radius (WGS-72)
$f_1 = 1/298.26$	-	Earth flattening (WGS-72)

Unfortunately, the model assumptions and travel-time sensitivity of each of these nominal values are not readily available. We have indicated a few error estimates in parts per million (ppm) below. (The ppm values are equivalent to 1 m at 10^6 m or about 540 nautical miles, a reasonable outer working range for good coverage. Some errors are not linearly range-dependent, so the ppm values are only intended to indicate the relative importance of parametric variations.)

Variable Coefficient Models

Propagation models which adapt their coefficients to space-time variations and which model many error terms could be applied to LORAN as they have been applied in Transit Satellite and GPS navigation. Although such models lose the attractive features of simplicity, they should allow greater accuracy where required. The information rate required for adaptive LORAN models is low, a few bits per hour. This input might come from special seasonal charts, local weather observations, or fixed-site "Local Area Monitors" (LAM's) functioning like the present "System Area Monitors" (SAM's) but with local feedback. Ultimately, the LAM correction vectors might be transmitted with the LORAN message. Harbor navigation research is currently studying LAM or differential LORAN techniques.

Calibration and Control

The latitude and longitude of the transmitters and SAM's are determined from Transit Satellite surveys and converted to WGS-72 coordinates. An atomic "Hot Clock" is then flown between Master and Secondary transmitters and used to directly measure the Emission Delay (ED), the time between the Master and Secondary transmissions. While the ED calibration is being made, the time difference (TD) at the SAM is also measured. This Controlling Standard Time Difference (CSTD) is used for routine control of the Secondary's transmission time relative to that of the Master. The latitudes, longitudes, nominal ED's and CSTD's are published (USCG,1981) and updated periodically. Corrections to the Secondary's timing, the Local Phase Adjustments (LPA's), are made in 20-nsec steps at 7.5-minute intervals. Timing control at the Secondary is such that only about one LPA per hour is required under normal conditions. Note that the LPA's attempt to maintain constant CSTD, not constant ED. The LPA's primarily track propagation variation; clock and transmitter changes are generally smaller and of longer period.

Steering the secondary in order to hold a constant TD at the SAM has several important consequences. First and foremost, it works rather well. Variations in the primary service area of 9960, for example, are typically less than 100 nsec (USCG, 1982). Second, the ED is not constant. Uniform changes in propagation speed are fully compensated along the locus of positions that are roughly the same land-length difference from the transmitters as the SAM. Third, stations at increasing distance from this SAM locus show increasing errors. Finally, the nonuniform components of propagation variations caused by local weather patterns, etc., are reflected in a complex manner throughout the service area. The USCG has recently established TD monitors at about 20 sites in the United States to routinely observe such variation. These observations (USCG, 1982) will hopefully lead to practical error models and/or real-time corrections for propagation variations. The SAM errors are the next largest term in the LORAN error budget after the ASF's.

Pulse Geometry

The ground-wave component of the hemispherically expanding LORAN pulse shell can be visualized as a cylindrical ring spreading over the curved earth. The ring has a width of about 50 km, a height of only a few kilometers, and grows at nearly the speed of light to a useful diameter of 3000 km or more while it's strength decreases rapidly with distance. We are interested in one particular electric field surface near the outer edge of the ring, the surface associated with the zero-crossing of the end of the third cycle. Its noise-limited width is only about 3-30 m.

The pulse phase-surfaces tilt slightly forward and increase in signal strength with altitude over land. The forward tilt produces a small radial component of the electric field in the ground which acts as a "lossy" dielectric, slowing and attenuating the wave. As the pulse moves out to sea, the surface losses are abruptly reduced by several orders of magnitude, exciting higher order propagation modes and allowing energy from modes aloft to advance the near-surface wave-front. The rapid advance at the surface actually reduces the accumulating phase lag and is thus called a "phase recovery." This effect is seen in the model predictions of Figure 1. The correction (bottom curve) grows rapidly at first and drops abruptly at the first conductivity boundary near the Hudson River. Before this recovery is complete, the error curve drops abruptly again at the shore at Weekapaug, R.I. The first phase recovery is undoubtedly a model artifact, but the second is quite real, as will be illustrated by the observational data in Fig. 7 below.

A similar sky wave arrives later than the ground wave via the ionosphere. The sky-wave delay and relative amplitude increase at night when the ionosphere is higher. By sampling early in the pulse at the end of the third cycle, most of the sky-wave interference is removed even when the sky wave is considerably stronger than the earlier arriving ground wave.

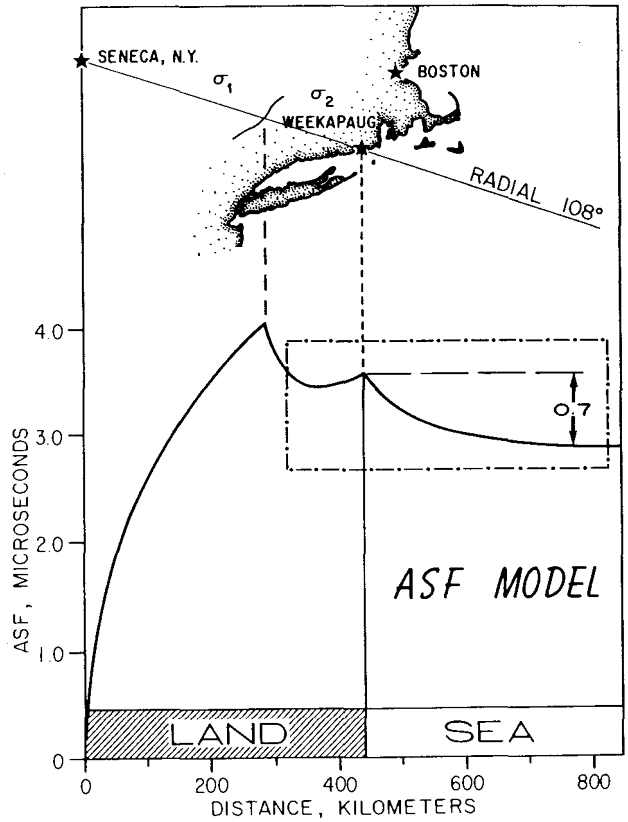

Figure 1. Range ASF model predictions along radial 108° from the 9960-MASTER at Seneca, NY. Phase-recovery is seen in the model at the conductivity changes near the Hudson River and at the shore near Weekapaug, RI.

PROPAGATION PREDICTION

The Van der Pol-Bremmer Propagation Method

The LORAN propagation prediction method used by DMA and the USCG is described by Van Der Pol and Bremmer (1937, 1938 and 1939) and Bremmer (1949 and 1958). It has been numerically tabulated by Johler et al. (1956), Brunavs (1976 and 1977), and Brunavs and Wells (1971a). The model assumes a smooth, spherical earth of finite conductivity, dielectric constant, and permeability with an electric point source near the earth's surface. Both the model and its numeric evaluation presented formidable problems for nearly half a century. It is now one of many models available (Hufford, 1952; Johler, 1970; Samaddar, 1979; and Wait, 1981).

The Van der Pol-Bremmer method assumes continuous wave (CW) propagation at a single frequency with no skywave interference. The phase of the far field wave, Ø, is

$$\phi = K_1 d + \phi_c \tag{1}$$

where the wave number K_1 is

$$K_1 = \frac{\omega n}{C_o} = \frac{2\pi}{\lambda}$$

and

$$\omega = 2\pi f \text{ and } \lambda = \text{wavelength} = 3 \text{ km}$$

The first term ($K_1 d$) accounts for propagation through the air and $Ø_c$ treats the effects of refraction, diffraction, modal propagation, boundary conditions, and initial conditions as seen in the far field.

$$\phi_c = \arg\left[\sum_{s=0}^{\infty} \frac{1}{2\tau_s - 1/\delta^2} \exp\left\{i\left[(K_1 a)^{1/3} \tau_s \alpha^{2/3} \frac{d}{a} + \frac{\alpha d}{2a} + \frac{\pi}{4}\right]\right\}\right] \tag{2}$$

and the time t_c associated with $Ø_c$ is found from

$$t_c = \frac{\phi_c}{\omega} \times 10^6 \ \mu\text{sec} \tag{3}$$

Where a = earth radius, d = distance from the transmitter; α and δ are discussed below. The factors τ_s are solutions to Riccati's differential equation (Howe, 1960; and Johler et al., 1959),

$$\frac{d\delta}{d\tau_s} - 2\delta^2 \tau_s + 1 = 0 \tag{4}$$

where δ is a frequency dependent conductivity and permittivity parameter for a vertical electric dipole,

$$\delta = \frac{i(K_2/K_1)^2 \alpha^{1/3}}{(K_1 a)^{1/3}((K_2/K_1)^2 - 1)^{1/2}} \tag{5}$$

where the earth wave number K_2 is

$$K_2 = \frac{\omega}{C_0}\left[\epsilon_2 + i\frac{\sigma \mu_0 C_0^{\ 2}}{\omega}\right]^{1/2} \tag{6}$$

Given d, the coefficients needed to solve for ϕ_c from equations 2-6 are: w, μ_o, C_o, a, n, α, ϵ_2 and σ. As the first four are known, ϕ_c is a function of the atmospheric parameters n and α and the earth effective impedence factors ϵ_2 and σ ie.,

$$\phi_c = f(n, \alpha, \varepsilon_2, \sigma) \tag{7}$$

Note that ϕ and therefore the scale and, to some extent, the rotation of the LORAN grid is a function of n, α, ϵ_2, and σ. Thus the selection of the air parameters n and α are critical and should be made independently of the earth boundary conditions treated by τ_s. From equation (1) it is seen that the primary factor time t_{PF}, $= \phi c/w$ is.

$$t_{PF} = K_1 d/\omega = nd/C_o$$

is not frequency dependent but the secondary factor time, t_{SF}, is.

Brunavs (1977) gives two polynomial approximations for t_c (Equation 3) and calculates their errors compared with direct solutions. Samaddar (1979, 1980) reviews the theory treated extensively in Watson (1918), Van der Pol and Bremmer (1937, 1938, 1939), Bremmer (1949, 1958), Johler et al. (1956), and Johler (1962). Wait (1964, 1981), and Fock (1965) provide modern perspective and entry to the extensive literature on this and other model approaches. The older Van der Pol-Bremmer method is outlined here because of its historic significance and its use by DMA and the USCG. With modern computers, it offers little advantage over the more flexible and direct numeric integration methods.

Sea Water Effects

Fortunately, sea-water variations have little effect on LORAN propagation. The skin depth (depth at which the signal is attenuated by 1/e., Terman, 1943) of the waves is about 75 cm. Although the temperature and salinity of sea water vary considerably near the ocean surface, associated conductivity changes produce only small propagation variations.

To illustrate this, the lower half of Figure 2 shows the variation of conductivity with temperature and salinity together with broad outlines of various near-surface water types. The upper half of the figure gives the error in meters relative to σ = 5 as a function of range. As seen, errors of only a few meters or so in the range estimates are expected from this source. The effect of ocean surface

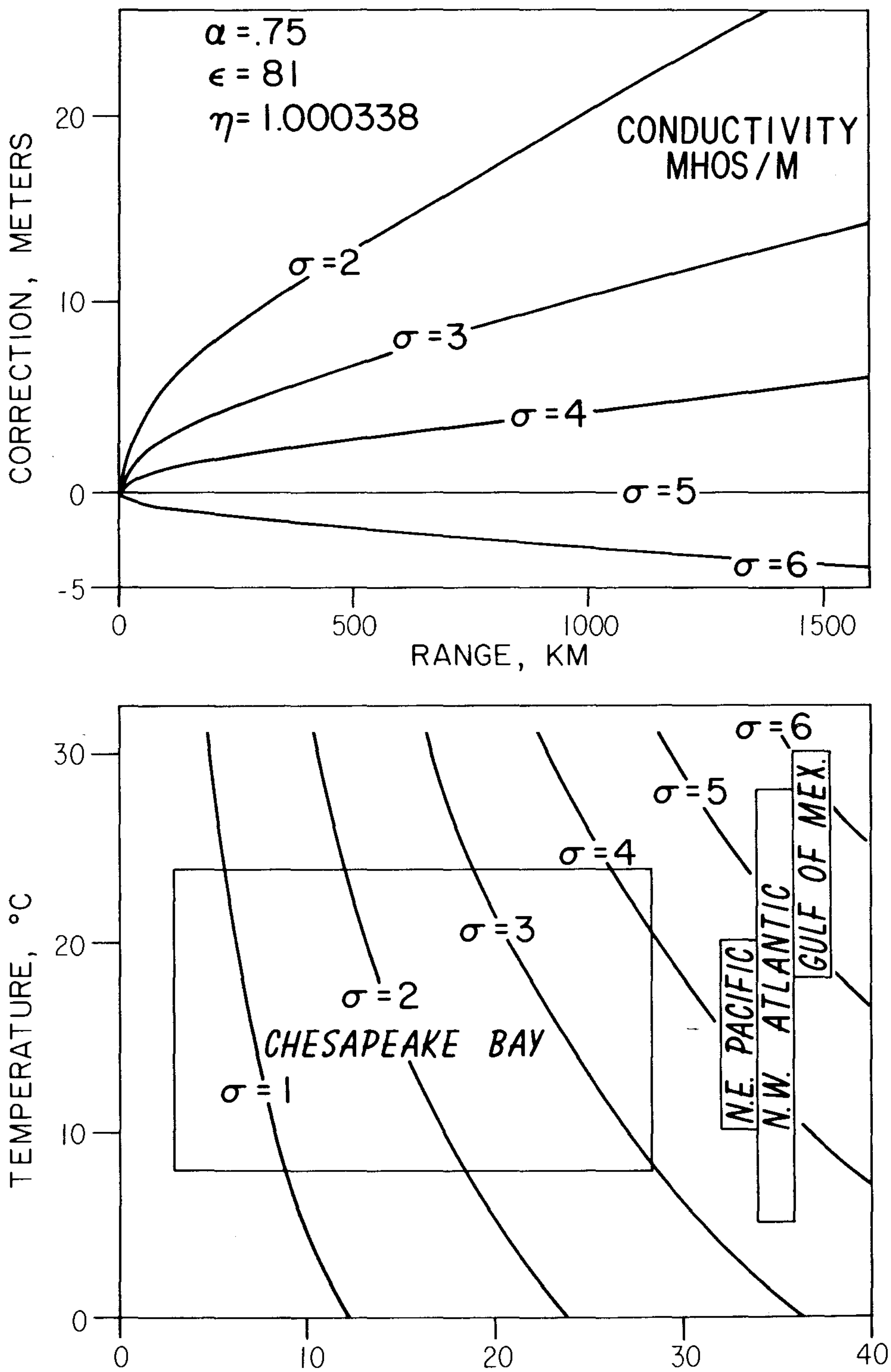

Figure 2. Relationship between salinity, temperature and conductivity (bottom) for sample near-surface ocean conditions (blocks at bottom). The range of conductivity shown can then be translated (top) to range errors in meters relative to the "standard" conductivity of 5 mhos/meter.

waves on LORAN timing has not, to our knowledge, been evaluated, but is expected to be small (Wait, 1969, 1971).

Speed of Light in Free-Space

The speed of light (C_0) in free-space adopted by the International Union of Geodesy and Geophysics, IUGG (1975), and by the USCG (1980) for LORAN is given above in Table 1. Note that this is not the same value used by Johler et al. (1956) which is 8.81 ppm faster. The change in C_0 is equivalent to a change in the nominal index of refraction discussed next.

Index of Refraction, n, and Refractivity, N.

The index of refraction (n) of radio waves in a medium is the ratio of the phase speed in free-space, C_0, to that in the medium C.

$$n = \frac{C_0}{C} \tag{8}$$

Because n in air typically has values ranging from 1.000250 to 1.000450, it is convenient to define the refractivity (N) as

$$N = (n-1) \times 10^6$$

Thus N for air is in the range 250-450.

Some representative values of N (Bean and Dutton, 1966) are:

	$\bar{N}$ Feb	$\bar{N}$ Aug	σ_N Feb	σ_N Aug
Denver	245	277	4	15
Boston	309	350	5	15
Miami	330	380	14	6

Here $\bar{N}$ is the monthly mean value of 8 years and σ_N is the standard deviation of the monthly means. On the U.S. East Coast, the extremes of the monthly mean values of N are about 50 N-units. Extensive tables and charts of many aspects of N-meteorology are also given by Bean and Dutton (1966).

Figure 3 illustrates the data given in Table 1. Three values for the speed of light in vacuum from the 1940s, 1956, and 1975 are shown at the top. Various estimates of the effective speed $\bar{C}$ of radio propagation (ratio of arc distance travelled to total travel time) are shown as a function of range from the transmitter. The DECCA values are shown as published (or inferred from the published data) without correction from DECCA frequencies to the 100-kHz nominal value of the LORAN and SALT-model data. The correction is both range and frequency dependent, but typically will reduce the DECCA $\bar{C}$'s by about 18 km/sec. The curve marked "SALT-model" shows the predicted effective speed at 100 kHz using the technique of Brunavs and Wells (1971-b). Example PF, SF, and ASF corrections are shown to suggest the relative size of each. The ASF corrections shown (inset) are for all land paths and are generally larger than the mixed land-sea paths of nearshore transmitters. Speed changes due to monthly mean n variations for three cities are given above the inset.

Historically, there has been a selection bias in reporting new observations of the speed of light (Aslakson, 1964; Sanders, 1965; and Froome and Essen, 1969). If one is close to the accepted value, he stops work and publishes; if he is not close, he tends not to publish. Thus, published values of C_0 for various decades have tended to cluster. A similar selection process may also be present in some of the radio ground-wave propagation velocity literature.

Values of n in air vary with pressure, temperature, and humidity. Thus, location, altitude, barometric pressure, time of day, weather, climate, etc., alter n. The relation of N to the absolute temperature (T) in degrees Kelvin, the total pressure (P) in millibars, and the water vapor pressure (e) in millibars is given by Smith and Weintraub (1953), Bean and Thayer (1959), Bean and Dutton (1966), and the CCIR (1978) as:

$$N = \frac{77.6}{T}\left(P + \frac{4810e}{T}\right) \tag{9}$$

Because e increases very rapidly with T in the range of interest ($\sim T^{18}$), N increases with temperature in humid air. Equation 9, derived from theory and laboratory measurements, is thought to accurately model N to within one N-unit. Instrumental errors in the determination of P, T, and e, however, limit practical accuracy to about $\pm$ 4 N-units. Direct measurements with radio-frequency resonators allow about an order of magnitude improvement in resolution.

Figure 4 shows the speed of propagation (C) for representative values of P, T, and humidity calculated from Equation 9 and standard tables of water vapor pressure. Notice the large (100 ppm) change in C from 0 to 100 percent humidity at room temperature.

TABLE 1

Effective propagation speeds for light in a vacuum (top), for DECCA and LORAN in the atmosphere (center), and for the RTCM (1981) LORAN salt-model approximation of various ranges (bottom)

PPM	Source	Value km/sec	Comments
-9	Johler et al. (1956)	299,795.1	C_o (1956)
0	USCG (1980)	299,792.458	C_o (1975)
65	Aslakson (1964)	299,773	C_o (1940s)
309	IHR, Laurila (1956)	299,700	Ocean, DECCA
322	Laurila (1956)	299,696 ± 26	Ocean, DECCA
338	USCG (1980)	299,691.16	C_o (1975) ÷ 1.000338
475	Larsson (1949)	299,650	Ocean, DECCA
505	LaCroix & Charles (1960)	299,641	Ocean, DECCA
609	Gray (1977)	299,610 ± 15	Ocean, DECCA
602	Brunavs & Wells (1971-a)	299,612 ± 28	Ocean, DECCA, 185 km
682	Brunavs & Wells (1971-a)	299,588 ± 28	Ocean, DECCA, 375 km
746	Lonars, Jerardi (1982)	299,569 ± 12	Ocean, LORAN
809	Dean et al. (1962)	299,550 ± 12	Ocean, LORAN, 812 km
913	Dean et al. (1962)	299,519 ± 9	Ocean, LORAN, 1840 km
1234	SALT-model	299,423	20 km range
666	SALT-model	299,593	100 km
786	SALT-model	299,557	500 km
870	SALT-model	299,532	1000 km
926	SALT-model	299,515	2000 km

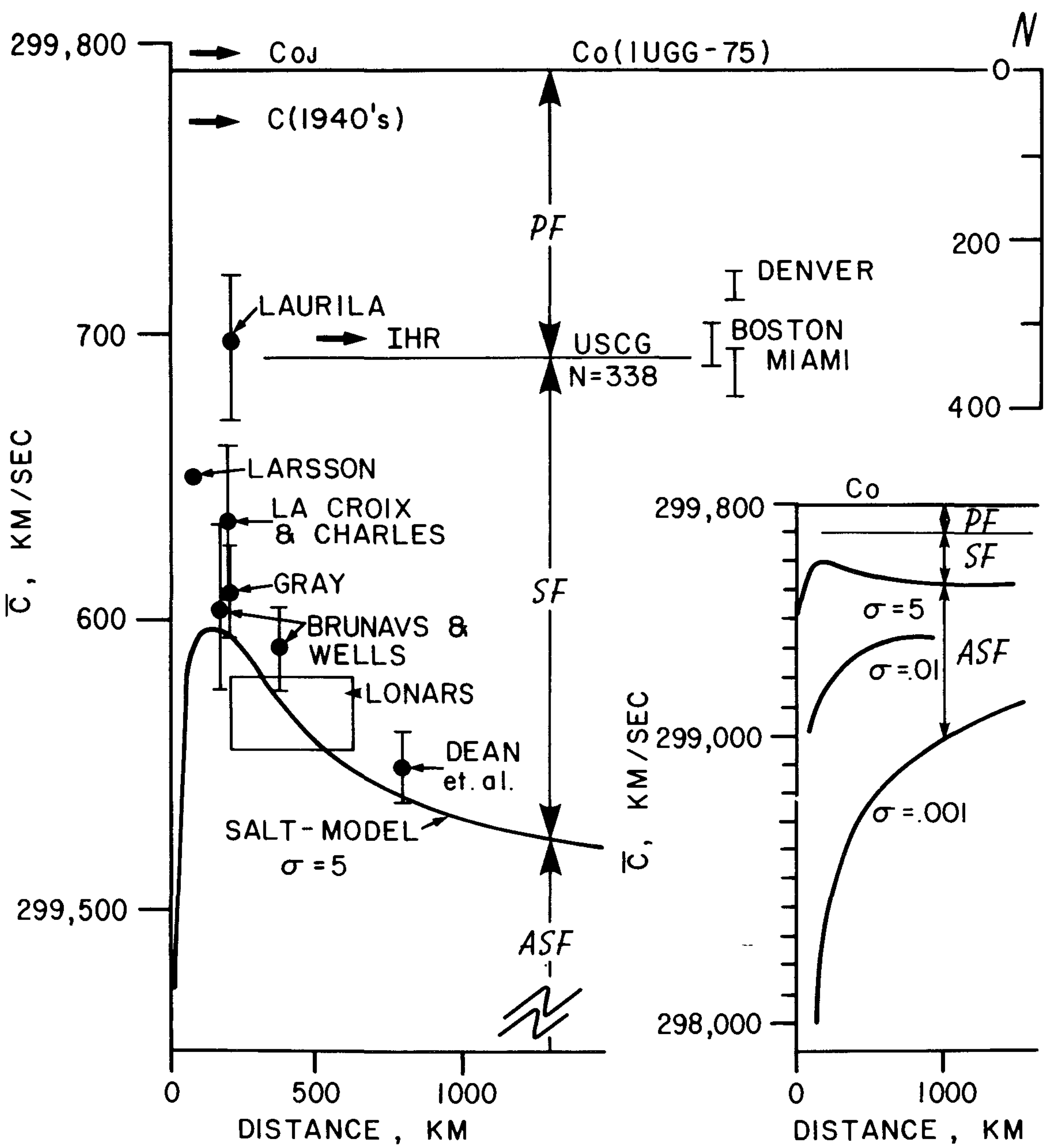

Figure 3. Effective propagation speeds $\overline{C}$ listed in Table 1 versus distance are indicated (left). Monthly mean variations of $\overline{C}$ due to index of refraction variations are shown for Denver, Boston and Miami. The inset figure (lower right) shows the PF, SF, and ASF corrections at reduced scale.

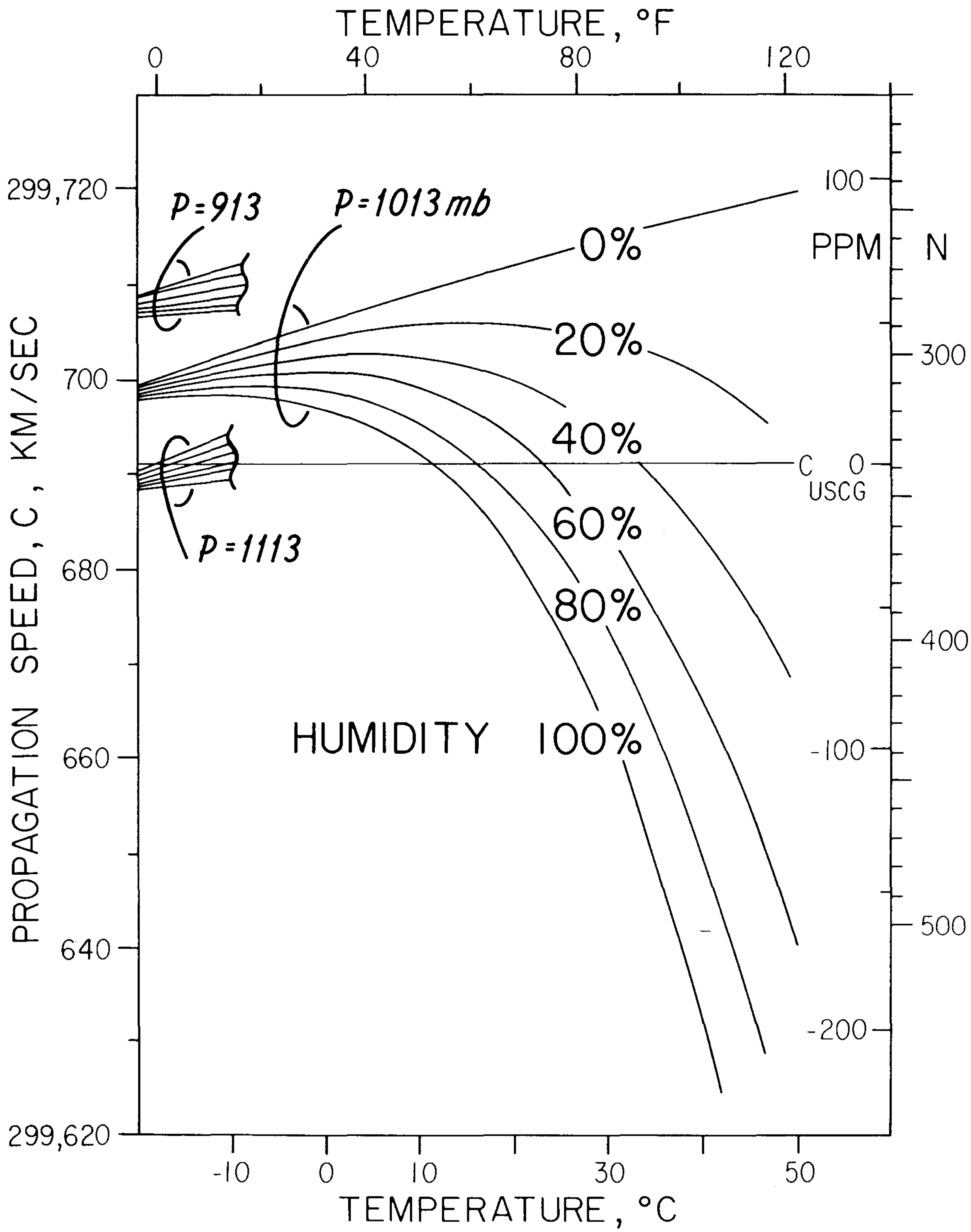

Figure 4. Variation of radio propagation speed with atmospheric pressure, temperature, and humidity. Scales of refractivity (N) and changes in parts per million (ppm) are shown at right. Pressure changes are suggested by truncated families of humidity curves at left.

As noted above, the arbitrary nominal value of n as adapted by the USCG is 1.000338. (This value is from Johler et al., 1956, p. 37, wherein $n = \sqrt{\epsilon_1}$, and apparently in turn from Schulkin, 1952, for summer conditions near Washington, D.C.) As seen in the figure, this is a reasonable nominal value in the range of general interest at sea. We wish to emphasize that this USCG value for n is a nominal model definition, not a measurement, and, as such, it serves the function of uniform normalization for the LORAN community. It may not represent the best nominal value, particularly in the tropics, at higher altitudes, nor for aircraft. Perhaps more representative seasonal and regional values could be established as well. Alternately, n can be estimated directly from weather observations and charts.

Effects of n Aloft

The net LORAN propagation rate at the earth's surface is influenced by propagation modes moving at higher altitudes and hence is influenced by values of n aloft. The index of refraction decreases from its surface value, slightly greater than unity, to exactly unity in free-space. The decrease of n with altitude refracts the signal toward the earth. Refraction and diffraction around the earth then allow over-the-horizon ground-wave transmission.

From 888 sets of monthly mean balloon soundings from 45 U. S. weather stations, Bean and Thayer (1959) show an exponential decay of N with altitude such that:

$$\Delta N = -7.32e^{.005577 N_s} \qquad (10)$$

where ΔN is the difference between the surface refractivity (N_s) and that at 1 km above the surface. The strong coupling of N_s and ΔN allows one to estimate the N-field near the earth without direct measurement aloft for most of the contiguous United States with the exception of southern California during the summer months.

The Van der Pol-Bremmer method, however, assumes a linear change of N with altitude. This convenient fiction gives surprisingly good results (Bean and Thayer, 1959) because most of the refraction of the low-angle ground-wave rays occurs in the lower atmosphere. The method then finds the radius of an "equivalent" earth (a_e) such that curvature of the real earth (1/a) plus that due to Snell's law of refraction in the linear gradient of n with height (h) dn/dh, is

$$\frac{1}{a} + \frac{1}{n}\frac{dn}{dh}\cos\theta = \frac{1}{a_e} \qquad (11)$$

where θ is the elevation angle of the ray, a is the earth radius, and n is the surface index of refraction. The method then introduces the factor alpha such that

$$\alpha = \frac{a}{a_e} = 1 + \frac{a}{n}\frac{dn}{dh} \qquad (12)$$

Finally, the value a_e is arbitrarily taken to be 4/3 a (α = .75) without further regard for N_s or the profile of N. It is not clear that the 4/3 model is the best nominal value at 100 kHz (CCIR, 1978). Table 2 shows α calculated from equations 10 and 12. Note that the arbitrary selections of α = .75 and n = 1.000338 are inconsistent (α = .75 corresponds to N = 301, not 338) with the model of equation 10.

TABLE 2

Mean surface refractivity N_s, vertical gradient of refractivity ΔN and the Bremmer factor α.

N_s	ΔN	α	$\alpha^{2/3}$
200	-22	.86	.90
250	-30	.81	.87
300	-39	.75	.83
350	-52	.67	.77
400	-68	.57	.68
450	-90	.43	.57
338	-48	.69	.78
301	-39	$(4/3)^{-1}$	.83

Such historical oddities suggest it may be time to review the nominal values used in the DMA/USCG method as well as the method itself. Are the nominal values consistent and representative? Might regional and seasonal coefficients improve performance? What are the general parametric sensitivities of the various terms of the method? How do its predictions compare with those of other models and observations? Partial answers to such questions exist in the literature; a definitive study is not yet available.

Effect of n on the TD's

How do changes in n effect the TD's? The actual situation is complicated, but for illustration assume the simplified case in which all variables except n are fixed and the real emission delay of one Secondary is constant and known. Then the received time difference, TD, after correction for the emission delay is

$$TD = \frac{D_1}{\bar{C}_1} - \frac{D_2}{\bar{C}_2} \approx \frac{1}{C_o} (\bar{n}_1 D_1 - \bar{n}_2 D_2) \qquad (13)$$

or

$$C_o \cdot TD \approx \bar{n}_1 D_1 - \bar{n}_2 D_2$$

$$\approx (n + \Delta n_1) D_1 - (n + \Delta n_2) D_2$$

$$C_o \cdot TD \approx n(D_1 - D_2) + (\Delta n_1 D_1 - \Delta n_2 D_2) \qquad (14)$$

where D_1, D_2, $\bar{C}_1$, $\bar{C}_2$, $\bar{n}_1$, $\bar{n}_2$ and Δn_1, Δn_2 are the length, average speed, average index of refraction, and the correction to a nominal index of refraction n, for paths 1 and 2, respectively. From the first term of Equation 14, we see that the nominal value of n is multiplied by the path length difference, which to some extent may reduce the effect of an inappropriate choice of n. The corrections Δn_1 and Δn_2, however, can have either sign and may tend to cancel or not. As an example, suppose $D_1 = D_2 = 10^6$m and $\Delta n_1 = - \Delta n_2 = 10^{-5}$ ($\Delta N = 10$).

The error, E_R, is

$$E_R = 2\Delta n D = 20 \text{ meters}$$

However, if the paths to the two transmitters differ in length by 100 km, for instance, then an error in n of 10 N-units would yield an error of only $10^5 \times 10^{-5} = 1$ m. Thus, the difference in n between the paths may be more important than the nominal value. Doherty and Johler (1975) treat effects of alpha and n in greater detail.

Conductivity

The propagation rate is affected by the complex impedence of the air-earth boundary layer with a skin depth ranging from about 0.75 m for sea water to more than 50 m for dry land. The land electro-magnetic boundary effects are determined by the curvature of the earth, the roughness of the terrain at the scale of the transmitted wave length (3 km) and the equivalent impedence of the ground. The impedence depends on the rock type, penetration depth, stratification, soil type, and, in particular, on the rock and soil moisture content. Such electrical effects are used for geo-electromagnetic prospecting (Rokityansky, 1982, and Wait, 1982). Typically, the travel-time variations are caused by changes in the resistive or conductive component of the impedence.

The integrated impedence effects over a zone are conventionally modeled as a single bulk conductivity determined empirically for that zone. The integrated effects over various zones are then estimated by Millington's (1949) method discussed below. Effects of mountains, woods, and buildings are lumped together with the impedence effects by adhoc adjustment of the effective conductivities.

Values of conductivity (mhos/meter) range from about 0.001 for dry earth to 0.010 for marshy woodland and sea ice. Water conductivity ranges from about 0.001 to 5 or more in the ocean (Terman, 1943). Mountains, woods, and buildings tend to reduce the effective conductivity (Gupta and Anderson, 1979; and Johler et al., 1979). Grant (1977) shows that the effective conductivity may change by a factor of 2 from a dry to a wet year, but short-period effects of heavy rains are relatively small, as LORAN waves penetrate well below the storm-wetted layer. At a range of 10^6 m, the travel-time is about 3,338 microseconds over the ocean. If the path were over smooth land, the travel-time would be increased by only about 5 microseconds, but LORAN surveyors require travel-times accurate to 0.1 microseconds or better, i.e., to about 30 ppm. This requires that we know the effective land delays to a few percent.

Land Delay Models

A number of interesting propagation models for LORAN and other electomagnetic waves have been developed since the first efforts early in this century (Samaddar, 1980; Wait, 1964; and

Wait, 1981). The Millington (1949) semi-empirical model (and its extension to phase by Pressey et al., 1956) is used by DMA. It combines relative computational simplicity with accuracy limited mainly by the empirical input constants, i.e. the effective conductivities of the ground segments. The delays for each segment are estimated in both directions, assuming a smooth homogenous earth of conductivity equal to that of the segment. The model then sums and averages the nonlinear range-dependent delays to the receiver and, in the opposite direction, back to the transmitter. The rational for this procedure (Fermat's principle) is nicely described in some detail by Monteath (1973).

The Millington model requires about half a page of BASIC-code and runs on an Apple II calculator in 10-20 seconds of computer time per estimate. Conductivity models utilizing only two segments give offshore results similar to those of the more detailed geometry used by DMA in large computers. For ships, the radial ASF predictions need only be updated every half hour or so, making both the computational and programming requirements small. The difficulty, therefore, is neither the model complexity nor the computing time, but the selection of appropriate conductivity boundaries and values.

Model Predictions

Model ASF's for the New York Bight area (DMA, 1981) are contoured in Figure 5. The DMA X-TD model data shown use detailed geography with five fixed conductivities (.0005, .003, .005, .03 and 5.0 mhos/m). Because the transmissions from Nantucket Island are nearly all over water, the contoured corrections are very nearly those of the ASF's due to Seneca alone. The published data end at the Coastal Confluence Zone (CCZ) but are easily extended indefinitely to sea by the model.

Some of the geometric complexity shown can be reduced by plotting the data in the natural radial coordinate system for each transmitter. Figure 6 shows the Seneca Master ASF data plotted in range/azimuth coordinates. Beyond the shoreline, (heavy line), the field is relatively less complex and could be stored in perhaps 2 K bytes of table values or polynomial coefficients at about the ± 0.2 microsecond level. Thus, the ASF data for offshore navigation looks quite manageable with present microprocessor techniques.

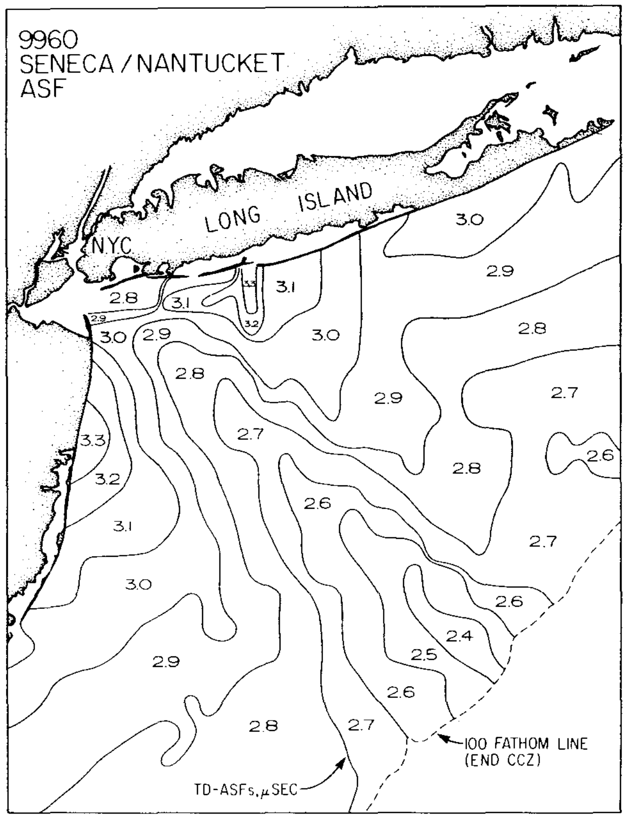

Figure 5. Contours of modeled overland delays (ASF's) in the New York Bite area. TD variations for Nantucket primarily reflect land effects from the master transmitter at Seneca, NY. Data is from DMA (1981).

COMPARISON OF THE MODEL WITH OBSERVATIONS

Nearshore

Observed nearshore effects are interestingly described by Pressey et al. (1956) for DECCA transmission (CW) in England. They find 5°-10° (about 0.2 microseconds) complex spatial phase variations within six wavelengths (18 Km) of shore; most of the effect is in the first three wavelengths. These spatial undulations occur, as might be expected, where the abrupt changes in boundary conditions excite higher order propagation modes which then decay rapidly with distance.

Figure 7 repeats the model delays shown in the dash-dot box of Figure 1, together with observations taken at sea

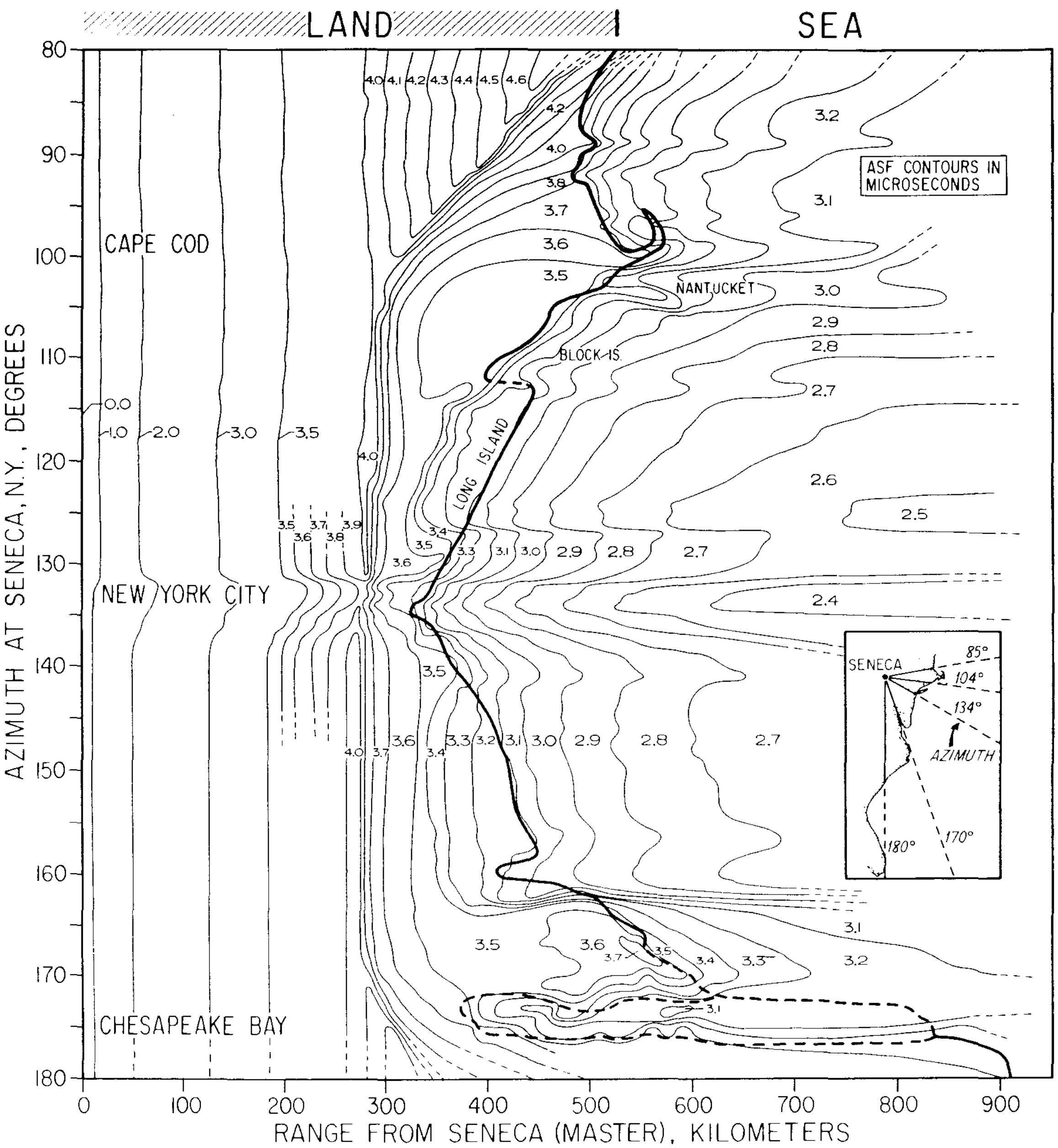

Figure 6. Model Range-ASF's for Seneca, NY, in range-asimuth coordinates. Heavy line marks the shore. Inset shows the general area covered. Contours are in microseconds. Note that sea contours (to right of shore line) would be relatively simple to store at say a ± 0.2 usec level of resolution.

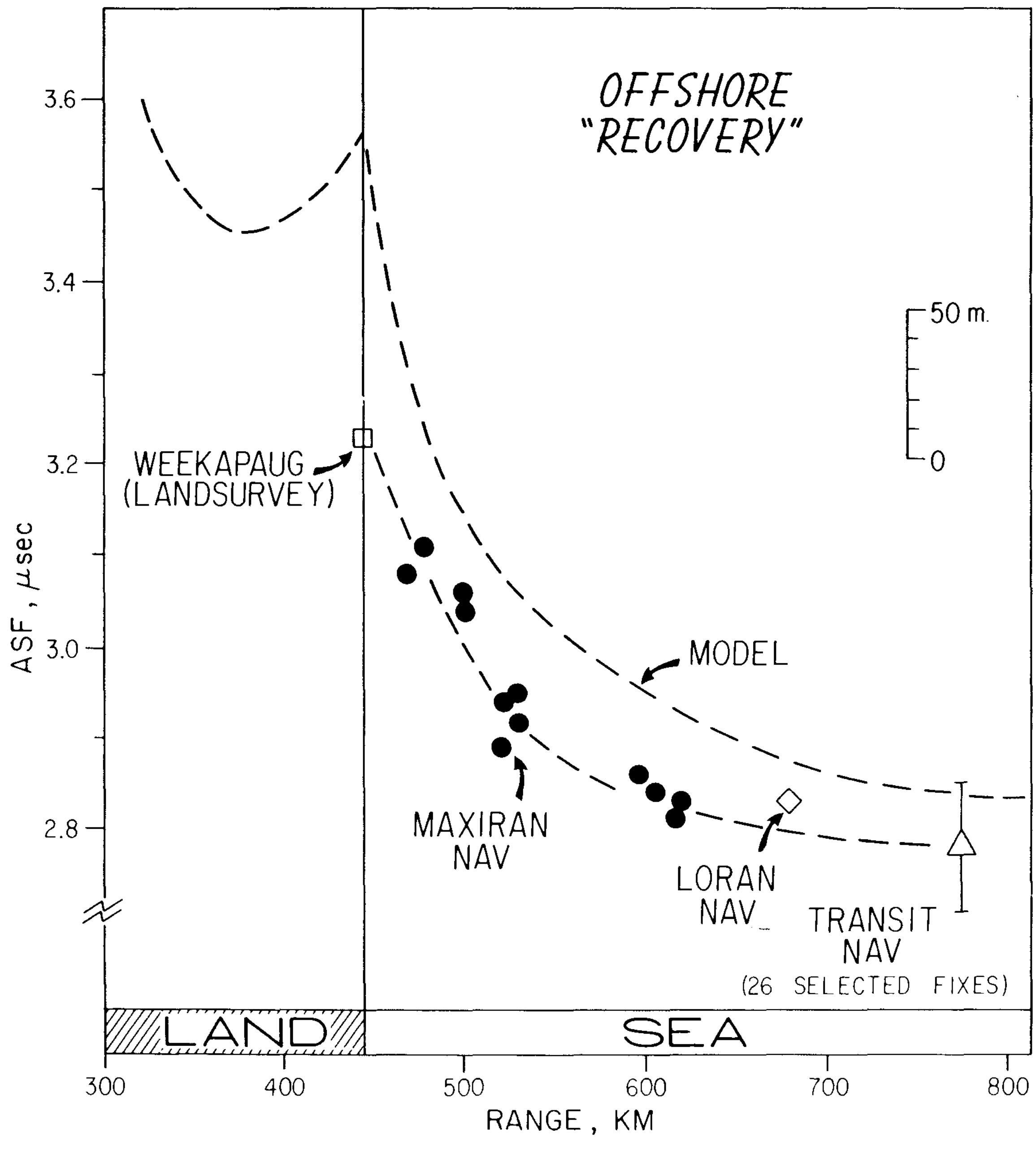

Figure 7. Model and offshore phase recovery observations are compared for the Seneca-9960, 108° azimuth radial shown in the dash-dot area of Figure 1, near Weekapaug, R.I. Four different types of X-TD observations show a systematic trend similar to, but slightly displaced (0.1 microseconds) from, the model prediction.

and ashore. Four types of observations were used: a) Land survey data taken at two locations in an open field at the USCG station at Watch Hill, R.I., using an Internav 404 receiver and local survey control converted to WGS-72; b) USCG survey observations using Austron 5000 receivers and Maxiran navigation from shore stations (Miller et al., 1981; and Weseman, 1982a, 1982b); c) A single mean estimate derived from time series of Internav 404 LORAN fixes and baseline crossing data; d) The average of 26 simultaneous Northstar-6000 LORAN and JMR-4a Transit Satellite fixes. The observational data shown are in general agreement with the model ASF at about the 0.1-microsecond level; however, the model curve does not include ASF delays from the Nantucket transmitter which are included in the observed X-TD on rate 9960 shown.

The complexity of the nearshore effects probably limits model predictions to the $\pm$ 0.1-microsecond level nearshore or perhaps twice this near rugged shores (Eaton et al., 1979). In addition, the Millington model introduces off sets of about 0.1 microseconds nearshore (Brunavs, 1976). Amplitude and phase measurements made in the vertical from aircraft would aid the model calibration and allow prediction beyond restrictive political boundaries.

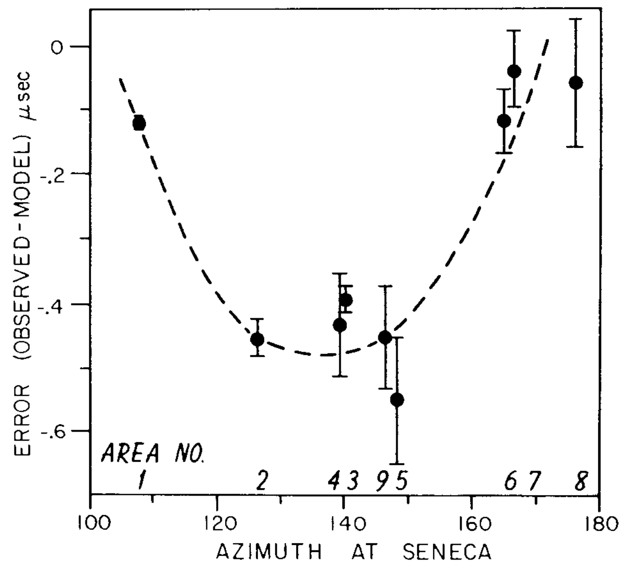

Figure 9. Trend of the X-Δ TD residuals of the previous figure. Scatter over 3-year period near azimuth 140° is of the order of 0.1 μ sec. Tentative systematic trend is suggested by arbitrary dash line sketched. Error bars represent $\pm$ one standard error of the means. Area numbers are shown along X-axis.

Far Offshore

How accurate are the ASF model predictions? We have given considerable attention to this question for the 9960-Chain and summarize our results in Figure 8. Several thousand simultaneous Transit Satellite and LORAN fixes have been collected, edited (Appendix B), and reduced to the nine sets of 219 observations shown in the figure and in Table 3. All observations were made from June to October when n and SAM anomalies are usually smallest. Figure 9 shows the X-TD residuals versus the azimuth at Seneca. The Y-TD residuals listed show a similar distribution except for area 7.

Test areas 3, 4, 5 and 9, surveyed with different ships and receivers in three separate years in a $\pm$ 5° band near Seneca azimuth 140° degrees (Figure 9), are consistent for both X and Y TD's at the 0.1-microsecond level. Paths from the X and Y transmitters to areas 6, 7, 8, and 9 are nearly all over water, so the unknown effects of the path delays from M can be eliminated by differencing the X and Y TD's. The resulting systematic trend merits further investigation. The signs of the W corrections (Table 3) are opposite to those for X and Y, suggesting that the primary ASF residuals from the DMA model for 9960 are on the Seneca and Caribou radials. It would be useful to have time series and spectra for periods of a year and longer of TD's and TOA's taken at fixed monitors at sea --- possibly on oil platforms, buoys, lightships, and on offshore islands. Additional details of the azimuthal structure nearshore are provided by the recent USCG ship surveys (see USCG Radionavigation Bulletin numbers 10 and 11).

SF AND ASF CONSIDERATIONS

Saltwater Correction, SF

The algorithm recommended by the RTCM (1981) and in general use by DMA is a two-segment polynominal fit (Harris, 1964) to Tables 18 and 20 of Johler et

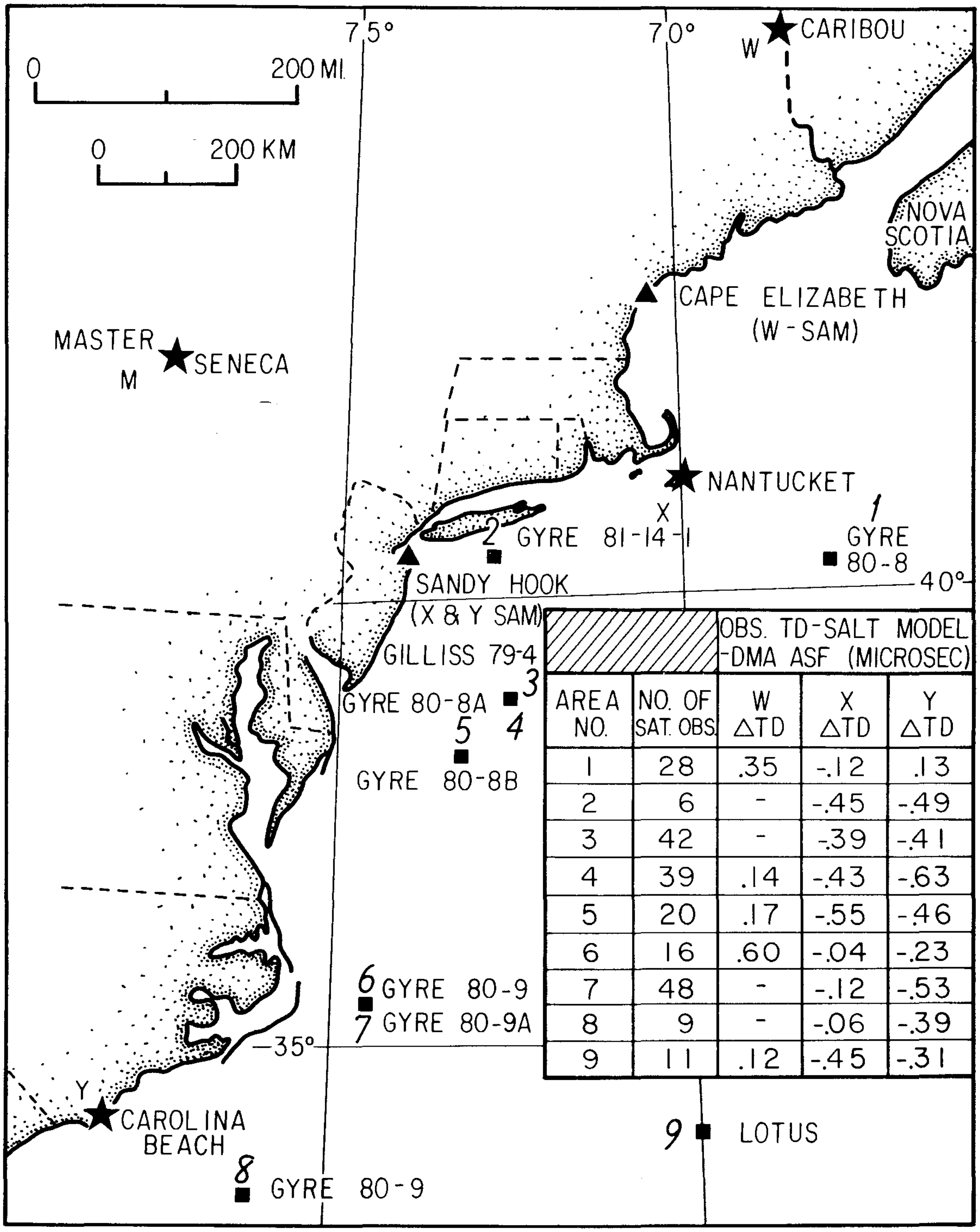

AREA NO.	NO. OF SAT. OBS.	OBS. TD-SALT MODEL -DMA ASF (MICROSEC) W ΔTD	X ΔTD	Y ΔTD
1	28	.35	-.12	.13
2	6	-	-.45	-.49
3	42	-	-.39	-.41
4	39	.14	-.43	-.63
5	20	.17	-.55	-.46
6	16	.60	-.04	-.23
7	48	-	-.12	-.53
8	9	-	-.06	-.39
9	11	.12	-.45	-.31

Figure 8. Residuals of observed values less model predictions for 9 offshore areas of LORAN Rate-9960. The residuals are based on Transit Satellite observations and ASF predictions using DMA model conductivities.

TABLE 3. Data and locations shown in Figures 8 and 9. Time differences (TDs) and standard errors (SEs) for rate 9960 W, X, and Y are listed (top) together with the number of satellite observations and residuals to the DMA SALT-model for areas 1-9 plotted in Figure 8.

		RESIDUALS IN MICROSECONDS								
Area. No.	No. SAT. OBS.	OBS. TD - SALTmodel						OBS.TD - SALTmodel - D.M.A. ASF		
		W		X		Y		W	X	Y
		TD	SE	TD	SE	TD	SE	△ TD'	△ TD'	△ TD'
1	28	1.33	.06	2.78	.01	2.71	.05	.35	-.12	.13
2	6	---	--	2.50	.03	1.48	.07	---	-.45	-.49
3	42	.17	.01	2.31	.02	1.62	.02	---	-.39	-.41
4	39	.14	.07	2.27	.08	1.40	.07	.14	-.43	-.63
5	20	.04	.09	2.25	.10	1.60	.14	.17	-.55	-.46
6	16	.90	.05	3.08	.06	2.83	.09	.60	-.04	-.23
7	48	---	---	2.95	.05	2.32	.07	---	-.12	-.53
8	9	---	---	3.24	.10	2.81	.19	---	-.06	-.39
9	11	.82	.06	2.25	.08	2.29	.12	.12	-.45	-.31

AREA NO.	LOCATION	SAT. RCVR.	CRUISE	DATES
1	40°10'N 67°40"W	JMR-2	GYRE 80-8	29 Aug to 02 Sep 80
2	40°25'N 72°50'W	MX702A-3	GYRE 81-14-1	15 Sep to 26 Sep 81
3	38°50'N 72°45'W	MX702A-3	GILLISS 79-4	27 Jun to 11 Jul 79
4	38°50'N 72°40'W	JMR-2	GYRE 80-8A	03 Sep to 10 Sep 80
5	38°15'N 73°15'W	JMR-2	GYRE 80-8B	10 Sep to 13 Sep 80
6	35°25'N 74°45'W	JMR-2	GYRE 80-9	19 Sep to 21 Sep 80
7	35°30'N 74°30'W	JMR-2	GYRE 80-9A	26 Sep to 14 Oct 80
8	33°15'N 76°00'W	JMR-2	GYRE 80-9	22 Sep to 25 Sep 80
9	34°00'N 70°00'W	MX 706	LOTUS	8 May to 12 May 82

al. (1956). The large number of digits of the coefficients shown in the code of Appendix A (Table 4a, lines 72 and 76) are clearly unnecessary, but are repeated here to indicate their origin.

Table 4 shows the residuals of the fit to the tabulated values in Johler et al. (1956) and to direct computations by Brunavs (1976, 1977). As seen in the table, there is a large discontinuity at 100 statute miles between the near field (flat earth) and far field (spherical earth) models. No significant discontinuity, however, is seen with Brunavs' values. Further comparison with Brunavs' values shows a cyclic residual of the fit with peaks of -21, +17, and -3 nanoseconds at 155, 497, and 1,864 statute miles, respectively. Below 1 mile or so, the RTCM model should not be used. The residuals are unfortunately largest ($\pm$6 m) in the 50-500 mile range, our primary interest at sea. The Brunavs and Johler model coefficients are not always those in present use by the USCG.

In short, the conversion from distance to time is considerably less accurate than is the distance determination alone. This will have practical implications for computer accuracy, speed, etc., for LORAN receiver manufacturer's development of latitude/longitude converters. The geodetic distance, of course, is not the distance traveled by the radio waves, but acts only as a scaling parameter in the effective speed calculation. The corrections to the actual distances traveled are absorbed in $\overline{C}$.

ASF Definitions

The phrase, Additional Secondary-phase Factor (ASF), has grown to mean land-induced propagation delays. Laying aside, for the moment, the interpretive problems associated with the phase of a zero-crossing time measurement of a broad-band pulse, let us consider ASF as a generic term referring to land-induced propagation travel-time delays -- a sort of spatial-temporal-modal mean-time interval. In this context, we look next at four of the several ASF definitions now in use.

Range ASF. The USCG (1980) definition of ASF is:

> "The amount, in microseconds, by which the time difference of an actual LORAN signal that has traveled over varied terrain differs from that of an ideal signal which has been predicted on the basis of travel over an all-seawater path. (LORAN signals travel slower over ground.)"

This is the clearest use of the term, i.e., the additional travel-time from one transmitter antenna to one receiver antenna relative to that calculated from a standard all salt-water model of the path. It is the anomaly of the travel-time component relative to an arbitrarily defined propagation SALT model.

$$ASF_R = PATH_{TT} - SALT_{TT}$$

The range ASF is equal to the actual (or best estimate) travel-time over the path less that predicted by the standard SALT-model. The net delays are caused mostly by land effects; but lakes, bays, and even ocean segments contribute to the sum of the nonlinear segment delays of the total travel-time and, hence, to the range ASF.

One need not be concerned with how representative the SALT-model is relative to local conditions (season, weather, topography, etc.); the model is only used to form a reference travel-time that accounts for most of the air and planetary boundary effects in a computationally expedient fashion. Note that although some salt-water propagation model is implied, a LORAN-chain model is not. Conceptually, one could directly determine such an ASF by measuring the mean actual travel-time with a portable clock. Comments on the nature of any particular mean (ground cover, ice, N_s, N-profile, number of observations, averaging methods, equipment, etc.) would complete the ASF estimate. Such measurements are now periodically made in the LORAN-C Emission Delay calibration. The results, however, are not generally presented as the ASF's of the baselines.

Delta ASF. The delta ASF is simply the difference between two range ASF's:

$$\Delta ASF = ASF_{R2} - ASF_{R1}$$

The published DMA (1981) Loran-C Correction Table is computed in this way relative to the DMA SALT-model first published by the RTCM (1981).

The Observed or TD-ASF. The observed or TD-ASF is the difference between the observed TD and the SALT-model TD at a location. It includes all causes of TD variations in the LORAN-chain. Operationally, it is much easier to measure than the range-ASF, but should not be confused with it. The TD-ASF might better be called a TD correction

TABLE 4. Residuals to the DMA-RTCM proposed fit. Columns 1 and 2 list the distance and SF correction from Johler et al. (1956, Tables 18 and 20). Columns 3 and 4, indicate the difference between the RTCM (1981) fit and the Johler et al. (1956) tables (RTCM-Johler). Column 5 gives the difference or bias between the RTCM (1981) fit and the direct Brunavs (1977) solution (RTCM-direct).

DISTANCE	SF	FIT RESIDUALS		BIAS
s. miles	μsec	μsec	m	m
0.1	4.4209	+.672	+201	-
0.2	3.5802	-1.039	-311	-
0.5	1.1807	-.170	-51	-
1.0	0.5038	-.003	-1	-
2.0	0.2448	+.003	+1	+1
5.0	0.1032	-.004	-1	-2
10.0	0.0593	-.002	-1	-3
20.0	0.0409	+.008	+2	-2
50.0	0.0368	+.050	+15	-1
100.0	0.0434	+.126	+38	-4
100.0	0.1755	+.004	+1	-1
200.0	0.4205	-.015	-4	-6
500.0	1.3579	+.017	+5	+6
1000.0	3.0811	+.004	+1	+2
2000.0	6.5466	-.005	-1	-1

and is:

$$ASF_{TD} = OBS_{TD} - SALT_{TD}$$

Note that this definition implies a Master/Secondary LORAN model as well as the SALT-model. (It is necessary to know the emission delay and SAM steering effects due to weather, ice, seasons, etc., in order to relate the observed TD to a nominal TD for the location.)

The RTCM (1981, p. 1) defines ASF as:

> "The amount, in microseconds, by which the time difference of an actual pair of LORAN-C signals that travel over terrain of various conductivities differs from that of signals which have been predicted on the basis of travel over all sea-water paths."

Although the wording is nearly identical with that of the USCG Range ASF definition above, the meaning has been changed to that of the TD-ASF.

The SAM-ASF. The TD-ASF at the SAM is an indirectly defined value set by the coordinates of the SAM antenna and the defined CSTD value. The TD-ASF at the SAM is held constant by changing the Emission Delay of the Secondary. The form of nominal ASF corrections such as those of Figs. 5, 8, and 9 are influenced by the arbitrary selection of the SAM-ASF.

It seems unnecessary to attempt to alter the varied general usage, but for mathematical clarity, some rigorous definitions are needed.

ASF Sign Conventions

Both positive and negative sign conventions are used for ASF's. DMA shows all additional secondary phase factor's (ASF's) as negative whereas secondary phase factors (SF's) are considered positive; yet, both increase the travel-time. When considered as receiver corrections, however, the ASF's used to adjust the observed TD's to positions charted from SALT-model predictions are negative. It is important here to distinguish between model anomalies and TD corrections.

Published ASF's (DMA)

DMA has calculated ASF's for military applications for many years. In April 1981, these values and the conductivities used to calculate them were declassified. DMA now offers LORAN-C correction tables for rates 5930, 9960, 8970, 7980, 9940, 5990, 7960 and 9990 (USCG, Radionavigation Bulletin). The published ASF values are for the CCZ from nearshore to the 100-fathom line, on a 5-arc-minute latitude/longitude (~5 mile) grid. With the exception of 9940 in Southern California, the ASF's are Millington model calculations based on USCG conductivity maps and do not include observations taken during the USCG LORAN verification surveys. Revised tables that include a "force-fit" of the offshore calibration data, but do not necessarily represent an adjustment of the model conductivities, are being prepared by DMA.

The next step might be to use tomographic or inverse techniques to adjust the model input parameters for a best fit to the weighted observational data available in each chain. Gressang and Horowitz (1978) proposed using a Kalman filter approach for such an adjustment. Although conceptually feasible, the conductivity adjustment procedures have not been implemented in the DMA LORAN ASF modeling.

Specifications for LORAN-C Propagation Models

There is no definitive specification of LORAN-C propagation models as there now is for the specification of the transmitted LORAN-C signal (USCG, 1981). Because propagation is not controlled, we can only specify how such models are constructed and how well they perform. The Minimum Performance Specification (MPS) report of the RTCM (1981) is the first major attempt at standardizing propagation models for LORAN-C. As such it represents a much needed breakthrough in a generally chaotic situation. Their position on specification and model improvements, however, was:

> "The report is designed to establish MPS for Automatic Coordinate Conversion equipment and is not to be considered as a standard way of computing. The material contained in the appendices to the SC-75 report are there for information only and should not be considered as a part of the MPS."

We submit that documentation of theory, methods of implementation, and worked examples are the kinds of information needed to make a paper standard generally usable. Means for implementing amendments and changes are needed to assure the health and utility of such standards.

What Next?

Now that DMA ASF's are declassified and microprocessors have made their use practical, we suggest that:

- Propagation model standards be developed and published.
- The observed TD's at a large number of locations in each LORAN chain be published as test-material for Latitude/Longitude Converter development and evaluation.
- Renewed effort for model and observational studies of LORAN propagation should be promoted.

OTHER CONSIDERATIONS

Temporal variations, SAM control procedures, and unmodeled terms all contribute to the observed errors. At Woods Hole, Mass., we routinely observe Time-of-Arrival (TOA) standard deviations of 7-40 nanoseconds for 2-hour averages at ranges of 40-780 nautical miles over water on rates 9960 and 5930. In addition to the ASF correction, it is probably appropriate to make at least SAM, seasonal, and catch-all corrections for survey applications. In the last 20 years, the accuracy of the Transit Satellite system on land has improved from about 2000 m to better than 1 m, largely through improved error models.

Weather and Seasonal Effects

Variations of several tenths of a microsecond of TOA measurements can accompany weather fronts. The variations observed at Woods Hole typically reach a maximum in about an hour and take several hours to recover. The controversial issue of storm and seasonal variation is discussed in Campbell et al. (1979), Charron (1981), Creamer and DePalma (1981), Doherty et al. (1979), Eaton et al. (1978), Illgen et al. (1979), Illgen and Feldman (1978), Mungall et al. (1981), Polhemus (1981), Potts and Wieder (1972), Samaddar (1980), Warren et al. (1978), Winkler (1972), and the referenced literature extending back into the 1950's. The longstanding puzzle concerning the size and cause of such effects now seems to favor about a one microsecond peak-to-peak seasonal variation per 500 km in New England with the primary cause being seasonal variations of n and alpha in addition to ground conductivity changes.

Effects Longer Than One Year

Grant (1977) observed variations in the ASF correction from 1972 to 1975 of 0.004-0.002 mho/m and noted they "may be due to the different meteorological conditions between the two years (1972 was notably wet while 1975 was notably dry)." The offset shown results in a range error of order 100 to 200 m for DECCA navigation over Newfoundland. The USCG (1982) monitors should allow detailed modeling of such effects, which were seen clearly in various other studies such as Doherty and Johler (1975).

System Area Monitor (SAM) Considerations

SAM control effects can be illustrated (Fig. 10) by a simplified

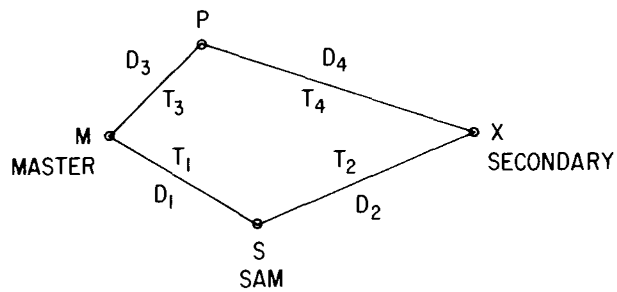

M = Master Station

X = Secondary Station

S = SAM

P = observer's location

$D_1 \ldots D_4$ = length as shown

$T_1 \ldots T_4$ = LORAN travel times

$C_1 \ldots C_4$ = mean propagation speeds along each of the paths

TD_S and TD_P = time differences at S and P, respectively

ED = nominal emission delay at X

t = time correction at X needed to keep the TD at the SAM constant

Fig. 10. Simplified model of SAM control.

model in which the TDs at the SAM and observer position are:

$$TD_S = T_2 - T_1 + (ED + t)$$

$$TD_P = T_4 - T_3 + (ED + t)$$

and the difference of these TDs is:

$$TD_P - TD_S = (T_4 - T_3) - (T_2 - T_1)$$

or

$$\Delta TD = TD_P - TD_S = \left[\left(\frac{D_4}{\bar{C}_4} - \frac{D_3}{\bar{C}_3}\right) - \left(\frac{D_2}{\bar{C}_2} - \frac{D_1}{\bar{C}_1}\right)\right] \quad (15)$$

If all the $\bar{C}$'s in Equation 15 change proportionally by a constant K then:

$$\Delta TD = \frac{1}{K}\left[\left(\frac{D_4}{\bar{C}_4} - \frac{D_3}{\bar{C}_3}\right) - \left(\frac{D_2}{\bar{C}_2} - \frac{D_1}{\bar{C}_1}\right)\right] \quad (16)$$

and the Δ TD change at P is seen to be proportional to 1/K, and the farther we are from the control TD (quantity in large brackets) the greater the change with K.

In actual use, the paths $D_1 \ldots D_4$ usually lie over different combinations of land and water which show significant seasonal and storm variations in $\bar{C}_1 \ldots \bar{C}_4$, causing lines of constant TD to move horizontally in a complex manner suggested by Equation 15. For modeling purposes, one might separate these effects into regional and local components. For practical applications such as harbor navigation, local reporting of the TD grid corrections may become as commonplace as tower barometric corrections are for aircraft altimeters. To be widely used, the correction vectors should be simple to receive and apply. From an operational point of view, they would be best implemented as TD offsets.

Because TDs can be controlled at only one point, it seems reasonable to locate this point near the area of greatest user activity in the chain. Then, at least that vicinity needs little or no LAM or differential LORAN-type correction. If, on the other hand, the Emission Delay were held constant, only areas along the baseline extensions and near the baseline ASF mid-point would show small variations. The baseline extensions are of no use for other reasons and the baseline ASF mid-point is relatively stable anyway (equation 15). Thus, while conceptually less satisfying, an observational rational can be made for constant CSTDs and variable EDs.

Pulse versus CW

LORAN propagation models are based on continuous wave (CW) phase assumptions, although the actual information comes from zero crossing time differences of a 20-kHz-wide pulse. As the ground wave is weakly dispersive, i.e., the propagation speeds depend somewhat on frequency, it is interesting to evaluate the correction anticipated between the CW model and the real LORAN pulse. For ranges of 1, 100, and 500 km; Johler et al. (1979, Part II, p. 25) estimate corrections of +0.11, +0.09, and +0.03 micro seconds, respectively, over smooth homogeneous ground. Errors at ranges less than a few kilometers from the transmitter are large for other reasons, but the errors shown at 100 and 500 km are significant and should be included in a detailed error budget. The logical distinction between signal, group, and phase velocity are described in many texts (i.e., Stratton, 1941; and Winkler, 1972). Fehlner et al. (1976), and Jespersen (1979) discuss possible methods of circumventing LORAN dispersion problems.

Height Gain

The height of the antennas above the ground and the elevation of the ground above sea level effect the propagation rate. Such effects are treated in the Van der Pol-Bremmer method, but are neglected in the DMA (1981) predictions. It would be useful to formally evaluate these effects for various situations.

Geodetic Datum

LORAN-C coordinates are given in World Geodetic System 1972 (WGS-72), whereas U.S. charts and maps use the North American Datum 1927 (NAD-27). Conversion from one sysem to the other is provided by the Molodenski formulas summarized in Stansell (1978) and shown graphically for the United States in Stansell (1973). Along the East Coast, residual errors after conversion by this method are estimated to be 10-20 m; they were found to be 11 m at Woods Hole, Mass. when the global ΔX, ΔY, ΔZ offsets of Stansell (1978) and Meade (1982) corrections were used. Conversion by DMA charts reduces this error to a few meters (about 3 m at Woods Hole). Several general texts (Hoar 1982; and Torge, 1980) and particularly the three International Geodetic Symposia on Satellite and Doppler Positioning at Las Cruces

NM-1976, Austin TX-1979 and Las Cruces NM-1982 provide background information.

Before 1976, LORAN WGS-72 Station coordinates were derived from on-site DMA Precise Ephemeris (PE) Transit Satellite Geodesy. More recently, Broadast Ephemeris (BE) have been converted to WGS-72. Transit Satellite navigation at sea utilizes the (BE), which require a small correction to convert to WGS-72 (Jenkins and Leroy, 1979; and Meade, 1982). Nearshore, we use NAD-27. In Canada and the United States, the change in 1984 to a new standard coordinate system should help eliminate confusion in the long run, but will add another system in the interim.

GDOP, ECD, Interference and Receivers

LORAN lines of position (LOP's) generally do not cross at right angles and are thus correlated. The fix becomes less accurate with small LOP crossing angles and with the hyperbolic spreading of the lines with distance from the transmitters. The TD's of a fix are also correlated through the shared signal from the Master and long-period noise/interference fluctuations (Amos and Feldman, 1977). Changes of pulse shape (envelop to cycle difference, or ECD) are caused by frequency-dependent propagation properties and contribute significantly to the error budget. Interference, man-made and natural, is at times the dominant error source. Bridges, powerlines, buildings, etc., can significantly distort the local LORAN grid. Receiver performance is equally important. These and other topics are beyond the scope of this paper but should not be overlooked in a general error-budget analysis.

CONCLUSION AND PROSPECTUS

Our studies at sea (Figs. 8 and 9) indicate that actual LORAN performance exceeds current error-model accuracy. By renewing interest in error modeling for LORAN, we might anticipate significant improvement in accuracy. Some major points discussed are:

1. Three major advances in LORAN calibration technology have been made in the last year and a half: The DMA ASF conductivities have been declassified, the DMA ASF values have been published, and the RTCM MPS has been published (DMA, 1981; and RTCM, 1981).

2. As a next step it would be useful to reduce the DMA-ASF books to microprocessor tables or coefficients to facilitate general use.

3. The USCG monitor program can now provide the data base for SAM error models. We encourage such model development.

4. LORAN propagation theory, coefficients, sensitivity, code and worked examples should be unified and published.

5. Model results should be compared with observations and the models adjusted accordingly.

6. The present ASF predictions need to be updated. A means for adjusting the conductivities should be implemented. LAM and other input data such as the baseline ASF's should be merged to make best estimates of the ASF model coefficients.

7. The LORAN ASF calibration effort needs to be consolidated and focused. One group should be responsible for the observations, procedures, and end products.

8. GPS will provide a superb tool for LORAN calibration and chain timing control. The improved accuracy of calibrated LORAN can be used to pace the civilian component of GPS and to serve as the primary navigation aid until GPS supersedes LORAN.

ACKNOWLEDGMENTS

It is a pleasure to thank J. Ligon, B. Schorr, D. Taggart, R. Wenzel and J. Weseman of the U. S. Coast Guard for their numerous contributions, data and valuable insights; also, E. Danford, L. Funakoshi and B. Swartwood of DMA for advice and the data used to compute ASF contours in Figures 1 and 6; and M. Eaton and S. Grant of the Canadian Hydrographic Service and D. Wells of the University of New Brunswick for programs, papers, comments, and general encouragement. Of the numerous others who have contributed to this paper we wish particularly to thank K. Chapman, H. Dahl, J. Hanna, D. Hill, S. Michaels, J. Morris, J. Moyer, and J. Wait, as well as J. Dodd, T. Jerardi, J. R. Johler, T. Aldrich, G. Tollios, and E. Winget for their review of the manuscript.

REFERENCES

Amos, D., and Feldman, D., 1977, A systematic method of LORAN-C accuracy contour estimation: The Wild Goose Association, Annual Technical Symposium, 6th, Proceedings, p. 77-98.

Aslakson, C. I., 1964, The velocity of light: Monaco, International Hydrographic Review, v. XLI, no. 1, p. 69-83.

APL (The Johns Hopkins University, Applied Physics Laboratory), 1981, Coordinate conversion, robust real time filtering of LORAN-C signals, and calibration of LORAN-C at sea: Radionavigation Journal 1980-1981, Wild Goose Association, Tenth Anniversary Edition, p. 17-88.

APL (The Johns Hopkins University, Applied Physics Laboratory), 1982, On the calculation of geodesic arc for use with LORAN: Radionavigation Journal, Wild Goose Association, p. 57-61.

Bean, B. R., and Dutton, G. J., 1966, Radio meteorology: NBS Monograph 92, Superintendent of Documents, Washington, DC, U.S. Government Printing Office, p. 163.

Bean, B. R., and Thayer, G. D., 1959, Models of the atmospheric radio refractive index: Institute of Radio Engineers, Proceedings, p. 740-755.

Bigelow, H. B., 1965, Electronic surveying: accuracy of electronic positioning systems: International Hydrographic Review, Monaco, Supplemental v. 6, p. 77-112, Sept. 1965, also Proceedings, American Society of Civil Engineers, p. 37-76, Oct. 1963.

Bremmer, H., 1949, Terrestrial radio waves, theory of propagation: Amsterdam, New York, Elsevier Publishing Co.

Bremmer, H., 1958, Propagation of electromagnetic waves: Encyclopedia of Physics (Handbuch der Physik), v. 16, p. 423-639.

Brunavs, P., 1976, Investigations of effects of inhomogeneous and irregular terrain on the groundwave propagation at 100 kHz, written communication.

Brunavs, P., 1977, Phase lags of 100 kHz radio-frequency ground wave and approximate formulas for computations, written communication.

Brunavs, P., and Wells, D. E., 1971a, Accurate phase lag measurements over seawater using DECCA Lamba: Atlantic Oceanographic Lab. Bedford Institute Report A.O.L. 1971-2, unpublished manuscript.

Brunavs, P., and Wells, D. E., 1971b, Accurate phase lag measurements over seawater using DECCA Lamba: Commonwealth Survey Officers Conference, Paper No. F3, p. 1-18.

Canadian Coast Guard, 1981, A primer on LORAN-C: Marine Aids Division, TP-2659, 2nd ed., p. 1-41, Mailing Address: Place de Ville, Tower A-6, Ontario, K1A0N7, Canada.

Campbell, L. W., Doherty, R.H., and Johler, J.R., 1979, Loran-C System dynamic model: temporal propagation variation study: U.S. Department of Transportation, U.S. Coast Guard, DOT-CG-D57-79, Government Accession No. AD-A076214.

CCIR (1978), International Radio Consultive Committee, 1978, Propagation in non-ionized media: Recommendations and Reports of the CCIR, XIV Plenary Assembly, Kyoto, v. 5.

Charron, L. G., 1981, Relationships between U.S. Naval Observatory, LORAN-C and the Defense Satellite Communication System: The Annual Precise Time and Time Interval Applications and Planning Meeting, 13th, Proceedings, p. 201-216.

Collins, J., 1980, Formulas for positioning at sea by circular, hyperbolic and astronomic methods: National Oceanic and Atmospheric Association Technical Report No. 81.

Creamer, P. M., and DePalma, L. M., 1981, Literature review of LORAN-C grid stability and warpage tests: The Wild Goose Association, Annual Technical Symposium, 10th, Proceedings, p. 103-127.

Dean, W. N., Frank, R. L., and Watts, P. C., 1962, Use of LORAN-C for intercontinental surveying: Monaco, International Hydrographic Review, v. 3, p. 77-84.

Defense Mapping Agency, 1981, LORAN-C correction table: Washington, DC, Defense Mapping Agency, Hydrographic/Topographic Center, DMA Stock No. LCPUB2211200-C.

DePalma, L. M., Creamer, P. M., and Anderson, E., 1980, Quantification of St. Marys River LORAN-C time defence GRID instability: The Wild Goose Association, Annual Technical Symposium, 9th, Proceedings, p. 51-61.

Doherty, R. H., Campbell, L. W., Samaddar, S. N, and Johler, J. R., 1979, A meteorological prediction technique for LORAN-C temporal variations: The Wild Goose Association, Annual Technical Symposium, 8th, Proceedings, p. 152-163.

Doherty, R. H. and Johler, J. R., 1975, Meteorological influences on LORAN-C ground wave propagation: Journal of Atmospheric and Terrestrial Physics, v. 37, p. 1117-1124.

Eaton, R. M., Schening, E., and Stuifbergen, N., 1978, A long range performance test of LORAN-C in Atlantic Canada: The Wild Goose Association, Annual Technical Symposium, 7th, p. 245-247.

Eaton, R. M., Mortimer, A. R., and Gray, D. H., 1979, Accurate chart latticing for LORAN-C: Monaco, International Hydrographic Review, v. LVI, no. 1, p. 21-33.

Fehlner, L.F., Jerardi, T.W., McCarty, T.A., and Roll, R.G., 1976, Experimental research on the propagation of LORAN-C signals, Vol. A: Summary Report: The Johns Hopkins University, Applied Physics Laboratory, APL/JHU TG 1298A, 77 p.

Fell, H., 1975, Comments on LORAN conversion algorithms: Navigation, v. 22, no. 2, p. 184-185.

Fock, Y. A., 1965, Electromagnetic diffraction and propagation problems: New York, Pergamon Press, v. 1, p. 203.

Froome, K. D., and Essen, L., 1969, The velocity of light and radio-waves: Academic Press, London and New York, 157 p.

Grant, S.T., 1973, Rho-Rho LORAN-C combined with satellite navigation for offshore surveys: Monaco, International Hydrographic Review, v. L, no. 2, p. 35-54.

Grant, S., 1977, A user-developed integrated navigation system: International Congress of Surveyors, XV, Stockholm, Sweden, p. 99-113.

Gray, D. H., 1977, The propagation velocity of DECCA-frequency transmissions over sea ice: Monaco, International Hydrographic Review, v. LIV, no. 1, p. 59-71.

Gressang, R. V., and Horowitz, S., 1978, Preliminary accuracy evaluation of a Loran grid prediction program: The Wild Goose Association, Annual Technical Symposium, 7th, Proceedings, p. 87-92.

Gupta, R. R., and Anderson, E., 1979, Application of semi-empirical TD grid calibration to the west coast LORAN-C chain: The Wild Goose Association, Annual Technical Symposium, 8th, Proceedings, p. 82-94.

Harris, L., 1964, Polaris FBM program navigation subsystem: Brooklyn, N.Y., Lab project 9500-1, Technical Memo 26, U.S. Naval Applied Science Laboratory (9110-P-IJ), p. 1-11 and A1-A3.

Hefley, G., 1972, The development of LORAN-C navigation and timing: Washington, DC, U.S. Government Printing Office, National Bureau of Standards Monograph 129.

Hoar, G. J., 1982, Satellite surveying: Torrance, California, Magnavox Advanced Products Division, Brochure MX-TM-3346-81, no. 10058.

Howe, H.H., 1960, Note on the solution of Riccati's differential equation: Journal of Research of the National Bureau of Standards, v. 64B, no. 2, p. 95-98.

Hufford, G.A., 1952, An integral equation approach to the problem of wave propagation over an irregular terrain: Quarterly Journal, Applied Math 9, p. 391-404.

Illgen, J.D., Mason, T., and Gambill, B., Jr., 1979, LORAN-C propagation and equipment timing fluctuations and conductivity estimates observed in the Great Lakes region: The Wild Goose Association, Annual Technical Symposium, 8th, Proceedings, p. 142-151.

Illgen, J.D. and Feldman, D. A., 1978, LORAN-C signal analysis experiments, an Overview: The Wild Goose Association, Annual Technical Symposium, 7th, Proceedings, p. 161-169.

International Union of Geodesy and Geophysics, 1975, Grenoble, XVIth General Assembly, Proceedings.

Jenkins, R.E. and Leroy, C. F., 1979, Broadcast versus precise ephermis - apples and oranges?: Austin, Texas, International Geodetic Symposium on Satellite Doppler Positioning, 2nd, Proceedings, p. 39-62.

Jerardi, T., 1982, The LONARS-aided Doppler solution - a new method for precise positioning at sea: Proceedings of the Third International Geodetic Symposium on Satellite Doppler Positioning, p. 755-782.

Jespersen, J.L., 1979, Some implications of reciprocity for two-way clock synchronization: Proceedings of the Eleventh Annual Precise Time and Time Interval (PTTI) Applications and Planning Meeting, p. 171-184.

Johler, J. R., 1962, Propagation of low-frequency radio signals: Institute of Radio Engineers, Proceedings, v. 50, no. 4, p. 404-427.

Johler, J.R., 1970, Spherical wave theory for MF, LF, VLF propagation: Radio Science, v. 5, no. 12, p. 1429-1443.

Johler, J.R., Doherty, R. H., and Cook, A. R., 1979, LORAN-C pulse transient propagation: Springfield, Va., U.S. Department of Transportation, U.S. Coast Guard Final Report, DOT-CG-D-52-79, NTIS Ad-A077551.

Johler, J.R., Keller, W. J., and Walters, L. C., 1956, Phase of the low radio frequency ground wave: Washington, D.C., National Bureau of Standards, Circular 573.

Johler, J.R., Walters, L.C., and Lilley, C.M., 1959, Low- and very low-frequency tables of ground wave parameters for the spherical earth theory: The roots of Riccata's differential equation: National Bureau of Standards Technical Note 7, PB 151266.

Lacroix, G. W., and Charles, D'A. H., 1960, The method and use of two range DECCA: Monaco, International Hydrographic Review, Supplementary v. 9-31.

Lambert, W.D., 1942, The distance between two widely separated points on the earth: Journal of the Washington Academy of Science, v. 32, no. 5, p. 125-130.

Larsson, H., 1949, Investigation of the accuracy obtained with the DECCA system for survey in the southern Baltic: Monaco, International Hydrographic Review, v. 26, no. 2, p. 25-45.

Laurila, S., 1956, DECCA in offshore survey: International Association of Geodesy, Geodesique, Bulletin no. 39.

Meade, B.K. 1982, NWL-10F versus WGS-72 Doppler results and broadcast versus precise ephemeris coordinates: Las Cruses, NM, International Geodetic Symposium on Satellite Doppler Positioning, 3rd, Proceedings, no. 11.

Miller, R., Illgen, J., Weseman, J., and Falconer, R., 1981, LORAN-C calibration of the Gulf coast and eastern seaboard: The Wild Goose Association, Annual Technical Symposium, 10th, Proceedings, p. 17-38.

Millington, G., 1949, Ground wave propagation over an inhomogeneous smooth earth: Institute of Electrical Engineering, London, Proceedings, Paper no. 794, Jan., 1949 (96, Part III, p. 53).

Monteath, G.D., 1973, Applications of the electromagnetic reciprocity principle: New York, Pergamon Press.

Mungall, A.G., Costain, C. C., and Ekholm, W. A., 1981, Influence of temperature - correlated Loran-C signal propagation delays on international time-scale comparisons: Metrologia, v. 17, p. 91-96.

Newman, J.N., 1980, LORAN navigation with a hand calculator: The Society of Naval Architects and Marine Engineers Symposium, Proceedings, Abstract, p. 6-1 to 6-13.

Polhemus, W. L., 1981, LORAN-C RNAV: The best near term solution to air operations in north eastern North America: The Wild Goose Association, Annual Technical Symposium, 10th, Proceedings, p. 153-182.

Potts, C.E., and Wieder, B., 1972, Precise time and frequency dissemination via the LORAN-C system: Institute of Electrical and Electronics Engineers, Proceedings, v. 60, no. 5, p. 530-539.

Pressey, B. G., Ashwell, G. E., and Fowler, C. S., 1956, Change of phase with distance of a low-frequency ground wave propagated across a coast-line: Institute of Electrical Engineers, Proceedings, No. 2082R, v. 103B, p. 527-534.

Radio Technical Commission for Marine Services, 1981, Minimum performance standards (MPS) for automatic coordinate conversion systems: Report of Radio Technical Commission for Marine Services Special Committee No. 75, RTCM Paper 378-81/DO-10.

Razin, S., 1967, Explicit (noniterative) LORAN solution: Navigation Journal, Institute of Navigation, v. 11, no. 3, p. 265-269.

Rokityansky, I. I., 1982, Geoelectromagnetic investigation of the earth's crust and mantle: New York, Springer-Verlag, p. 1-381.

Samaddar, S.N., 1979, The theory of LORAN-C ground wave propagation - a review: Navigation Journal, Institute of Navigation, v. 26, no. 2, p. 173-187.

Samaddar, S.N., 1980, Weather effect on Loran-C propagation: Navigation, Journal, Institute of Navigation, v. 27, no. 1, p. 39-53.

Sanders, J.H., 1965, The velocity of light: Pergamon Press, 141 p.

Schulkin, M., 1952, Average radio-ray refraction in the lower atmosphere: Institute of Radio Engineers, Proceedings, v. 40, p. 554-561.

Sodano, E.M., 1965, General non-iterative solution of the inverse and direct geodetic problems: Bulletin Geodesique, Annee, Nouvelle Serie, no. 75.

Smith, E. K., Jr., and Weintraub, S., 1953, The constants in the equation for atmospheric refractive index at radio frequencies: Institute of Radio Engineers, Proceedings, v. 41, p. 1035-1037.

Stansell, T. A., 1973, Accuracy of geophysical offshore navigation systems: Torrance, California, Magnavox Advanced Products Division, Brochure, no. MX-TR-2035-73.

Stansell, T. A., 1978, The transit navigation satellite system: Torrance, California, Magnavox Advanced Products Division, Brochure, no. R-5933/Oct., 1978.

Stratton, J. A., 1941, Electromagnetic Theory: New York, McGraw Hill Book Company, 615 p.

Stuifbergen, N., 1980, Intersection of hyperbolae on the earth: Technical Report #77, University of New Brunswick, Canada.

Terman, F. E., 1943, Radio Engineer's Handbook: New York, McGraw-Hill, p. 1-1019, Section 10.

Thomas, P. D., 1970, Spheroidal geodesics reference systems, and local geometry: U.S. Naval Oceanographic Office, SP-138, Jan 1970. (Now: Defense Mapping Agency, SPPUB-138).

Torge, W., 1980, Geodesy: Translated from German by C.

Jekeli: Berlin, Walter de Gruyta and Co., ISBN 3-11-007232-7.

U. S. Coast Guard, Department of Transportation, 1982, Harbor monitor system quarterly status review for 1 Jan 1982 through 31 March 1982: Groton, Connecticut, U.S. Coast Guard Research and Development Center.

U. S. Coast Guard, Department of Transportation, 1980 to 1981, Radionavigation Bulletin, Washington, D.C., Nos. 1-9, June 1980 to June 1982.

U.S. Coast Guard, (G-WAN-2), Department of Transportation, 1980, LORAN-C user handbook: Washington, D.C., Comdtinst M16562.3, p. 1-82.

U.S. Coast Guard, (G-NRN-1), Department of Transportation, 1981, Specification of the transmitted Loran-C signal: Washington, D.C., Comdtinst M16562.4, July, 1981.

Van der Pol, B., and Bremmer, H., 1937, 1938, 1939, The diffraction of electromagnetic waves from an electrical point source round a finitely conducting sphere: Philadelphia Magazine, Series 7, v. 4, p. 141-176, 825-864; v. 25, p. 817-834; v. 26, p. 261-275.

Wait, J.R., 1964, Electromagnetic surface waves, Advances in Radio Research, New York, Academic Press, v. 1, p. 157-217.

Wait, J. R., 1969, Concerning the theory of scatter of HF radio ground waves from periodic sea waves: Boulder, Colorado, Electronic Probing in Geophysics, Golem Press, Appendix B, p. 361-369.

Wait, J. R., 1971, On the theory of radio propagation over a slightly roughened curved earth: Boulder, Colorado, Electronic Probing in Geophysics, Golem Press, Appendix C, p. 370-381.

Wait, J. R., 1981, Wave propagation theory: New York, Pergamon Press, p. 1-346.

Wait, J. R., 1982, Geo-Electromagnetism: New York, Academic Press, p. 1-268.

Warren, R. S., Gupta, R. R., and Shubbuck, T. J., 1978, Design and calibration of a grid prediction algorithm for the St. Mary's River LORAN-C chain: The Wild Goose Association, Annual Technical Symposium, 7th, Proceedings, p. 134-143.

Watson, G. N., 1918, The transmission of electric waves around the earth: The Royal Society, Proceedings, v. A95, p. 546-563.

Weseman, J. F., 1982a, Preliminary data from the September, 1981, New England Coast Calibration or Rate 9960, private communication.

Weseman, J. F., 1982b, LORAN-C: Present and future: Navigation, Journal of the Institute of Navigation, v. 29, no. 1, p. 7-21.

Winkler, G.M.R., 1972, Path delay, its variations, and some implications for the field use of precise frequency standards: Institute of Electrical and Electronic Engineers, Proceedings, v. 60, no. 5, p. 522-529.

APPENDIX A

The arc-length tables and code shown below give:

1. Arc-length differences versus range and azimuth for the Sodano (1965), Collins (1980), and Lambert (1942), methods, using computer software with 7, 8-9 and 11 significant digit precision.

2. Program "check-out" examples giving distance, azimuth and time computed by the Sodano (1965) and DMA (RTCM, 1981) methods.

3. Station coordinates used for the tables in 2A.

4. Double precision Fortran subroutine of the Sodano (1965) arc-length method used in computations of Tables 1A and 2A.

Sodano (1965) proved least sensitive to computer precision as shown in Tables 1A, 2A and 3A. The data shown were generated by the HP-1000 RTE IV double precision ($\pm$ $2^{39}-1$, i.e. 11-12 places), the HP-1000 RTE IV single precision ($\pm 2^{24}-1$, i.e., 7 places) and an Apple II$^+$ computer (8-9 places). As seen in table 1A (column 3), both Collins and Sodano agree within

$\pm$ 1 meter. Collins (1980) shows much greater differences (column 5) at short distances with the lower (7 places) precision. Conversely, Lambert (1942) has the larger differences with higher precision (column 4) and greater differences at all distances (column 6) with the lower precision (7 places). Additionally, checks were run against examples given by Thomas (1970) on the Apple II$^+$ and agreed within $\pm$ .5 meters at distances of 8,466 and 10,102 Km. The results are in general agreement with the recent work of APL (1982).

TABLE 1A. Differences (meters) in arc length found by three different methods (S=Sodano, C=Collins, L=Lambert) and three levels of computer precision shown in the last row. Sodano double precision was used as the reference value. The symbol code is: HP double precision S_D, C_D, L_D; HP single precision S, C, L; and Apple II$^+$ S_A, C_A, L_A.

n.miles	Azimuth	C_D-S_D	L_D-S_D	C-S_D	L-S_D	S-S_D	S_A-S_D	C_A-S_D
.5	70°	.40	.14	-950.75	3458.8	-.44	-.002	5.37
1.0		.10	.06	1471.61	3521.1	-.17	0	3.66
10.0		.02	-.01	57.69	622.8	-.77	.003	.44
25.0		.01	-.03	30.40	205.7	-.72	-.002	.13
50.0		.02	-.06	50.30	124.2	-.28	-.002	.10
100.0		.03	-.13	-2.50	32.9	-.72	-.001	.07
200.0		.06	-.26	-13.60	27.3	-.30	.001	.08
300.0		.10	-.39	-1.75	15.2	.37	.003	.11
400.0		.13	-.52	2.59	8.6	-.41	.002	.13
500.0		.17	-.65	.28	.9	.28	-.001	.17
800.0		.29	-1.04	.11	-24.1	-.09	-.001	.29
1000.0		.38	-1.30	1.02	-52.7	-.98	.004	.39
1200.0		.50	-1.56	4.02	-93.0	.52	-.001	.50
.5	180°	0	.43	-.45	2192.0	-1.10	-.036	-.40
1.0		0	.30	-.89	1263.0	-.37	-.077	-.08
5.0		-.01	.12	.58	66.8	.45	-.038	-.04
10.0		-.01	.20	.29	133.6	.25	-.076	.09
25.0		-.03	.44	.23	-85.0	1.26	-.077	-.11
50.0		-.06	.87	.81	-9.7	-.77	-.038	-.10
100.0		-.12	1.72	.97	.4	.31	.036	-.08
500.0		-.53	7.48	.87	7.6	.74	-.038	-.57
1000.0		-.78	10.75	.13	-24.9	-1.67	-.071	-.85
1200.0		-.78	10.53	-.76	-45.8	.74	-.005	-.78
.5	40°	.11	.68	-61.10	2265.0	.88	.002	1.18
.9		.03	.22	-123.20	1413.8	.26	.002	1.15
90.0		0	.05	6.28	23.8	-.67	.003	.07
45.0		-.03	.15	-2.14	36.2	.10	.004	-.02
91.0		-.06	.31	-1.93	4.6	.79	.002	-.05
452.0		-.30	2.30	-.68	.1	.94	.001	-.30
890.0		-.61	5.97	-.33	-28.8	-.63	-.001	-.61
1060.0		-.73	7.60	-1.38	-58.2	-1.38	-.003	-.72
No. of Sigificant digits		11	11	7	7	7	8-9	8-9

TABLE 1A (continued): Example calculations using the 9960 rate (see tables 2A and 3A, also).

Loran Stations	Distance ($Sodano_D$) M	C_D-S_D	L_D-S_D	C-S_D	L-S_D	S-S_D	S_A-S_D	C_A-S_D
X-M	590091.87	.06	-.30	-1.87	7.75	.75	-.003	.07
X-W	638597.15	-.40	5.56	-2.15	17.10	.35	.001	-.40
X-Y	1060726.66	-.35	2.65	-.66	4.04	-.46	-.004	-.35
X-Z	1488635.85	.26	-.85	1.85	-25.65	1.35	-.001	.27
X-"opposite M"	602389.83	.06	-.23	-2.08	4.17	-.21	.001	.06
M-W	837863.03	-.07	.66	-1.53	-4.53	-.28	-.003	-.06
M-X	590091.87	.06	-.30	-1.87	7.75	.75	-.003	.07
M-Y	964985.76	-.58	8.17	.24	-2.51	-1.01	-.002	-.57
M-Z	947140.79	.06	-.26	.21	-8.29	.83	.007	.06
No. significant digits	11 places	11 places			7 places		8-9 places	

Table 2A: Example solutions made with the Sodano (1965) arc length subroutine, the positions listed in table 3A, and the H.P. double precision routine listed in table 4A.

LORAN Stations 9960	Distance $Sodano_D$ (meters)	Azmuth Forward (degrees)	Azmuth Backward (degrees)	PF + SF (microseconds)
X to M	590091.87	288.23	103.64	1969.93
X to W	638597.15	14.21	195.63	2131.88
X to Y	1060726.66	223.76	38.90	3541.31
X to Z	1488635.85	269.78	78.34	4970.06
X to "Opp.M"	602389.83	103.37	287.82	2010.99
M to W	837863.03	54.07	240.35	2797.20
M to Y	964985.76	185.99	5.31	3221.65
M to Z	947140.79	253.99	66.94	3162.06
M to "Opp.M"	1191407.66	101.18	290.24	3977.64

TABLE 3A. Latitudes and longitudes of Loran stations used in Table 2A (from USCG, 1981). Position for "Opposite-M" was arbitrarily chosen to complete data set to include all quadrants.

NORTHEAST U. S. LORAN-C CHAIN - GRI 9960

STATION	FUNCTION	COORDINATES DEG MIN SEC	COORDINATES DEGREES
SENECA, NY	MASTER	42° 42' 50.''60N 76 49 33.86W	42°.71405556 -76.82607222
CARIBOU, ME	WHISKEY	46 48 27.20N 67 55 37.71W	46.80755556 -67.92714167
NANTUCKET, MA	XRAY	41 15 11.93N 69 58 39.09W	41.25331389 -69.97752500
CAROLINA BEACH, NC	YANKEE	34 03 46.04N 77 54 46.76W	34.06278889 -77.91298889
DANA, IN	ZULU	39 51 07.54N 87 29 12.14W	39.85209444 -87.48670556
"OPPOSITE M"	--	--	39.79262776 -63.12897778

```
      TABLE 4A:   DOUBLE PRECISION FORTRAN SUBROUTINE OF SODANO ARCLENGTH
                  METHOD USED IN COMPUTATIONS OF TABLES 1A AND 2A.
C
FTN4
      PROGRAM SODDP
C
C                          ARCLENGTH  (SODANO 1965)
C
      SUBROUTINE ARCL2 (Y,X,D,AS,AB,T)
      DOUBLE PRECISION Y,X,D,AS,AB,T,
     *                   PI,PI2,AA,BB,C,K1,K2,F1,F2,
     *                   LO,G1,G2,G3,H,G4,G5,
     *                   AN,C1,AM,G6,G7,R,
     *                   D1,D2,D3,D4,D5,
     *                   XY,XX,W
      DIMENSION Y(2),X(2)
      COMMON PI,PI2,AA,BB,C,K1,K2
      LO=LOGLO(ILO)
      PI=3.1415926535890D0
      PI2=PI*2.D0
      AA=6378135.0D0
      BB=6356750.5D0
      C =299.69116D0
      K1=PI/180.D0
      K2=180.D0/PI
      F1=1.D0-(BB/AA)
      F2=F1**2
C
      LO = X(2) - X(1)
      IF(DABS(LO).LE.PI) GOTO 5
      LO=-DSIGN(PI2,LO)+LO
    5 G1=DATAN(DTAN(Y(1))*(1.D0-F1))
      G2=DATAN(DTAN(Y(2))*(1.D0-F1))
      G3=DSIN(G1)*DSIN(G2)
      H=DCOS(G1)*DCOS(G2)
      G4=G3+H*DCOS(LO)
      G5=DSQRT((DSIN(LO)*DCOS(G2))**2
     *   +(DSIN(G2)*DCOS(G1)-DSIN(G1)*DCOS(G2)*DCOS(LO))**2)
      AN=DATN2(G5,G4)
      C1=H*DSIN(LO)/G5
      AM=1.D0-C1**2
      G6=(F1+F2)*AN+G3*((-F2/2.D0)*G5-F2*AN**2/G5)
      G7=AM*((-5.D0*F2/4.D0)*AN+(F2/4.D0)*G5*G4+F2*AN**2/DTAN(AN))
      R=(G6+G7)*C1+LO
C
C                 AS = AZM FORWARD
C
      XY=DSIN(R)*DCOS(G2)
      XX=DSIN(G2)*DCOS(G1)-DCOS(R)*DSIN(G1)*DCOS(G2)
      AS=DATN2(XY,XX)
      IF(AS.LT.0.D0) AS=AS + PI2
C
C                 AB = AZM BACKWARD
C
      XY=DSIN(R)*DCOS(G1)
      XX=DSIN(G2)*DCOS(G1)*DCOS(R)-DSIN(G1)*DCOS(G2)
      AB=DATN2(XY,XX)+PI
      IF(AB.LT.0.D0) AB=AB + PI2
```

Table 4a (Continued)

```
      C
      C                 ARC DISTANCE
      C
            D1=(1.D0+F1+F2)*AN+G3*((F1+F2)*G5-(F2/2.D0)*AN**2/G5)
            D2=AM*((F2/2.D0)*AN**2/DTAN(AN)-(F1+F2)*.5D0*AN-(F1+F2)*.5D0*G5*G4)
            D3=G3**2*(-F2/2.D0)*G5*G4
            D4=AM**2*((F2/16.D0)*AN+(F2/16.D0)*G5*G4-(F2/2.D0)*AN**2/DTAN(AN)
           *   -(F2/8.D0)*G5*G4**3)
            D5=G3*AM*((F2/2.D0)*AN**2/G5+(F2/2.D0)*G5*G4**2)
            D=(D1+D2+D3+D4+D5)*BB
      C
      C                   DISTANCE TO TIME+SF
      C
            W=D/C
            IF(W.GT.537.D0) GO TO 230
            T=2.7412979D0/W-.011402D0+3.2774624D-4*W + W
            GO TO 240
      230   T=129.04398D0/W-.40758D0+6.4576438D-4*W + W
      240   RETURN
            END
            END$
```

APPENDIX B

The following equipment and procedures were used in the offshore ASF survey.

1. Equipment used:

   a) JMR-4 Sealand Surveyor Satellite Receiver w/program G-1.
   b) NORTHSTAR 6000 (stand alone).
   c) Integrated Navigation System (INS) including Hewlett Packard 21 MX Computer, Magnavox MX702A-3 Satellite Receiver, NORTHSTAR 6000 LORAN-C Receiver, Sperry 301 Doppler Speed Log, and Sperry Mark 29 Gyro Compass, Western Geophysical Transit Satellite software.

2. General Notes:

   a) Integrated Navigation System (INS) used for survey control (course and speed).
   b) MX702A-3 uses a real time input of course and speed VIA INS.
   c) JMR-4 uses a manually entered course and speed, usually the "averaged" values prior to lock on.
   d) TD's are interpolated (.01 microseconds) from 5 minutes spot values to match satellite fix times.
   e) NORTHSTAR 6000 receiver resolution is 0.1 microseconds.

3. Data selection criteria for MX and JMR receivers.

   a) Maximum satellite elevation in the range 15^{o} to 60^{o} inclusive.
   b) Continuous 150 and 400 MHz, $\pm$ 2 minutes from closest approach.
   c) Sigma of doppler residual less than 6.
   d) No change of course or speed noted.
   e) No recomputed fixes used.
   f) No asymmetric passes used.
   g) Sea state less than about 5.

4. Data selection criteria for NORTHSTAR 6000 LORAN-C

   a) SNR greater than 250 North Star units.
   b) No obvious receiver errors.
   c) No adverse log comments.

SESSION III

POSITIONING II

THE LONARS-AIDED DOPPLER SOLUTION
A NEW METHOD FOR PRECISE POSITIONING AT SEA

T. Jerardi, Applied Physics Laboratory
Laurel, Maryland
B. Merritt, Defense Mapping Agency
Hydrographic Topographic Center,
Washington, D. C.

ABSTRACT

LONARS is a precision position-fixing system based primarily on the use of LORAN-C Radionavigation. This system is used to precisely position test platforms in a 2500 square mile ocean area off the Florida coast. To meet future stringent accuracy requirements, APL and DMA personnel undertook an at-sea calibration of LONARS during April 1980.

The single pass Doppler solution using the Magnavox Geoceiver and DMAHTC precise ephemeris was chosen as the calibration standard. The LONARS system was used to model ship's drift during each Doppler pass. Included in the paper is an analysis of significant error sources in the Doppler fix, the utility of shore-ship single pass translocation, and a summary of operational problems encountered during the at-sea calibration. The estimated accuracy of LONARS-Aided Doppler was found to be 10 meters one-sigma.

INTRODUCTION

During the first half of 1980, a task to calibrate Loran-C over a 2500 square mile area off the coast of Cape Canaveral, Florida was jointly undertaken by the Applied Physics Laboratory of the Johns Hopkins University (APL/JHU) and the Defense Mapping Agency Hydrographic Topographic Center (DMAHTC), under the sponsorship of the U.S. Navy. The geodetic reference coordinates for this calibration were based on the Transit navigation satellite system. The Loran-C data was obtained by LONARS (Loran Navigation and Receiving System) developed by APL/JHU for the U.S. Navy.

A description of this calibration effort which focuses primarily on Loran-C issues has recently been reported by Fehlner and Jerardi [1]. The following discussion will be focused on the geodetic reference supplied by the Transit system after a brief introduction to the LONARS system.

THE LONARS SYSTEM

LONARS is a precision navigation system based on Loran-C*. The superior performance of LONARS is achieved by a novel application of robust statistics to the tracking filters within the LONARS receiver [2]. Figure 1 displays a shipboard LONARS system. The core of the LONARS system is a Hewlett Packard 21MX-E minicomputer. The robust tracking filters are implemented in software within the 21MX-E.

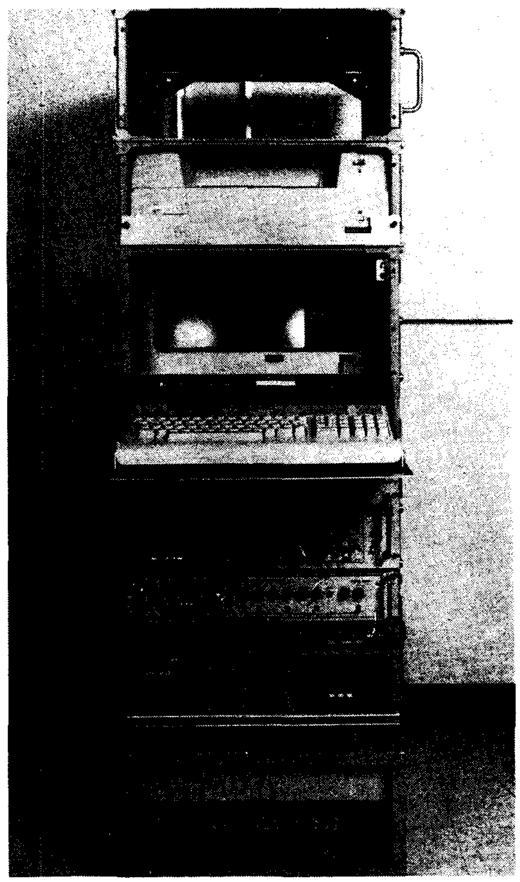

Fig. 1 LONARS shipboard equipment.

*A short description of the Loran-C system is given in Appendix A.

CALIBRATION CONCEPT

To fully realize the potential of the LONARS signal processing algorithms, a system calibration is required. The purpose of the LONARS calibration is the development and validation of a procedure to convert loran time differences to geodetic coordinates. This conversion process is composed of two components, a geodetic component and a propagation component. The geodetic component is the computation of geodetic arc lengths, from which range differences may be readily computed. It was determined that the geodetic component represented no particular problem, given the coordinates of the end points and that any of several arc length algorithms could be used. The Andoyer-Lambert [3] algorithm was used for the model development due to its simplicity. The propagation component is a model which accounts for Loran-C groundwave propagation in order to derive range differences from loran time differences.

The general plan for any loran calibration is therefore defined as obtaining a coordinated set of loran time differences and corresponding geodetic coordinates. From the geodetic coordinates the range differences can be computed. These range differences and time differences are then the inputs to a regression procedure to determine various propagation parameters.

From statistical design considerations a uniformly spaced data set offers the most flexibility and accuracy for the subsequent regression analysis. Figure 2 graphically displays the overall data acquisition plan. The small solid circles represent the primary calibration data to be used for model development. The small solid squares represent a secondary data set to be used for model validation. A simple rectilinear "site-code" grid is used for identification.

The quality of the geodetic coordinates is of vital importance in any such calibration. A clear choice for the reference system is a current state-of-the-art Transit Integral Doppler point position system, which could be adapted to handle platform motion. DMAHTC's DOPL79 program was thus chosen.

EVOLUTION OF DOPL79

The Defense Mapping Agency Hydrographic Topographic Center (DMAHTC) has had a solitary point position reduction capability since 1971. The original software DOPPLR [4] was developed in 1970 as part of the effort in the geodetic community to achieve station position solutions of geodetic quality from the Doppler tracking of Transit Satellites (Navy Navigation Satellites, NNS), using the then newly developed Geoceiver. Extensive testing of DOPPLR occurred during the Department of Defense Geoceiver Test Program [5] which concluded that the solitary point posi-

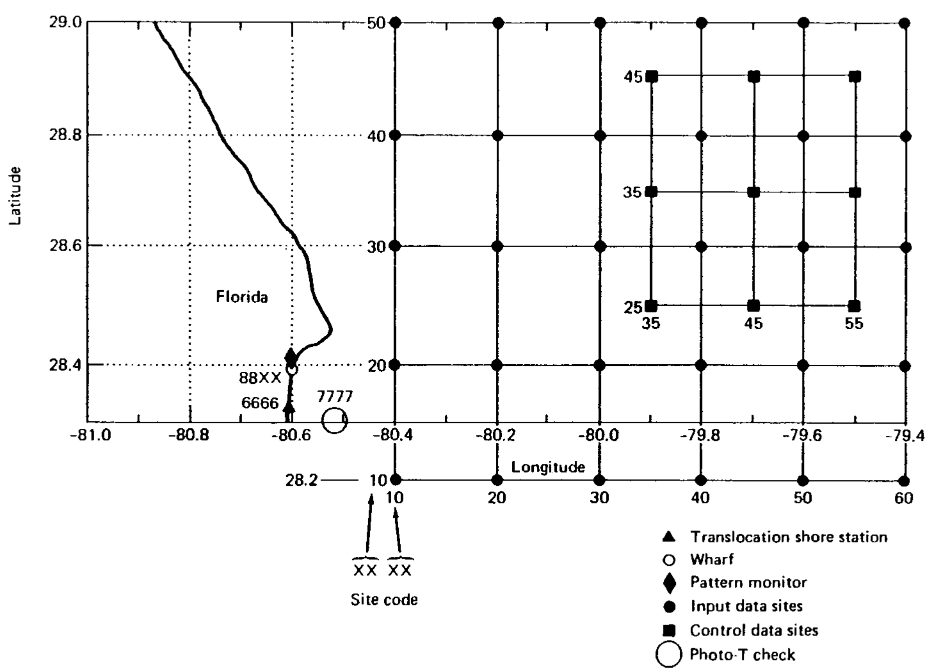

Fig. 2 Calibration area showing planned survey sites

tioning mode of operation (NWL Precise Ephemeris held fixed) would be the primary approach to reduction of Geoceiver data within DoD. The report assigned an accuracy of 1 meter for each component at the one sigma confidence level for a balanced set of 30 - 50 Transit passes. The stated accuracy was arrived at through comparisons with the High Precision Geodimeter Traverse in the United States.

As a result of great interest in achieving submeter positioning accuracies, an updated and recoded version of the original program began production use in January, 1979. The new version, called DOPL79, carried a number of minor model changes, in the data editing function, and a more accurate ephemeris interpolation procedure [6]. Although no external comparisons have been done, the one sigma precision estimate for 30 - 50 TRANSIT passes, assuming properly functioning standard equipment, is 0.70 meters for each axis. This number is based on reductions of several thousand passes from a number of semi-permanent tracking stations.

Program DOPL79 is the last processing stage of a complex of Fortran 66 computer programs, together called the Doppler Geodetic Point Positioning (DGPP) system residing on the Univac 1100/81 computer at DMAHTC. The DGPP system will process a variety of receiving equipment formats into nominal 30 second Doppler count data, access the appropriate Precise Ephemeris (PE) spans which reside on removable disk packs, and perform the adjustment. Raw data on magnetic tapes created on an Interdata mini computer is the normal input mode for DGPP. The PE has been computed since May 1975 in a routine production fashion at DMAHTC.

CALIBRATION DATA FLOW

Prior to this calibration the geodetic accuracy of LONARS was dominated by errors with very high spatial correlation. This fact allowed LONARS data to be used to compensate for platform motion in the Transit solution. To minimize the effect of correlated errors within the Transit system a translocation technique was used.

Figure 3 indicates the overall data flow to support this scheme. The Doppler data from the ship and shore sites was forwarded to DMAHTC via Autodin where it was handled independently through the reformatting and preprocessing steps. The LONARS data was processed by APL/JHU and a tape file of ship's position was supplied to DMAHTC. A file of loran time differences was also created for the actual calibration computation. As figure 3 indicates, the final doppler adjustment program requires three data inputs: fixed site doppler related data, ship doppler related data, and LONARS ship motion data.

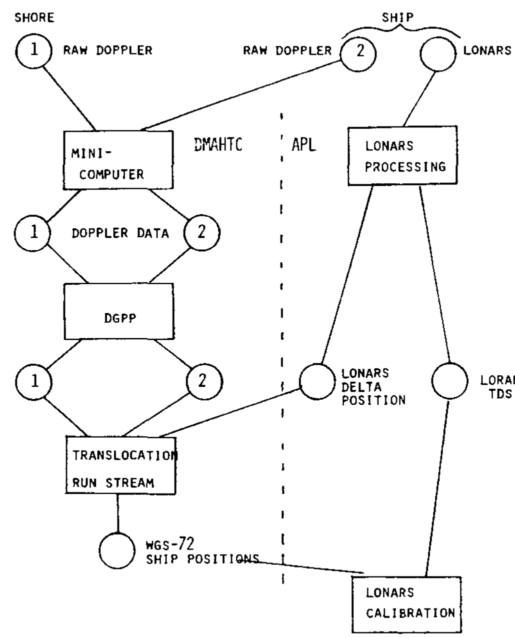

Fig. 3 LONARS project data flow.

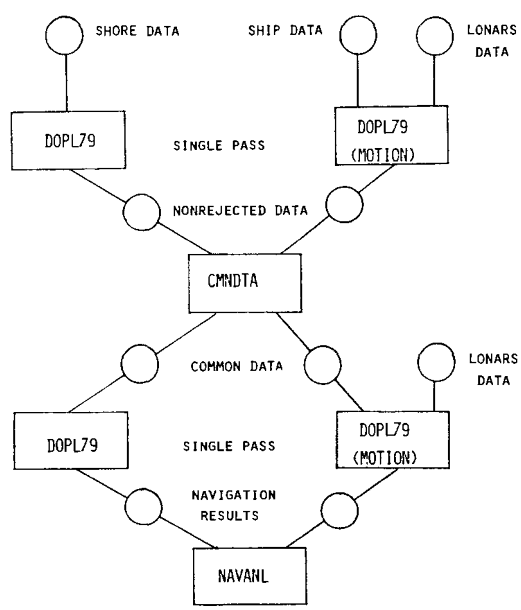

Fig. 4 Translocation runstream.

MODIFICATIONS TO DOPL79 SOFTWARE

The motion compensated, height constrained single pass solution with ship - shore data point matching was used to determine the relative position of the ship at a chosen epoch with respect to the shore station. This involved the following steps (See Figure 4).

a. Perform a single pass solution for the shore station with 2.5 sigma data editing.

b. Perform a motion compensated single pass solution for the ship with 2.5 sigma data editing.

c. Determine the non-deleted observations common to both solutions.

d. Repeat a. and b. except disable data edit function and only allow common points from c. into the solutions.

e. Difference cartesian coordinates from d. and apply to the shore station reference coordinates to obtain the final ships coordinates.

To perform the listed steps in a more or less automated fashion required modifications to existing software. A breakout of DOPL79 into functional modules is shown in Figure 5 with modifications for this project shown in parentheses.

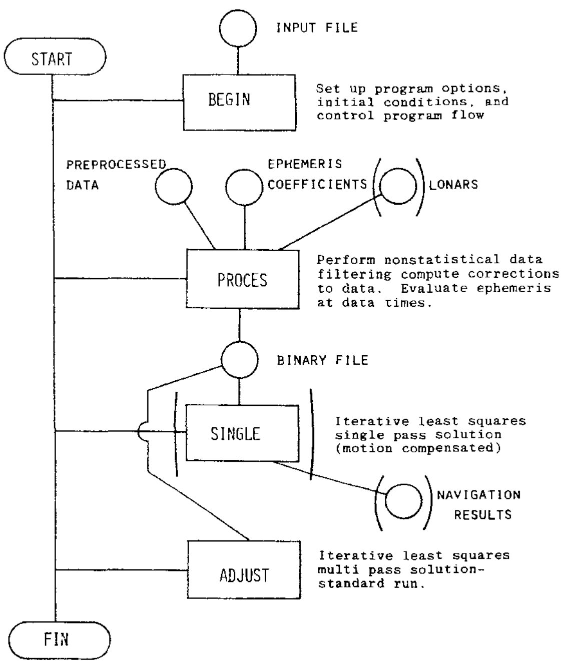

Fig. 5 (5) DOPL79 program flow with modifications for project in parentheses.

SINGLE PASS PROCESSING CAPABILITY

Production multipass processing in DOPL79 involves a batch fit to all non-rejected data, and the navigation solution is not required. This capability was coded as an additional functional module (SINGLE) in the program. A two-dimensional solution in either the horizontal plane or the Guier plane may be output. The measurement model used was identical to the multipass case, except the time delay parameter was assumed known and the tropospheric scaling parameter was not determined. The model is given in more detail in Appendix B.

SHIP MOTION COMPENSATION

To solve for ship's coordinates at a particular epoch, the change in ship's position with respect to its position at epoch must be known a priori over the duration of a Transit pass. Including these "delta position" corrections into the normal computation of slant range difference will correct the data for the effect of a drifting platform, leaving only the signal due to a fixed site (Fig. 6).

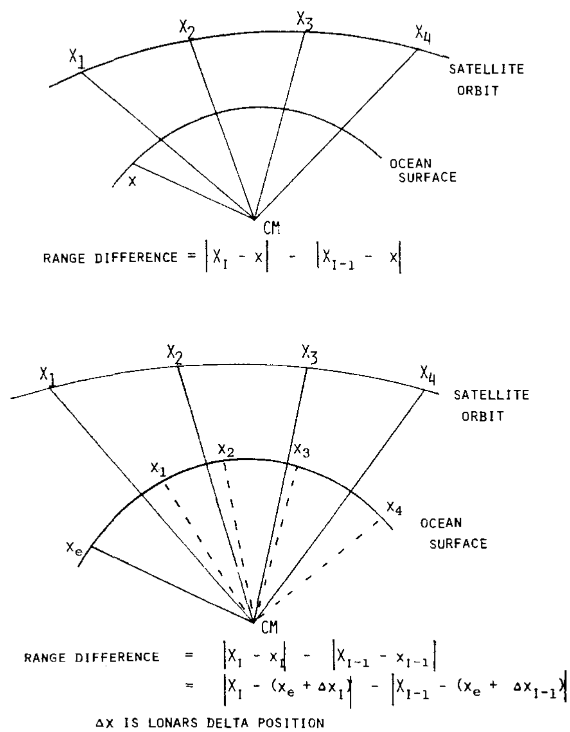

Fig. 6 Doppler measurement models.

Note that the nature of the measurement model requires that the position corrections be known only at the end times of each Doppler counting interval.

The LONARS position measurements were smoothed and interpolated for Transit emit times at APL. Satellite alerts generated at DMAHTC provided the appropriate time spans. An epoch was chosen several minutes before scheduled rise time and LONARS delta positions (LDP's) were generated with respect to that epoch. This epoch became the epoch time of the Doppler fix, and the LONARS derived horizontal coordinates became the initial horizontal coordinates in the solution. The ellipsoid height at which the solution was constrained was obtained by adding the known MSL height of the antenna to the NASA GEM 10-B geoid height, interpolated from a grid generated for the survey area.

The LDP's were input to DOPL79 as an additional input file in a pass by pass matchup with the standard Doppler data and PE coefficients. In module SINGLE, the observation equation and the data partials were modified to accommodate the LDP's. The following mathematical approximations were made due to the small drift over a pass (less than 3 Km) or the small instantaneous velocity (less than 3 meters/sec) of the ship:

a. The ships velocity contribution to the equipment delay range rate terms ($\dot{\rho}$) was ignored.
b. The LDP's were evaluated at the satellite emit times instead of the station receive times.
c. The initial coordinates were used in all tropospheric model computations.

These modifications are detailed in Appendix B.

TRANSLOCATION RUNSTREAM

Because no orbit corrections were applied, the proper name for the method used is "Simultaneous single pass point positioning with common data enforced". Once the processing sequence was automated, computations generally proceeded smoothly. Normally 15-20 pairs of passes were processed at a time. The shore station reference coordinates were the result of a 40 pass DOPL79 solution observed before the start of the at-sea campaign. The modified program provided data residual correlation analysis and quality control flags for each pair of passes. Among the quantities monitored were data residual rms, two-frequency ionospheric corrections, shore station navigation errors, numbers of times loss of lock occurred, and amount of common data.

PRE-MISSION STUDIES

Prior to the field data collection operation a number of small studies were conducted to understand the effect of various error sources. These studies also allowed the modified software to be tested under controlled conditions.

An enumeration of the error sources in a single pass Doppler fix would include the following:

a. Satellite ephemeris

b. Satellite antenna electrical center

c. Satellite oscillator

d. Higher order ionospheric refraction

e. Residual tropospheric refraction

f. Constrained height of solution

g. Preamp, receiver noise

h. Tracking antenna electrical center

i. Local environment (RFI and multipath effects)

j. Unmodeled station motion during a pass (LDP errors)

Simultaneous Doppler tracking by two stations in geometrically similar positions with respect to the satellite allows a more accurate relative positioning because terms (a. - f.) tend to be of the same magnitude and sign, and have a cancelling effect. Error sources (g. - j.) are independent by station and define the theoretical limit of accuracy attainable using translocation methods.

Note that for a ship-shore tracking pair, item j. is a non-cancelling error. The LDP corrections turned out to be the single largest error source in this project, some what limiting the normal improvement allowed by translocation.

Some pre-mission testing with existing land based data sets was done to exercise the single pass software and to develop insights into PE/DOPL79 single pass accuracies. In all runs, a 5 degree data end point cut off was used, and reference coordinates were taken from the multipass solution results. Unweighted rms navigation errors for individual stations and between stations are given in Table 1.

Two Ohio, USA data sets tracked at separations of 0.5 degrees in latitude and 0.8 degrees in longitude had 16 common passes. With no selective pass editing, a slight improvement in relative precision over individual station precision is seen (Table 1, Test 1). If certain pass pairs are deleted based on output statistics from each solution, improved relative results are obtained (Table 1, Test 2). Whily only about half of the data were used, the repeatability is at the several meter level. Edit cirteria were developed empirically and included quantities such as solution data variance, but did not include the size of the individual navigation errors.

Two standard geoceiver sets (separate antenna, preamp, and oscillator) tracked 33 common passes at the DMAHTC Herndon, Virginia Electronics Lab in February, 1980. The antenna separation was roughly 4 meters. The relative positioning results (Table 1, Test 3) indicate that the noise

Table 1

Translocation testing with real data

TEST	STATION	PASSES INPUT/USED	RMS Navigation Errors ϕ,m	λ,m	$\Delta\ \phi$,m	$\Delta\ \lambda$,m
1	Ohio 1	16/14	3.0	5.2	1.3	4.9
	Ohio 2		2.4	3.9		
2	Ohio 1	16/8	3.9	4.0	1.2	2.0
	Ohio 2		3.1	3.6		
3	30682A	33/29	1.3	1.7	0.4	0.7
	30682B		1.3	1.9		
4	Ohio 1	16/8	3.9	4.0	1.6	7.9
	Ohio 2		3.5	6.3		
5	Ohio 1	16/8	4.2	5.0	1.2	2.9
	Ohio 2		3.5	6.3		

contribution of the tracking equipment to translocation accuracies is below the 1 meter level. The low single station errors are due to collacation with TRANET STATION 407, which is used to reduce the PE.

Twenty five passes from Station 1 (Ohio) were used to simulate data and model errors which would be encountered in the reduction of the ships Doppler data. Two of the errors, ship motion due to waves and linear growth in ship's position, are related to the LDP corrections. The third error studied was constraint of the solution at a height which may be inconsistent with the PE system. RMS of navigation errors were examined as in the previous section.

Data were generated from a sine wave with period of 15 seconds and 2 meters peak to peak. The perturbation was applied separately in the North, East and Up directions. RMS navigation errors were always 3 meters or less, and the solution did not appear overly sensitive to this effect.

A ramp error in station location of 1 meter/minute was applied as an LDP error separately in the North and East directions. Longitude navigations were found to be very sensitive to the ramp in the North direction, with an RMS navigation error of over 20 meters clearly exceeding the error budget. Other combinations were all less than 7 meters.

For a ship at sea the station height is the most natural coordinate to be considered completely known in the Transit navigation solution. To study the propagation of height error into the navigation, the Ohio translocation results (Table 1, Test 2) were taken as a standard. The run was repeated with the height of Station 1 constrained at 5 meters above its optimal (multi-pass) value as shown in Table 1, Test 4. Note that the relative latitude precision is about the same, but the relative longitude precision degrades by a factor of 4. A second run was made with both station heights increased by 5 meters, and the relative longitude was similar to the standard run (Table 1, Test 5).

These results imply that the differential height error in a translocating pair is a critical factor. It is apparent that some inconsistency may result in using a PE-derived ellipsoid height for the shore station and a gravimetric (geoid plus MSL) height for the ship. Thus the NASA GEM 10-B geoid model was used to generate heights for both shore and ship reductions.

The solution longitude shows the greatest sensitivity to the aforementioned errors. It was decided that passes below

15 degrees at Time of Closest Approach (TCA) would not be tracked to reduce the effect of propagation errors and wave induced ship motion. To alleviate adverse error propagation into longitude due to translocation geometry, motion errors, and differential height errors, passes with TCA above 70 degrees were not considered. Also an attempt was made to balance a pass east of station with a pass west of station in a given area to average geometry dependent errors.

It was concluded that the error budget of 15 meters could bemet if the GEM 10-B geoid was differentially accurate to 1-2 meters and if motion errors were .5 meter/ minute or less.

DATA COLLECTION

The data collection effort was conducted during April of 1980, using the Research Vessel EL TORO (see Figure 7). The instrumentation (Geoceivers and LONARS) was housed in an equipment module located aft on the upper deck of the EL TORO (see Figure 8).

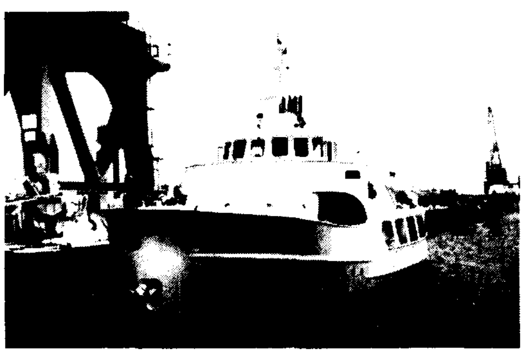

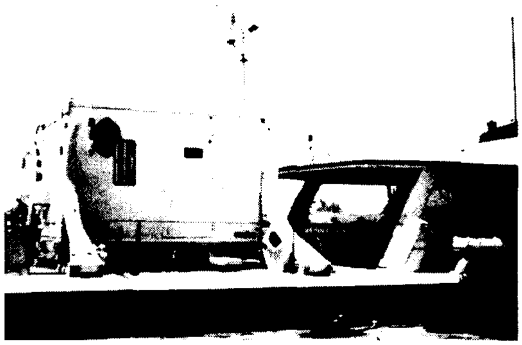

Fig. 7 and 8 R. V. EL TORO and equipment module.

Figure 9 indicates the actual data collected. The Transit data collected was from satellites 30130 (59), 30140 (60) and 30190 (68). As indicated in Figure 9, five Transit passes were taken at a point denoted "Photo-T area". In this area, precision Photo-Theodelite tracking was used during the initial checkout. This checkout allowed for both equipment performance evaluation and to prove-in the data collection procedures.

The essential feature of the data gathering procedure was that the vessel was dead-in-water during the Transit passes. This drift process allowed for simpler models to be used to describe the platform motion during the Transit passes. Premission analysis indicated that if the vessel were "driven" during the pass, the various "controlled" ship tracks might prove difficult to accommodate.

DOPPLER DATA ANALYSIS

A total of 68 valid passes were taken between 15 April and 25 April 1980 by the ship while at sea. During that same period 86 passes were recorded at the shore station. Three passes were recorded by the ship while moored to the wharf.

It appears that less than 5% of the Doppler fixes taken were bad due to ephemeris quality or receiver malfunction. Histograms of single pass RMS data residuals and navigations for the shore station are given in Fig. 10. Note that the shore navigations are generally of excellent quality, with mean errors of 2.3 meters in latitude and 3.3 meters in longitude. The shipboard RMS data residuals (Fig. 11), with a mean of 0.90 meters, are nearly 5 times greater on average than those of the shore station, reflecting the error effects discussed earlier. The magnitude of this superimposed noise effectively disabled the outlier rejection process that would occur at lower noise levels. Correlation coefficients computed for the ship and shore Doppler residuals were generally less than ±0.2. The ship residuals consistently showed greater structure. Several of the shipboard passes recorded during periods of high sea state were rejected because their data residuals were significantly higher than shown in Fig. 11.

The 5 Photo-T and 3 dockside passes allow for an independent evaluation of the overall system performance. Figure 12 is a plot of the position errors from these two sets. The dockside fixes used the LONARS data for platform motion compensation, even though the actual ship's velocity was zero. A number of dockside passes were lost due to an equipment malfunction, which went unnoticed for several days. We were thus left with only 8 independent samples. Even this small sample size indicated the validity of the pre-mission studies and the full scale data collection proceeded.

CALIBRATION RESULTS

A detailed discussion of the Loran-C propagation model that was developed is given in Reference 1. We will summarize

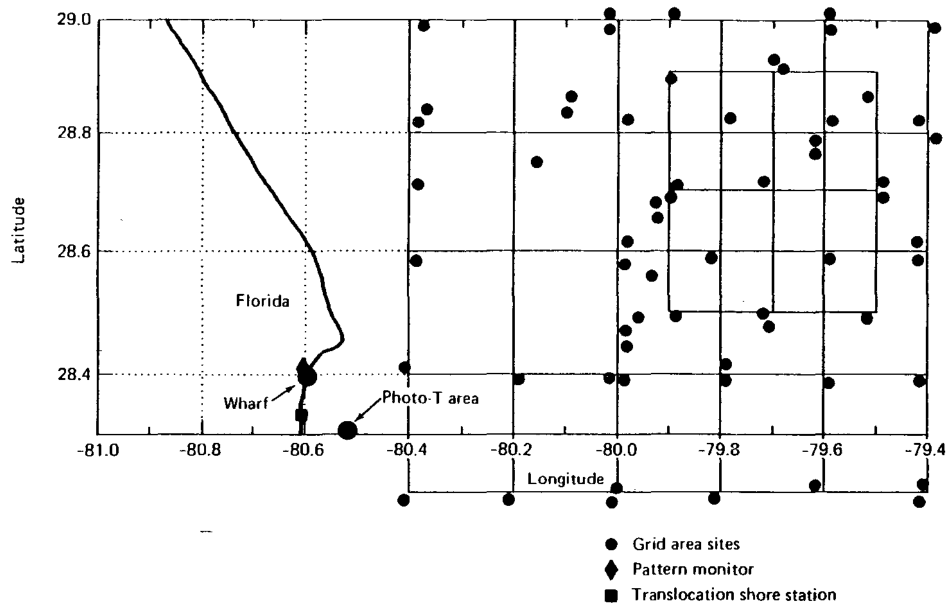

Fig. 9 Calibration data collected.

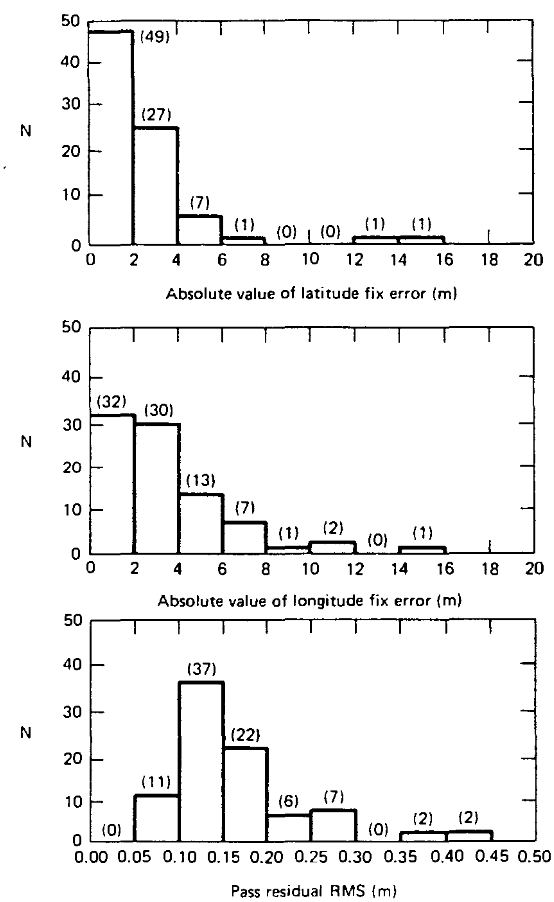

Fig. 10 Shore station single pass statistics.

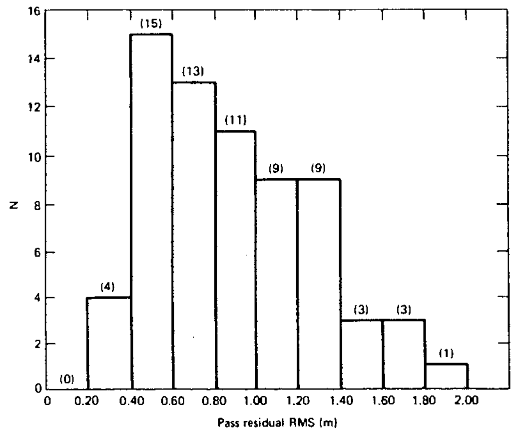

Fig. 11 Mobile station single pass statistics.

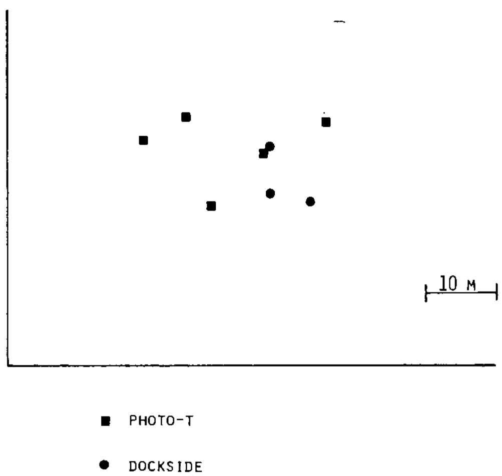

Fig. 12 Position error plot.

here the major findings. A single ground-wave propagation velocity could be used for all 3 propagation paths (Malone, Jupiter and Carolina Beach). The value of this sea-water (4-5 mhos/meter) propagation velocity is 299.569 ± 0.012 meters/microseconds. Since the Jupiter and Carolina Beach paths are almost totally over sea-water, this leaves only an offset parameter (emission delay, see Appendix A) to be determined.

The propagation from Malone is a mixed path, part over land and part over sea. The effect of this mixed path can be accommodated by a correction term dependent on the azimuth to the Malone transmitter. The rational of the correction term is based on the fact that over the area of interest the faction of land path to total path varies linearly with azimuth. As above, there is also an offset term (emission delay) required.

There are several facets of this mixed path that have not been explored (e.g., coastal refraction). The overall LONARS system accuracy using the above model is estimated to be better than 16 meters radial over the entire area. Since the requirements were met there has been little support for further study of this mixed path propagation.

As a byproduct of the LONARS calibration data analysis we obtained estimates of LONARS-Aided Doppler fix accuracy. The error distribution is elliptical with the longitude about 10 meters 1 sigma and latitude about 5 meters 1 sigma.

CONCLUSIONS

From the point of view of "surveying" at sea, we feel that 10 meters accuracy per pass can be readily achieved with current equipment and software. In order to substantially reduce this, further development is needed. The magnitude of the longitude error clearly indicates where the effort is required. Additional instrumentation for roll, ptich and heave (vertical velocity) will likely be required.

The use of "Translocation" did not significantly reduce the position errors but this procedure provided an excellent quality control tool for detecting errors in the ephemeris data. For this reason translocation is recommended even when using the Precise Ephemeris.

APPENDIX A

THE LORAN-C SYSTEM

Loran-C is a low frequency (100 khz), pulsed, hyperbolic navigation system. The geographic arrangement of the Southeast U.S. Loran-C chain is given in Fig. A.1.

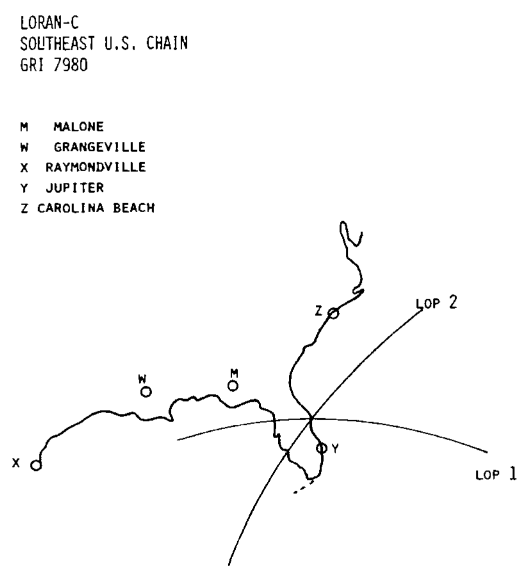

Fig. A.1 Southeast U. S. chain.

A chain is composed of 3 or more stations. One station is designated as the master and all other stations are designated as secondaries. A chain is identified by its Group Repetition Inverval (GRI) which is the period (in tens of microseconds) between pulse groups that each station transmits. The Southeast U.S. chain has a GRI of 7980 which means the stations transmit periodically with a period of 79800 microseconds.

Each station transmits a group of 8 pulses that are separated by one millisecond. This group of pulses allows a phase coding process to be used so that the master can be distinguished from the secondaries. The overall chain signal format is by time sequencing the stations so that no two signals are received simultaneously.

The transmission pattern is as follows:

1. The master transmits its coded group of 8 pulses.
2. At a fixed time after the master transmission (known as emission delay) the first secondary transmits its coded group of 8 pulses.
3. Sequentially the other secondaries transmit each at a unique emission delay as in 2.
4. At the GRI, the master again transmits and the entire process is repeated.

A receiver in the service area tracks (i.e., measures the phase with respect to a local clock) the various stations in a chain. This process yields the times of arrival (TOA's) of the various stations with respect to a local clock. From three such TOA's two time differences (TD's) can be formed by using one of the TOA's as a reference TOA. These time differences are the fundamental Loran-C coordinates. The lines of constant time difference are hyperbolas with the stations as foci.

APPENDIX B

TRANSIT POSITION FIXING OF A MOVING PLATFORM

B.1 Standard (Stationary Receiver) Solution

A single pass solution modeling of Geoceiver Doppler observations in the reduction program DOPL79 (program file DOPPLR-test) can be described by the following observation equation:

$$O_1 \approx C_i = DR_i/\lambda + \Delta F \Delta T_i + ION_i + TROP_i + CORR_i + \dot{DR}_i * TD/\lambda$$

Where

O_i = iTH observed Doppler count

C_i = iTh computed Doppler count

DR_i = iTH station to satellite range difference, computed from the iTH and i + 1TH station to satellite ranges. DR_i implicitly contains the station location parameters $\overline{X}$.

Thus

$$DR_i = R_{i+1} - R_i$$

And

$$R_i = \sqrt{(X_{SATi}-X)^2+(Y_{SATi}-Y)^2+(Z_{SATi}-Z)}$$

λ = wave length of transmitter Doppler signal

ΔF = satellite-station frequency offset parameter

ΔT = ith integration interval at the satellite

$\dot{ION}_i$ = ith two frequency ionospheric correction

$TROP_i$ = ith tropospheric refraction correction (Hopfield)

$CORR_i$ = a set of correction terms applied to the ith observation including the following:

- CL_i = corrects ith count for propagation times of the Doppler signal
- PC_i = corrects ith count for residual difference between ground clock and satellite clock intervals
- ERC_i = corrects ith count for earth rotation correct effect

$\dot{DR}_i$ = same as DR_i except applies to instantaneous range rate instead of range

TD = equipment delay, assumed known.

The three cartesian coordinates and frequency offset are carried as unknowns in a linearized, iterative, constrained least squares solution. The a priori constraint (Guier plane [7,8] or station height) is applied to the normal matrix as a weight matrix in cartesian space. Convergence is satisfied when the current coordinates change less than 0.01 meter between iterations. Outlier data point stripping is done at 2.5 times RMS of residuals.

In the standard solution the following terms are computed from an approximate initial coordinate $\vec{X}^o$):

$$TROP_i = TROP_i\ (\vec{X}^o)$$

$$PC_i = PC_i\ (\vec{X}^o)$$

The values of $\vec{X}^o$ in error by more than 10 kilometers will show decimeter level changes in the fix position. For the constrained height solution the weight matrix is recomputed if $\vec{X}^o$ is more than 100 meters off.

B.2 Modifications for a Moving Platform

The fundamental difference is that $\vec{X}$ becomes $\vec{X}(t)$ where t is time. Thus any computation involving station position becomes time dependent. The LONARS delta position inputs are correction terms $\Delta\vec{X}_i$ at time T_i to the station position $\vec{X}_E$ at a certain epoch T_e. The constant $\vec{X}$ is replaced by

$$\vec{X}_i = \vec{X}_E + \Delta\vec{X}_i$$

The station location parameters are now $\vec{X}_E$.

a. The range is then

$$R_i = \sqrt{(X_{SATi}-X_i)^2+(Y_{SATi}-Y_i)^2+(Z_{SATi}-Z_i)^2}$$

b. The partial derivative with respect to station location is updated with $\vec{X}_i$

c. The terms Cl_i and ERC_i are computed with $\vec{X}_i$

d. The contribution of ground station instantaneous velocity to the DR_i terms is ignored.

e. The terms $TROP_i$ and PC_i are evaluated with the initial epoch position $\vec{X}^o{}_E$ only:

$$TROP_i = TROP_i\ (\vec{X}^o{}_E)$$

$$PC_i = PC_i\ (\vec{X}^o{}_E)$$

f. $\Delta\vec{X}_i$ are evaluated at satellite emit times instead of station receive times.

For a vessel freely drifting on the ocean surface with $\vec{X}^o{}_E$ derived from the LONARS system, the approximations made in d., e., and f. are valid.

REFERENCES

1. Fehlner, Leo F. and Thomas W. Jerardi, "The Calibration of Loran-C at Sea," Radionavigation Journal 1980-81, The Wild Goose Association, Acton, Ma.

2. Jerardi, Thomas W. "Robust Real Time Filtering of Loran Signals," Radionavigation Journal 1980-81, The Wild Goose Association, Acton, Ma.

3. Aeronautical Chart and Information Center, Geodetic Distances and Azimuth Computation for Lines under 500. Miles, ACIC Technical Report No. 59, September 1960.

4. Smith, R. W., C. R. Schwarz, and W. D. Googe, "DOPPLER - A Point Positioning Program Using Integrated Doppler Satellite Observations," DMATC Report No. 76-1, April 1976.

5. "Report of the DoD Geoceiver Test Program," published by the DoD Coordinating Committee for Geoceiver Test Program Report, DMA Report 001, July 1972.

6. Jenkins, R. E., B. D. Merritt, D. R. Messent, and J. R. Lucas, "Refinement of Positioning Software (DOPPLR)," Proceedings of the Second International Symposium on Satellite Doppler Positioning, Vol. I, pp. 233-266.

7. Guier, W. H., "Studies on Doppler Residuals - I: Dependence on Satellite Orbit Error and Station Position Error," APL/JHU Technical Report: TG-503, June 1963.

8. Guier, W. H., "Geodetic Problems and Satellite Orbits," in Space Mathematics Part 2, Lectures in APplied Mathematics Vol. 6, American Mathematical Society, Providence, Rhode Island, 1966.

LORAN-C 1982: A HIGH TECHNOLOGY NANOSECOND ACCURACY SYSTEM FOR HHE AND RESTRICTED WATERWAY NAVIGATION

John D. Illgen
Kaman Tempo
816 State Street
Santa Barbara, CA 93102

ABSTRACT

This paper provides a definition of the new 1982 Loran-C high-technology, nanosecond accuracy system that is being used for HHE and restricted waterway navigation. Significant technological and operational changes and improvements that have occurred in the past ten years are highlighted. Temporal and spatial errors are presented in quantitative terms. Most important, existing and proven compensation techniques for Loran-C sources of error are defined including Loran-C receiver related issues.

SECTION 1
INTRODUCTION AND SUMMARY

Introduction

The objective of this paper is to define the maximum potential accuracy and resolution achievable with the Loran-C radio-navigation system and describe techniques for achieving this capability in a harbor navigation environment.

Over the last several years, the Coast Guard and the marine community have been investigating techniques for using Loran-C for precise navigation in harbors and confined waterways. These investigations include analytical studies supplemented by field tests in selected ports and inland waterways to develop performance and operational data. The US Coast Guard Office of Navigation, Short Range Aids to Navigation Division, desires to assimilate the base of knowledge on Loran-C precision navigation and present this information in a form that will encourage and stimulate the marine industry to exploit the full capability of the Loran-C system.

This paper includes a compilation of research information on Loran-C performance and operational capabilities from Government and industry studies, analyses, tests, and experiments to characterize the maximum potential accuracy and resolution achievable with the Loran-C system used by marine vessels in a typical harbor environment. Specific attention has been given to:

1. Description of the Loran-C error sources and means to compensate.
2. Description of geographically dependent effects, especially the land/sea interface.
3. Definition of Loran-C coverage contours.
4. Definition of various Differential Loran-C concept alternatives, including: automatic corrections, manual corrections, initiate and go, and on-the-fly correction.
5. Definition of receiver performance specifications and limitations, with particular attention to resolution and accuracy.

Section 1 provides a definition of the new 1982 Loran-C navigation system. The literature includes numerous Loran-C navigation descriptions; however, Section 1 not only defines the system but highlights significant technological and operational changes and improvements that have occurred in the past 10 years. These new Loran-C system features are summarized below in Table 1.

Table 1. Loran-C system features.

Improvement	Technological	Operational	Impact
Loran-C Pulse Control	X	X	Textbook shape pulse (leading edge)
Solid State Transmitters	X	X	99.9 percent time availabilities
Improved Chain Control Equipment (positioning, processing, and communications)	X	X	Increased chain stability, reliability
Improved Chain Control Procedures		X	Increased chain stability (better compensation for temporal fluctuations)
Increased Automation	X	X	Reduced labor and increased reliability
Improved Loran-C Survey Methods	X		Improved compensation for land-sea boundary changes (CCZ) and spatial effects (bridges, islands, etc within harbors)
Improved Planning (GDOP considerations)		X	Improved accuracy
User Equipment	X	X	Improved resolution, automation, and reliability

Summary

Section 3 of this paper defines in quantitative terms the source and magnitude of Loran-C temporal and spatial errors. Transmitter timing fluctuations, propagation (temporal and spatial), noise (atmospheric), and frequency interference are presented in quantitative terms. Section 4 provides a description of the compensation techniques that can be used to minimize Loran-C errors. Compensation techniques for temporal and spatial fluctuations are presented in Section 4. Since noise, frequency interference, receiver error, and cycle selection problems are reduced or eliminated by good receiver design practices mitigation techniques for these are presented in Section 5.

The error sources, causes, and proven compensation techniques that are dealt with herein are summarized in Table 2. A few important observations referring to items listed in Table 2 should be made:

1. (Items 1,2,3) Data in Section 3 includes examples of very large errors caused by both temporal and spatial errors. We no longer care how large these errors are since there is a proven compensation technique for each error source as demonstrated in Section 4. Of course, knowing the origin of these errors is a requirement.
2. (Items 4,5,6) Limitations may actually be associated with the user equipment. Two differential Loran-C tests have shown 25- to 50-foot accuracy is achievable. When examining the raw test data it is obvious these values

Table 2. Loran-C error sources and compensation techniques.

Error Source	Cause	Compensation Technique
1. Transmitter timing fluctuations	Cesium, timer, and transmitter variations	Accurate and stable time base frequency, phase adjustments on short- and long-term basis, cycle compensation loop
2. Temporal fluctuations	Refractive index changes along propagation path	Differential Loran-C and variations of this method
	Surface impedance variation along propagation path	Differential Loran-C and variations of this method
3. Spatial effects	Bridges (such as Golden Gate) Docks; Buildings; Terrain Elevation (islands, peninsulas in vicinity of harbor, river, etc)	Conduct grid survey. Reflect warpage in grid. This is a one-time fix. Use position reference system or visual grid survey methods (PLAD)
4. Noise (atmospheric and manmade)	Electrical discharges in the atmosphere and power generation equipment	Band limiting and switched Q in the receiver. Linear: filtering done at low-level ahead of amplifier and clipped linear amplifier. Hard limiter: all linear processing at low-level output has square wave shape. Signal processing filters to minimize effects of interference and noise, shape the envelope, and minimize unwanted distortions. Narrow band switching of the filters is provided to gain SNR.
5. Frequency interference	In-Band 90-110 kHz Near-Band 70-90 kHz Out-of-band 70 kHz and 130 kHz	Band limiting. Interference filters (notch filters) - number depends on operational area. Filter the analog signal or change cross-correlation process to eliminate synchronous interference.
6. Receiver	Error measurement technique	Linear and hard limiter amplifiers have wide-band amplifier with low internal noise.

are in the receiver noise. This is a definite challenge for the Loran-C manufacturers.

3. (Items 2,3) A compendium of test data has been collected over the past 10 to 15 years and presented in Section 3. A clear distinction has been drawn between spatial and temporal effects (terrain elevation, effects of structures, time varying effects such as surface impedance, refractive index changes, etc). This distinction is of great importance when recognizing the limitations of techniques such as PLAD or positioning reference systems (Trisponder, Mini-Ranger, Maxiran, etc) used for Loran-C surveys. These techniques strictly provide a calibration of spatial effects. Differential Loran-C methods or variations thereof are required to compensate for temporal fluctuations.
4. (Items 1,2) A functional flow diagram of all the major subsystems required to design an automated differential Loran-C system is included in Section 4.
5. (Item 2) Automatic differential systems appear more practical than manual due to the frequency update (correction interval) requirements for most harbor and river areas.
6. PLAD type systems are effective. However, caution is a necessity since the presurveyed points only include a measure of spatial error and not real-time corrections for temporal fluctuations. The data in this paper shows the need for real-time corrections (100-second correction interval preference, 15 minutes in certain situations) to compensate for temporal errors.
7. Operation of initialization techniques are presented in Section 4. Additionally, a review of these techniques starting in 1968 to the present is provided.
8. To compensate for spatial changes requires a Loran-C grid survey. Both the visual aid and position reference systems are defined. Issues associated with grid survey standardization are summarized.

The impact on Loran-C receivers resulting from the phenomenal boom in the microprocessor industry and microprocessor developments is described. The fact that microprocessors will improve error measurement techniques implies that manufacturers have in hand the technology to design receivers with resolution in nanoseconds.

Regulatory and legislative issues do play a major role and an urgent need does exist to examine potential legal problems for restricted waterway use as was achieved by the Coast Guard for the CCZ.

Functions and requirements for radionavigation aids vary depending on harbor, river, seaway dimensions (depth and width of the channel), vessel type and size (cargo, pleasure craft, and several other categories), and equipment performance characteristics associated directly with the electronic navigation system being used. The remainder of this paper focuses on the Loran-C electronic navigation system—a proven system for Coastal Confluence Zone and restricted (harbors, rivers, and seaways) waterway navigation.

SECTION 2
LORAN-C NAVIGATION SYSTEM DEFINITION

Loran-C is a low-frequency, radionavigation aid operating in the radio spectrum of 90 to 110 kHz. Although primarily employed for navigation, transmissions are used for time dissemination, frequency reference, and communications. These other applications of Loran-C do not affect the navigation accuracy. The Loran-C system consists of transmitting stations in groups forming chains—a coverage area specific to each chain, receiving equipment, a propagation medium between transmitters and receiver, and methods of application. At least three transmitter stations make up a chain. One station is designated master while others are called secondaries. Chain coverage area is determined by the transmitted power from each station, the geometry of the stations, including the distance between them and their orientation. Figure 1 shows subsystem interconnections for a 3-station chain. Within the coverage area propagation of the Loran-C signal is affected by physical conditions of the earth's surface and atmosphere which must be considered when using the system. Natural

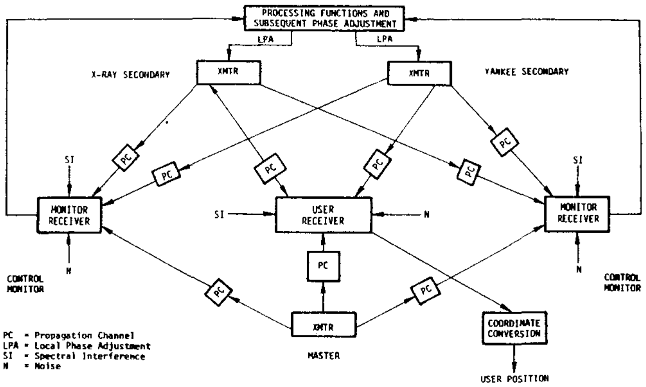

Figure 1. Loran-C subsystem interconnection for 3-station chain.

and manmade noise is added to the signal and must be taken into account. These physical conditions and noise effects can be troublesome and impact Loran-C signals. However, as will be demonstrated later, all known error sources can be minimized by using existing error compensation techniques and good receiver design practices. Receivers determine the applied coverage area by their signal processing techniques and can derive position velocity and time information from the transmission. Methods of application provide for conversion of basic signal time of arrival to geographic coordinates, bearing and distance, along track distance and cross error, velocity vectors, and time and frequency reference.

All transmitters in the Loran-C system share the same radio frequency spectrum by sending out a burst of short pulses and then remaining silent for a predetermined period. Each chain within the system has a characteristic repetition interval between the pulse bursts that enables receiving equipment to be uniquely synchronized thereby identifying the chain and stations within the chain being employed.

The U.S. Coast Guard has introduced present day technology into the Loran-C system as follows:

1. Use of solid-state transmitters.
2. Better chain control procedures.
   - Improved algorithms to provide corrections
   - Automated unmanned control monitors
   - Increased number of monitors, and, strategically locating the control monitors.
   - Use of microcomputers.
3. Using present day grid calibration techniques (position reference* systems and PLAD* type systems) for Loran-C surveys. Charts are now reflecting real-world data rather than pure predictions.
4. Increased redundancy and back-up procedures to provide continuous service.
5. Good chain planning is now resulting in shorter baselines and higher signal-to-noise ratios.
6. Transmitting antenna improvements.
7. Improved communications control between stations.

*To be defined and discussed in Section 4.

Results of the above can be stated quantitatively in terms of the traditional gauge of performance (ie, the percentage of usable time the service is available each month). The availability and reliability of Loran-C systems throughout the world continues to improve (Reference 2).

The worldwide Loran-C chains have provided 99.9-percent service (less scheduled outages). Periods of scheduled off-air are linked to the same deficiencies which have plagued Loran-C chains for years (ie, maintenance of the towers, transmitters, and couplers which are part of third- and fourth-generation equipment). The new chains are displaying a significant decrease in off air time due to; the installation of solid state transmitters and dual antenna couplers.

Coverage Area

The coverage area of a chain is usually defined in terms of signal strength and geometry of the transmitting stations with respect to each other, as they will support a specified position accuracy from a Loran-C receiver having certain minimum performance characteristics. Coverage area as defined herein is the term applied on charts prepared by the US National Ocean Survey and the US Defense Mapping Agency and in the Loran-C implementation plan by the Coast Guard.

Figure 2 displays worldwide Loran-C coverage. Loran-C coverage now encompasses over 20-million square miles around the US (including Hawaii and Alaska), Japan, Canada, Pacific Ocean, Atlantic Ocean, Mediterranean Sea, and the Norwegian Sea. The shaded area in Figure 2 shows coverage area where there is a high probability of obtaining a good groundwave fix to an accuracy of better than 0.15 nmi (900 feet). The outlined areas show skywave fix where there is high probability of obtaining a good skywave fix. The stars show regions where users have reported good groundwave fixes well beyond the expected coverage area. Not shown in Figure 2 are the coverage expansions that include: Red Sea, Gulf of Aden, Arabian Sea, Persian Gulf, portion of the Indian Ocean, Saudi Arabia, Iran, Jordan, UAR, Israel, Egypt, Sudan, Ethiopia, Pakistan, India, Mexico, and extended coverage in Europe.

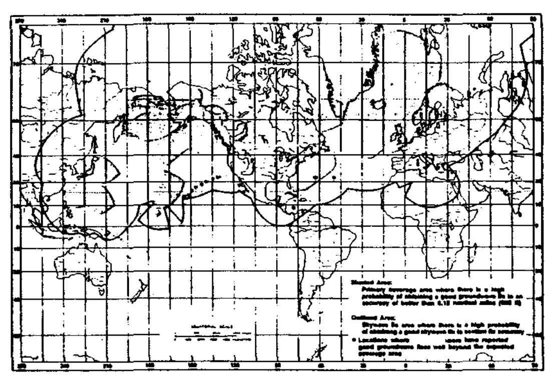

Figure 2. Loran-C worldwide coverage.

These new chains are being designed to provide high accuracy (well below 500 feet). Privately-owned Loran-C chains are being considered in the Arctic (northern frontiers of Canada) and other areas. The applications are requiring accuracies better than advertised for the CCZ

(Coastal Confluence Zone). To achieve higher accuracies for harbor, restricted waterway navigation, offshore applications, etc augmentation techniques (such as differential Loran-C) and Loran-C mini-chains have been demonstrated.

SECTION 3
LORAN-C ERROR SOURCES

The US Coast Guard has conducted numerous efforts to determine the source, magnitude, and statistics of Loran-C error sources. These error sources are significant in terms of magnitude and frequency of occurrence; however, in each case there is a compensation technique. Fortunately the Loran-C system has matured over the years and proven compensation techniques have been developed. Additionally, Loran-C today includes the use of high technology and good design practices developed from many years of experience for both Loran-C transmission and user equipment. Estimates for each category of error source will be provided based on a review of tests conducted over the past 10 to 15 years. Then this section will be followed by a description of compensation techniques and good receiver design practices.

Sources of Fluctuations in Transmitted Signals

Predicted transmitted error in terms of timing synchronization, pulse shape control, phase control, and parameter drift will now be estimated.

Timing Synchronization. The time when each pulse is transmitted is controlled by a cesium beam frequency standard that provides stable and accurate time base frequency of 5 MHz and 1 MHz which are used as inputs to the Loran-C timer set. Together these two equipments form a "Loran-C clock." Synchronization of the clocks at all the stations in a chain is accomplished by LPAs (Local Phase Adjustments) on a shortterm basis and frequency and phase adjustments on a long-term basis.

The frequency standard used at Loran-C stations is a Hewlett-Packard Model 5061A Cesium Beam Atomic Frequency Standard. The setability of these standards is $\pm 10^{-13}$. In other words the fractional frequency offset between two 5061A standards cannot be reliably reduced below this level. A fractional frequency offset of 7×10^{-13} corresponds to 60-nanosecond gain or loss of time per day between the two clocks. If the frequency of the two clocks remained constant after being set then three 20-nanosecond LPAs per day would correct for this drift and the maximum error during one day would be ±10 ns. However, the frequency of cesium beam oscillators changes with time in an unpredictable manner. In addition there is phase noise and the timer certainly adds some additional phase noise or jitter and the information used to derive LPAs is corrupted by all the other temporal fluctuations.

In Reference 3 a model of cesium beam standards was developed. The state space equations of this model are given by

$$\begin{bmatrix} X_{k+1} \\ Y_{k+1} \end{bmatrix} = \begin{bmatrix} 1 & \Delta t \\ 0 & 1 \end{bmatrix} \begin{bmatrix} X_k \\ Y_k \end{bmatrix} + \begin{bmatrix} 1 & 0 \\ 0 & 1-\theta_k \end{bmatrix} \begin{bmatrix} a_k \\ b_k \end{bmatrix}$$

where

$\{a_k\}$ = zero mean sequence of uncorrelated random variables on constant variance $\sigma_a{}^2$ corrupting the phase offset

$\{b_k\}$ = zero mean sequence of uncorrelated random variables of constant variance $\sigma_b{}^2$ corrupting the clock frequency

Y_k = fractional frequency values at day k

X_k = daily phase offset

θ_k = constant.

Based on 3 to 4 years of clock data at the Naval Observatory, values for σ_a of 5 ns and σ_b of 8.9×10^{-14} have been determined.

We assume that the noise sequence that drives the frequency offset is actually a series of small jumps occurring once every GRI. Then the value of σ_b would be given by

$$\sigma_b = 8.9 \times 10^{-14}/(86400/\mathrm{GRI})^{1/2}$$
$$= (8.9 \times 10^{-14})/(8.64 \times 10^4/0.0994)^{1.2}$$
$$= 1 \times 10^{-17} \quad .$$

Thus in the short term most of the fluctuations due to frequency standard instability are due to phase noise since the longer term frequency effects are removed by LPAs. Thus we estimate that the short-term variations are about 5-ns rms. Due to the fact that the timer has a quantization level of 6 ns, we roughly estimate an rms error of about 10 ns due to the Loran-C timer set.

Not all of the fluctuations in the transmitted signal are due to cesium standard instability. The transmitter itself is also a source of signal fluctuation. However, the transmitter is maintained in phase lock with the 5-MHz output of the cesium standard to within ±20 ns by the cycle compensation loop. Plots produced at Loran-C transmitting station Middletown, California (the X-secondary on the West Coast USA Loran-C chain), have been examined that show these slight adjustments (Reference 4). The cycle compensation loop function is recorded continuously and the records are saved. This loop compensates for changing bias levels within the transmitter and changing delay times. It is estimated that because of the fact that the cycle compensation loop only makes 20-ns corrections, fluctuations in the signal due to the transmitter are roughly estimated to be 6 ns.

The rss of the cesium variations, the timer variations, and the transmitter variations yield an equipment error of

$$[(10)^2 + (5)^2 + (10)^2]^{1/2} = 15 \text{ ns} \quad .$$

Loran-C Temporal Timing Fluctuations

There are three categories of important error sources that can cause TD Loran-C timing fluctuations. These are: receiver-induced, transmitting equipment, and propagation fluctuations. To determine the magnitude and source of Loran-C transmitting induced timing fluctuations it would be necessary to locate receivers near (50 to 70 km) two or more transmitters in a service area. Through simple addition and subtraction of TDs significant propagation and equipment fluctuations could be separated as long as the fluctuations are larger than receiver error (typically 25 ns). Specifically this measurement configuration requires the following assumptions:

1. The propagation fluctuations in a signal traveling in one direction over a given baseline are equal to the propagation fluctuations in a signal traveling in the opposite direction.

2. Propagation fluctuations over the short paths are small compared to other timing fluctuations.

3. Receiver-induced fluctuations are small compared to chain and propagation fluctuations.

4. Chain fluctuations are the same for all receivers in the service area of interest (ie, chain fluctuations are not spatially dependent).

We have been able to separate equipment and propagation induced fluctuations.

TD and TOA measurements have been conducted over a large area in the Southern Triad of the West Coast, USA (Reference 5). One of the West Coast experiments was aimed at determining the stability of Loran-C signals. No Loran-C timing fluctuations could be attributed to large atmospheric changes even though numerous cold and warm weather fronts (parallel and perpendicular to the propagation paths) passed over the various propagation paths. The timing fluctuations were typically below 35 ns (rms, standard deviation) each week for 12 weeks. Propagation fluctuations (rms, standard deviations) were below 20 ns and masked by receiver noise. Additionally, two receivers (LC204 and BRN-5 linear) were colocated at Ft. Cronkhite (near San Francisco) monitoring TDX and TDY for ten continuous months. The propagation paths ranged between 50 nmi and about 475 nmi. The mean values over the entire 10 months (which included winter—the most severe fronts cross the paths) did not change more than 60 ns and standard deviations were <35 ns. The Ft. Cronkhite measurement site is only 100 miles north of the control monitor (located at Point Pinos, CA). This shows good control when the receiver (user) is near the monitor.

The West Coast results show a very stable (Southern Triad) Loran-C system that was not significantly affected by frontal systems passing over the propagation paths. Additionally, the results at Ft. Cronkhite show good control when the user is in the vicinity of the control monitor.

Previous Experiments on the East Coast. The expectations, based on earlier East Coast data collections, that weather phenomena might change the groundwave phase by as much as 0.5 to 1 microsecond or more were not borne out in any of the data collected on the West Coast (USA) and more recently in the Canadian Great Lakes region.

Diurnal fluctuations measured over a propagation path (753 nmi) between Carolina Beach and Dana have revealed 1-microsecond changes in the winter and 0.5-microsecond changes in the summer (Reference 6). The propagation paths in the Great Lakes experiment are as long as the Carolina Beach-Dana path (in both cases typically 550 to 650 nmi). There is a difference in conductivity of about a factor of 2 which should not have significant impact. These large timing fluctuations have been attributed to the passage of frontal systems. Attempts to explain the above changes in Loran-C TDs based on meteorological (ie, changes in temperature occurs the same time as the change in TD) explanations have been attempted by several researchers (References 7, 8, and 9). Even though the Loran-C data compares well with a specific weather parameter (temperature), the fact remains that diurnal TD timing fluctuations are about 4 to 5 times as great as can be explained by simple calculations using expected changes in the index of refraction.

Figures 3 and 4 (taken from Reference 9) show the idealized cold front in terms of N units (variation of the refractive index from unity). In the case of the cold front the variation in N would result in a prediction of a rapid change in the primary phase of 100 ns and a change of -60 ns for secondary phase. This yields a total phase lag increase of 40 ns. From Figure 4 it appears that warm fronts would not produce significant phase changes. It is estimated that shifts in TD's due entirely to atmospheric changes would not exceed 20-ns rms and are probably about 10-ns rms.

Temporal Fluctuations Summary. Tables 3 and 4 show Loran-C temporal tilming fluctuations measured over the past 10 to 15 years. Several observations can be made about this tabulation:

1. The largest peak-to-peak temporal fluctuations have occurred in the winter season.

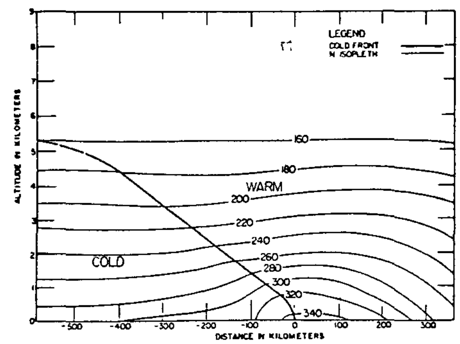

Figure 3. Idealized cold front in N units (from Reference 9).

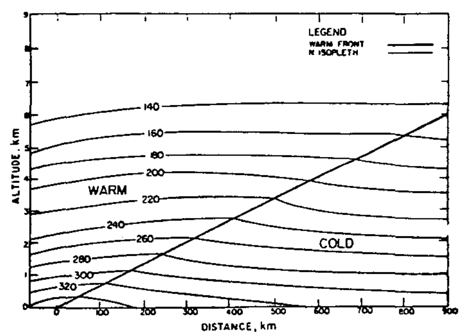

Figure 4. Idealized warm front in N units (from Reference 9).

2. These effects in the Northern areas may be related to surface impedance changes (snow, ice, and freezing conditions).

3. These fluctuations are all smaller than reported before approximately 1973 (perhaps improved chain control, better geometry, shorter baselines, higher SNR, and careful placement of control monitors are impacting these new results).

Table 3. Test results showing temporal fluctuations.

Sponsoring Organization	Results	Refs.
Canadian Hydrographic Service/ Kaman Tempo	TD fluctuations vary from 0.05 to 0.3 μs peak-to-peak over two to three days depending on location wrt control monitor. Weather fronts produce 0.05 μs TD change.	10
US Coast Guard/Kaman Tempo	Seasonal TD variations 0.06 μs at Ft. Cronkhite. Weekly TD variations are typically 0.035 μs.	4,11,12 5,13
US Coast Guard/Magnavox	Weekly TD variations are 0.3 μs.	14
US Navy/Sperry Systems Management	Seasonal TD variations are highly correlated with refractivity. Weather fronts reported to induce large TD variations.	15
FAA/TSC	Seasonal variations in Vermont at 0.8 μs peak-to-peak (largest in winter).	16
US Coast Guard/TASC	Seasonal TD variations in St. Marys River Chain are 0.4 μs peak-to-peak and largest in winter. Diurnal TD variations are 0.04 μs peak-to-peak.	17
US Coast Guard/Internav	Differential Loran-C errors of 1 μs reduced using Differential Loran-C. 50-foot accuracy demonstrated.	18

4. Reports produced by the sponsoring/performing organizations have explained these computations reasonably well and have demonstrated the means to compensate for temporal errors.

Spatial Error

The time-of-arrival of a Loran pulse depends on the electrical properties of the earth's surface over which these signals propagate. These electrical properties include the impedance or conductivity of the ground, the roughness or terrain variations of the surface, the refractive index of the atmosphere at the surface, and the lapse rate or rate of change of refractive index with altitude above the surface. Spatial variations of the transmitted Loran signal are primarily influenced by the nonhomogeneous surface impedance and by variations in terrain elevation.

Temporal Effects

Temporal effects may be produced by time changes on these spatial features but are more easily influenced by the surface refractive index and the lapse rate of the refractive index of the earth's atmosphere, which are known to change diurnally and with changing weather conditions as discussed earlier.

Spatial Effects Testing. One of the objectives of the Loran-C Signal Analysis Harbor Navigation project conducted by the US Coast Guard was to improve the accuracy and control of Loran-C through a better understanding of Loran-C signal characteristics. An important step in achieving this objective was to better define the predictability of the Loran-C signal phase and amplitude characteristics and to explain differences between observed time differences (TDs) and predicted TDs using current prediction and calibration techniques with emphasis on terrain and surface impedance behavior.

Four groundwave propagation prediction models or techniques have been reviewed and tested against each other and against a carefully controlled experimental data base by Gambill and Schwartz (Reference 11). This work has been instrumental in understanding the behavior of spatial effects on Loran-C. Therefore, the prediction models used to explain the experimental results will be discussed. The four techniques are:

1. Honogeneous Spherical Earth—A well-researched technique which includes comprehensive published literature.

2. Millington's—A semi-empirical technique currently used for system calibration.

3. Wait's Multisegment Spherical Earth—A theoretical model to account for inhomogeneous earth.

4. Integral Equation Solution—A computer program to calcluate signals over irregular inhomogeneous terrain.

Paragraphs below include comparisons between Millington and Integral Equation predictions, and the mesured data base to better explain the significance of spatial and surface impedance effects on Loran-C signals. Comparisons have also been conducted using the flat-earth homogeneous spherical earth, and Wait's multiple segment techniques by Gambill and Schwartz in Reference 11 will not be shown here.

Experimental Configuration. Measurements of phase time difference (TD) and signal arrival times (TOA) were taken at eight sites over a period of 60 days, as nearly as possible along the Yankee to San Francisco Harbor path, between Searchlight, NV, and Ft. Cronkhite, CA. The main reason for these measurements was to compile a comprehensive experimental data base for comparison with predicted results from prediction techniques previously mentioned. Analysis and interpretation of the differences between measured and predicted data were to lead to a better understanding of Loran-C signal characteristics.

The Searchlight/Ft. Cronkhite path was selected for the experiment because of its extremely variable terrain and demonstrable history of short-term weather fluctuations. The assumption was that irregular terrain and variable surface impedance along the path would produce experimental results that differed significantly from simple model predictions and therefore would provide a data base for thoroughly testing models that account for irregular terrain and impedance.

It was also expected that weather variations typical of the time of year might occur during data collection periods along the path. If large variations in measured data occurred concurrently with significant weather pheomena, then the data could provide additional guidance to improve models of weather produced variations in the prediction codes.

Figure 5 identifies the nearest town where data collection sites were established to take TOA measurements. The figure is not drawn to scale, but is intended to show the approximate, relative off-set distance of these locations from the geodesic. The precise (receiver) antenna locations were used to compute predictions. The latitude and longitude in WGS-72 coordinates and the distance from each site to the Searchlight transmitter can be found in Reference 13.

Before proceeding with the experimental results a discussion of modeling techniques used to analyze the test data is in order.

Model Intercomparison.

Classical Techniques. This idealized technique will not produce phase delay estimates with useful accuracy for irregular paths (such as defined in Reference 11). However, because

Table 4. Test information.

Sponsoring/Performing Organizations	Completion Date	Loran-C Chain	Number Of Sites	Test Duration	Measurements	Location	Data Sampling Interval	Data Sample Size (Approx.)	Application	Data Quality (μsec)	Motivation
Canadian Hydrographic Service/Kaman Tempo	1978	Northeast US	3	3 wk	TDW, TDX	Great Lakes Region	100 sec	Oct 80 to Nov 80	Great Lakes Navigation	0.02	Temporal effects and relation to chain control
US Coast Guard/Kaman Tempo	1978	US West Coast	18	10 mo	TDX, TDY	West Coast (Southern Triad)	100 sec	Aug 77 to May 78	Harbor Navigation	0.02	Temporal fluctuation evaluation and means to compensate
US Coast Guard/Magnavox	1977	US East Coast	3	3 mo	TOAM	Fort Wayne, IN Newark, OH Washington, DC	15 min	Feb 77 to April 77	Loran-C System Support	0.02	Cause of Diurnal TD variations
US Coast Guard/Internav	1973	US East Coast	8	2 mo	TDY, TDZ	Delaware River	100 sec	Jul 73 to Aug 73	Harbor Navigation	0.02	Differential Loran-C evaluation
US Navy/Sperry Systems Management	1971	US East Coast	3	1 yr	TDW, TDY	Nantucket, MA Carolina Beach Jupiter, FL	15 min	Oct 67 to Sep 68	Strategic Submarine Navigation	0.01	Potential Improvement afforded by Propagation Corrections
FAA/TSC	1980	Northeast US	3	14 mo	TDW, TDY, TDX	Burlington, Newport, & Rutland, VT	3 hrs	Aug 79 to Oct 80	Civil A/C Navigation	0.1	Seasonal, Diurnal variations in TD grid bias
US Coast Guard/TASC	1980	St Marys River	3	1 yr	TDX, TDY, TDZ	Northern Michigan	15 min	May 79 to May 80	Ore Carrier Navigation of St Marys	0.02	Month-to-Month TD variations

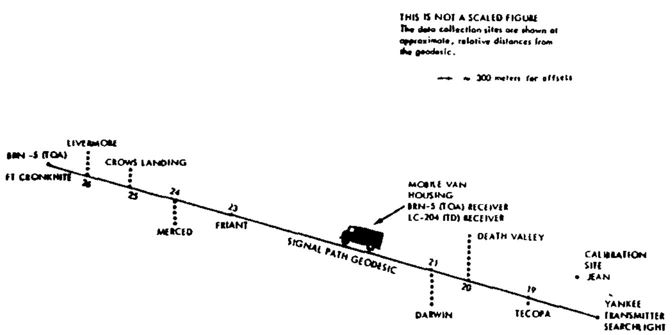

Figure 5. Propagation path data collection sites relative to the geodesic.

the classical technique is imbedded in other techniques, the numerical procedures should be considered.

The general classical theory solution results in an infinite series representation for the complex groundwave loss function. The series converges rapidly for long paths but requires many terms for paths less than 100 km in length. Two short-path approximations are available, one for high surface impedance and the other for low surface impedance.

The evaluation of the classical theory determined the required number of terms in the series for a specified path length and level-of-accuracy, and also defined appropriate distances to switch from the accurate series solution to the short-distance approximations (Reference 11).

Millington's Technique Compared to Wait's Multiple Segment Technique (MULSEG). Both these techniques account for inhomogeneous impedance along the path. The results produced by these two techniques have been compared for several hypothetical cases. One example is shown in Figure 6 for a five-segment path. The results are typical of results obtained for a number of other cases (Reference 11). As a result of this comparison, we concluded that the prediction differences were small compared to errors caused by the neglect of terrain variations.

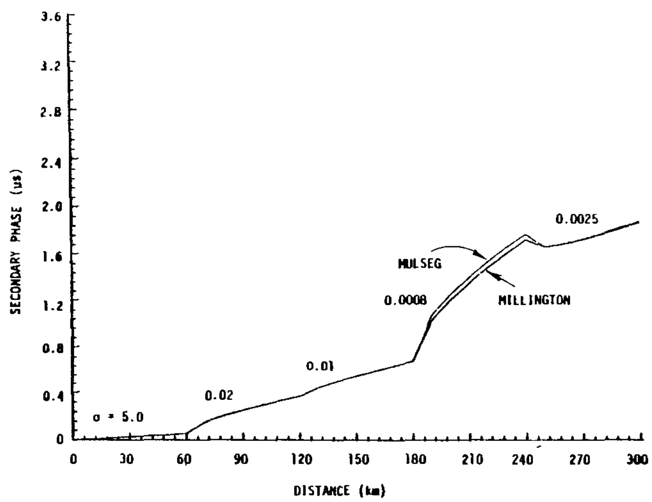

Figure 6. Comparison of MULSEG and Millington for a five-segment path (sea to land).

Millington's Technique Compared to the Integral Equation Solution. Results from Millington's technique and the integral equation technique have been compared for two cases: one where terrain effects are important, and one where terrain effects are suppressed. These comparisons were made during the process of comparing experimental and predicted results and are discussed later.

Data Preparation. All methods considered require an accurate definition of geodetic path length as input. Also, all methods currently use a single value for the effective earth radius along the path. The classical approach requires a single value of surface impedance for the entire path. Millington's technique and MULSEG require surface impedance data for as many segments as are required to account for inhomogeneity along the path. The integral equation requires inhomogeneous impedance data for segments along the path and terrain variations relative to a smooth spherical reference.

Path Length. For accurate prediction, path length needs to be determined within a few tens of meters. Phase prediction errors resulting from path length error are approximately 3.3 ns per meter. Accurate site position surveys and geodetic distance calculations using Sodano's technique provided path length accuracy that should limit the phase error to less than 10 ns in this experiment.

Effective Earth Radius. An effective earth radius, a_e (usually larger than the earth's actual radius, a), is used to approximately account for the refractive effects of the lower atmosphere. Approximate relationships defining the effective radius in terms of surface refractive index are provided in Reference 19 and elsewhere. A ratio of a to a_e of 0.85 was used in the calculations reported here.

Surface Impedance. Crude estimates of surface impedance can be obtained from existing surface conductivity maps or from maps providing general surface and topographic features. These estimates are usually adequate for Millington's technique, where the typical application is to adjust original estimates of surface impedance to match selected experimental data before using the surface impedance values to make predictions.

To make more accurate predictions, surface impedance is estimated using best available data defining geophysical and electrical properties of surface and subsurface layers. The availability and detail of these data depend strongly on location.

Figure 7 shows (thin lines) the best estimate of the surface impedance along the propagation path, using geophysical data from the US Geological Service and the California and Nevada Bureaus of Mines. Data were obtained at various locations for one, two, three, or four layers and processed using a multilayer surface impedance model. The details of the data and processing are provided in Reference 19. Figure 7 shows amplitude data only. The surface impedance phase in all cases was very close to 45 degrees.

Also shown on Figure 7 (heavy lines) is a twelve-segment approximation that was used later in comparing Millington's technique calculations to the integral equation results.

Terrain Data. Terrain data are required only for the integral equation approach. For many areas of the world, digitized data are available that provide more detailed definition of terrain variation than can be used in the computations. Proper automation of data search and smoothing routines can reduce this data preparation task to a reasonable computer effort.

In the experiment described here, digitized data were not available over the entire path and terrain variations were obtained from the most detailed topographic maps available. Digitizing the data from the maps and subsequent verification of the data took 2 to 3 manweeks. Data preparation for the integral equation technique can be a formidable task unless a digitized data base and associated software to scan and select appropriate data are available.

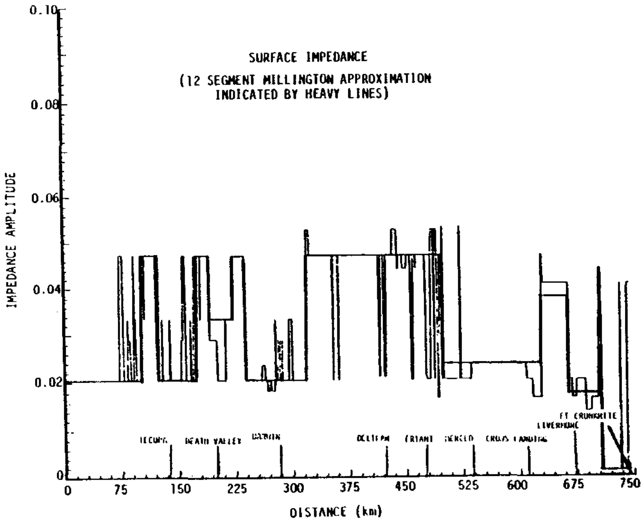

Figure 7. Approximation to the surface impedance for a Millington calculation.

The original data defining terrain along the propagation path are plotted in Figure 8. The detail shown in the figure is more than is required in the integral equation and some data smoothing was applied. Phase predictions shown later used terrain data that were smoothed by averaging data over a 3-km interval.

Comparison Between Predictions and Experimental Data. One primary goal of this effort was to compare pure predictions (ie, no tuning of input data using measured signal phase or amplitude data) with measured data. Figure 8 shows the predicted secondary phase (signal phase lag in excess of the free space phase lag) for the integral equation results and Millington's technique results. The integral equation results were obtained using the detailed impedance estimates shown in Figure 7 and the terrain variations shown in Figure 8 (after smoothing). The Millington results were obtained using the twelve-segment approximation to the detailed impedance estimates shown on Figure 7.

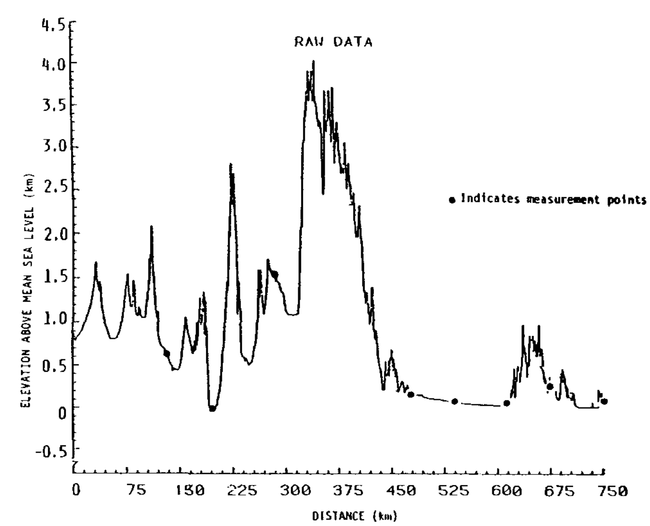

Figure 8. Original worst case path terrain data.

The experimental results are shown on Figure 9 by the bars above the measurement sites. The length of the bar indicates approximate bounds on experimental error as defined earlier. Since only relative (not absolute) secondary phase measurements were obtained, a reference point for the data must be selected. In this comparison we chose to equate predicted and measured secondary phase at Tecopa, the site nearest Searchlight. The origin could also be selected to minimize mean rms difference between measured and predicted values. However, it can be observed from Figure 9 that no origin selection can be made that will remove all large prediction and measurement differences. The maximum difference as shown on the figure between integral equation predictions and measurements is about 0.5 microsecond.

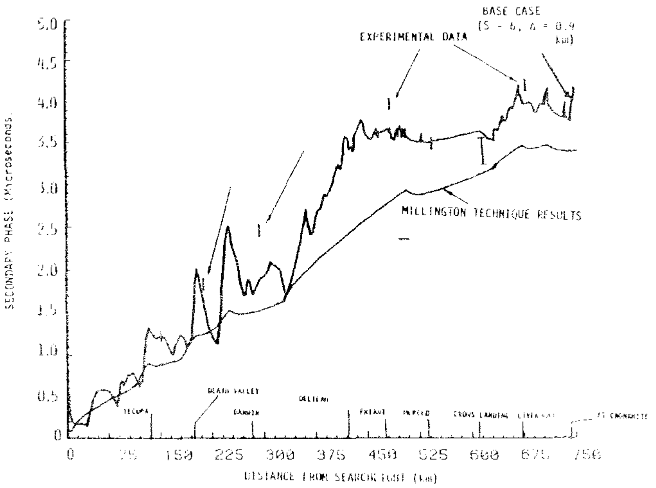

Figure 9. Comparison between the integral equation and Millington's technique results.

It can also be noted from Figure 9 that the integral equation results produce better agreement with the measured data than Millington's results (ie, inclusion of the terrain effects provides an apparent improvement).

To verify that the differences between the Millington and integral equation predictions are due to terrain effects, a second calculation was performed with the integral equation, but with terrain effects suppressed. These results, with Millington's technique results repeated, are shown in Figure 10. The agreement between predictions is very good and provides confidence in the computational models. The results provide further verification that Millington's technique is useful when terrain effects are minimal.

Additional Comparison. Two additional sets of calculations were performed to provide a crude measure of sensitivity of predicted versus measurement difference to input parameters. We believe that terrain data is adequately defined and input value errors would most likely be the surface impedance definition. Figure 11 shows the original integral equation predictions, the measurements, and a new integral equation prediction made with the conductivity of all segments along the path decreased by a factor of 2 (this increases the surface impedance by approximately a factor of 2). Note that the two predictions now almost bracket the measured data. It is clear that selective adjustment of the conductivity of different segments by a factor of approximately 2 could produce good agreement between measured and predicted values. These adjustments were not performed because of the computer costs for repetitive calculations with the integral equation program.

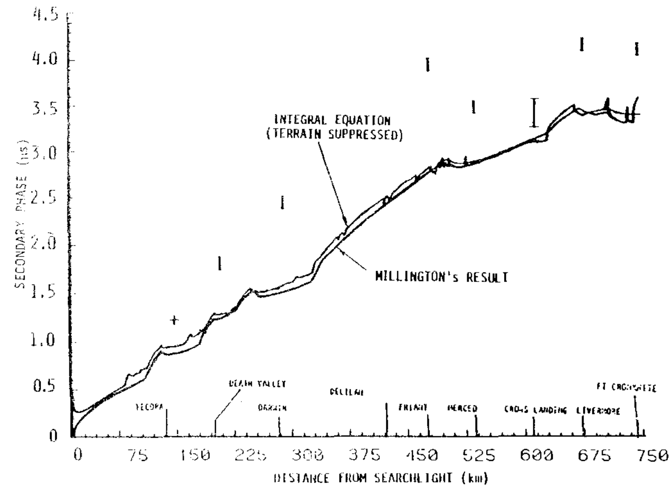

Figure 10. Comparison of Millington's technique with the integral equation technique (with terrain variations suppressed).

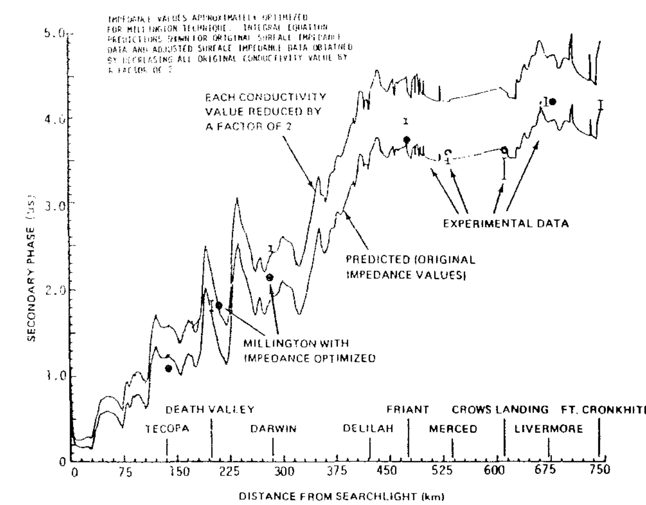

Figure 11. Comparison of measurement of Millington and integral equation predictions after surface impedance adjustment.

Also shown on Figure 11 by the filled-in circles are results obtained with Millington's technique with the impedance of the twelve-segment apprxoimation adjusted to approximately minimize the rms difference between Millington's predictions and measurements. Impedance values had to be generally increased to compensate for terrain effects and/or errors in the original impedance values. The results obtained by varying the impedance values indicate that the impedance values need to be known much better than a factor of 2 for accurate (100 ns) predictions over long overland paths.

Clearly it has been demonstrated that deterministic prediction techniques alone are not adequate for precise navigation. However, a careful balance between predictions and measured data (empirical models) may have some merit.

Predicted Weather Effects. Except for one isolated incident, no significant weather-produced fluctuations were observed during the West Coast experiments. As a result, little emphasis was placed on prediction of weather effects. One example of predicted weather-produced fluctuations was produced using surface weather data from a station (Reno, NV) near the Master transmitter. The atmospheric pressure in millibars, the temperature, and dew point temperature were taken at Reno. These values were used to compute the surface refractive index and a corresponding value of effective earth radius. Phase fluctuations, which are the sum of the primary and secondary phase fluctuations, were computed for path lengths of 100, 300, 500, and 700 km. The predicted phase fluctuations were small, showing a maximum value of 15 ns. These values agree in order of magnitude with the experimental observations during the Loran-C Signal Analysis West Coast Experiment with one exception, where it is postulated that a larger change was produced as a result of precipitation-induced surface impedance changes. A discussion of this exceptional case was provided in Reference 13.

Conclusions. Detailed conclusions and recommendations are provided in Reference 11. A summary of the discussion in Reference 11 is provided below.

1. For a smooth, inhomogeneous earth, Millington's technique and Wait's multiple segment technique produce nearly identical results. Therefore, Millington's technique should be used in preference to Wait's because of its greater simplicity and shorter running time.

2. Millington's technique and the integral equation technique give nearly identical results for a path with highly inhomogeneous impedance when the terrain variations are suppressed for the integral equation calculations.

3. The integral equation calculations show that both terrain and surface impedance variations are important in predicting secondary phase. Our numerical computations indicated that the terrain can be defined with sufficient accuracy with data points spaced at approximately an integration step size of 1 km. Our experimental observations and predictions indicate that to obtain prediction accuracy on the order of 100 ns or better, the surface impedance uncertainty must be much less than a factor of 2 for overland paths.

4. The effect of terrain variations (in this case elevations greater than one wavelength above the mean geoid) was to increase the secondary phase. Thus, matching calibration data with impedance variations alone requires higher than actual impedance values to compensate for the terrain effects.

5. Data preparation for the integral equation method is a formidable task. The hand preparation of the data for the worst-case path required an effort of about 1 man-month. Digital terrain data tapes for the path were not available. Hand preparation of data for a coverage area would not be practical.

6. The highly variable terrain and surface impedance along the worst-case path and the differences between predicted and measured values indicate the need for more closely spaced measurement points to adequately calibrate phase change along the overland portion of the path from an experimental standpoint. On the other hand, measurements made beyond the region of major terrain variations can be used to compensate for the integrated effects of terrain-induced fluctuations. A good example is the match between measurements and predictions at Ft. Cronkhite shown in Figure 9. Ft. Cronkhite is the last measurement point along the path and is located in San Francisco Harbor.

Spatial Effects Measured from Previous Experiments. Tables 5 and 6 provide a summary of spatial test data collected over the past 10 to 15 years. Several interesting points can be made about Tables 5 and 6 and the propagation path experiment previously discussed:

1. Present conductivity maps are not adequate for chart preparation using predictions alone.

2. Caution must be exercised by the user when purchasing Loran-C receiver systems that claim to include propagation corrections if these corrections are prepared using conductivity values from outdated or inaccurate maps.

3. Effects of terrain elevation are pronounced.

4. Surface impedance is time varying (ie, significant TD variations occur with extremes--dry-to-freezing conditions, precipitation, etc). Loran-C surveys do not account for these seasonal changes. Such surveys only include terrain elevation and surface impedance is reflected in the measurement for an instantaneous period of time.

Compensation techniques do exist to account for all of the above.

Atmospheric and Manmade Noise. There are a number of types of noise that may influence Loran-C signal reception, although, usually only one type will predominate. Broadly the noise can be divided into two categories depending on whether it originates in the receiving system or externally to the antenna. The internal noise is due to antenna and transmission line losses, or is generated in the receiver itself. It has the characteristics of thermal noise and, in many cases, its effects on signal reception can be determined mathematically with a high degree of precision. External noise can be divided into several types each having its own characteristics. The most usual types are of atmospheric, galactic, and manmade origin.

In the low frequency 100 kHz part of the spectrum noise is developed almost entirely from electrical discharges in the atmosphere and manmade sources, such as power generation equipment. The strength of the Loran-C signal is stable, so it is this electrical background interference that varies with weather.

Atmospheric noise is generally characterized by short pulses with random recurrence superimposed upon a background of random noise. Averaging these short pulses of noise power over several minutes yields average values that are nearly constant during a given hour.

The noise can be better understood by examining the model shown in Figure 12. The model consists of the impulsive disturbances, I(t); Gaussian noise, W(t); and the desired signal, S(t). The impulsive-noise atmospheric noise model is characterized by a randomly occurring impulse of the form

$$I_\ell = g_\ell e^{n_\ell} \quad ,$$

where I is the area under the signal curve (ie, EΔ, where E is the amplitude of a pulse of duration Δ seconds, g_ℓ is a random variable with equal likelihood of being ±1, and n is a normal

Table 5. Spatial test information.

Sponsoring/Performing Organizations	Completion Date	Loran-C Chain	Number of Sites	Coverage (km)	Measurements	Spacing (km)	Application	Data Quality (μsec)	Motivation
US Coast Guard/TASC	1979	US West Coast	27 land 23 sea	1500	TDW, TDX, TDY	20-100 km	CCZ Navigation	0.1 - 0.2	Loran-C chart errors
US Air Force/MITRE	1979	Southeast US	126	80 x 140	TDW, TDY	10 km	A/C navigation using ARN-101 RCVR	0.1 - 0.2	Grid warpage caused by land paths
US Coast Guard/TASC	1978	St Marys River	25	120	TDX, TDY, TDZ	4 km	Ore carrier navigation of St Marys River	0.2	Chain calibration
Canadian Hydrographic Service/Kaman Tempo	1978	Northeast US	10	1000	TOAM*, TOAW*	200 km	Great Lakes Navigation	0.1 - 0.2	Conductivity map improvement
US Coast Guard/Kaman Tempo	1978	US West Coast	8 on radial 14 in harbor	800 40	TOAY* along radial TDX and TDY in harbor	100-km along radial 4 km in harbor	Harbor Navigation	0.07 - 0.2	Grid Prediction evaluation
Canadian Hydrographic Service/Same	1977	Canadian West Coast	200	1000	TOAM, TOAX, TOAY	30-km offshore continuous near straits	CCZ Navigation	0.5 offshore 0.1 near straits	Chain calibration
US Army/Same	1975	US East Coast	61	100x100	TDY, TDZ	10 km	Terrestrial navigation using manpack RCVR	0.2	Coordinate conversion model development
US Army/Same	1973	US East Coast	54	3x8	TDY, TDZ	0.5 km	Terrestrial navigation using manpack RCVR	0.1	Coastline-induced anomalies
Commerce Dept/Same	1972	US East Coast	74	100x100	TDW, TDZ	5 km	Basic propagation research	0.1	Local grid warpage

*Measured site-to-site change in TOA

Table 6. Spatial test results.

Sponsoring/Performing Organization	Results
US Coast Guard/TASC	San Joaquin Valley introduces 1 to 2 μs TDX anomaly.
US Air Force/MITRE	Large area warpage. Warpage independent of altitude below 13K feet.
US Coast Guard/TASC	Conductivity is nonuniform in 70 km x 130 km coverage area.
Canadian Hydrographic Service/ Kaman Tempo	Conductivity map is incorrect by factor of 2 to 10 in certain regions.
US Coast Guard/Kaman Tempo	Accurate prediction requires terrain and conductivity data. TD residual changes rapidly at land-sea interface.
Canadian Hydrographic Service/Same	Effects of land-sea interface and mountains are pronounced.
US Army/Same	TD residuals after large-area calibration of linear model are 0.3 μs rms.
US Army/Same	TD anomaly is observed at sea/land interface.

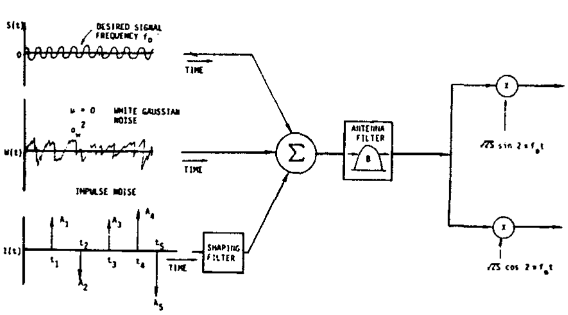

Figure 12. Model of signal and noise at the input to Loran-C receiver.

random variable with mean μ_ℓ and variance $\sigma_\ell{}^2$. The subscript ℓ refers to a particular cycle being examined (given that the impulse occurred in that cycle). The impulse occurrence rate μ is the range 30 to 2000 impulses per second, and the occurrences are assumed governed by a Poisson distribution.

For the Loran-C model carrier, the quantity V_{dm} (median value of the voltage deviation as tabulated in Reference 27) can be related to the noise model by

$$V_{dm} = 20 \log_{10}[\exp(\sigma_\ell{}^2/2] \quad ,$$

where V_{dm} is given in dB. It can be shown that

$$E_u = 20 \log_{10} = \left(\frac{\sqrt{u}}{0.0073} \exp[\mu_\ell + \sigma_\ell{}^2]\right)$$

or

$$E_n = F_a = 95.5 + 20 \log_{10} f_{MHz} + \log_{10} B \; (\mu V/m) ,$$

where E_n is the rms noise field strength, F_a is called the noise parameter (effective noise factor that results from the external noise power available from a loss-free antenna where $F_a = 10 \log_{10} f_a$, f_{MHz} is the frequency of the measurement in MHz ($\cong$ 0.1), and B is the bandwidth (20 kHz). In the noise model, values of μ_ℓ are obtained for F_{am} and σF_{am} $\pm F_{am}$. Table 7 summarizes the results obtained from the model for the San Francisco harbor area. The model can be exercised for any desired location worldwide. The table indicates that the median noise values, F_{am}, differ the greatest between summer and winter and expected (the difference is approximately 7 to 17 dB) depending on the time block. Table 7 shows a substantial change for time of day for the three time blocks shown for each season.

Table 7. Noise results for San Francisco harbor (carrier frequency 100 kHz and bandwidth of 20 kHz).

Season	Time of Day	F_{am} (dB)	σF_{am} (dB)	V_{dm} (dB)	σ_L (dB rel. 1 μV/m)	μ_L (dB rel. 1 V/m) Average	Lower	Upper
Winter	0000-0400	108	4.6	28.7	2.57	11.24	10.71	11.77
	0800-1200	85	6.4	29.5	2.61	14.08	13.34	14.81
	1600-2000	97	5.5	29.0	2.58	12.58	11.95	13.21
Spring	0000-0400	115	4.0	29.0	2.58	10.51	10.05	10.97
	0800-1200	93	6.7	30.5	2.65	13.38	12.61	14.61
	1600-2000	103	6.5	29.2	2.59	11.93	11.19	12.68
Summer	0000-0400	115	5.0	28.6	2.57	10.41	9.84	10.99
	0800-1200	98	7.4	31.5	2.69	13.04	12.19	13.89
	1600-2000	115	5.8	29.0	2.58	10.51	9.84	11.17
Fall	0000-0400	115	4.9	29.4	2.60	10.60	10.03	11.16
	0800-1200	95	6.6	31.1	2.68	13.29	12.53	14.05
	1600-2000	109	6.3	29.2	2.55	11.01	10.29	11.74

Atmospheric noise, manmade noise, and spectral interference can be most troublesome sources of degradation when using Loran-C. Section 4 defines good design practices that can minimize noise.

Spectral Interference

In the frequency bands 60 to 90 kHz and 100 to 180 kHz there are broadcast stations that operate with keyed CW, AM, PSK, and FSK modulation schemes. Several of these stations are located near coastlines and also in the vicinity of the Great Lakes region and are used for long-range communications. These transmitters have radiated powers in excess of 100 KW. Users of Loran-C in the vicinity of one or more of these sources must be able to cope effectively with the interference. Not all spectral interference is from outside the 90- to 110-kHz band. Both skywave interference and cross rate interference sources also adversely affect receiver performance.

Data Summary. It is customary to futher classify spectral interference by frequency band location of the interference relative to the 90- to 110-kHz band. The classifications are as follows:

1. In-Band Interference: Interference whose carrier frequency lies in the band 90 to 110 kHz.

2. Near-Band Interference: Interference whose carrier frequency lies in the frequency bands 70 to 90 kHz and 110 to 130 kHz.

3. Out-of-Band Interference: Interference whose carrier frequency lies in the frequency bands below 70 kHz or above 130 kHz.

Special tests were conducted in the field (Reference 4) to observe interfering signals, to determine the signal acquisition time of a typical user receiver throughout the Great Lakes region, and to monitor receiver operation. Figure 12 illustrates sites along each radial where measurements occurred. The site code from this figure is used in Table 8 to identify locations. Paragraphs that follow include results of each of the above.

During the field experiment several interfering frequencies were detected using a spectrum analyzer and are summarized in Table 8. The input to the analyzer was from an LC204 receiver (RF output jack). The notches were not used on the receiver during the tests that resulted in the data displayed in Table 8. Table 8 shows all the frequencies that were scaled from spectrum analyzer photographs. Some general comments regarding Table 8.

Table 8. Frequencies scaled from polaroid photographs.

Radial	Measurement Site	Time J. Day	Hr/Min	Frequency
A	Flint (A0)	284	0800	71.2 122 60
	Welland (A1)	281	1630	60
	Woodstock (A2)	276	1730	71.2 122 60
	Grand Bend (A3)	289	0800	71.2 122
B	Wallaceburg (B3)	289	1945	71.2 122
	Wallaceburg (B3)	290	0730	71.2 122
	Wallaceburg (B3)	291	0730	71.2 122 60
C	Port Hope (C1)	298	0900	76.4 122
	Massey (C3)	300	0800	122 71.2 60
	Victoria Harbor (C2)	298	0900	71.2 122
0	Peshu Lake (D2)	302	1645	71.2 122 60
	Wawa (D3)	306	1700	71.2 83.5
E	Ft Francis (E1 & F1)	316	1000	110 60
	Mine Center (E2)	319	0800	83.5 125.9
	Mt Cauley Lake (E3)	321	0800	83.5 125.9
	Atico Gold Mine (E4)	323	0830	60
F	Ash Lake (F2)	327	1400	110, 130, 60, 54, 71.2
	Armstrong Lake (F3)	329	0830	60 125.9
	Superior Nat. Forest (F4)	330	1430	60
	Ottawa	268	1415	125.9

1. The Eastern portion of the Great Lakes is affected by frequencies of 71.2, 122, and 60 kHz.

2. The Northwestern portion of the Great Lakes region is affected by several frequencies but when examining the photographs the effects are not nearly as severe as the Eastern Great Lakes region.

3. Ash Lake had an unusual amount of interference as compared to other sites. Again, this may be due to the randomness of broadcast times from these interfering transmitters rather than anything unique about the Ash Lake site location.

Interference from out-of-band signals was also examined in the Chesapeake Bay. One source (an 88-kHz, high-power, narrow-band transmitter located in Annapolis, MD) reduced the receiver's sensitivity by several dB. When properly adjusted, successful operation occurred in the presence of this interfering signal as long as the vessel was greater than approximately a few hundred meters away from the transmitter.

Bench tests indicated that the narrow-band notch filters (that are manually controlled) did not adversely affect the receiver's accuracy or ECD characteristics if they were adjusted outside the Loran-C band (below 90 or above 110 kHz).

SECTION 4
AUGMENTATION TECHNIQUES TO COMPENSATE FOR ERRORS

The previous section has defined and provided quantitative information for the following Loran-C error sources:

a. Transmitter
b. Temporal (including refractive index and surface impedance)
c. Noise
d. Frequency interference
e. Spatial.

Some of the above error sources vary with geographical location and time; while others are dependent on equipment design or geometry. The approach in this section is to define compensation techniques that are presently available to minimize these error sources.

Differential Loran-C to Compensate for Temporal Errors

Loran-C signals are monitored at a fixed site, and the TD (Time Difference) can be compared with a reference TD for the monitor site. A correction can then be computed and transmitted to users. This techique, called Differential Loran-C, whereby realtime corrections are applied to Loran-C TD readings has been shown to provide improved accuracy (Reference 13), and this technique shows promise for marine navigation in the harbor and harbor entrance (HHE) areas (Reference 13).

A general differential Loran-C system is shown in Figure 13. The important features of this system are:

- Multiple monitors.
- Use of Loran-C control monitor information.
- Use of an estimator/predictor.
- Improved correction algorithm.
- Multiple communication links.

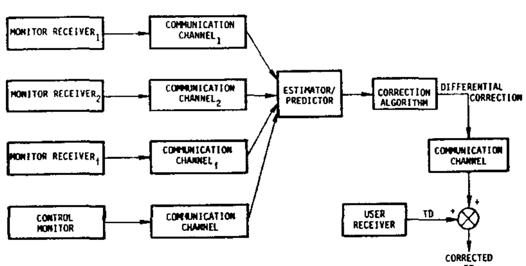

Figure 13. Differential Loran-C system.

These features all represent departures from the traditional differential concept and are expected to improve system performance.

The central idea of differential concept is to estimate the errors in user time differences and then transmit the error estimates to the user so that he may correct his TD readings and hence obtain improved accuracy.

Before installing a differential Loran-C there are several fators that must be considered during the design phase. These are summarized below. Standard covariance analysis (Reference 28) should be used to investigate the performance sensitivity to correction updates, estimator complexity, SNR, modeling errors, and estimator/predictor design parameters such as weighting factors. Simulation using existing Loran-C system models should be used to deter- mine performance versus the following:

- Number of monitors
- Orientation and spacing of monitors
- Characteristics of user and monitor receivers
- Location of control monitor
- Availability of control monitor data
- Length of sample time for computing monitor reference TD means.

The impact of the communication channels should be analyzed separately using standard techniques for communication systems. The more important parameters are

- Size of differential coverage area
- Frequency of correction
- Magnitude and precision of correction
- Site and frequency choice
- Modulation and error correction
- Number of monitors.

Communication channel requirements should be defined and communication channels postulated. Bit error rates should be determined and input to the system simulation and their impact on system performance evaluated. Validation tests to verify the above should be conducted prior to installation and operation.

Review of Past Work and Performance Expected

The concept of using a monitor receiver to correct a user receiver was originally proposed by the Naval Electronics Laboratory (NEL) for the Omega radio navigation system and was called differential Omega (Reference 29). The purpose of the original concept was to estimate the average phase velocity to a monitor receiver and then determine a phase velocity correction factor that would be used to crrect published charts and tables. These correction factors would then be broadcast to the Omega users in the vicinity of the monitor receiver. Experiments were performed where the difference between the charted reading of the monitor location and the monitor receiver reading was used as a correction factor.

One very significant observation was made concerning the experiments. Three stations, Aldra, Haiku, and Trinidad, were tracked. The station at Aldra had only been in service a very short time and was not properly synchronized. As might be expected, the error in user position from the use of charts for the Aldra-Trinidad pair was very large. However, the error in user position after the differential correction factor was applied was quite small. In other words, differential Omega was not affected by improper system synchronization.

In the summer of 1973 an experiment was conducted in the Delaware Bay area to collect data for analyzing the potential of Loran-C for high-accuracy, all-weather navigation in river, harbor, and harbor entrance environments (Reference 18). The definition of the differential Loran-C correction factor used in this study was somewhat different than the differential Omega correction factor described above. Instead of taking the difference between the actual monitor TD reading and the charted value of the TD, the correction factor was computed by differencing the actual TD from its long-term sample mean. Thus the differential concept was being applied to the repeatable mode instead of to the normal mode of system operation. Using this concept one does not need to know the monitor location at all. All that is required is that the monitor receiver be in operation long enough to compute a long-term sample mean.

The experiment specifically examined the improvement versus distance and improvement versus monitor TD averaging (correction update rate). The long-term sample means were computed using 1 week of data. The significant results of this experiment were as follows:

- Maximum improvement was obtained for a 100-second update interval (the data sampling interval) with little or no improvement for update intervals longer than 15 minutes. The corrections for the longer intervals were based on TD averages over the interval preceding the correction.
- Signals with high SNR showed the most improvement.
- There was no apparent tendency for differential errors to increase with increasing distance from the monitor (maximum separation was 69 miles).
- Errors attributed to differential changes in path transmission times were insignificant.

A second differential Loran-C study (Reference 3) was commissioned by the Coast Guard as part of the Loran-C Signal Analysis project. Its purpose was to provide necessary data for the evaluation of the potential use of Loran-C for high accuracy, all-weather navigation in a harbor, harbor entrance (HHE) environment. Four modes of system operation were considered:

1. Absolute location
2. Relative location
3. Differentially augmented absolution location
4. Differentially augmented relative location.

To provide an assessment of the absolute mode, a means of converting TDs to absolute geodetic position is necessary. The mariner normally performs this conversion with the aid of nautical charts which have Loran-C grid lines drawn on them. However, there are no such published charts for the San Francisco harbor, and an intermediate step to provide a calibrated grid for the harbor is necessary.

The specific objectives of this experiment were thus to provide a calibrated grid of the San Francisco harbor and estimates of the spatial distortion, and obtain the data required to assess the performance of Loran-C in the above mentioned modes.

To accomplish these objectives, a series of measurement deployments were planned which included both land site and vessel measurements. The measurements began 8 April and were terminated 9 May 1978.

The harbor experiment was divided into three phases: (1) a planning phase; (2) a land site measurement phase at sites around the periphery of the harbor and on Treasure, Angel, and Alcatraz Islands; and (3) a vessel measurement phase conducted aboard the USCG research vessel Polaris. Figure 14 shows the location of the 13 land sites and an outline of the areas covered by the

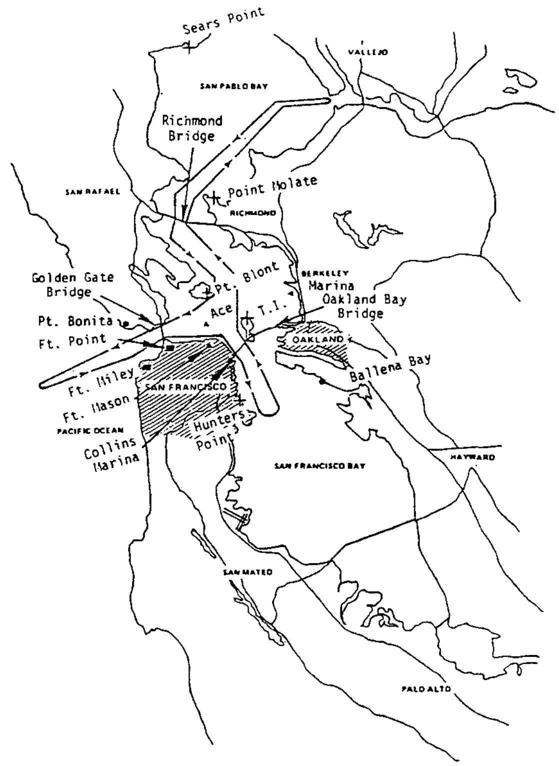

Figure 14. San Francisco Harbor test area.

Polaris. The vessel measurements will be described in later paragraphs where spatial error compensation is discussed.

Planning Phase. The specific objectives of the planning phase were to (1) select the land measurement sites; (2) select vessel tracks; and (3) estimate spatial grid anomalies. To aid in the planning phase, data analyzed from Fort Cronkhite, USCG calibration data collected at Treasure Island, and data from the propagation path experiment discussed earlier were used.

An idealized grid was first prepared for the harbor and harbor entrance of San Francisco Bay as a visual aid in planning and experiment control. For example, TDs from these grids were provided to site technicians to verify proper receiver operation. For two LOPs (lines of position) an idealized grid is parametrized by six quantities: four average phase velocities and two secondary emission delays. The time differences for a user at latitude L and longitude λ are given by

$$TDX(L,\lambda) = E_X + d_X(L,\lambda)/V_X - d_M(L,\lambda)/\bar{V}_{MX} \qquad (1)$$

$$TDY(L,\lambda) = E_Y + d_Y(L,\lambda)/V_Y = d_M(L,\lambda)/\bar{V}_{MY} ,$$

where

L = latitude of user position

λ = longitude of user position

E_X = emission delay for X-ray (μs)

E_Y = emission delay for Yankee (μs)

$\overline{V}_{MX}$ = average phase velocity from Master for TDX ($km/\mu s$)

$\overline{V}_{MY}$ = average phase velocity from Master for TDY* ($km/\mu s$)

$\overline{V}_X$ = average phase velocity from X-ray ($km/\mu s$)

$\overline{V}_Y$ = average phase velocity from Yankee ($km/\mu s$)

$d_M(L,\lambda)$ = geodetic distance to Master (km)

$d_X(L,\lambda)$ = geodetic distance to X-ray (km)

$d_Y(L,\lambda)$ = geodetic distance to Yankee (km).

Note that TD measurements at three positions (3 TDX, 3 TDY) are sufficient to determine all of the parameters in the idealized model. When less than three measurements are available, parameters must be estimated by predictions or obtained from other sources. To obtain the necessary parameters for the initial idealized grid from available data, Fort Cronkhite data and USCG chain calibration data were used. From the chain calibration data the values of the emission delays were determined by averaging TD data taken on the baseline extensions. The values obtained were:

$$E_X = 28094.467 \quad \mu s$$

$$E_Y = 41967.620 \quad \mu s \quad .$$

The phase velocity V_Y was estimated using the phase predicted from the integral equation program for the Yankee path to Fort Cronkhite. Then values were assigned to V_X, V_{MX}, and V_{MY} which, when adjusted for the land-to-sea interface effects, matched the Fort Cronkhite data for TDS and TDY reasonably well. The phase velocities determined were

$$\overline{V}_{MX} = \overline{V}_{MY} = \overline{V}_M = 0.299061 \quad km/\mu s$$

$$V_X = 0.2983804 \quad km/\mu s$$

$$V_Y = 0.299150 \quad km/\mu s \quad .$$

As a first approximation, we assumed that spatial grid distortions were primarily the result of phase recovery at land-sea interfaces and the scattering of signals from large metallic bridges. At land-sea interfaces, the secondary phase of the Loran-C signal undergoes a rapid decrease (see Figure 15, which is typical for all lower to higher conductivity changes). When the interface is far from the transmitter, the phase recovery is primarily determined by the overwater distance after the transition, as illustrated in Figure 16. This effect was employed to calculate first-order grid distortions relative to the idealized grid. A typical example of the distortion is shown in Figure 17.

*Obviously, in the real world, V_{MX} and V_{MY} must be equal, and they are treated so in this subsection. However, Equation 1 can be used as a numerical fit to data, as it is in later sections, and a better fit can be obtained by allowing $V_{MX} \neq V_{MY}$.

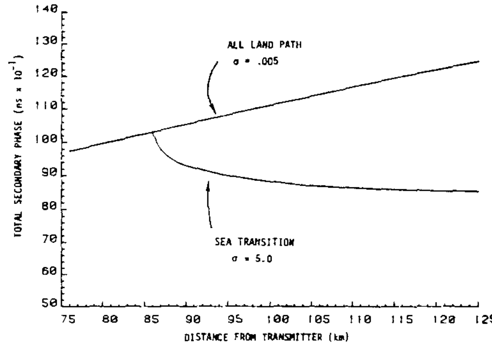

Figure 15. Effect of a land-sea interface on the seconday phase.

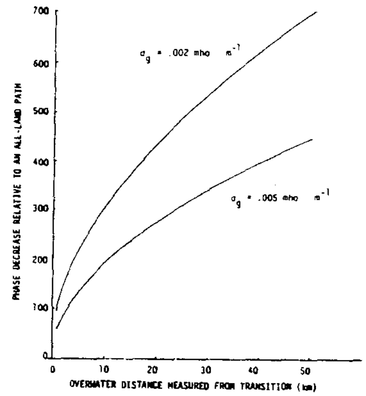

Figure 16. Phase change versus distance from the land-sea transition.

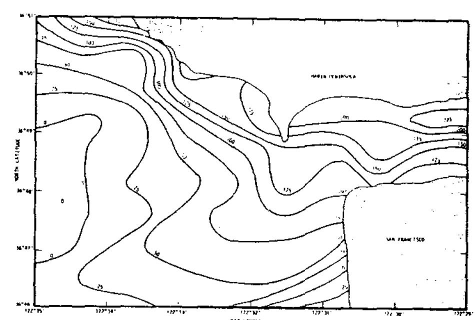

Figure 17. First-order TDX variations (ns) produced by the land-sea boundary effect in the outer harbor.

Two areas were considered: (1) the area outside the Golden Gate bridge to the sea buoy, and (2) the inner harbor. Examination of the estimated TD errors outside the Golden Gate revealed that TDX errors ranged from +200 ns to -25 ns, while TDY errors were in the range +50 ns to -75 ns. For the inner harbor TDX errors ranged from +200 ns to -400 ns, while TDY errors were in the range +50 ns to -75 ns.

To study grid distortion caused by large metallic structures such as bridges, it was assumed that scattering was the major effect. The bridge structure was modeled as a rectangular conducting plate, and both cw and pulsed operation were considered. Figure 18 shows estimated

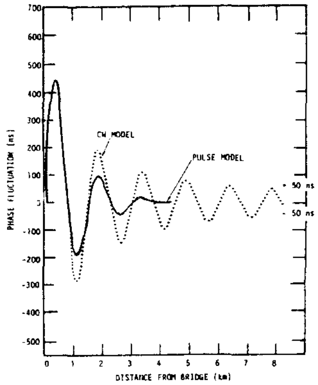

Figure 18. Phase error produced by reflection from Golden Gate Bridge.

phase fluctuation versus distance from the bridge. In the pulsed mode of operation, the fluctuations damped out more quickly than in the cw mode. Based on this analysis, it was predicted that the largest distortion would occur on the harbor side of the Golden Gate Bridge. This results because the X-ray signal is parallel to the bridge, producing little interfering reflection and the Master signal arrives perpendicular to the bridge, producing maximum reflection. For the Bay Bridge the distortion was predicted to be less severe than for the Golden Gate Bridge, with TDY being most affected. No significant distortion was expected near the Richmond Bridge since its height is only a small fraction of a wavelength at 100 kHz.

The land harbor sites and the vessel tracks were selected on the basis of the analysis described above. For details of the selection process, see Reference 12. As an example, a closely spaced series of parallel vessel tracks in the vicinity of the Golden Gate Bridge was selected to map the scattering effects predicted.

Fixed Land Site Phase. The purpose of the land site measurements was to provide data necessary to obtain: (1) a calibrated, accurate harbor grid; (2) an evaluation of grid accuracy and anomalies; (3) an evaluation of relative (repeatable) mode Loran-C; and (4) an evaluation of differentially augmented relative mode Loran-C. The land harbor site measurements were made using five receivers in three deployments of approximately 1 week each. Since two sites were visited twice, data were collected at a total of 13 sites. Figure 14 shows the location of the sites. The crosses represent deployment 1 sites, the circles represent deployment 2 sites, the triangles represent deployment 3 sites, and the squares represent sites which were common to deployments 2 and 3.

Data Collection and Analysis. The data collected are summarized in Table 9. The values in Table 9 were computed using 7 to 9 days of data (data sampling interval of 100 seconds) for each site (the actual number of days of data for each site is indicated in the data sample column of Table 9). All standard deviations are small (ie, below 30 nanoseconds). Week 2 showed the largest standard deviations. As already mentioned in Section 4, this is attributed to problems at the Point Pinos SAM. Note the shift in mean TDX and mean TDY at Fort Point and Fort Mason between weeks 2 and 3. Fort Cronkhite data also exhibited similar behavior.

To evaluate the accuracy of the idealized grid and calibration techniques, a series of

Table 10. Harbor experiment data summary (values in microseconds).

Deployment	Measurement Site	Data Sample (days)	Mean TDX	Mean TDY	Std. Dev. TDX	Std. Dev. TDX
1	1. Sears Point	7	27159.2852	43306.6406	0.0218	0.0195
	2. Point Molate	7	27203.0703	43241.7578	0.0181	0.0185
	3. Angel Island	7	27221.6641	43211.2812	0.0222	0.0177
	4. Hunters Point	7	27256.0820	43167.8594	0.0278	0.0217
	5. Treasure Island	7	27238.0508	43201.4687	0.0243	0.0203
2	6. Ballena Bay	7	27272.6992	43178.0156	0.0249	0.0205
	7. Collins Marine	7	27241.4961	43188.1641	0.0210	0.0255
	8. Fort Mason	9	27226.5898	43196.8047	0.0271	0.0220
	9. Fort Point	7	27217.5937	43197.5937	0.0250	0.0230
	10. Point Bonita	8	27199.4922	43204.2031	0.0292	0.0276
3	11. VA Hospital Fort Miley	7	27211.7305	43191.1250	0.0227	0.0227
	12. Fort Point	9	27217.5781	43197.5625	0.0189	0.0223
	13. Fort Mason	9	27226.5820	43196.7969	0.0175	0.0193
	14. Alcatraz Island	9	27225.4258	43202.5547	0.0174	0.0196
	15. Berkeley Marina	8	27248.7695	43211.9375	0.0218	0.0276

grids were prepared based on the data from selected land sites. The accuracy of the resulting grids was estimated by comparing the predicted TD for the measurement sites with the actual measured values. A thorough discussion of these procedures can be found in Reference 11. The idealized grids were derived from the following data: (1) the original grid parameters estimated in the planning phase; (2) fixed sites with all over-land paths (Fort Cronkhite, Sears Point, Ballena Bay, and Berkeley Marina); (3) fixed site data with both on-shore and mid-harbor locations (Sears Point, Alcatraz, and Fort Miley); and (4) data from all sites using a least squares fit. The accuracy of the grids fits to the data progressively improved from (1) to (4). This comparison is summarized in Table 10.

Conclusions from Fixed Site Data. The error contours from the planning phase did not explain the difference between measured values and the initial idealized grid. It was discovered that an additional major error source was due to the nonlinear phase distance relationship (ie, phase is not really a linear function of distance even for a short homogeneous path segment as assumed in Equation 1. Additionally, it was determined that the land-sea recovery was not as large as predicted when the parameters of Equation 1 are estimated from data taken at a carefully selected set of calibration sites. The effects of the nonlinear phase-distance effect are worst at moderately close distances to the transmitter, where the phase versus distance function has significant curvature. Thus, grid fits may have larger errors for short baseline systems than for long baseline systems (given equal accuracy in the calibration data). The sensitivity to conductivity changes is greater, thus temporal changes in the ground conductivity due to precipitation or freezing can cause significant grid instabilities.

The use of grids based upon phase velocity as a polynomial function of range and bearing from each transmitter was not considered. It was reasoned that the additional complexity of these grid models would only yield slight accuracy improvement, since the required smoothness in the spatial derivatives of the phase is clearly not attained in the complex signal path impedance structure found in harbors.

The analysis of grid calibration techniques found in Reference 11 provides an upper bound for grid fit error of 250 ns for the area bounded by the calibration sites. This error analysis also predicted larger grid errors for TDX

Table 10. Summary of harbor fixed site data reduction and grid preparation.

Site	Distances to Master, X-ray, and Yankee			Measured (Predicted Using →)		Estimated Parameters Used in Experiment Plan		Overland Path Data		On Shore and Mid Harbor Data		Least Square Fit to 13 Sites	
	D_M(km)	D_X(km)	D_Y(km)	TDX (μs)	TDY(μs)	TDX(μs)	TDY(μs)	TDX(μs)	TDY (μs)	TDX(μs)	TDY(μs)	TDX(μs)	TDY(μs)
Fort Cronkhite	374.588	104.539	746.697	192.402*	210.969*	192.363	211.134	192.402	210.796	191.975	211.100	192.191	211.027
Fort Miley	375.085	110.973	741.214	211.731	191.125	212.271	191.143	212.307	190.780	211.731	191.125	211.908	191.052
Point Bonita	374.455	106.654	744.558	199.492	204.203	199.899	204.427	199.937	204.082	199.456	204.392	199.653	204.321
Fort Point	370.808	108.400	738.861	217.586	197.579	217.947	197.581	217.984	197.242	217.398	197.482	217.511	197.438
Point Blunt	364.550	103.375	736.769	221.664	211.281	222.026	211.511	222.065	211.213	221.496	211.293	221.526	211.290
Alcatraz Island	366.363	106.368	735.957	225.426	202.555	226.000	202.736	226.037	202.420	225.426	202.554	225.468	202.540
Fort Mason	368.020	108.381	735.873	226.586	196.801	227.207	196.916	227.243	196.587	226.611	196.767	226.670	196.742
Hunter's Point	368.596	117.796	727.833	256.082	167.859	256.842	168.113	256.873	167.749	256.019	167.983	256.020	167.960
Ballena Bay	360.146	114.395	722.439	272.699	178.016	273.694	178.335	273.726	178.016	272.812	178.049	272.674	178.082
Collins Marina	366.266	111.073	731.574	241.496	188.164	242.097	188.410	242.131	188.078	241.403	188.231	241.408	188.220
Treasure Island	362.770	106.589	732.047	238.051	201.469	238.754	201.678	238.790	201.375	238.112	201.431	238.084	201.441
Berkeley Marina	356.070	103.164	728.493	248.770	211.938	249.675	212.202	249.713	211.938	249.005	211.830	248.873	211.884
Point Molate	359.703	92.988	741.023	203.070	241.758	203.415	241.942	203.459	241.698	203.063	241.626	203.077	241.650
Sears Point	350.111	70.240	750.937	159.285	306.640	159.229	307.152	159.285	307.021	159.285	306.639	159.283	306.716

Measured Minus Predictions → Site	TDX(ns)	TDY(ns)	TDX(ns)	TDY(ns)	TDX(ns)	TDY(ns)	TDX(ns)	TDY(ns)
Fort Cronkhite	+39	-165	-0.1	+172.6	+426.7	-130.6	+210.8	-57.9
Fort Miley	-540	-18	-575.6	+344.7	+0.3	+0.5	-176.7	+73.2
Point Bonita	-407	-224	-444.5	+121.5	+36.2	-189.1	-161.1	-118.3
Fort Point	-353	+13	-397.6	+336.8	+188.1	+97.1	+74.5	+141.5
Point Blunt	-362	-230	-400.7	+68.1	+167.9	-12.5	+137.9	-8.6
Alcatraz Island	-574	-181	-600.1	+134.6	+0.5	+0.8	-42.3	+15.4
Fort Mason	-617	-111	-657.2	+213.6	-24.6	+34.4	-84.2	+59.3
Hunter's Point	-760	-254	-791.3	+110.5	+63.0	-124.4	+62.5	-101.0
Ballena Bay	-995	-319	-1027.1	+0.4	-112.8	-32.8	+24.9	-65.5
Collins Marina	-601	-246	-635.1	+86.4	+93.4	-67.0	+87.8	-55.7
Treasure Island	-703	-209	-739.3	+94.0	-61.3	+37.8	-32.7	+27.6
Berkeley Marina	-905	-264	-942.9	+0.0	-235.1	+107.9	-102.6	+53.7
Point Molate	-345	-184	389.0	+59.8	+7.0	+131.5	-7.1	+108.1
Sears Point	+56	-512	+0.1	-380.5	+0.3	+0.8	+1.6	-76.3

	Original Estimated Parameters	Overland Paths	On Shore + Harbor	Least Squares
Mean TDX Error	505	544	-39	0.5
Std Dev. (TDX)	307	302	154.5	111
Mean TDY Error	207	-97	10.4	0.3
Std Dev. (TDY)	127	173	93.4	81
Max Error (TDX)	995	1027	426	211
Max Error (TDY)	512	380.5	124	141

*Add 27000 to TDX
Add 43000 to TDY

than TDY, which was confirmed by the measurements. The final idealized grid had about 100-ns accuracy for the harbor area best sampled by the calibration sites. An obvious means of improving grid accuracy would be to use multiple grids. The number of grids and their boundaries could be selected based on an error analysis which bounds the error of each subgrid.

An alternative grid parametrization considered was the linear grid, which is a linearization of Equation 1 about some fixed location. Obviously a linear grid is less accurate over a large area, but errors near the linearization point may be quite small. Thus, one might consider the use of multiple linear grids to achieve the same accuracy as the idealized grid. This essentially trades increased parameter storage needed for the simpler coordinate conversion algorithm (ie, one only needs to solve a set of linear instead of nonlinear equations). The linear grid is of interest from the standpoint that it is simple, easily implemented, and need not provide absolute position (see Reference 31). Both the idealized grid and the linear grid have the very desirable property that the grid calibration can be completely automated and performed in real time. This has been implemented for the linear grid by the USCG.

Evaluation of Differentially Augmented Relative Mode (Differential Loran-C). The fixed site data from the first deployment were processed to simulate a differential Loran-C system. The concept of differential Loran-C was tested in the Differential Loran-C Time Stability study (Reference 18) as stated earlier. In this study, conducted in 1973, it was shown that the differential mode of operation resulted in improvement factors of 1.5 to 3 over the repeatable mode. In the differential mode a monitor receiver at a known, fixed location is used to compute a correction that is provided to users in the area. The user then adds this correction to his receivers TDs to obtain more accurate TDs. The basic formula for computing the correction for X-ray from data at site G is

$$DC(t_i) = \overline{TDGX} - TDGX(t_i) \quad , \qquad (2)$$

where $DC(t_i)$ denotes the differential correction at time t_i, $\overline{TDGX}$ is the average monitor or control TD, and $TDGX(t_i)$ is the monitor TD at t_i. The error in the differential correction, or the differential error DE, is the sum of the signal variation at the mobile location and the DC, namely

$$DE(t_i) = (TDSX(t_i) - \overline{TDSX}) + (TDGX(t_i) - \overline{TDGX}) , \qquad (3)$$

where S is the mobile user site. If the time differences are highly correlated and the two receivers measure without error, then the DE would be quite small.

Consider the problem of finding the optimal estimate of the user TD given the TD at the monitor. It is well known that the linear minimum variance unbiased estimate is given by

$$\widehat{TDSX}(t_i) = K(TDGX(t_i) - \overline{TDGX}) + \overline{TDSX} \quad , \qquad (4)$$

where $\widehat{TDSX}(t_i)$ denotes the minimum variance estimate of $TDSX(t_i)$ and the gain K is given by

$$K = \frac{E\ (TDSX(t_i) - \overline{TDSX})(TDGX(t_i) - \overline{TDGX})}{E\ (TDGX(t_i) - \overline{TDGX})^2} \qquad (5)$$

where $E\{\cdot\}$ is the expectation operator. If we multiply Equation 4 by -1 and add $TDSX(t_i)$ to both sides we get

$$(TDSX(t_i) - \overline{TDSX}) - K(TDGX(t_i) - \overline{TDGX}) = TDSX(t_i) - \widehat{TDSX}(t_i) \quad . \qquad (6)$$

We see that this represents a general expression for the differential error. Since $\widehat{TDSX}(t_i)$ minimizes the variance of Equation 6, we conclude that

$$DC^*(t_i) = -K(TDGX(t_i) - \overline{TDGX}) \qquad (7)$$

is the optimum differential correction. It is clear that Equation 2 is a special case of Equation 7 where K = 1.

If K = 1 as computed by Equation 5, then we conclude that

$$COV(TDSX,TDGX) = COV(TDGX,TDGX) \quad , \qquad (8)$$

or TDSX and TDGX are perfectly correlated. It is obvious that using Equation 7 as a correction rather than Equation 2 should reduce the variance of the differential error. The form of Equation 7 has a nice intuitive explanation. Since we are dividing up the variance of the monitor TD, we see that as the variance goes up, the gain goes down. However, since the numerator of Equation 5 is the covariance of the mobile and monitor TDs, we see that for highly correlated TDs the gain will approach unity no matter how large the variance of the monitor becomes. This is a very satisfying logical result.

The terms in Equation 5 can be estimated from experimental data. To do this we can estimate the covariance and variance by computing the sample covariance and the sample variance. The formulas are given by

$$COV(TDSX,TDGX) = \frac{1}{2} \sum_{i=1}^{N} [TDSX(t_i) - \overline{TDSX}][TDGX(t_i) - \overline{TDGX}] \qquad (9)$$

and

$$COV(TDGX,TDGX) = \frac{1}{N} \sum_{i=1}^{N} [TDGX(t_i) - \overline{TDGX}]^2 \qquad (10)$$

where N is the number of data samples. Thus Equation 5 becomes

$$K = \frac{\sum_{i=1}^{N} [TDSX(t_i) - \overline{TDSX}][TDGX(t_i) - \overline{TDGX}]}{\sum_{i=1}^{N} [TDGX(t_i) - \overline{TDGX}]^2} \qquad (11)$$

Equation 11 is fine for investigating the differential concept. However, it is not very useful for real-world use. There are several immediate reasons for this. Among them is the fact that although the sample variance can be computed for the monitor receiver, it may be difficult to compute for the covariance of the mobile receiver against the monitor unless a large sample of data is available from the mobile receiver. For the real-world use of differential Loran-C, we need an expression for COV(TDSX,TDGX) which can be precomputed without the need of experimental data from the mobile receiver.

We can use the fluctuations model described in Reference 13 to compute the desired covariance, if we make the following assumptions: (1) that chain, propagation, and receiver variations are mutually independent; (2) the monitor and mobile receiver are close enough so that the propagation fluctuations are identical at both receivers for each signal; (3) the signals from each transmitter are mutually independent; and (4) the receiver fluctuations at each receiver are independent. If these assumptions are satisfied, then

$$E\{tdsx \times tdgx\} = E\{x_\theta(t_i)^2\} + E\{m_\theta(t_i)^2\} + E\{[x_\Omega(t_i - m_\Omega(t_i)]^2\} \quad . \qquad (12)$$

Using data from the stability experiment (Reference 13), we can estimate the value of K for TDX to be 0.98 and for TDY to be 0.88.

Data Collection and Analysis. One week of data collected at Sears Point, Point Molate, Angel Island, Treasure Island, and Hunters Point was used to simulate differential Loran-C. Sears Point was arbitrarily designated as the monitor receiver to correct Point Molate, Angel Island, and Hunters Point, while Angel Island was designated monitor to correct Treasure Island. The differential error was computed for five different averaging intervals: 100 s, 15 min, 2 hours, 6 hours, and 24 hours. For each averaging interval, the differential error was computed for two differential gains, 1.0 and the value computed by Equation 11. Histograms of each of these differential error sequences, sample standard deviations, and improvement ratios were produced. Improvement ratio is defined as the ratio of the standard deviations of the uncorrected mobile TD to the corrected mobile TD.

Figures 19 and 20 show the improvement ratio versus correction averaging inteval for TDX and TDY, respectively. Each plot has two curves, one for the standard differential gain (ie, K=1) and the other for the optimal differential gain as computed using Equation 11. For TDX the curve

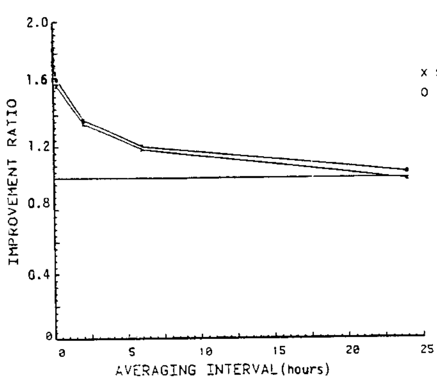

Figure 19. Improvement ratio versus correction interval for TDX.

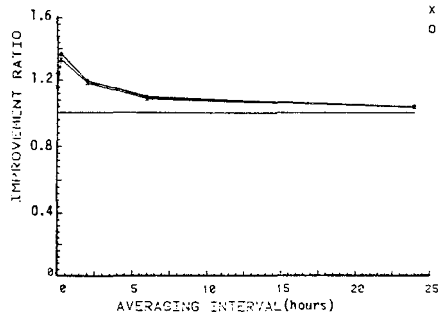

Figure 20. Improvement ratio versus correction interval for TDY.

exhibits the expected behavior of an exponentially decaying improvement ratio with a maximum for no averaging. Of course the curve for the optimal gain remains above the curve for standard gain, but the improvement is not dramatic. Figure 20 for TDY is much more interesting. Notice that the improvement ratio is a maximum for 15-minute averaging of the correction. Since the Yankee signal has a lower signal-to-noise ratio than X ray, the variation in TDY at the two sites has a larger independent component, which is reduced by averaging. However, averaging the correction also reduces the components that are correlated with the user TD. Apparently there is sufficient time correlation in TDY to yield improved results even though the correction is averaged longer.

While the standard gain yields degraded performance for 24-hour averaging of the correction on TDX, it yields improvement for this long averaging interval on TDY. This is further proof that TDY has signifiant long-term correlation. In general, though, the improvement ratios for TDX are higher than those for TDY, as one would expect due to the higher signal-to-noise ratio on the X-ray signal.

In Figures 21 and 22 the improvement ratio versus distance from the monitor are plotted. There does not appear to be any consistent pattern. In fact, for TDX this curve peaks at 33 km, with the general trend of increasing improvement with distance. TDY, however, behaves more as one might expect with improvement decreasing with distance. A strong negative correlation between distance from the monitor and improvement ratio implies that propagation fluctuations are dominant in the differential error. However, the verification and stability experiments have clearly shown that propagation fluctuations are much smaller than chain fluctuations and are on the order of receiver fluctuations. Since the Yankee signal path is the longest, one would expect propagation fluctuations to be more pronounced. Examination of the stability data also reveals that Yankee chain equipment fluctuations are somewhat smaller than for X ray. This seems to explain both the decrease in improvement ratio with distance and the larger low-frequency spectral components observed for TDY.

Sears Point correcting Angel Island showed the best performance of the five pairs. The standard deviation of the corrected time differences was 0.2 ns for TDX, and 12.6 ns for TDY. A careful examination of the data reveals the following points: (1) the data sample for this pair was by far the largest; (2) portions of days 102 and/or 106 were missing at Point Molate, Hunters Point, and Treasure Island due to

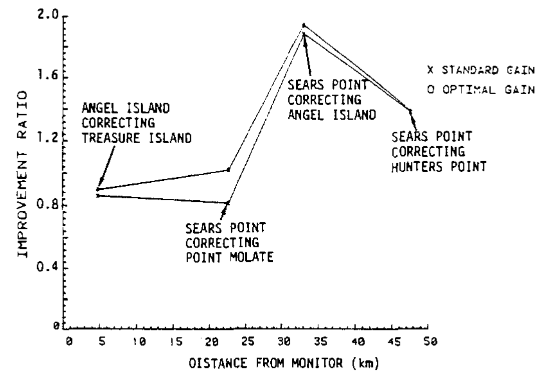

Figure 21. TDX improvement ratio versus distance from monitor.

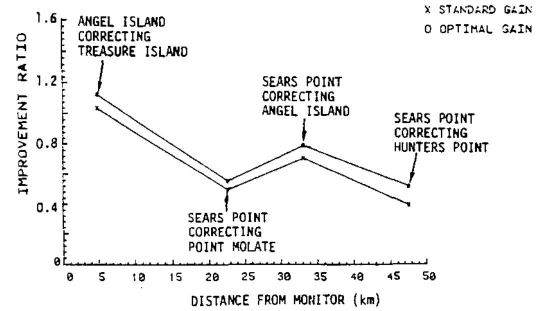

Figure 22. TDY improvement ratio versus distance from monitor.

receiver simulator tests or receiver problems; and (3) these particular days showed significant chain fluctuations that were highly correlated at both Sears Point and Angel Island. These facts tend to make the improvement for Sears Point correcting Angel Island look much better than for the other pairs. Results from the Differential Loran-C Time Stability study show that 7-ns rms was the smallest DE standard deviation obtained (based on 1 week of data). Simulator tests performed on the receivers for comparable signal-to-noise ratios suggest that no further improvement is possible beyond this level.

The TDX data for most site pairs were highly correlated ($\rho > 0.85$). Thus, the improvement gained by using the optimal differential gain was only slight. The exception was Sears Point and Point Molate. The correlation between TDX at these locations was $\rho = 0.75$. The standard deviation of TDX was 18 ns at Point Molate and 21 ns at Sears Point. The standard deviation of the differential error for $K = 1$ was 14 ns and 12 ns for $K = 0.66$, about a 15-percent improvement. The improvement gained by using the optimal K was generally larger for TDY than TDX as expected, due to the lower signal-to-noise ratio on Yankee. The improvements due to the use of the optimal K are encouraging enough to warrant further investigation.

The optimal K derived here is based only on instantaneous signal fluctuations. We have already seen that there is significant time correlation in TDY. This suggests that the differential correction should be based on the output of a Kalman (or Weiner) filter that could exploit this time correlation in an optimal manner. Other extensions naturally handled by the Kalman filter structure would include multiple monitors.

Differential Loran-C Recommendations. Since there is little or no correlation between differential improvement and distance from the monitor, we conclude that differential propagation fluctuations are not as significant as receiver and chain (equipment) fluctuations. Furthermore, it appears that chain fluctuations are a significant error source in TDs measured in the San Francisco Bay area even though the Control Monitor is nearby at Point Pinos.

Automatic initialization and update would be far superior over manual initialization because of the frequency update (100 sec) requirements to obtain maximum accuracy (25 to 50 feet) as defined in the preceeding paragraphs. This maximum accuracy is required in large portions of most rivers, harbors, and other narrow waterways. The limiting factors for achieving higher accuracies than presently available using differential Loran-C are equipment related (ie, further reduction in receiver error is required). Automation of differential Loran-C implies carefully designed software, communication links, and devices to avoid errors in processing and transmitting corrections.

Initialization Techniques Using Loran-C (Initiate and Go/Initialize on the Fly)

The ability to initiate and go and initialize on the fly has been under development by the US Air Force and US Coast Guard since 1968. This is not a new technology to the military sector. In 1968 a Loran Assist Device (LAD) was developed for a unique military aircraft requirement and was followed by several other military versions. In 1970 a Coast Guard Loran Assist Device (COGLAD) was developed to evaluate Loran as an aid to laying buoys. With the development microprocessors in 1973, a small, simple processor (CLAD) was developed and tested by the Coast Guard. The original COGLAD was upgraded and tested on the Great Lakes in 1976. PILOT (Precision Intracoastal Loran Translocation) was developed in 1979 and tested aboard ore carriers on the Great Lakes in late 1980. PILOT is a preproduction microprocessor-controlled graphics terminal using Loran and prerecorded charts to aid ships piloting rivers and harbors. Each new system used increasingly sophisticated data processing techniques, required less operator training and attention, and represented a lower potential production cost. These improvements were largely the result of the phenomenal developments in the integrated circuit and microprocessor industry in the last decade.

The design objective of the PLAD system was to demonstrate that Loran repeatability (ie, return to presurveyed way points) could be successfully used to pilot harbors and rivers, and that the system be sufficiently portable for professional pilots to hand cary aboard commercial vessels. PLAD can be used in any harbor or river that has good Loran-C coverage (geometry and SNR) and has been surveyed. To change the PLAD operational area requires that one memory data chip in PLAD be replaced but no hardware or software modifications are required. PLAD and this interchangeable chip are both identified in Figure 23.

There are numerous variations in applying initialization. One such procedure is summarized below using the PLAD system:

1. Approximately one hour before boarding a vessel, PLAD should be taken to a calibration point, set up, allowed to lock on, and commanded to execute an automatic calibration run.

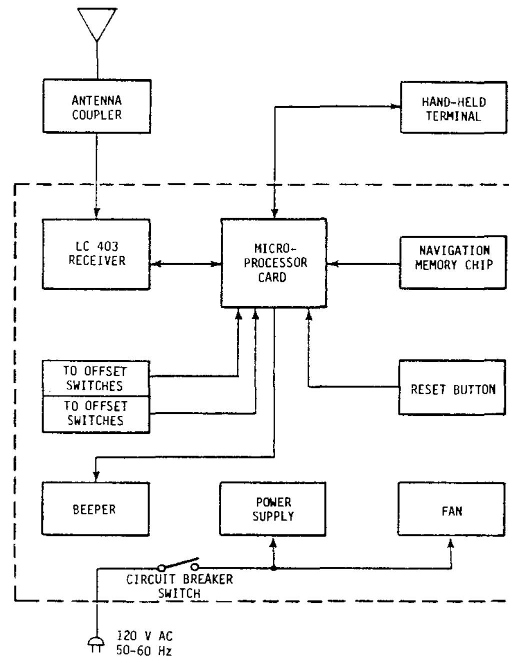

Figure 23. PLAD system block diagram.

2. After the calibration samples are taken, the TD bias values from the auto calibration run are loaded into the TD bias section of PLAD and the unit is shut down in order to carry it aboard the vessel.

3. The unit is taken aboard the vessel and set up at a convenient point for the navigator or user taking into account proper location to avoid shipboard noise* and antenna problems*.

4. When the receiver indicates lock on (approximately 5 to 15 minutes), the user can select a course and be sure that the PLAD display settles on the proper range.

5. Select appropriate displays (Along track distance, cross track distance, along track speed, cross track speed, etc) with which to navigate.

With sufficient data collection, initialization can also occur at the departure point and previously surveyed waypoints can be used for navigation. Specifically at each waypoint the nominal Loran time differences are obtained from a survey and known to the navigator. In the neighborhood of a waypoint the difference between the TD measured by the navigator and the surveyed TD of the nearby waypoint is a differenced TD. The TDs obtained from the two secondary transmitters are unique to the position (x,y) at which they are measured, where x and y denote horizontal displacements relative to the waypoint.

The relationship between the two TDs and x and y is nonlinear. For given TDs the solution for x and y is obtained by an iterative procedure. Once the navigation algorithm has converged to final values of x and y the ship's horizontal velocity components are also readily calculated as linear

*Most Loran-C receiver manufacturers provide sound guidance for optimum antenna locations and information on how to avoid shipboard noise.

combinations of the time derivatives of the measured TDs. The TD time derivatives are available from the TD filters.

The St. Marys River minichain used the above technique in 1979 successfully. The St. Marys Loran-C minichain features short propagation paths, and good geometry. Therefore it was possible to reduce the geometry to a single plane tangent to the earth at the origin. No account was taken of the earth's curvature in computing the theoretical transmission path lengths. Reference 34 extended this technique used in the St. Marys to allow the computation to be used with the most general configurations of Loran transmitter and waypoint geometry.

The previously surveyed TDs do fluctuate with time as demonstrated earlier in this report. Depending on the accuracy requirements (harbor or river dimensions) differential Loran-C may also be required when using systems such as PLAD. There is a clear tradeoff when employing the above augmentation techniques individually or combined that must be made for each individual harbor, river, and waterway (accuracy requirement versus harbor, river dimensions, and system geometry must be considered). These considerations have been discussed earlier. See References 32 through 34 for further detail.

Grid Calibration

There are two techniques (and variations thereof) that are used for grid calibration:

1. Position Reference System — This technique requires the simultaneous (time synchronized) recording of both Loran-C TDs and range values or phase differences from a position reference system. These signal values are all converted to latitude and longitude for comparison of Loran-C with the positioning reference or "truth" system. The positioning system is calibrated to a known accuracy.

2. Visual Grid Survey — This method was developed to determine TD coordinates of the physical features of an HHE area. The process consists of selecting route waypoints; computing estimates of TDs; estimating position of surrounding navigation features; surveying (measuring) TDs along visual ranges, channel edges, and at aids to navigation in the vicinity of the waypoint; statistically defining the TDs for the waypoints. This technique is used to determine the evaluate navigation parameters for repeatability and accuracy.

These grid survey techniques only account for spatial change in a harbor or river environment. After a successful survey the spatial features (bridges, terrain elevation, large structures, islands, etc) are built into the grid (ie, the grid is warped). To control Loran-C temporal timing fluctuations still requires the use of differential Loran-C with correction intervals less than 15 minutes for high accuracy. Based on data evaluated to date daily broadcasts may not be sufficient to represent changes in the time varying components of the Loran-C grid for locations featuring narrow waterways. In open bay areas (such as the Chesapeake) daily broadcasts may be sufficient (ie, less accuracy required).

Each of the grid calibration tecnniques will now be described.

Position Reference System. Kaman Tempo (Reference 13) collected data on a research vessel in San Francisco harbor for the US Coast Guard. This was the first intensive harbor calibration ever sponsored by the Coast Guard.

While measurements were being made at fixed land sites, data were also being collected on board the research vessel Polaris in the harbor and harbor entrance. Figure 15 shows an outline of the area covered by the vessel. Both TOA and TD receivers collected data. The vessel position was measured quite accurately using the Trisponder radar system. The vessel position measurements should be an order of magnitude better than expected Loran-C errors to reasonably measure any errors in the Loran data. Summer data collected at Fort Cronkhite had suggested a 30-meter ($2D_{rms}$) Loran-C error, which dictates a requirement for a 3-meter ($2D_{rms}$) error in locating the vessel. The Trisponder radar system (a master unit and track plotted on the vessel and four transponders on the shore) provided this accuracy. This accuracy was proven based on calibrating the Trisponder position between two known points at distances that were similar to those used during the Loran-C harbor calibration. Vessel position was recorded every second. A total of 11 days of data were taken, 9 with 100-second averaging and sampling, and 2 with 10-second averaging and sampling of the Loran-C data.

The object of this phase of the experiment was to provide data for an assessment of absolute mode Loran-C in a typical harbor environment and to study grid anomalies produced by bridges. To assess the abolute mode, idealized grid parameters which were obtained by a least squares fit of land site data were used for conversion of time differences to latitude and longitude and vice versa.

Before comparison between the Trisponder position data and Loran-C data could be accomplished, a number of technical problems had to be addressed. These included: (1) correction of the Loran-C data to compensate for dynamic errors due to vessel motion and the long averaging times of the receivers; (2) the editing and filtering of the Trisponder data; and (3) proper handling of large data gaps in the Trisponder data. These are briefly discussed below.

To correct the Loran-C data for averaging errors, the Trisponder data were used to estimate vessel heading and speed. The receiver averaging was modeled and an expression was obtained for the error as a function of heading and speed. This expression was used along with the heading and speed data to estimate the error due to averaging for each TD. Finally, this estimate was subtracted from the Loran-C data.

The Trisponder data were found to have some bad data points and outliers. Much of this bad data was caused by signal scattering from large vessels that passes near the Polaris. A Kalman filter was used to edit these bad data. The Trisponder data were filtered in cartesian coordinates, and data editing was performed by comparing the data with its prediction from the filter. If the difference was too large, the data point was rejected and replaced by the prediction.

At other times the line-of-sight to the transponders was interrupted by large vessels. In this case data gaps up to 60 seconds occurred. To fill these gaps the predictions from the Kalman filter were used. However, if the filter covariance became too large, no comparison was made for that Loran-C sample and the Kalman filter was reinitialized.

To test the validity of the dynamic error removal algorithm, simulator tests were performed by Kaman Tempo at EECEN (US Coast Guard Electronic Engineering Center). The LRTC-II (Loran-C Receiver Test Complex) simulator was programmed to produce a series of TDs which simulated a vessel steaming at 6 knots. It was found that the dynamic error was corrected to within 10 ns.

Data Collection and Analysis. A block diagram of the processing system used to compare the Loran data to the Trisponder data is shown in Figure 24. An example vessel track is shown in Figure 25 along with the corresponding vessel position obtained from Loran-C. Figure 26 compares latitude and longitude as computed by the Trisponder (truth system) represented by the small dots and the Loran-C system as represented by the "fat" dots. Figure 27 shows time difference errors as arrows emanating from the "true" vessel position and pointing in the direction of time difference gradient. For TDX the arrows are at angles from the vertical of approximately 120 degrees for positive errors and -30 degrees for negative errors. TDY errors are represented by arrow points up (0°) for positive errors and down (180°) for negative errors.

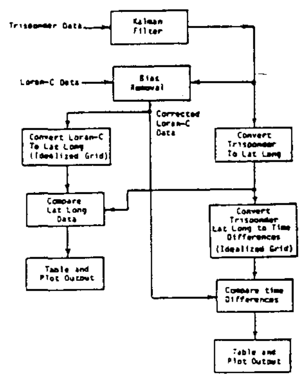

Figure 24. Block diagram of vessel data processing system.

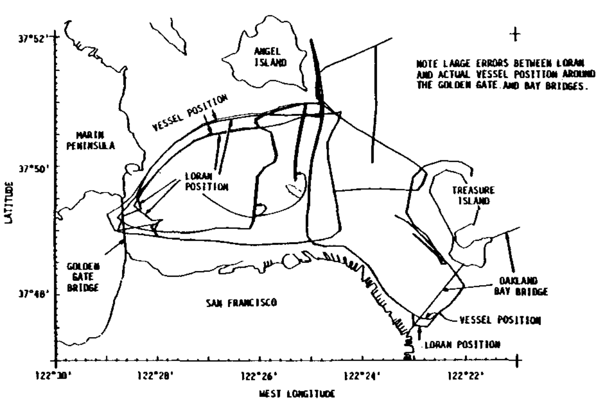

Figure 25. Vessel track from Trisponder and Loran-C data.

The difference between true and measured position was generally low in the inner harbor, which follows from the fact that the placement of the land harbor sites used in the grid fitting is such that the grid is optimized for this area. Two areas exhibited systematic charting errors. They were near Angel Island and Alcatraz for both the X-ray and Yankee time differences. Pre-experiment analysis based on the land-sea interface phase recovery indicated that only X ray would show large errors in these areas.

In an attempt to explain the systematic TD errors around Angel Island in both TDX and TDY,

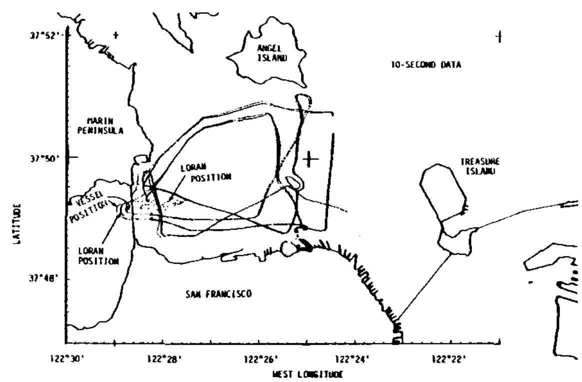

Figure 26. Detailed comparison of Trisponder and Loran-C measured vessel positions.

we considered prediction errors at Point Blunt and Alcatraz. For Point Blunt grid fit errors were 138 ns for TDX and -9 ns for TDY, while at Alcatraz we have -42.3 ns for TDX and 15 ns for TDY. The large error for TDX at Point Blunt seems to correlate well, and the errors in TDX for Alcatraz are in agreement for the area east of Alcatraz but not to the west. Furthermore, if we attempt to use the error contours from the planning phase, we again find good agreement for TDX. However, the large TDY errors around and to the west of Angel Island are predicted to be zero. Further analysis is needed to explain the behavior of TDY by considering other error sources. However, one cannot rule out the possibility that the error is really in the "truth" system and not Loran-C.

The errors around the three bridges follow the general pattern predicted by analysis in Reference 12. It was predicted that errors in TDX would be worst around the Golden Gate Bridge while errors in TDY would be worst around the Bay Bridge. The Richmond Bridge was not expected to produce severe errors in either TDX or TDY. The reasons for these predictions are as follows: (1) the Golden Gate has the largest cross section; (2) the X-ray signal passes almost parallel to the bridge while Master is almost perpendicular; (3) the reflection of Yankee from the Golden Gate would approximately cancel the effect of Master; and (4) the Richmond Bridge is too small to cause significant scattering. The TDY errors around the Golden Gate Bridge are somewhat larger than around the Bay Bridge but are smaller than the TDX errors around the Golden Gate. TDY errors around the Bay Bridge were larger than TDX errors as expected.

One day of Loran-C data with 10-sec averaging was collected in the Golden Gate Bridge area. The closer spaced samples gave a good picture of what happens as a vessel approaches the Golden Gate Bridge. An error buildup in TDX began about 1000 to 1200 meters from the bridge. This compares quite well with the start of the major lobe in Figure 19. The signal then became totally useless when the vessel approached within 400 to 600 m of the bridge, in that the received signal became so unstable that it could not be used for navigation. The signal was again usable about 400 to 600 m from the bridge on the seaward side.

Errors in position were higher in the San Pablo Bay area and seaward from Golden Gate Bridge. These areas were not effectively sampled by the calibration sites, and thus the grid fit should be poor in these areas.

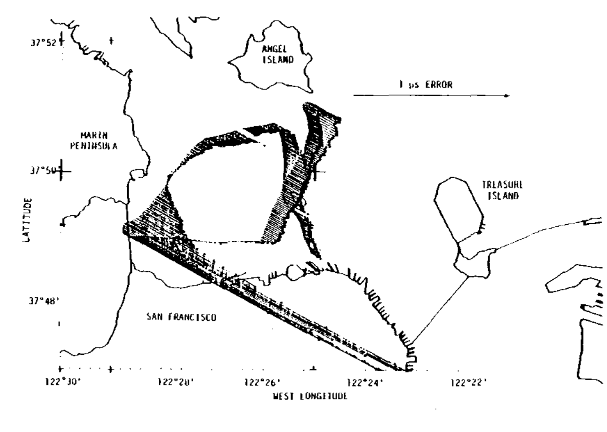

Figure 27. Loran-C time difference errors at a position measured by the Trisponder system.

The means and standard deviations of the differences between grid predictions and measured data for the inner harbor (excluding the areas near the Golden Gate and Bay Bridges) are:

$$\overline{TDX} = 34.1 \text{ ns} \qquad \sigma_{TDX} = 65.1 \text{ ns}$$

$$\overline{TDY} = -0.6 \text{ ns} \qquad \sigma_{TDY} = 64.7 \text{ ns} \quad .$$

Note the mean offset in TDX could be corrected by changing the X-ray emission delay. In general the performance is quite good. If one considers that the standard deviations of the received signals are about 20-ns rms, then we see that approximately 60-ns rms is due to charting errors.

Conclusions. The results of this experiment show that Loran-C can provide reliable and accurate navigation for use in piloting San Francisco Bay and other harbors and restricted waterways provided proper precautions are exercised near bridges and the proper equipment is used. The quality of the results is encouraging and shows that the software and techniques developed to process the vessel data form a solid basis for user equipment design and automated harbor calibation techniques.

Some general conclusions are also possible concerning the distortion caused by large bridges. Bridge height must be a significant fraction of a wavelength to produce significant signal distortion. This conclusion is based on a simplified analysis and the fact that the Richmond Bridge produces little or no distortion compared to the large Golden Gate and Bay Bridges. The simple scattering theory predicts fairly well the general behavior and spatial pattern of measured signal distortion.

Visual Grid Survey/Waypoint Navigation. The Visual Grid Survey technique was developed to determine the TD coordinates of the physical features of an HHE area. The process consists of:

- Choosing route waypoints
- Computing estimate of TDs
- Estimating position of surrounding navigation features
- Surveying (measuring TDs along visual ranges, channel edges, and at aids to navigation in the vicinity of the waypoint
- Statistically defining the TDs for the waypoint.

There are two basis ways of visually determining waypoint TDs. In the ideal case, the ends of all channel segments are makred by the intersection of two ranges. The survey vessel proceeds back and forth through the waypoint along each range. Linear regression techniques are employed to fit a straight line to the TD data. The intersection of the TD lines marks the waypoint.

In the case where ranges are not available, the channel features near a desired waypoint are surveyed, including if available, any fixed aids in the vicinity. An estimate of the waypoint is made and the location of the channel features predicted. The waypoint TDs are adjusted as necessary until the resultant graphical representation of the channel features matches the real world.

In those cases where distance to land or a fixed aid precludes an accurate visual check on the waypoints derived from floating aids, a short-range, transponder system is set up to act as the reference for waypoint determination. This is necessary in areas such as lower Delaware Bay and Chesapeake Bay. Use of a positioning system in the CCZ is of paramount importance for chain calibration because of the lack of visual aids several miles offshore.

Recommendations. The federal government must establish standards of Loran-C surveying. This incudes setting standards on specific survey techniques (positioning systems and visual), type of equipment (and calibration procedures for equipment being used), positioning, coordinate conversion algorithms, and variables, use of Kalman filters, and standard techniques to account for vessel motion and dynamics during survey.

Commercial surveying of Loran-C grids minimize government involvement and facilitate transference of costs directly to the users, it is quite likely Department of Transportation will endorse commercial navigation survey to account for spatial error. However, the need for differential Loran-C to compensate for temporal fluctuations will most likely require DOT involvement.

SECTION 5
RECEIVER PERFORMANCE SPECIFICATIONS

The Loran-C Receiver

Loran-C receivers are complex and their use requires other elements of the system (proper geometry, and means to compensate for temporal and spatial effects) discussed previously to be matched properly for successful performance.

A typical installation consists of 4 basic elements. These include: antenna system, analog signal processing, digital signal processing, and control and display. References 4 and 35 have defined the operation of these four receiver functions. This section will concentrate on a review of past test data and the compensation techniques that can be used to reject noise, frequency interference, and reduce error. Reference 36 provides a summary of data collected for 28 receivers.

One, the antenna, consists of a 1- to 3-meter steel whip mounted in such a location as to minimize its capacitive reactance. Since any short (compared to a wavelength) antenna exhibits low resistance and high capacitive reactance, a coupler is employed to provide noise attenuation, passband filtering, and impedance matching to a 50 Ohm coaxial cable.

Within the receiver, individual manufacturers use different signal processing techniques, time constants, etc to process Loran-C signals as demonstrated in the receiver survey updated for this effort. A typical Loran-C receiver employs a hard limited, microprocessor controlled digital design. It operates in a differential* envelope mode to determine proper cycle selection.

A good Loran-C receiver must include the following performance characteristics:

- Sensitivity/selectivity (measure of receiver's ability to lock on to desired signals, eliminating those which are out-of-band).
- Dynamic range (range of signals that can be processed in the receiver).
- ECD range (range of ECD values for which the receiver will initially achieve lock and stay in lock).
- Lock-on time (time taken for the receiver to initiate proper tracking of the Loran signals).
- Dead reckoning time (time after a receiver has lost signal before it starts the acquisition, settle, and track process over again).

The sensitivity of a Loran-C system is controlled by the combined characteristics of the receiver and antenna coupler, including front-end bandwidth, noise and gain characteristic, and receiver signal processing and averaging technique. Typical marine Loran-C receiver specifications state a -10-dB SNR performance at 5- to 7-minute lock-on time as shown in the survey. Based upon laboratory tests the 3-dB coupler/receiver bandwidth of typical Loran-C receivers are set to about 20 to 25 kHz. New design such as the Mieco includes wider bandwidths. At this bandwidth, the lock-on sensitivity is measured to be about -2-dB SNR over a range of ±3 μs ECD offset. Once the typical receiver is locked-on, its tracking sensitivity (minimum SNR at which it continues to maintain proper track) was measured to be -7 dB. When tracking below this value, receivers have been observed to lose lock. The receiver must then reacquire if the "lost signal" time was greater than the dead reckoning time.

Typically, signal dynamic range of 20 to 30 was observed in the tests. The dynamic range capability of the typical Loran receiver exceeded signal variations encountered in various tests. Thus, dynamic range is not considered to be a very critical receiver characteristic unless a receiver is operated in close proximity to one of the several continental Loran-C transmitter sites or the source of a strong interfering signal.

To prevent cycle slip, a Loran-C receiver must tolerate a wide range of ECD. In addition, it is essential that no skywave signals be introduced at the sampling point. Trade-offs have been studied between sampling the pulse at the third cycle (no skywave contamination) versus sampling the pulse at a later cycle yielding a higher SNR reading at the expense of skywave contamination and envelope distortion. It was found that skywave contamination increases the range of ECD observed on incoming signals, which already possess local phase variations and initial ECD offset. This added ECD range often exceeded the receiver's ECD limits and resulted in loss of lock or cycle slip.

*Compares the envelope of the secondaries to the measured slope of the master.

Time for Search, Time to Correct Cycle, and Envelope Times

The typical Loran-C user is also concerned with other important receiver performance characteristics. These include:

1. Time for search.
2. Time to correct cycle (sometimes referred to as settling time).
3. Envelope times (time to return to third cycle from adjacent cycle).

An Internav LC204 receiver (very typical of hard-limiter type receivers) was chosen to assess typical user receiver performance based on the above three criteria. Several times at each site throughout the Great Lakes Region the LC204 was turned off and then on again to test the reacquisition times of a typical user receiver.

All of the results are presented in tabular form in Reference 4. As an example we have chosen Table 11 which is representative of the signal acquisition times obtained. Table 11 shows time for search, time to the correct cycle and envelope times for Loran-C station Seneca (Master), Loran-C Station Caribou (W), and Loran-C station Carolina Beach (Y). Under the column entitled "Envelope Times" the U represents up 1 cycle and the D represents down 1 cycle. The time to return up or down to the original cycle is the value indicated in sec- onds. Key points regarding Table 11 are listed below:

1. Time for search for M ranges between 2 and 11 seconds and W and Y ranges between 4 and 26 seconds.
2. Average time to correct cycle for M, W, and Y are 196.8, 401.3, and 267 seconds, respectively.
3. Envelope times for M, W, and Y averages are:

M		W		Y	
Up	Down	Up	Down	Up	Down
6	5	91	85	146	93

Table 11. LC204 acquisition (all times in seconds).

Time			Time for Search			Time to Correct Cycle			Envelope Times					
									M		W		Y	
Day	Hr Mn	Site	M	W	Y	M	W	Y	U	D	U	D	U	D
275	1945	A-2 Woodstock	4	8	9		392	388	10	2	68	16	148	14
277	1510	A-2	11	20	26	210	385	370	7	6	149	124	120	124
277	1535	A-2	4	8	12	185	344	245	7	5	150	190	340	280
278	1006	A-2	4	6	8	197	365	270	7.5	5	104	165	200	125
278	1030	A-2	2	6	9	170	384	190	8	5	120	134	259	190
279	1310	A-1 Welland	3	12	15	120	332	220	5	4	130	80	135	72
279	1340	A-1	4	5	7	205	570	275	4	4	26	20	30	18
279	1355	A-1	5	8	10	203	410	230	4	4	26	12	30	18
279	2000	A-1	4	16	20	252	434	270	4	4	150	160	282	150
280	1830	A-1	2	4	7	216	458	220	4	3	44	18	70	18
284	0745	A-0	2	4	7	210	340	260		14	35	18	25	11

To summarize, the LC204 had no trouble in initially acquiring the Loran pulse throughout the test area. The time required to settle to the correct cycle was generally 3 to 4 minutes on Master, 6 to 8 minutes on Caribou, and 4 to 7 minutes on Carolina Beach. At Peshu Lake, Caribou would not reliably cycle select. At Wawa, neither Caribou or Carolina Beach would reliably cycle select. Most of the receivers conducted in the survey do not have characteristics much different than the above.

Compensation of Frequency Interference and Noise

To mitigate against these noise and interference effects the Loran-C receiver design should include use of the four design principles defined below:

1. Band-limiting is required in the Loran-C receiver for noise reduction and elimination of out-of-band signals. In most designs, bandpass limiting is achieved in the antenna coupler, with some final tuned circuits, in some cases with switched Q, in the receiver. The switched Q circuit permits narrowband RF for the search mode, and wideband for Pulse Group Time Reference Identification (PGTRI) and tracking. The exact bandwidth (4 to 30 kHz) selected depends on the SNR design goal, number of poles in the filter, and trade-offs of the cost of the filter versus costs of processing sampled data.

2. There are two basic design types of the analog signal processing. The types differ by virtue of the two different amplifier types: linear and hard limited. With linear amplifiers, filtering is done at low level ahead of the amplifier. The amplifier has a wide range automatic gain control that adjusts the gain in each interval such that the amplifier output is the same amplitude for all stations' signals. Envelope shape processing is done at high level, so that there are two outputs, an envelope and a cycle channel for sampling. A modification of this amplifier type is the clipped linear amplifier, that operates linearly over the expected signal ranges but limits high amplitude signals such as atmospheric noise bursts or crossing rate Loran-C signals.

The alternative type of amplification is the hard limiting amplifier. In this case, all linear processing must be done at low level. Two hard limited RF amplifiers are then required to make envelope and cycle signals available for the sampling process. The amplifier then amplifies the signal and limits the amplitude until the output has a squarewave shape with the polarity equal to the instantaneous polarity of the input waveform.

In both types of amplifier, the overriding requirement is that delay through the amplifier not vary with received signal amplitude or AGC setting. In general, this means a very wide-band amplifier (10 to 100 MHz), with very low internal noise.

3. The signal processing circuits are essentially filters that minimize the effects of interference and noise, shape the envelope appropriately, and minimize unwanted distortions. The bandpass limiting circuits are designed so that when their effects are considered with the filtering in the antenna coupler, the exact bandpass is achieved which minimizes atmospheric noise, while maintaining the envelope shape undistorted for good cycle selection, and maintaining an overall linear phase shift characteristic over the passband for good timing accuracy. Narrowband switching of the filters is provided to gain SNR during search, at the expense of envelope shape. This envelope distortion is of no consequence during search.

4. Interference filters are narrowband rejection filters (notch filters) for reduction of the effects of near-band signals, which can adversely effect the operation of the receiver. The number of notch filters is a design decision that must be based on interference known to exist in the operating area, the receiver bandpass characteristics, and any sampled signal processed that have interference rejection capabilities. Interference effects can be classed in two general types: high level signals that cause the receiver circuits to act nonlinearly, and signals that are coherent with the spectrum of the sampled data process (cross correlation), called "synchronous interference." High level continuous signals must be reduced by filtering the analog signal, ahead of the active stages. In the case of high level atmospheric noise bursts and crossing rate Loran-C signals, a form of limiting is more effects. Synchronous interference can be handled by either notch filters or changing the cross correlation process to eliminate the synchronism, or both.

Control and Display. In addition to performing signal processing functions, the receiver also provides for control and display functions. In a microprocessor-based receiver, the control display group is simply a keyboard/display peripheral of the microprocessor. This provides for the input and storage of initialization conditions and for output either through a visual display or electronic interface. Several receivers surveyed in Section 6 have this capability.

Through the use of microprocessors and related signal processing circuits, modern Loran-C receivers provide high quality navigation data at a low cost. As microprocessor techniques continue to grow, it is reasonable to expect receiver prices to be reduced somewhat further; however there is a point at which the price will be controlled by the packaging, installation and servicing costs, and not by the cost of the integrated circuits used to perform the signal processing functions.

What is actually possible is real-time input from a Loran receiver combined with other variables of vessel movement, permitting rapid calculation of fixes, currents, and courses to steer to reach desired waypoints or destinations. This is just the result of following the trend of more and more logic and memory density.

The existence of more memory implies storage of more and more secondary-phase factor data that gives the conversion process its accuracy. Probably in the final analysis, it will not be the limitations of calculator memory that determine performance, but the availability of the secondary-phase factor data to fill that memory that will be the pacing element.

ACKNOWLEDGMENTS

The author would like to express his appreciation to Mr. William O'Halloran and Mr. Bahar Uttam of Jaycor, and Mr. John Heurtley of Transportation Systems Center for their comments and support during the preparation of this paper. The author would especially like to thank Captain J. Terry Montonye (US Coast Guard) who spearheaded this effort. Appreciation is also extended to Mr. Mort Rogoff and Mr. William Buebel for their time and discussions.

REFERENCES

1. Montonye, J.T., "All-Weather Precise Piloting Options for Mariners," ISOSO 81 Proceedings, November 1981.

2. Harvey, R.L., "West Coast Loran-C -- A Model for the Future," Wild Goose Association, Proceedings of the Seventh Annual Technical Symposium, 18-20 October 1978.

3. Nelson, L.W., Loran-C: System Analysis Interim Report No. 1, KT77TMP-44, Kaman Tempo, December 1977.

4. Illgen, J.D., B. Gambill, and L.W. Nelson, Loran-C Great Lakes Experiment: Coverage and Accuracy Determination, Volumes I, II, and III, KT79TMP-19, Kaman Tempo, 26 March 1979.

5. Illgen, J.D., and D.A. Feldman, "Loran-C Signal Analysis Experiments -- An Overview," Wild Goose Association, Proceedings of the Seventh Annual Technical Symposium, 18-20 October 1978.

6. Frank, R.L., and D.L. McGrew, Real Time Compensation of Loran-C/D Temporal Variations, paper presented at Wild Goose Convention, 2-4 October 1974.

7. Doherty, R.H., and J.R. Johler, Analysis of Groundwave Temporal Variations in the Loran-C Radio Navigation System, Technical Memorandum 76-222, US Department of Commerce, Office of Telecommunications, June 1976.

8. Doherty, R.H., and J.R. Johler, Meteorological Influence of Loran-C Groundwave Propagation, paper presented at Second Annual Convention, Wild Goose Association, Washington, DC, September 1973.

9. Bean, B.R., and E.J. Dutton, Radio Meteorology, National Bureau of Standards, Monograph 02, 1 March 1966.

10. Illgen, J.D., T. Mason, and B. Gambill, "Loran-C Propagation and Equipment Timing Fluctuations and Conductivity Estimates Observed in the Great Lakes Region," Proceedings of Eighth Annual Technical Symposium of the Wild Goose Association, Williamsburg, VA, October 1979.

11. Gambill, B., and K. Schwartz, Loran-C Signal Analysis Propagation Model Evaluation, General Electric-Tempo, CG-D-20-80, July 1979.

12. Illgen, J.D., et al, Harbor Experiment Analysis Plan, February 1978, Kaman Tempo.

13. Nelson, L.W., Loran-C Signal Analysis Final Report, CG-D-4-80, prepared by kaman Tempo for USCG, December 1979.

14. Dean, W.N., Diurnal Variations in Loran-C Ground Wave Propagation, Magnavox Government and Industrial Electronics Co., Unpublished report, 1978.

15. Final Report on Loran-C Propagation Study, Sperry Systems Management Division, Report No. CJ-2232-1892, April 1971.

16. MacKenzie, F.D., Flight Evaluation of Loran-C in the State of Vermont, Transportation Systems Center, Draft Report, July 1981.

17. DePalma, L.M., P.M. Creamer, and E. Anderson, "Qualification of St. Marys River Loran-C Time Difference Grid Instability, Proceedings of Ninth Annual Technical Symposium of the Wild Goose Association, Boston, MA, October 1980.

18 Goddard, R.B., Differential Loran-C Time Stability Study, US Coast Guard, Report No. DOT-CG-31146-A, November 1973.

19 Gambill, B., and K. Schwartz, Loran-C Signal Analysis -- Propagation Model Evaluation, DOT (TBD), KT78TMP-51, Kaman Tempo.

20 Specification of the Transmitted Loran-C Signal, Department of Transportation, Coast Guard, COMDTINST M16562.4, July 1981.

21 Gupta, R.R., and E. Anderson, "Application of Semi-Empirical TD Grid Calibration to the West Coast Loran-C Chain," Proceedings of Eighth Annual Technical Symposium of the Wild Goose Association, Williamsburg, VA, October 1979.

22 Marchand, M.A., J.L. Kennedy, L.A. Kellett, Loran Warpage Coefficients Generation Program (WARP), Hanscom Field, Technical Report ESD-TR-81-116(III), Feburary 1981.

23 Warren, R.S., R.R. Gupta, and T.J. Shubbuck, "Design and Calibration of a Grid Prediction Algorithm for the St. Marys River Loran-C Chain," Proceedings of Seventh Annual Technical Symposium of the Wild Goose Association, New Orleans, LA, October 1978.

24 Mortimer, A.R., R.M. Eaton, and D.H. Gray, "Calibration of the West Canadian Loran-C Chain," Canadian Aeronautics and Space Journal, Vol 24, No 3, May/Jun 1978, pp 129-136.

25 Pearce, D.C., and J.W. Walker, "Ground Effects on Loran-C Signals," Proceedings of the Sixth Annual Precise Time and Time In- terval Applications and Planning Meeting, Washington, DC, December 1974.

26 Anderson, C.W., D.C. Pearce, and J.W. Walker, Coastline Induced Loran-C Anomalies, US Army Electronics Command, Report No. ECOM-4075, February 1973.

27 CCIR 322, International Radio Consultative Committee, Documents of the 10th Plenary Assembly, Geneva, 1963, Report 322, World Distribution and Characteristics of Atmospheric Radio Noise, published by International Telecommunications Union, Geneva, 1964.

28 Sage, A.P., and J.L. Melsa, Estimation Theory with Applications to Communications and Control, McGraw Hill, NY, 1971.

29 Brodgen, J.W., and O.L. Luken, Differential Omega, NRL Memorandum Report 1716, Naval Research Laboratory, Washington, DC, August 1966.

30 Nelson, L.W., Loran-C Signal Analysis: Final System Analysis Report, KT78TMP-108, Kaman Tempo, June 1979.

31 Ligon, J.M., and C.R. Edwards, PILOT, Precision Intercoastal Loran Translocation-Exploiting Loran-C in the Harbor and River Environment, presented at the 8th Annual Wild Goose Association, October 1979.

32 Olsen, D.L., et al, Precision Loran-C Navigation for the Harbor and Harbor Entrance Area, CG-D-34-80, prepared by USCG, May 1980.

33 St Marys River Loran-C, prepared by Teledyne Systems Company, Northridge, CA, February 1977.

34 Schwab, Navigation Algorithm and Switchover Doctrine for Multiple-Option Loran Position Fixes, Space Department AOL SDO5949, March 1981.

35 Poppe, M.C., Jr., "The Loran-C Receiver A Functional Description," Cambridge Engineering, Cambridge, VT, ION, Vol 29, No 1, Spring 82.

36 Illgen, J.D., Loran-C 1982 A High Technology Nanosecond Accuracy System for HHE and Restricted Waterway Navigation, KT-82-050(R), December 1982, Kaman Tempo, Santa Barbara, CA.

SESSION IV
OPERATIONS

RADIONAVIGATION IN THE YEAR 2001

David C. Scull
U.S. Department of Transportation
Research and Special Programs Administration
400 Seventh Street, S.W.
Washington, D.C. 20590

ABSTRACT

What will be the radionavigation system mix at the turn of the century? It is easy to envision satellite systems providing the necessary functions of communication and navigation, but to what degree will these systems accomplish it? How will NAVSTAR GPS supplement or replace such systems as LORAN, OMEGA, VOR-DME AND TRANSIT? These are the questions that are before the radionavigation planning groups within the Department of Defense (DOD) and the Department of Transportation (DOT). The goal is to establish through an integrated DOD/DOT planning and budgeting process, a cost-effective mix of federally provided multi-user systems for the post 1995 time frame. Two key events stand out in the process: the 1983 DOD/DOT preliminary recommendation on the future navigation system mix and the 1986 decision at the national level. The 1986 decision becomes the basis for navigational system implementation. Following the 1986 decision, it is intended that this process will be continued to reflect, in the ongoing radionavigation planning, such factors as new requirements and advances in technology.

INTRODUCTION

Why are concerned about the Radionavigation Systems of the next century? In spite of present economic conditions, there will be significant growth in the number of ships, aircraft, and land vehicles. There will be attempts to make their operation more efficient using new technology. There will be new requirements for personal as well as cargo security. Existing systems will need refurbishment or replacement of their essential parts. There also will be new procedural changes as we attempt to incorporate new navigation systems and further improve the flow of traffic. And finally, as is becoming more evident in our national ecomony, stability is being tied to an international system of economics and multi-national cooperation. Institutional problems dealing with user acceptance, cost recovery, and international standardization must be dealt with as we look to the future. This is why the planning process right now is so important to our future viability in the field of radionavigation. I believe we face the danger of either not maintaining or improving our existing radionavigation systems where warranted or proceeding too slowly in the adoption of new satellite navigation systems.

DEVELOPMENT OF THE PLANNING PROCESS

The radionavigation planning process is not a new concept. It consists of two basic processes: 1) defining navigational requirements and 2) finding that system or mix of systems that will meet such requirements. In addition, there must be a sound economic basis for the choice of one system over another. There has been some type of governmental planning process since radionavigation systems, released for civil use, were introduced after World War II. In the 1960's, the DOD planned its implementation of new systems through the use of Technical Development Plans (TDP's). Such planning was later unified, formalized, and coordinated among the Services and documented in the Joint Chiefs of Staff (JCS) Master Navigation Plan. After the DOT was formed in 1967, its National Plan for Navigation was developed and published in 1970 to provide the first focal point for civil radionavigation planning. As requirements for the Coastal Confluence Zone (CCZ), and the North Atlantic Minimum Navigation Performance Specification (MNPS) were developed in the early 1970's, candidate systems were evaluated in the DOT National Plan for Navigation. But let's look at the past few years and see why DOD and DOT have had to further coordinate their planning activity and produce a combined Federal Radionavigation Plan.

Congress gave limited attention to radionavigation in the early 1970's. The GAO, however, gave its blessing to DOT plans to implement LORAN-C as the government provided radionavigation service for the United States CCZ and OMEGA as the oceanic en route system. Within this same time period, we saw concepts such as Project 621B, TIMATION and the Defense Navigation Satellite System (DNSS) evolve into what today is known as NAVSTAR GPS. When NAVSTAR GPS emerged, two things became evident: 1) its potential for technological contribution to both military and civil users and 2) its huge cost to the taxpayer. Perhaps anticipating the requirement for a unified federal radionavigation plan, the Office of Management and Budget and the National Telecommunications and Information Agency chaired a series of interagency meetings with DOD and DOT and other government departments on detemining the means of establishing a government-wide radionavigation plan. It was decided ultimately that this responsibility should rest with those who operate the systems, namely the DOD and DOT. Possibly not satisfied with progress made in the Executive Branch, Congress, with considerable prompting by GAO, Congress passed the International Maritime Satellite (INMARSAT) Act of 1978. This legislation required the President to develop a plan to reduce the so called "proliferation" and overlap of systems. The Plan was to include both air and marine radionavigation systems. The radionavigation process was further strengthened through a DOD/DOT memorandum of understanding signed in April, 1979. After exhaustive meetings of the working groups involved, a Presidential report and the accompanying first edition of the Federal Radionavigation Plan (FRP) were forwarded to Congress in January, 1981.

The purpose of the FRP is first to provide an integrated DOD and DOT plan. It incorporates much of the DOD JCS Master Navigation Plan and the now superceded DOT National Plan for Navigation. The FRP compares systems on the basis of common characteristics such as accuracy, reliability, and coverage. It considers the consolidation of systems, it determines and resolves common issues and establishes a common planning schedule. Very importantly, it provides planning information for users and equipment manufacturers. The thrust of the FRP is directed at determining the optimum mix of radionavigation systems through examining the use of existing radionavigation systems and determining if they may be replaced by either an existing system or a future system such as NAVSTAR GPS. For example, can VOR/DME be replaced by LORAN-C or OMEGA or can all three be replaced by NAVSTAR GPS? The answers to these questions will be the basis for a joint DOD/DOT recommendation and eventual national decision on the future radionavigation system mix. Now let us look at planning process in radionavigation and how we will arrive at the DOD/DOT preliminary recommendation.

DOD/DOT JOINT RECOMMENDATION AND A NATIONAL DECISION ON THE FUTURE RADIONAVIGATION SYSTEM MIX

As was mentioned previously in this paper, there are many factors to consider in choosing systems that will either satisfy user requirements or provide user benefits. These include operational, technical, economic, and institutional considerations. Although much experimentation and operational evaluation must be performed, most technical and operational factors are definable. The economic and institutional factors are not so easily defined. Nonetheless they must be examined and evaluated before making any final choice.

The point at which to begin the radionavigation planning process is in the definition of requirements. Let's look at a method of structuring a table of navigation requirements. In the FRP, the reader for the purposes of analysis is asked to divide the navigation process into discrete phases of navigation e.g. Marine navigation consists of three phases: Oceanic, Coastal, and Harbor Approach/Harbor; Air Navigation consists of two phases: En route/Terminal and Approach/Landing. Accuracy of a system although not the only factor is probably the most important technical factor in determining whether or not a radionavigation system will meet requirements.

Table 1 provides the accuracies required in controlled airspace to meet the current requirements for the En Route/Terminal and the Approach/Landing phases of air navigation. These accuracies are based on standards that have been developed from such documents as the FAA Advisory Circular AC 90-45A and North Atlantic Minimum Navigation Performance Specification (MNPS). Similar standards are used to develop accuracy requirements for marine navigation, however, accuracy requirements can also be mandated by regulation. This is the case in the U.S. Coastal Confluence Zone where LORAN-C or an acceptable substitute such as a satellite navigation is required on vessels larger than 1600 gross tons.

Civil Aviation Radionavigation Accuracy Criteria

Phase of Flight	Source	System Use
Oceanic	—	6.2nm 2drms
En Route	1,000m 2drms	3,600m 2drms
Terminal	500m 2drms	1,800m 2drms
Non-Precision Approach	100m 2drms	150m 2drms
Precision Landing		
Horizontal	4.5m 2σ	6.1m 2σ
Vertical	0.5m 2σ	0.6m 2σ

Once these accuracy requirements are established then candidate systems can be tested to see if they meet the requirements. For instance, Volume III of the FRP states that NAVSTAR, GPS (without selective availability *applied) for the most sophisticated user will provide a best predictable positioning accuracy at 18.1 meters (2drms**) horizontally and 29.7 meters (2 sigma) vertically. As can be seen in Table I the accuracy requirements for precision landing sytems can not be met. If the accuracy of the Standard Positioning Service (SPS) is degraded to 500 meters 2 drms, NAVSTAR GPS is also not a candidate system for non-precision approaches but is acceptable for en route navigation.

Accuracy is just one of many technical factors considered, others such as signal coverage, environmental effects and human factors also must be evaluated. The FAA places a strong emphasis on system reliability and integrity.

*Selective avalability is a technique whereby the the accuracy of navigational signals are purposedly degraded.

**Drms is the square root of the sum of the squares of the one sigma error components along the major and minor axis of a probability ellipse. Values of drms such as 2 drms are derived by using the corresponding values of sigma. There is a range of values of probability associated with a single value of 2 drms. The variation is not large but it ranges from 95.4% to 98.2% as a function of the ellipticity. The ellipticity is defined as the ratio of σ_1 to σ_2.

Equipment should have a minimal chance of failure during flight and should not provide false information without warning. Operational factors are also addressed in the selection process. Areas of operation, mission, economics, personal preference and Federal regulations influence the choice of which system is to be used. Operational suitability generally can only be determined after a system has been made available for operational use. User acceptance is often strong evidence that a system is operationally suitable, but unfortunately radionavigation systems can not be fully operational the minute implementation takes place.

This was particulary true of the OMEGA system where ten years elapsed before the full network of transmitting stations became operational. Very little was known concerning the propagation of OMEGA signals in the Southern Hemisphere before the system was conceived. Perhaps the system design would be much different than it is now if the propagation characteristics had been fully understood. On the other hand, satellite navigation systems, due to the nature of their signals, may be evaluated using only a few satellites. The FAA has already made an extensive technical evaluation of NAVSTAR GPS. What is really not known beforehand, however, is the economics which will influence civil acceptance of a new radionavigation system or the desire to retain an old one. A economic planning model has been developed that examines these factors.

THE DOT ECONOMIC PLANNING MODEL FOR RADIONAVIGATION SYSTEMS

The concept of an economic model that could be used in making decisions concerning radionavigation systems originated in 1976 when the FAA started an economic analysis of civil air navigation alternatives. (Reference 1.) The result of that effort identified the cost impact of various navigation system implementation/operating scenarios on the FAA and on aviation users through use of a Requirements Analysis of Air Navigation Systems (RAANS) model. The scenarios tested with RAANS model provided for varying levels of transition from VOR/DME to other potential air navigation systems, such as LORAN-C, NAVSTAR GPS and Differential OMEGA. As possible multimodal (Air, Marine and Land) applications for NAVSTAR GPS became increasingly evident and a planning structure within DOT was formalized, the need for a broader and more sophisticated model was recognized. The basic RAANS model was therefore modified and greatly expanded. The operator costs were distributed among various agencies, i.e., the Coast Guard FAA, and the DOD. In addition to quantifying user costs, the capability of estimating user benefits was incorporated in the DOT model. The number of user groups has been expanded to include civil, marine and land users, in addition to air. The model was delivered to the Transportation Systems Center, Cambridge, Massachusetts by the Contractor, Systems Control Technology, Inc. in June 1982.

Radionavigation Model Operation

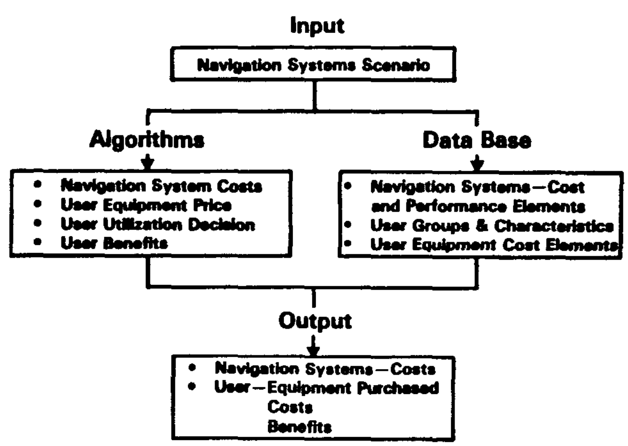

The operation of the model is illustrated in figure 1. A scenario has to be defined, for example, replacing VOR/DME with LORAN-C in the continental US. The scenario must specify not only where but when the transition to another system will take place. The DOT economic planning model is also divided into two functional parts. The first includes the model processing elements, i.e., the software containing the required logic, algorithms and processing options. The second part is the nominal data base wherein are stored the characteristics of the candidate navigation systems, user groups characteristics and the user equipment cost elements. The output is the cost of operating the specified navigation systems, the type of equipment the user is likely to purchase and the point in time when he is likely to purchase it. Also some relative idea of the benefits to be gained by transitioning to a new system are included in the output.

The first economic planning model scenarios have been run and the results are being analyzed. Various sensitivity analyses will test the model to ensure that the results used in formulating the DOT preliminary recommendation are valid.

INSTITUTIONAL ISSUES TO BE RESOLVED

Of the institutional issues there are three that must be dealt with before we can look forward to a significant change in the field of radionavigation. All of these are complex issues and need resolution in the immediate future. Unfortunately they probably will not be resolved before the joint DOD/DOT preliminary recommendation is made in 1983 but may be resolvable before a national decision is due in 1986. They are: first, the accuracy to be afforded to civil users by NAVSTAR GPS; second, the acceptance, internationally, of a military navigation system and; third, the imposition of user fees for navigational services.

In examining the technical requirements for radionavigation systems it can be seen that NAVSTAR GPS has the capability of meeting most requirements if its full accuracy is available but only a few if is degraded in accordance with present policy. With an accuracy of only 500 meters 2 drms NAVSTAR GPS is not capable of meeting the commercial fishing needs for a high repeatable accuracy (15-18 meters, 2 drms) or the future needs for precision navigation within harbors. Therefore, it is not at present a candidate for replacing LORAN-C. As was discussed previously, this degree of accuracy is also not acceptable for aircraft non-precision approaches either, hence, it is not a candidate system for replacing VOR. The only system that NAVSTAR GPS might replace from a technical standpoint under these conditions is OMEGA.

Still there is another aspect of NAVSTAR GPS to consider, its use in the differential mode. Recent studies have shown that Differential NAVSTAR GPS is capable of two-dimensional accuracies in the order of 10 meters (2 drms). These studies also assume the use of filtering, reducing bias errors to zero and an typical HDOP of 1.5. (Reference 2.) There have been no plans announced by the Department of Defense, to apply selective availability techniques to point they would defeat Differential NAVSTAR GPS, hence, it can be considered as a possible alternative. Of course, with a differential system comes the requirement for a communications channel. Thus the technical and cost considerations are also a part of an implementation decision on Differential NAVSTAR GPS. The policy on selective availability, which is under DOD purview, will be reviewed periodically. With similar satellite navigation systems such as the Soviet's GLONASS in the offing, it possible that the policy of selective availability may be relaxed in the future with greatly increased accuracy available in the post 1995 time frame. (Reference 3.) NAVSTAR GPS with full accuracy available to the civil community, then again becomes a very likely replacement for many systems.

*HDOP - Horizontal Dilution of Precision. A value of 1.5 is chosen as a typical figure for this error.

Radionavigation systems know no state or national boundaries but, provide coverage anywhere their signals are propagated at reasonable levels for detection. The world's transportation systems are also interrelated through the use of radionavigation systems. Any, future mix of radionavigation systems will have to include those that will meet some type of international standards. VOR/DME is a recognized air navigation system and is listed as an International Civil Aviation Organization (ICAO) standard. Other systems such as OMEGA, LORAN-C and TRANSIT although not officially recognized as standards by ICAO or the International Maritime Organization (IMO) are used extensively by the international civil community. International standardization will of course have be considered in any future recommendation.

Administration policy stresses the need for each user to pay his fair share of government provided services. The issue of cost recovery and user charges is still very much with us.

The civil aviation community now pays user charges in the form of fuel taxes, excise taxes, ticket taxes and registration fees. The marine community probably will pay for its use of radionavigation services in the future. The user charges levied in civil aviation are not broken out for radionavigation services but are collected as a general tax to pay for a host of FAA provided services including operation of the Air Traffic Control (ATC) system. Still it is possible to attribute a portion of these total costs to navigation services. This was done in recently proposed legislation that was based on a plan submitted by the Coast Guard. The Department of Defense has looked at another means of collecting a fee for navigation services. This is in connection with NAVSTAR GPS whereby the user would be charged for his specific use of the system. (Reference 4.) A direct assessment could be made by requiring the user to purchase a commerically constructed cryptographic key to gain access to the system. This is a different approach than that to be used by DOT in collecting users fees. Some means of rectifying this difference in philosophy will have to be found.

Although difficult, the resolution of the above issues is possible. Hopefully, such resolution will come quickly. There has been recent discussion of an international satellite navigation system operated by the civil community as a consortium similar to INMARSAT. Any delay in resolution of the issues concerning NAVSTAR GPS makes this more of a possibility. It may be an answer to the question of international civil acceptance of a military system. A lot will depend on world economics and if aviation and marine users are willing to pay for more navigation services than they already have. In the meantime, we should not overlook the potential in NAVSTAR GPS and the investment this country has already made in the system. Neither should we forget the existing systems that will need upgrading or other improvements in the future. It is probably safe to say that most of our existing systems, e.g., LORAN-C, OMEGA and VOR/DME have not reached their fullest potential. Still, the time will come when attempts to improve or continue the operation of these systems will provide only minimum benefit. The purpose of the Federal radionavigation planning process is to continually review the mix of radionavigation systems and ensure that are operated in the most effective manner. The process also should not stop at a "status quo" but be a vigorous attempt to introduce new technology into the field of radionavigation that will improve the safety and efficiency of transportation.

CONCLUSION

It is difficult to determine the full role that satellite navigation will play in year 2001. Who?, at the end of World War II could have predicted that within 15 years a doppler satellite navigation system such as TRANSIT was to be operational. The fact that TRANSIT receivers that originally cost $30,000 are now being replaced by $3,000 receivers is astonishing, and we have probably not seen an end to this revolution in electronics and computer technology. To what extent this technology is capitalized on will depend on the economy and the willingness of industry and government to invest in research and development. We should not hesitate, however, to make plans that will improve the radionavigation services in this country. Vessels can be moved more efficiently in harbors and aircraft can save additional fuel by flying the most direct routes. More lives can be saved by the rapid response of rescue forces to the exact location of an accident. We will also still need some back-up all-weather navigation system in case of equipment failure, either at the transmitter or the receiver. We can not overlook the fact that inertial systems are getting more reliable and attractive with respect to the cost of ownership. Is it possible that inertial systems will become so accurate and dependable that regardless of time, no external reference will be required. It is hard to imagine, however, that there will not be some redundant ground-based radionavigation systems.

The user should have the most say in what system or systems will be used in the future. How does the user have a say in this matter? One of the most active ways is through direct comment on the Federal Radionavigation Plan (FRP). An address to write to express your feelings to the DOT Navigation Working Group is in the FRP. Another way is through user groups and through participation at user conferences. The FAA recently had a meeting of this type in Washington, D.C. A similar meeting for surface transportation users is scheduled for November 16-17, 1982 in Washington, D.C. With input from the users, the Coast Guard, FAA and other DOT administrations, DOT can present a stronger case before Congress and the Administration in obtaining funds and support in maintaining our very important national resource in radionavigation services.

REFERENCES

1. Solomon, H. and Stephenson, A. "A Navigation Systems Planning Model" Proceedings of the ION National Aerospace Meeting Trevose, Pennsylvania, April 1981.

2. Beser, J. and Parkinson, B. "The Application of NAVSTAR DIFFERENTIAL GPS in the Civilian Community" Proceeding of the ION Annual Meeting" Annapolis, Maryland June 1981.

3. "Advance Publication of a Planned Satellite Network", Special Section No. AR11/A/3 annexed to IFRB Circular No. 1522, 8 June 1982.

4. DOD Preliminary Report to the Senate and House Committee on Armed Services on NAVSTAR GPS User Charges, March 1982.

Disclaimer

This paper expresses the views of the author and are not necessarily those of the Department of Transportation.

ALASKA LORAN-C FLIGHT TEST EVALUATION

Larry D. King and Edwin D. McConkey
Systems Control Technology, Inc.
2326 S. Congress Ave., Suite 2-A
West Palm Beach, Fl. 33406

ABSTRACT

This paper contains the description and results of a Loran-C flight test program conducted in the State of Alaska. The testing period was from August 1982 to September 1982. The purpose of the flight test was to identify applicable Loran-C accuracy data for the Alaskan air taxi and light aircraft operators so that a Supplemental Type Certificate (STC) can be issued in the Alaska Region for the Loran-C system tested (Teledyne TDL-711). Data was also collected both on the transition and return flights across the continental United States from West Palm Beach, Florida.

Navigation system errors were quantified for the Loran-C unit tested. The errors were computed from knowledge of position calculated from ground truth data and the indicated position of the navigator. Signal coverage, bias and flight technical error data were also obtained. Multilateration ground truth, photographic ground truth, and data acquisition systems were carried aboard the test aircraft. Over 15,000 nm were flown and more than 100 hours of Loran-C data from Florida to Alaska were recorded.

The tests were concentrated in the southwest part of the Alaskan mainland. An interconnecting network of routes west of Anchorage and south of a line from Fairbanks to Kotzebue were flown for data collection. Of particular interest was the area around, and to the west of, Bethel where there are currently very few aids to air navigation.

The North Pacific chain with stations at St. Paul (Master), Port Clarence (Yankee) and Narrow Cape (Zulu) was used in this area. Preliminary results indicate that Loran-C has sufficient signal coverage and accuracy to support aircraft enroute navigation in much of the test area. In the area around Anchorage the test unit failed to consistently acquire and track the signal, however. Further analysis of the data and testing are required in the Anchorage area.

INTRODUCTION

This document describes the results of a program for the collection of flight test data in Alaska using Loran-C (a wide area coverage navigation system). The purpose of the flight test was to evaluate a Loran-C receiver as an enroute navigation aid in Alaska and to collect data that can be submitted to the FAA in support of an application for a Supplemental Type Certificate (STC). Ultimately the Loran-C performance data collected will be utilized in the consideration of Loran-C by the Alaskan Region as an enroute navigation aid for the Alaska Air Taxi operators and light aircraft operators.

Navigation system errors (NAT and NCT: navigation error in alongtrack and crosstrack coordinates) were quantified for the Loran-C unit tested (Teledyne TDL-711). Total system crosstrack error (TSCT) and alongtrack error (TSAT) were also quantified in this report. Signal coverage, bias and flight technical error data were collected for position analysis obtained from a multilateration ground truth, photographic ground truth and data acquisition system carried aboard the test aircraft. Included in the test were equipment shakedown flights for the data acquisition system, transition data collection flights and Alaska data collection flights.

OBJECTIVES

The objectives of this project was to collect Loran-C performance data in Alaska that would be applicable in the consideration of Loran-C by the FAA as an enroute navigation aid. The specific objectives of this flight test were defined as follows:

- Collect Loran-C data relating to signal coverage and navigation system accuracy in the Alaska Enroute structure.
- Collect and analyze Loran-C data while enroute to Alaska.
- Collect and analyze signal information; such as propagation errors, signal to noise ratios, etc.
- Collect and analyze fixed site Loran-C data so that the effects of signal anomalies can be identified in the flight data.
- Qualitatively evaluate the potential for, and the effects of;

blunders using the Loran-C airborne system selected.

- Collect and analyze Flight Technical Error (FTE) data associated with the airborne Loran-C system selected.
- Provide the necessary installation and accuracy data so that a Supplemental Type Certificate (STC) can be issued by the FAA for the Loran-C system tested.

FLIGHT TEST ROUTES AND PROCEDURES

A total of 6,300 data miles were flown in the State of Alaska during a period from September 1, 1982 to September 10, 1982. Test locations were chosen to include as many geographically diverse situations as is possible within the constraints of a flight test. The aircraft was based in Anchorage, Alaska and was stationed at the FAA hanger on the airport.

In order to meet the major objective of obtaining an STC for the TDL-711 Loran-C receiver, the specific objectives of this flight test were defined as follows: 1] determine useable accurate signal coverage, and 2] determine avionics accuracy within that coverage. As depicted in Figure 1, the test routes were concentrated in the southwest part of the state where there is published coverage from the North Pacific Loran-C chain. Typically, single triad coverage was available from the Master Station at St. Paul (in the Pribilof Islands) and the secondary stations at Port Clarence and Narrow Cape. The other secondary station in the chain at Attu Island was utilized only as a backup station. Little overland coverage was available from the Gulf of Alaska chain according to published United States Coast Guard Loran-C charts.

Accuracy data were collected whenever the ground truth system was operational; minimum of two DME stations being received. In those cases where DME coverage was poor (west of Bethel) the photographic ground truth system was utilized.

To demonstrate compatibility with the existing VOR/DME system and air taxi operator routes, all of the flight test routes were along published, low altitude airways in the Southwest area. The Alaska Loran-C flight test program consisted of an area roughly defined by Anchorage, Fairbanks, Nome, Kodiak and McGrath (see Figure 1). Three basic flight test routes were flown. Test route 1 consisted of three [3] segments while test routes 2 and 3 consisted of four [4] and five [5] segments, respectively. Each leg was approximately 430 nm in length (2.9 flight hours). These legs consisted of enroute segments only. Segments were identified by the following number system:

Segment	Origin	Destination
1	Anchorage	Nome
2	Nome	McGrath
3	McGrath	Anchorage
4	Anchorage	Galena
5	Galena	Nome
6	Nome	King Salmon
7	King Salmon	Anchorage
8	Anchorage	King Salmon
9	King Salmon	McGrath
10	McGrath	Galena
11	Galena	Nome
12	Nome	Anchorage

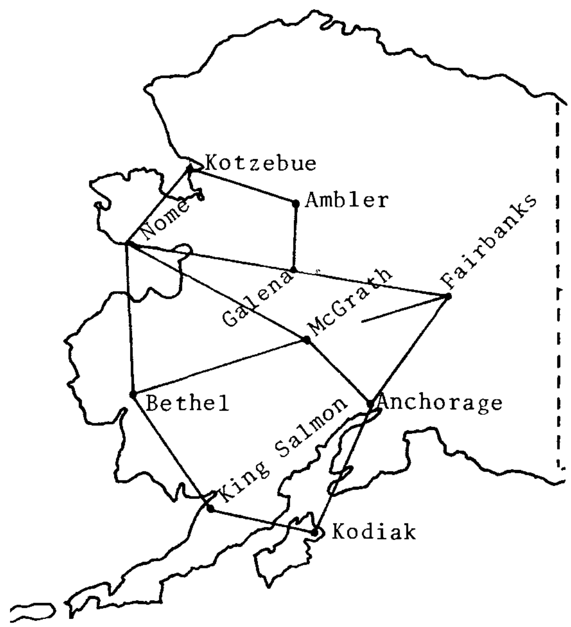

Figure 1 Alaska Loran-C Flight Test Routes

An additional flight was flown west of Bethel at the following locations: Kipnuk, Mekoryuk, Nightmute, Cape Romanzof and Russian Mission. The purpose of this segment was to explore overall signal accuracy and coverage and to demonstrate operations similar to those normally made by local air taxi operators. As mentioned earlier, photographic data were collected to verify the accuracy of the Loran-C navigator in this area.

Alaska enroute segments included flight over a variety of topographic and geographic conditions. Availability of DME transmitters along the route was adequate for data acquisition at flight altitudes in the range of 10,000-12,000 feet.

In addition to the enroute segments

flown in the Alaska area, five Loran-C RNAV approaches were accomplished. The approaches, with the exception of Anchorage, were flown in an ad hoc manner, that is they were executed without the aid of approach plates or published procedures. Typically, the approaches were flown utilizing two waypoints, the runway threshold and the FAF (Final Approach Fix) waypoint located five nautical miles out on centerline. Five approaches were executed in total at the following locations:

Anchorage	Nome
Bethel	King Salmon
Fairbanks	

The transition portion of the flight test program consisted of an area roughly defined by West Palm Beach, Florida; Denver, Colorado; Reno, Nevada; Vancouver, British Columbia; and Anchorage, Alaska (see Figure 2 and 3). Ten [10] flight legs were flown for the transition portion of the flight test with each leg being approximately 430 nm in length (2.9 flight hours). These legs consisted of departure, enroute and appraoch segments. Segments were identified by a number as follows:

Segment	Origin	Destination
1	W. Palm Beach, Fl	Mont., AL
2	Mont., AL	Little Rock, AR
3	Little Rock, AR	Amarillo, TX
4	Amarillo, TX	Denver, CO
5	Denver, CO	Roosevelt, UT
6	Roosevelt, UT	Reno, NV
7	Reno, NV	Seattle, WA
8	Seattle, WA	Ft. Nelson, CA
9	Ft. Nelson, CA	Whitehorse, CA
10	Whitehorse, CA	Anchorage, AK

Each segment was flown twice, once in transition to Anchorage, AK and once on the return flight to West Palm Beach, FL. The transition portion of the flight to Alaska was flown during a period from August 29, 1982 to September 1, 1982. The return portion of the flight was flown from September 17, 1982 to September 21, 1982.

Enroute segments included over water, coastal plain, central plain and rocky mountain overflight. Availability of DME transmitters along the route was adequate for data acquisition at flight altitudes in the range of 10,000 to 12,000 feet. The areas of reduced accuracy are predictable based on transmitter geometries and the route of flight for this test was selected to include areas of both good geometry and bad geometry. For example, the Denver, CO area was selected because it is on the outer fringe of current Loran-C coverage.

In addition to the transition enroute data collected during this flight test, a limited amount of approach data were collected. An RNAV non-precision approach using information from the Loran-C system being tested was attempted at the termination of each segment. During the portion of each approach that multiple DME coverage was adequate for operation of the data acquisition ground truth system, approach phase navigation system error values were determined. Low altitudes during the final phases of the approach, in most cases, limited the availability of adequate DME coverage. However, FTE data was collected during the entire approach phase in all cases. Data collected during this flight test represent a comprehensive baseline data base of both flight technical error and navigation system error values over a variety of topographic and geographic conditions.

Eleven approaches were completed at eight different airports during the transition enroute phase of the Loran-C testing. All of the approaches were published RNAV approaches with the exception of the Anchorage International approach. The eight approach locations were as follows:

Palm Beach Int'l., FL	-RNAV Rwy 13
Dannelly Field, AL	-RNAV Rwy 3
Adams Field, AR	-RNAV Rwy 22
Tradewind Airport, TX	-RNAV Rwy 35
Jeffco Airport, CO	-RNAV Rwy 29R
Roosevelt Mun., UT	-RNAV Rwy 25
Reno Int'l., NV	-RNAV Rwy 16
Anchorage Int'l., AK	-RNAV Rwy 6R

Although every effort was made to select those destination RNAV approaches most likely to supply DME signal sources required by the data acquisition system, primary emphasis was placed on selecting terminal locations which were indicative of a variety of navigation system transmitter geometries, and potential signal propagation effects. It is felt that the route and destinations selected for this flight test represented the greatest variety of signal variations available.

FLIGHT CREW

Three subject pilots were utilized for this test effort. All of the pilots were commercial and instrument rated, and all had previous experience flying long range navigation equipment. Table 1 presents a breakdown of the flight hours and qualifications for each pilot.

All enroute and approach segments were flown by the primary subject pilot. The copilot acted as safety observer and was also responsible for ATC communications and data entry into the TDL-711 Loran-C system. The flight test observer was tasked with operation of the data acquisition system and the manual logging of unusual flight situations.

Table 1 Project Pilot Experience

Pilot	Total Time (hrs)	Comm.	Inst.	ATR	Long Range Nav. Exp.
A	35,000	√	√	√	Omega
B	35,000	√	√	√	Omega
C	2,000	√	√		Loran-C

TEST VEHICLE AND EQUIPMENT

The aircraft used in the test was a twin engine Beechcraft Queen Air Model 65. During the data collection activity, a dedicated course deviation indicator (CDI) display was utilized to display Loran-C steering commands at all times. The safety observer monitored aircraft position by standard VOR navigation using a standard CDI display on the right side of the front instrument panel.

The Loran-C airborne system used for the flight test program was a Teledyne TDL-711 micro-navigator system consisting of an E-field vertical antenna; a receiver/computer unit mounted on the data acquisition rack; a control display unit (CDU) mounted on the aircraft's center console; and a CDI in the center of the pilot's instrument panel to display Loran-C course deviation.

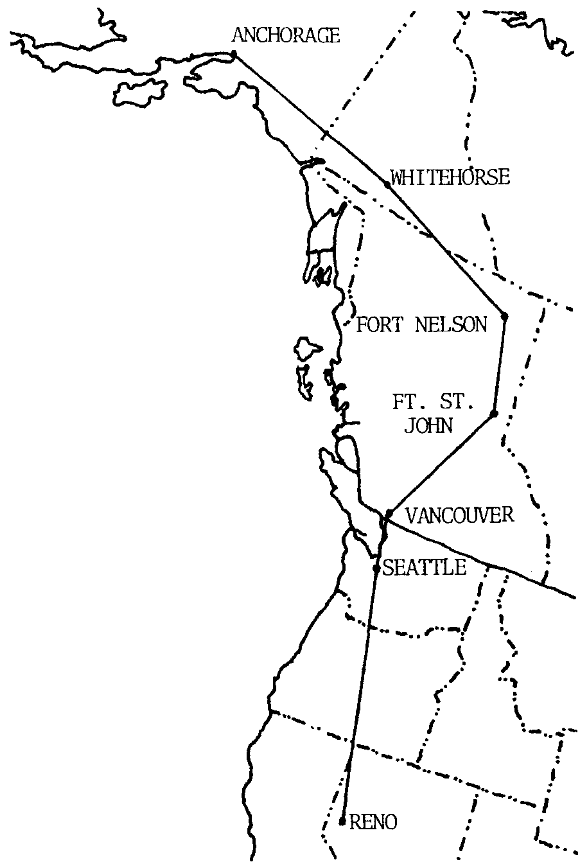

Figure 3 Transition Flight Test Route

Figure 2 Transition Flight Test Route

The control display unit, shown in Figure 4, is the operator's interface with the Loran-C system. It displays position information both in latitude/longitude and time differences, shows which waypoint, or waypoint pair, has been selected, displays all navigation and test modes, and shows the information being entered through the keyboard.

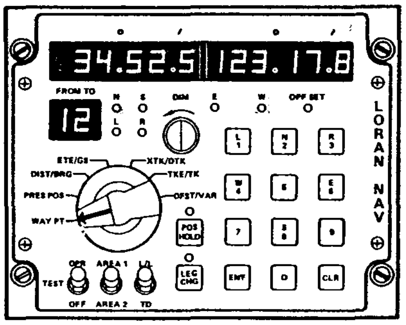

Figure 4 TDL-711 Control Display Unit [1]

There are six decimal points for use with the data shown in each upper display window (two of the six in each are shown in Figure 4). These same decimal points are also used to warn the crew of non-standard Loran-C system operation. All the decimal points blink when the processor is operating in the master independent mode (the master signal is unable or non-existent and a third secondary has been added to the computations, with one of the secondaries selected as master). They remain on steadily when navigation information (and thus, the computer position) is unuseable.

The rotary data selector switch chooses the information to be displayed:

- "WAY PT": the selected waypoint position is displayed, or the coordinates to be entered for the selected waypoint are shown.
- "PRES POS": position displays present position or allows entry of present position.
- "DIST/BRG": displays in the left and right ~~windows~~ range and bearing to the selected "TO" waypoint in the "FROM-TO" window.
- "ETE/GS": the processor shows time to go to the "TO" waypoint and present ground speed.
- "XTK/DTK": shows crosstrack distance on the left and desired track angle on the right.
- "TKE/TK": displays track angle error and track angle.
- OFST/VAR": shows the current parallel offset distance (or allows selection of a new offset), and lets the operator either see the current magentic variation, if any, or enter a new variation.

The "MODE SELECTOR", (lower left corner) is a three position switch which, at the operator's discretion, either shuts off power to the system, initiates the self-test sequence, or puts the system into normal operation.

One of two pre-programed coverage areas can be chosen with the area switch.* This switch selects the traid (a three-station set of master and secondaries) which is to be used for position computation and navigation. All of the Programmable Read Only Memory's (PROM) for all test coverage areas were available in the system. The "L/L-TD" switch chooses the mode of the selected position display or entry of latitude/longitude or time differences.

Pressing the "POS HOLD" switch stores the aircraft's present position at the moment it is depressed. If the rotary data selector is in the "PRES POS" mode, the displays will freeze. In any event, position continues to be updated once per second. The indicator light stays on until the switch is pressed a second time.

To effect a leg change, the "LEG CHG" switch is depressed and the next waypoint pair is entered using the keyboard. On the TDL-711, the leg change light will flash when the "TO" waypoint has been reached, and the new waypoint "FROM-TO" pair must be entered manually. There is no automatic leg change function. The selected waypoint pair appears in the "FROM-TO" window.

The keyboard is for information entry. Certain keys have double functions depending on the position of the rotary data selector switch. The "ENT" key inserts the keyboard entry into the ~~processor~~. The "CLR" key is used to clear keyboard entry errors.

The "N" and "S" lights indicate latitude, and the "E" and "W" longitude. Whenever an offset course has been entered, the "OFFSET" light remains on.

When the aircraft is left or right

*This particular Loran-C unit was modified with Teledyne's 16 triad option.

of desired track, when the track angle error is left or right of desired track heading, or when the offset course is left or right of nominal, the "L" or "R" lights will be on to show the direction of displacement. The "DIM" control regulates all CDU lights except the "OFFSET", "LEG CHG" and "POS HOLD" indicators. They are controlled with the cockpit dimmer controls.

The output of the Loran-C navigator drives a deviation indicator (CDI), giving linear deviation from the selected "TO" waypoint course. Full scale deflection left or right of center is 1.28 nautical miles. The "TO" flag indicates that the aircraft is located short of the "TO" waypoint. The "FROM" flag indicates a position beyond the "TO" waypoint. The red "NAV" flag indicates that steering commands are invalid.

The Loran-C receiver is designed to run a remote display unit (RDU), and the information it provides to that remote display can be externally programmed through the PROM.

REFERENCE SYSTEMS

A multiple DME positioning system and a photographic positioning system were used to fix the aircraft's actual position. The multiple DME positioning system used was a Rockwell-Collins DME-700. The DME-700 transmits pulsed signals to a ground station and receives responses from the station. Slant range is determined by measuring the transmit time from the aircraft to the station and back to the aircraft. The DME-700 is capable of operating in several modes including: standby, single channel, diversity, and scan (which was utilized for the purpose of this test). The scan mode provides a capability to service up to five stations at a high rate, and can scan the other 274 channels for valid replies at the same time. The DME-700 receives serial digital control information on one of two ARINC 429 input data buses. The control information also instructs the DME as to what mode of operation to use. The DME-700 delivers serial digital distance data over two ARINC 429 output data buses. DME data (distance and frequency) from the five closest DME stations are transmitted via the data output buses at 3.5 sec intervals. Depending on the number of stations, received data for an additional 15 DME stations can also be transmitted via the data output buses.

The photographic positioning system used was a Minolta X-700 camera system. The Minolta X-700 is a 35 mm Single Lens Reflex (SLR) camera system. Options available for the X-700 system that were utilized for this flight test program are as follows:

- Multifunction back
- MD-1 Motor Drive
- Remote Control

The multifunction back allows the user to imprint on each negative one of several items: time (hours, minutes and seconds), calendar date (month, day and year) or it can be programmed to number each negative in sequence from 1 to 999,999. For this flight test application the time option was utilized. This allowed the data to be time correlated with the airborne system data collector. The motor drive and remote control options allowed the flight test engineer to operate the camera while observing other necessary data collection parameters.

The camera was mounted inside the aircraft pointing through the bottom of the fuselage. Two lenses were used (35 mm and 70 mm), depending on the altitude above the ground, to yield a reasonable field of view. Photographs were taken of airport runways and VOR stations so that an accurate indication of actual aircraft position could be determined. Photographs were developed on site to insure the validity and quality of the data.

DATA ACQUISITION SYSTEM

The data acquisition package utilized during the flight test program consisted of eight major components. They were as follows:

- MFE 452B w/414 PAR Cassette Recorder
- Collins DME-700
- Microcomputer Chasis. Logic and Interface Boards
- Keyboard and Alphanumeric Display
- System RPU Loran-C

The appropriate data parameters were digitally recorded on the MFE 452B with 414 PAR option cassette recorder. These data were recorded from three distinct sources via the microcomputer logic and interface boards. The three sources were as follows: Collins DME-700, analog voltages representing aircraft systems and the wide area coverage system RPU. The operator/system interface components consisted of a keyboard, alphanumeric display and a CRT console, to be used for post-flight quick-look dumps. The primary power for the data acquisition system was 28 VAC.

DATA PROCESSING

The data obtained during the flight test consisted of digital data recordings on magnetic tape, photographic data at selected sites and observations of the pilots and flight test observer. The digital data recording system, used in the test, recorded three generic types of navigation and aircraft system data. These types were:

- Analog voltage or phase angle data
- DME digital data
- TDL-711 Loran-C digital data

All data were time tagged by the data collector clock to the nearest .01 second. Data were recorded at a 1 Hz rate on magnetic tape cassettes. On the transition flight from West Palm Beach to Anchorage, data were recorded at periodic intervals of approximately five minutes on line and five minutes off line. During the Alaskan flight testing and the return flight to West Palm Beach, data were recorded continuously. In all, 120 cassettes of test data were obtained. Due to the large amount of data, processing was performed at a 0.1 Hz rate thereby providing data at ten second intervals.

The following analog data were recorded during the test and utilized in the data reduction procedure:

- Dynamic pressure (indicated airspeed)
- Altitude reference } Potentiometer voltages
- Altitude wiper }
- Aircraft heading synchro
- CDI indicator voltage
- CDI flag voltage

Seven DME data channels from the Rockwell-Collins DME-700 were obtained each second. Each channel contained a time tag, co-channel VOR frequency and DME distance. In areas where there were five or more DME stations available, the DME-700 provided DME measurements from five separate stations. The additional two channel's contained data from two of the five channels taken about a half second later. When fewer than five stations were available, the DME-700 provided repeated measurements from the available stations to complete the seven channels of data.

The TDL-711 Loran-C navigator was equipped with a specialized PROM for providing a considerable amount of Loran-C receiver information through the remote display unit (RDU) data line. The Loran-C information is divided into three general categories, display replica data, Loran-C signal processing data and Loran-C navigation data. Specific parameters recorded in these categories are:

<u>Display replica data</u>

- CDU annunciators
- Left hand digital display
- Right hand digital display
- From/to waypoint display
- Decimal points and other CDU lamps
- Distance to waypoint register for display
- Ground speed register for display

<u>Loran-C signal processing data</u>

- Time difference A
- Time difference B
- Loran-C track status
- Loran-C signal to noise ratio
- Loran-C station blink status
- Loran-C envelope detection status
- Loran-C envelope numbers
- Triad in use
- Group repetition interval's (GRI's) per CDI update

<u>Loran-C navigation data</u>

- Loran-C latitude and longitude
- Crosstrack error
- To/from waypoint latitude/longitude
- To/from waypoint numbers
- Parallel offset value
- Magnetic deviation value
- CDI scale factor

All Loran-C data were recorded at a 1 Hz rate and were time tagged to the nearest .01 seconds.

Through the use of the aircraft's true position, and the navigation and Loran-C data recorded from the Loran-C navigator, many accuracy parameters could be determined. These include:

- Easting and northing position errors
- Loran-C time difference errors
- Total system alongtrack and crosstrack errors
- Navigation sensor alongtrack and crosstrack errors
- Navigation computer alongtrack and crosstrack errors
- Flight technical error

A diagram defining these error relationships is shown in Figure 5. The navigator RDU data stream provides Loran-C derived latitude and longitude, crosstrack deviation (flight technical error) and distance to waypoint (DTW) data.

From these parameters, and the waypoints which define the course, the other error components are calculated.

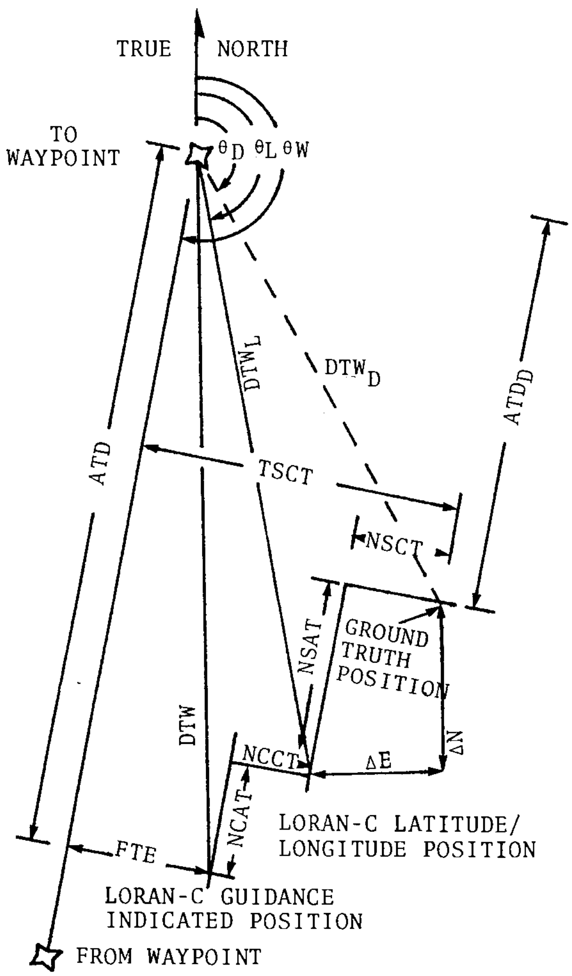

Figure 5 Loran-C System Error Geometry

Time difference errors were computed at each point where valid Loran-C and DME position data was available. The procedure involves reversing the coordinate conversion process performed by the TDL-711 navigator. Using the true aircraft position from the DME system, distance to Loran-C station values are computed for a spheroidal earth model. The procedure for this computation was taken from FAA Advisory Circular 90-45A, Appendix J. However, earth radii used in the procedure are taken from Reference 2, which uses the World Geodetic System-1972 Datum. The error components are evaluated statistically by computing their mean values and standard deviations according to standard formulas.

OPERATIONAL RESULTS

General

As found in this test and previous Loran-C tests with the TDL-711, the system has been designed reasonably well from the pilot's point of view. Most of the features or modes were, at one time or another, used by each of the subject pilots. some pilots preferred to keep the digital display readout in the "XTE" mode in order to fine tune their steering performance, since this readout is to .01 nm. Other pilots primarily used the distance to waypoint mode in order to maintain cognizance of their alongtrack position, and used the CDI needle for crosstrack steering. In any event, in the majority of situations the Loran-C signal stability was good enought that pilot FTE, or steering error, was quite low. Even when flying the CDI, needle movement was only affected by aircraft heading or wind, and did not exhibit the significant variations often encountered with either flying VOR radials, or, to a lesser extent; when flying VOR/DME RNAV. It is to be expected that the FTE element in a Loran-C RNAV system use error budget will be substantially lower than the values currently used for the enroute and terminal phases of VOR/DME system certifications.

Four operationally significant circumstances were observed during the conduct of these tests. The first is of somewhat lesser importance and has been both observed and documented in a previous test (Reference 3). When initiating a leg change (i.e., changing from a waypoint 1-2 leg to a waypoint 2-3 leg), a period of several seconds is required, during which time the CDI needle is centered and the flag is in view. In an enroute environment, where course changes between legs are usually moderate, this denial of steering information is not critical. However, if this situation occured in a terminal area situation where course changes of up to 90° can be expected, this system characteristic could possibly result in undesirable airspace utilization under conditions where airspace is at a premium. The principal cause of this problem is the saturation of the computer currently used in the TDL-711. Use of a faster computer or more optimized software design should reduce this "dead" time to a more desirable level.

The second problem is of a potentially more serious nature, and has also been observed previously. On several occasions, such as flying east from McGrath to Anchorage, the Loran-C accuracy markedly degrades, with no overt indication to the pilot that such a situation exists. In some cases the

Loran-C accuracy diverged from a value of approximately 1 nm to a value approaching 20 nm. From the pilot's point of view the system is performing perfectly (i.e., the system is locked on with an adequate set of signal strengths, the CDI flag is pulled out of view, and CDI steering signals are available). However, without some supplemental position fixing aid, such as VOR and DME, or visual fixes, the pilot is not aware that his guidance could be in error by 20 nm. The cause for these errors has not yet been quantified. Some measure of errors appear to be a function of the specific design characteristics of the Loran-C airborne unit used in this flight experiment, such as the propagation model and/or cycle slip. Operational procedures to eliminate or reduce the possibility of this situation occurring should be investigated.

The third problem has again been both observed and documented in a previous test (Reference 3). The TDL-711 system offers a diagnostic mode which can be utilized to display certain internal navigator data, such as signal to noise ratios (SNRs) and other important signal data. This mode is entered by moving the selector to the "LEG CHG" position and then through a series of keystrokes initiated by the pilot. On several occasions when the pilot tried to exit the diagnostic mode, the system would lock up. To resume normal navigation the system had to be reinitialized in flight.

The fourth very disturbing problem occured on two occasions. For reasons unknown, when a leg change was initiated the CDI needle moved full left then right, repeatedly. Again the system was locked up and required reinitialization before navigation could be resumed. Both of the problems are most likely software related.

Finally, no noticable problems were experienced due to precipitation static. Several of the flights were flown in rain, ice and snow for extended periods of time and never once was there experienced a system failure or loss of lock situation due to precipitation static. Even at times when the rainfall rates were heavy, no noticable problems were experienced due to precipitation.

Transition Segments

During the enroute transition phase of testing, no "mid continent gap" was encountered per se. Although at times signals were weak and coverage was poor, the navigator continued to operate and provide good guidance for most of the flight. There were times when the system lost lock for brief periods of time enroute, but these occurences were limited.

On approaches into both Montgomery, Alabama and Little Rock, Arkansas, the system lost lock on the transition and return flights from Anchorage. This problem could be due possibly to some local industrial noise in the area. Further approach testing in these areas might reveal some additional information. Although some bias errors were experienced, the approaches to all of the other airports were accomplsihed without a break in lock.

Alaska

The main purpose of the Loran-C flight test in Alaska was to determine in which areas the system could meet the AC 90-45A airspace requirements so that a STC can be issued for those particular geographical areas using the TDL-711.

One of the serious problems mentioned earlier occured virtually every time the system was utilized in the Anchorage, Alaska area. The Loran-C accuracy markedly degraded in the Anchorage area (approximately a 60 nm radius), with no overt indication to the pilot such a situation existed. Only on one occasion at Anchorage did the Loran acquire signals on the ground. On all of the other flights the Loran did not lock on until well clear of the Anchorage area. This was true for all directions of flight. In some cases the error value approached 20 nm. Again, this is without any indication to the pilot unless of course the pilot uses VOR/DME or some other means to establish his actual position.

In the extreme southwest areas, especially around Bethel, Alaska, the system performed very accurately. On the Bethel Spur Route the Loran-C navigator guided the pilots to the exact location of the airports. Navigation during this flight was steady and at no time did the system lose lock. Since there are few other means of navigation in these areas, local air taxi operators could benefit greatly by having Loran-C in their aircrafts. The Bethel area offers good geometry from the master at St. Paul Island and the secondaries at Port Clearance and Narrow Cape. In addition, this area is right in the heart of good Loran-C coverage where good strong signals can be reliably received.

In the northern areas around Galena, Ambler and Kotzebue, the system experienced what appeared to be some type of cycle slip. Errors in excess of five miles were observed in this area. Navigation was always steady with no breaks in lock, but large bias errors were experienced. This area is outside of the predicted USCG Loran-C coverage, mainly because it is so far from St. Paul Island, the master station.

Further testing should be conducted in this area to determine the cause of the errors.

Overall, the TDL-711 Loran-C navigation system performed very accurately over the course of the flight test experiment. Although several anomalies were noticed in certain geographical areas, the TDL-711 was found to be very accurate when it received good signals and was straightforward to operate. In good coverage areas, the system locked on within 2.5 minutes. Two generic operational problems arose during the tests. In areas where the SNRs were very low, the system often did not acquire the Loran-C signals on the ground or in the air. In addition, the system will acquire a false position with no indication to the operator that it has done so.

CHAIN PERFORMANCE

During the Alaska flights the North Pacific chain was utilized almost exclusively. On a few occasions in the Anchorage area when the receiver would not lock onto the North Pacific chain, attempts were made to acquire the Gulf of Alaska chain. These attempts were equally unsuccessful and so the only useful navigation data were obtained with the North Pacific chain. The triad used for navigation was:

Time difference A - Port Clarence/ St. Paul Island

Time difference B - Narrow Cape/ St. Paul Island

A review of the Coast Guard monitor data showed that the time difference errors, as recorded at the Kodiak monitor site, were usually less than 40 nanoseconds. On some occasions however, particularly on flights 9-04, 9-06 and 9-07, the TDA error at Kodiak was as large as -80 nonoseconds. This error value however, is on the order of the minimum time difference resolution of the TDL-711 and is not considered significant in affecting Loran-C operational accuracy.

It should be noted that while the Kodiak station monitors the Port Clarence signal, it does not control that stations phase adjustment.

Five instances of unuseable time were recorded for the master station at St. Paul Island during the period of time from 9-01-82 to 9-18-82. None of these times coincided with the times that the test flights were in progress. The unuseable times totaled 23 minutes for the 19 days, producing a system availability rate of 99.92% during the test period. The availability was 100% during the tests.

In summary, the North Pacific chain was operating within the normal accuracy and availability ranges during the performance of the flight tests.

RECEIVER PERFORMANCE

The remainder of the text discusses the accuracy results obtained from the flight test program. More detailed results can be found in the flight test report (Reference 4). The data presented in this report and in this paper reflects only the data collected during the Alaska portion of the flights.

In the Anchorage and Fairbanks area, the availability of Loran-C guidance from the TDL-711 was very poor. This was consistently true on each day that the unit was flown in these areas. For example, on a flight flown on 9-4-82, the unit failed to lock on for about one hour until the aircraft was about 100 nm south-south west of Anchorage near Homer. Two brief loss of lock occurences happened outside the Anchorage area, one near King Salmon and one near McGrath. The first of these was operator induced to demonstrate airborne reinitialization. On the return trip from Fairbanks to Anchorage, the unit had large errors throughout this flight segment and completely failed to operate for a constant seven minute period.

Time difference errors were determined by applying the data processing procedure outlined previously. Evaluation of the time difference error provided information on the receiver's ability to process the Loran-C signal and identify the proper cycle crossing and evaluate the propagation model used by the TDL-711 navigator for position determination.

Table 2 presents the detailed statistical time difference error data for the five days of flight testing. These data are taken within a 50 nm radius of the cities and villages shown. As a general rule the following rules apply to interpreting the time difference errors:

- TDA refers to the Port Clarence/ St. Paul Island time difference
- TDB refers to the Narrow Cape/ St. Paul Island time difference
- Positive time difference error implies one or more of the following conditions:
  - propagation model error in the master signal
  - cycle slip in the master signal
  - cycle jump in the secondary signal

- negative time difference error implies one or more of the following conditions:
  - propagation model error in the secondary signal
  - cycle slip in the secondary signal
  - cycle jump in the master signal
- A cycle slip is defined as the receiver tracking on the fourth or greater cycle, a cycle jump occurs if the receiver tracks the first or second zero crossing in the Loran-C pulse.
- Normally propagation model errors are in the 2-3 μ second range with errors occasionally reaching 4-5 μ seconds. Cycle slip and cycle jump errors are multiples of 10 μ seconds which is the period of the 100 KHz Loran-C signal.

Table 2 indicates that near Kodiak the TDA error approaches -5 microseconds indicating a large error in the Port Clarence signal. This signal is traveling over the mountains north of Kodiak and a large modeling error is quite normal. Similarly, at Bethel the TDB signal approaches -5 to -6 microseconds. The Narrow Cape signal passes over the same mountains causing a similar error in TDB at Bethel. In the Anchorage and Fairbanks area, all signals travel over the mountains and a cancellation of modeling errors probably occurs due to the time difference nature of the signal.

Table 2 shows errors observed on flight 9-06 which was flown throughout the northern region of the test area. Only about 10 minutes were obtained in the Anchorage to Fairbanks segment. In this area both TDA and TDB were very large, about 21 μ seconds, indicating a

Table 2 Mean Time Difference and Position Errors

CITY	DAY	#PTS	TDA	TDB	ΔN	ΔE
Kodiak	9-04	70	- 4.587	2.429	- .804	- .334
	9-07	90	-26.431	- .085	-4.126	- 2.723
King Salmon	9-04 in	31	- 4.190	- 2.521	- .583	- .365
	9-04 out	117	- 3.715	- 3.545	- .421	- .374
	9-07	139	- 3.423	- 3.413	- .398	- .360
Bethel	9-04	134	- 2.211	- 5.563	- .116	- .530
	9-07 in	61	- 2.565	- 5.356	- .149	- .497
	9-07 out	12	- 1.376	- 5.153	- .021	- .499
	9-09	97	- .528	- 5.011	- .056	- .507
	9-10	4	- 2.391	4.216	- .369	.427
Aniak	9-04	26	- .528	- 3.610	- .007	- .379
	9-07	41	- .219	- 3.228	.020	- .341
	9-09	133	- 1.271	- 3.593	- .086	- .383
	9-10 out	35	75.055	3.261	8.876	1.273
	9-10 in	42	- .126	6.443	- .117	.669
Nome	9-06 in	117	9.961	3.423	1.301	.247
	9-06 out	148	- .830	3.171	.039	.455
	9-09 in	126	- .887	- 6.545	- .289	- .886
	9-09 out	123	- .374	- 5.968	- .131	- .819
Galena	9-06 out	39	11.410	7.255	2.722	2.088
	9-06 in	97	1.630	6.769	.639	1.174
Fairbanks	9-04 in	88	.846	1.384	.284	.615
	9-04 out	140	31.583	31.486	9.771	17.631
	9-06 in/am	21	21.099	20.661	6.889	11.994
	9-06 out/am	90	11.615	11.228	3.700	6.027
	9-06 pm	127	.534	10.921	.370	3.066
Anchorage	9-04 in	105	46.425	39.844	6.665	17.340
	9-06 in	137	8.861	19.452	.842	5.606
	9-07 out	119	10.877	35.313	.117	8.673
	9-07 in	14	- 9.513	- 7.827	-1.330	- 2.719
	9-09 out	88	45.863	47.217	6.230	16.294
	9-09 in	125	- .155	1.788	- .091	.294
	9-10 out	99	32.407	34.241	4.268	11.492
	9-10 in	107	- 2.232	11.073	- .734	1.642

probable cycle slip in the master signal.

Upon leaving Fairbanks the unit was reinitialized, but as shown, large errors on the order of +10 to +12 seconds are apparent. At Nome there is almost precisely a 10 μ seconds jump in the TDA data of Table 2 between the incoming flight 9-06 and the outgoing flight (9.961 μ seconds versus -0.830 μ seconds). At the same time, the TDB error is essentially constant on the inbound and outbound segments (3.423 μ seconds versus 3.171 μ seconds). This would tend to indicate a cycle jump in the secondary signal of TDB rather than a cycle slip in the master signal which would affect both TDA and TDB. Near Anchorage, on the return segment, a large TD jump occurs after the aircraft passes Nenana. Since it occurs in both TDA and TDB, the evidence indicates a probable cycle slip in the master signal.

Cycle slips or cycle jumps are apparent in both TDA and TDB as the aircraft exits and enters the Anchorage area. TDA error is about -10.9 μ seconds upon leaving Anchorage and -9.7 μ seconds upon return. TDB error is -35.5 on the outbound segment and -7.8 on the return segment in the evening.

The TD errors shown in Table 2 for flight 9-09 from Anchorage to Nome to Bethel to Anchorage were the most consistent data obtained during the test. Upon leaving Anchorage, TD errors in both channels exceed 40 μ seconds, however, the system was reinitialized and consistent performance was observed throughout the remainder of the flight.

Errors in TDA are near zero throughout the flight. Errors in TDB of about -6 μ seconds were observed at Nome. The error at Nome is consistent with propagation model error in the Narrow Cape signal as it travels over land and mountains north of Kodiak. The system appears to function well even into the Anchorage area on this flight.

The flight of 9-10 consisted of a direct flight from Anchorage to Bethel, the Bethel Spur segment and return from Bethel to Anchorage. During the Bethel Spur segment photographic data was obtained. On this flight the system was initialized in the Anchorage area and allowed to operate without operator intervention from Anchorage to Bethel. The system indicated that it was operating properly, but large errors are shown in both TDA and TDB throughout the segment. Apparently the system, once locked on to a signal, did not attempt to verify if it was locked on to the correct signal. This observation strongly suggests that the system should be checked for proper operation and reinitialized in known, good signal areas.

The limited amount of TD error data obtained on this flight indicates that the error in TDB was about 10 μ seconds greater than that obtained in previous flights at Bethel and Aniak. This is shown in Table 2. At Aniak the error is about +6.4 microseconds instead of -3.2 to -3.6 as measured on flights 9-04, 9-07 and 9-09. At Bethel the error, based on only 4 points, is +4.2 μ seconds instead of the -5.0 to -5.6 μ seconds, which was measured on other days. This difference strongly suggests a receiver cycle jump in the secondary signal from Narrow Cape.

Propagation model errors, where they could be separated from cycle errors, were quite consistent with expected performance. The TDL-711 propagation model uses a faster propagation velocity than that predicted by theoretical means. It is especially true in the case of signals which propagate over mountainous terrain of poor conductivity, such as the areas west of Fairbanks, Anchorage and Kodiak. These mountains, some of which are the most rugged in North America, appear to have a significant slowing effect on the propagation velocity of the 100 KHz Loran-C signal.

The apparent cycle slip and cycle jump problems experienced during the test could arise from a number of possible sources. Included among these are:

- Poor signal to noise ratio
- Interference from other radio systems
- Multipath distortions to the signal

It is quite possible that all three problems exist in the Anchorage area. Industrial noise from electrical machinery coupled with the great distance (900 nm) between the St. Paul Island master station could cause low signal to noice ratio problems. In addition, three AM broadcast stations in Anchorage are separated by 100 KHz:

KENI - 550 KHz - 5 KW (daytime)

KYAK - 650 KHz - 50 KW (daytime)

KFQD - 750 KHZ - 50 KW (daytime)

Although the receiver has high out-of-band rejection, it is possible for some energy from these frequencies to be present in the receiver front-end and cause synchronous interference at 100 KHz

The rugged mountains in the test area create the likelihood of multipath distortion of the Loran-C pulse. This type of distortion could create difficulties in identifying and tracking the third cycle zero crossing which is generally used by Loran-C receiver designers for phase tracking.

The widespread occurrence of cycle tracking problems throughout the test area tends to enforce the multipath theory. However, the amount and character of the recorded data are not sufficient to confirm or deny any of the three listed problem sources nor to rule out other possible sources of problems.

Of major concern are large numbers of cycle tracking problems observed in these tests. These errors produce large position errors as shown in Table 2 under the northing and easting error columns. The TDL-711 system is incapable of detecting these cycle tracking problems at the present time and therefore provides no warning to the pilot.

A statistical combination of the time difference and position errors for four cities in good coverage areas are shown in Table 3. These data show generally good position accuracy capability inspite of the occasional occurrences of cycle slip.

and moderate turbulence. In spite of these conditions, the data shows that FTE is considerably smaller than the 2.0 nm value contained in Advisory Circular 90-45A for enroute performance. The 95% level (2σ) for FTE as determined by the test data was 0.35 nm. This is approximately one-sixth of the value used in the advisory circular.

Table 4 Flight Technical Error

FLIGHT DATE	NUMBER OF POINTS	MEAN	STD DEVIATION
9-04-82	582	+.036	.103
9-06-82	578	+.033	.160
9-07-82	249	-.074	.193
9-09-82	872	-.005	.205
TOTAL	2281	+.007	.175

PHOTOGRAPHIC DATA

Table 5 summarizes the results of the Alaska Loran-C data collected with the photographic data collection system

Table 3 Statistical Combination of Time Difference and Position Errors

LOCATION	# PTS	μS TDA		μS TDB		NM ΔN		NM ΔE	
		$\overline{X}$	$\overline{\sigma}$	$\overline{X}$	$\overline{\sigma}$	$\overline{X}$	$\overline{\sigma}$	$\overline{X}$	$\overline{\sigma}$
King Salmon	287	-3.62	.92	-3.37	.46	-.43	.15	-.37	.06
Bethel	308	-1.72	1.07	-5.21	1.19	-.10	.09	-.50	.12
Aniak	242	- .81	.61	-1.79	3.81	-.06	.06	-.19	.40
Nome	514	1.72	4.53	-1.34	4.80	.21	.64	-.22	.62

PILOT PERFORMANCE

During the transition flights to and from Alaska and the test in Alaska, a linear CDI scale factor of ±1.28 nm full scale was used. Through use of the observers notes, the portions of the flight that Loran-C was being used for guidance were identified. These times were coupled with times when both Loran-C and DME position data were valid. Statistical aggregation of the flight technical error data for these times are presented for flights 9-04, 9-06, 9-07 and 9-09 in Table 4.

The data from flight 9-10 are essentially similar to those obtained on the first four days. However, because of the unavailability of DME positioning data during most of the flight, the data was not included in the statistical processing.

The flights often encountered high winds on the Bethel Spur Route. Table 5 shows in the northing error case that the calculated mean is -.197 nm and the one-sigma value is .126 nm. The results for the easting errors were a total mean value of .436 nm and a one-sigma value of .067 nm. The error statistics in Table 5 show that the calculated mean is .145 nm and the one-sigma value is .408 nm, for the cross-track case. In the along track direction the calculated mean was -.019 nm and a one-sigma of .285 nm.

Table 5 Bethel Spur Route Statistics

	N ERROR	E ERROR	XTK ERROR	ATK ERROR
$\overline{X}$	-.197	.436	.145	-.019
σ	.126	.067	.408	.285
Points	12	12	12	12

The values indicated in Table 5 support the fact that the TDL-711 system performs very accurately in the Bethel area. The table reflects data collected at six different locations where each location was flown twice, therefore, demonstrating the repeatable accuracy of the system in good coverage areas.

Comparison of the photo data with the DME positioning data for Bethel on the same day shows excellent agreement. The DME system produced northing and easting errors of -.369 and +.427 nm, respectively. These values agree very well with the northing errors of -.352 and 0.325 nm, and fall inbetween the easting errors of .489 and .329 nm.

OVERALL SYSTEM PERFORMANCE

Overall, the performance of the navigator during the Alaska flights was quite variable. The performance in the Anchorage and Fairbanks areas, at the present time, is not acceptable for IFR navigation. Performance in areas west of the mountainous portions of the test area around King Salmon, Bethel, Aniak and Nome was sufficient to meet Advisory Circular 90-45A standards for RNAV enroute accuracy.

Statistical processing of the data was performed to produce total system alongtrack (TSAT) errors and total system crosstrack (TSCT) errors. These data are shown in Table 6.

Table 6 Total System Errors

FLIGHT DATE	ERROR TYPE	# PTS	MEAN (X)	STD DEV (σ)	MEAN +2σ	MEAN -2σ
9-04	TSAT	582	-.245	.241	.237	- .727
	TSCT	582	.359	.347	1.053	- .355
9-06	TSAT	578	-.428	.889	1.350	-2.206
	TSCT	578	.226	.428	1.082	- .630
9-07	TSAT	249	-.194	.129	.064	- .452
	TSCT	249	.268	.287	.842	- .306
9-09	TSAT	872	-.229	.441	.653	-1.111
	TSCT	872	.013	.457	.927	- .901
TOTAL	TSAT	2281	-.280	.546	.812	-1.372
	TSCT	2281	.183	.431	1.045	- .679

/NOTE/ TSAT = Total System Alongtrack Error
TSCT = Total System Crosstrack Error

The data shows that TSCT was within the 2.5 nm enroute criteria throughout the test program. TSAT does exceed the 1.5 nm criteria in some instances on flight 9-06. However, the aggregation of alongtrack error over the total test program stays within the 1.5 nm limit as shown in Table 6.

The data shows that TSCT was within the 2.5 nm enroute criteria throughout the test program. TSAT does exceed the 1.5 nm criteria in some instances on flight 9-06. However, the aggregation of alongtrack error over the total test program stays within the +1.5 nm limit as shown in Table 6.

CONCLUSIONS/RECOMMENDATIONS

— Total system errors (TSAT and (TSCT) were measured during the Alaska test at times when:

- Loran-C was used for guidance
- DME position data was available
- The Loran-C system was functional

These errors met Advisory Circular 90-45A criteria at these times.

— Flight technical errors of 0.35 nm (2σ) were measured during the test.

— The TDL-711 system performed very poorly within at least a 60 nm radius of Anchorage. Position errors in excess of 15 nm were not uncommon. System accuracy in the Fairbanks area was also very poor.

— One of the most important problems encountered is that the system can be locked onto, and track, an erroneous signal and calculate erroneous guidance with no indication to the operator that it has done so.

— The major source of errors in the Alaska flights is time difference error. This error is translated into position and guidance error through the coordinate conversion process. The most probable cause of the time difference error is cycle slip or cycle jump where the receiver tracks the wrong cycle of the Loran-C signal. Apparent cycle slips of up to 70μ seconds were observed. Cycle slips on the order of 10 to 40μ seconds were not uncommon in the Anchorage and Fairbanks area.

— A second probable source of time difference error observed during the test is propagation modeling error. This error was most apparent when operating near Nome and Kodiak. At these locations the modeling error approached -5 to -6 microseconds. This produced position errors on the order of 0.9 nm at these locations.

— The conversion process from time difference coordinates, to position coordinates, to guidance coordinates, produces negligable system errors.

— The TDL-711 was easy to operate and imposed no undue burden on the flight crew.

— The TDL-711 met or exceeded the accuracy requirements of Advisory Circular 90-45A in the areas around Nome, Bethel, Aniak and King Salmon. It is recommended that STC certification be granted in an area bounded by the 156°W meridian, the 168°W meridian, the 58°N parallel and by the 65°N parallel.

— Operation of the system in IFR enroute conditions should be subject to the following conditions:

- The system should be initialized (either in the air or on the ground) in known areas of good signal coverage.
- The performance of the system must be checked through an approved position check prior to commencing IFR navigation. Position check procedures include:
  - navigation station passage (VOR or NDB)
  - position check utilizing two VOR stations
  - position check utilizing VOR/DME

The system should meet ±1.5 nm accuracy criteria in crosstrack and alongtrack directions.

ACKNOWLEDGEMENTS

Much of the material for this paper was derived with the aid of associates at the Champlain Technology Industries Division of Systems Control Technology, Inc. Dr. Donald W. Richardson, President of the CTI Division, provided overall program management and participated as one of the subject pilots. Mr. Eric H. Bolz, Senior Engineer, provided technical expertise in the instrumentation coordination of the aircraft.

Mr. Harvey Barnett and Mr. Howard Meyers were contracted to participate as the primary subject pilots on the project.

Mr. George H. Quinn of the Federal Aviation Administration, Systems Research and Development Service provided technical guidance for the program.

REFERENCES

1. Anonymous, "TDL-711 Loran Micro Navigator - Operations Manual", Offshore Navigation, Inc., July 1978

2. Roland, W.F., Editor, "Radionavigation Journal 1978", Wild Goose Association, Inc., Acton, Mass. 1978

3. Scalise, T.E., Bolz, E.H., McConkey, E.D., "West Coast Loran-C Flight Test", Systems Control, Inc. (Vt), Champlain Technology Industries Division for the Federal Aviation Administration, Systems Research and Development Service, FAA-RD-80-28, March 1980

4. King. L.D., McConkey, E.D., "Alaska Loran-C Flight Test Evaluation", Systems Control Technology, Inc., Champlain Technology Industries Division for the Federal Aviation Administration Systems Research and Development Service, DOT/FAA/PM 83/4, February 1983

THE FUTURE OF LORAN-C IN EUROPE

CDR Roger W. Hassard
USCG Activities, Europe
Box 50
7 North Audley Street
London W1Y 1WJ
England

Present Loran-C operations in Europe are under the control of the U.S. Coast Guard which exercises regional and chain manager functions from its office in London. The system is there to meet precise navigation requirements of the Department of Defense (DOD) but, as in the U.S. and Canada, it has seen rapidly increasing use by commercial interests over the past decade. Now that the first non-U.S. chain for northern Europe is being developed, interest in the system seems to be increasing. As fate would have it, DOD requirements for the system are simultaneously decreasing and U.S. funding (and USCG presence in Europe) will undoubtedly end in the 1990s. Since interest has been expressed in a unified radionavigation system for Europe, a logical option, either as a long term solution or as a transitional system, is Loran-C. The existing system and plans for its improvement are discussed. Also presented are some reconfigurations which would provide coverage for commercially important areas. A major challenge awaits those who will attempt to co-ordinate the funding and operation of such a multi-national system. Planning for it would need to start soon.

PRESENT SITUATION

The North Atlantic (7930), Norwegian Sea (7970) and Mediterranean Sea (7990) Loran-C chains are under the operational control of U.S. Coast Guard Activities, Europe with Regional and Chain Manager functions. Other radionavigational services in the area and in the same spectral region are the U.S. Air Force Loran-D chain in West Germany and the Netherlands, the western Loran-C chain of the Soviet Union, and a mini-chain at the Suez Canal, as well as numerous Pulse-8 and Decca chains. Saudi Arabia and France are each in the process of constructing Loran-C chains. This paper concentrates on northern Europe and thus does not consider the Mediterranean and Middle East regions.

The present day configuration of the North Atlantic and Norwegian Sea Chains is shown in Figure 1. In mid-1984, when the new Canadian station at Fox Harbor becomes operational, the North Atlantic Chain will be reconfigured as shown in Figure 2 and its GRI will be changed to 9980 (the present 7930 rate will be assigned to the Labrador Sea Chain).

A major change is presently being made in the monitoring and control arrangements for our two northern chains. We have already completed an equipment replacement project at the Keflavik, Iceland monitor station. The faithful but archaic AN/FPN-46 timers were turned off in July 1982 and the modern Primary Control Monitoring System (PCMS), based on the Austron 5000 receiver, is now doing the job. This new equipment will also allow Keflavik to monitor and control two legs of the Norwegian Sea Chain (Sandur and Jan Mayen) while simultaneously handling the North Atlantic Chain.

Modern technology is also catching up with our Shetland Islands monitor station. We are currently engaged in a project which will result in 'unmanning' of the station by 1 October 1983. Here also the AN/FPN-46's will be replaced by PCMS. In this case, however, all of the receiver data will be transmitted in real time to Keflavik which will be the control station for both chains. A secondary monitor for the entire Norwegian Sea chain will be at LORSTA Ejde in the Faeroe Islands. This secondary data will also be transmitted to Keflavik. Table I summarizes the monitor and control plan.

Another operational European chain, the USAF operated Loran-D system, is shown in Figure 3. The government of the Netherlands is presently voicing interest in commercial use of this system as the result of recent tests conducted with standard Loran-C receivers along their coast. At present the chain is operated for a very limited set of users and is frequently off-air, making commercial use doubtful.

Finally, the French government is in the process of establishing a two station (rho-rho) chain as shown in Figure 4. This chain is planned to become operational on GRI 8940 in June 1985. As will be shown, numerous possibilities exist for expansion of this chain into a multi-station hyperbolic system. Initially, however, it will simply provide rho-rho coverage for the Bay of Biscay and precise time data. The monitor, located at Brest, will synchronize the system with UT via a television or similar link to the Paris Observatory.

Even with all these government operated systems, major bodies of water in Europe are

TABLE I

MONITOR AND CONTROL PLAN SUMMARY

Present North Atlantic and Norwegian Sea Loran-C Chains

	7930			7970			
	M-X ANGISSOQ -EJDE	M-Y ANGISSOQ -SANDUR	M-Z ANGISSOQ-CAPE RACE	M-W EJDE-SYLT	M-X EJDE-BØ	M-Y EJDE-SANDUR	M-Z EJDE-JAN MAYEN
PRIMARY MONITOR	KEFLAVIK (PCMS-1)		ST ANTHONY (PCMS-1)	SHETLANDS (AN/FPN-46)			
SECONDARY MONITOR	KEFLAVIK (PCMS-2)		ST ANTHONY (PCMS-2)	NONE (DELTA CONTROL)			
CONTROL	KEFLAVIK		ST ANTHONY	SHETLANDS			

Planned North Atlantic and Norwegian Sea Loran-C Chains

	9980		7970			
	M-W SANDUR-ANGISSOQ	M-X SANDUR-EJDE	M-W EJDE-SYLT	M-X EJDE-BØ	M-Y EJDE-SANDUR	M-Z EJDE-JAN MAYEN
PRIMARY MONITOR	KEFLAVIK (PCMS-1)		SHETLANDS* (PCMS)		KEFLAVIK* (PCMS-1)	
SECONDARY MONITOR	KEFLAVIK (PCMS-2)		EJDE* (PCMS)		KEFLAVIK* (PCMS-2)	
CONTROL	KEFLAVIK		KEFLAVIK			

* To be confirmed by operational tests in 1983

not adequately covered for commercial use. Much of the North Sea and all of the heavily travelled English Channel remain outside the good coverage areas for these systems. However, commercial systems have filled many of these voids in order to provide accurate position fixing for the oil exploration industry. Figures 5 and 6 show the Pulse-8 and Decca chains operating in the region.

FORECAST

The Federal Radionavigation Plan (FRP) of March 1982 states that the Navy has a continuing requirement for these chains through 1992. Meanwhile, DOD and DOT are continuing to work towards a 1983 "preliminary recommendation on the future navigation system mix" and, in 1986 a "national decision on selection of navigation systems of the future". The only decision which is of importance to the European Loran-C system, however, is that of DOD and it will be dictated almost exclusively by implementation of GPS.

If GPS becomes operational in the late 1980s and sufficient numbers of adequate receivers are available in the field in the early 1990s, it is a safe bet that DOD will eliminate all of their Loran-C requirements. As a result, the Coast Guard will immediately turn off transmissions and dispose of the stations and their equipment

What happens to the European Loran-C user when these stations are turned off? What are the alternatives?

GPS: This is viewed as a purely U.S. military system. European users do not want to be so closely tied to the whims of the Pentagon. Furthermore, the initial accuracy to be provided to the civil users will be comparable to Loran-C predictable accuracy and not nearly as good as Loran-C repeatable accuracy. Receiver costs and user charges are also valid concerns.

PULSE-8: Basically a low-power, commercial version of Loran-C widely available in the region. Many additional stations would be required to cover the English Channel, the Skagerrak, the Irish Sea and Norwegian, Icelandic and Faeroese waters. It is highly unlikely that large areas of the Norwegian Sea and North Atlantic, presently covered by Loran-C, could be accommodated. User charges would be necessary to support the commercial operation and continued operation would be a corporate policy decision.

DECCA: Also a commercial system which is widely available in the region, but with more limited range than either Loran-C or Pulse-8 because of skywave degradation.

TRANSIT: This satellite system, also called NAVSAT, is planned to be phased out in the early 1990s in favor of GPS.

OMEGA: Accuracy is much less than Loran-C. Although its future is uncertain, its international status will probably ensure its presence into the 2000s.

Short of developing their own independent system, retention of high accuracy position fixing capability after Loran-C will require European users to depend on GPS or on commercial systems with restricted coverage.

An additional possibility does exist, in the continued operation of Loran-C by some non-U.S. entity. The major problem to be resolved would be funding the continued operation. Navigation interests of the various European nations would require extensive co-ordination.

The remainder of this paper deals with possible Loran-C chain configurations for Europe and with some of the plans currently under consideration by various European governments.

FUTURE POSSIBILITIES

On 8 June 1982 the government of the Netherlands hosted a meeting at Urk concerning the possibilities of using Loran-C and Loran-D in the southern portion of the North Sea. The meeting was held at the request of the Dutch Federation of Fishermen Association which had expressed concern over poor coverage in the area from existing systems. Representatives from both civilian and military agencies of the Dutch government as well as from the USCG, USN and USAF attended. Among the possibilities raised by the Dutch was a low power secondary station in Belgium. This station could be used on either the Norwegian Sea or the Loran-D chains; either of these approaches would improve the coverage provided, but both are far from optimal solutions and treat only one of many areas where coverage for commercial usage would be needed. Figures 7 and 8 show the approximate coverage areas which would be added by the Dutch recommendations. The additional station would be funded by the Netherlands.

If the Loran-D chain were to be made available for commercial use, a better solution would be to add the French station at Lessay or the former Loran-D station at Wycombe, England, as shown in Figure 9. To achieve the coverage shown, the Loran-D stations' output power would need to be increased. The stations are presently transmitting 35 kW in Loran-D format. Because of the way we define output power, Loran-C users also 'see' 35 kW transmitters even though they are using only half the radiated signals.

Disregarding the Loran-D chain, which should be considered solely as a U.S. military asset within Europe, Figure 10 presents a Loran-C chain which would provide complete coverage of the North Sea, the entire United Kingdom and Ireland.* This chain would require dual rating of the French station at Lessay and construction of a new station in the vicinity of Bergen, Norway. The French have already voiced a willingness to tie their new stations into other European Loran-C chains and their transmitting equipment, initially to operate at 250 kW, will be capable of expansion to 500 kW dual rate operation. The Bergen, Norway station has been under consideration by Norway for a number of years (albeit for a different chain configuration) and is presently included within a document prepared by the Norwegian Board of Navigation and now under review by their Department of Communications (Samferdseldepartementet).

An improvement to the North Sea Chain of Figure 10 can be obtained by inclusion of the most westerly station of the Soviet Union's western chain. This would improve coverage between Denmark and Sweden by eliminating the base line extension problem seen in Figure 10. It would also provide improved coverage for the Baltic Sea. The improved chain is shown in Figure 11. Although no contact has been made with the Soviet Union in this matter, it should be noted that they have previously called for joint chain operations and in fact proposed dual rate operations between their eastern chain and our North-West Pacific Chain in 1980.

An alternative to the North Sea Chain of Figure 10 is an expansion of the French chain as shown in Figure 12. This is under consideration by the French and involves one new station in southern Ireland. Coverage quality in the North Sea would not be as great as that of the chain in Figure 10 due to significant overland propogation from the Ireland secondary. In addition to the expanded chain shown, the French have considered more secondaries in northwestern Spain and in the Azores!

Further to the North, interest in Loran-C navigation exists for the Norwegian coast, including offshore oil fields, the Faeroe Islands and Iceland. If Loran-C is to be a viable navigation system for shipping in U.S./Canadian waters and the major ports of northern Europe, it would also be reasonable to maintain coverage between the Labrador Sea Chain and mainland Europe.

The easiest problem to resolve is that of Icelandic coverage. After all, there are very few land masses available and those where stations already exist would seem to be best, with just one change. To provide complete coverage of Icelandic waters with a single chain would involve addition of Jan Mayen to the reconfigured North Atlantic Chain as shown in Figure 13. This change has been recommended by Iceland in the past and is included in recent correspondence from Norway.

The Norwegian coverage presents the most interesting problems. Poor ground conductivity, severe terrain and winter snow conditions combine to make overland propagation paths a major problem. Recent tests with Coast Guard monitoring equipment at a number of sites in the vicinity of Bergen confirmed that there is no mainland Norway

* The coverage diagrams provided show only the 30° crossing angle limitation, being a physical limitation due to station locations. SNR limitations are a function of radiated power which is not considered in this paper.

location where both Sylt and Bø can be reliably monitored. Fortunately, there are offshore island groups which can simplify the problem.

As mentioned earlier, Norwegian interest in a station near Bergen is not for a North Sea Chain as previously discussed and shown in Figure 10, but for improved coverage of Norwegian coastal waters as shown in Figure 14. Note that each of these proposed chains includes a Bergen to Sylt leg, so there is certainly hope for a combined solution.

Norway has also been interested in coverage of the far northern waters and the chain shown in Figure 15 would extend coverage all the way to the Barents Sea. Because of the limited areas where coverage is considered important (oil fields), it is probable that coverage in this area will be provided by 'mini-chains'. Another complicating factor is that Bear Island (Bjørnøya), shown as the master station of the chain, comes under the Svalbard Treaty of 1925 between Norway and numerous other governments. An additional complication of the chain shown (which is not one proposed by Norway) is that it requires dual rating of Jan Mayen and Bø. Tests on the AN/FPN-39 transmitters at these stations indicate that dual rating would noticeably reduce the service life of these equipments.

CONSOLIDATION

The final two figures, 16 and 17, show two ways of fitting the various chains together.

It appears feasible on paper, but there is no way that this can come to pass without a strong commitment by all those nations which would benefit from the coverage provided. Iceland, for example, with fewer than 300,000 people, could never afford to operate and maintain the four stations required for coverage of her waters. But those waters are prime fishing grounds for many other European nations. Furthermore, the U.K., Holland, Belgium, Sweden and other nations would benefit but might be reluctant to share costs as none of the facilities would be located on their lands.

If anyone is interested in European Loran-C coverage after the U.S. pulls out, now is the time to start taking action.

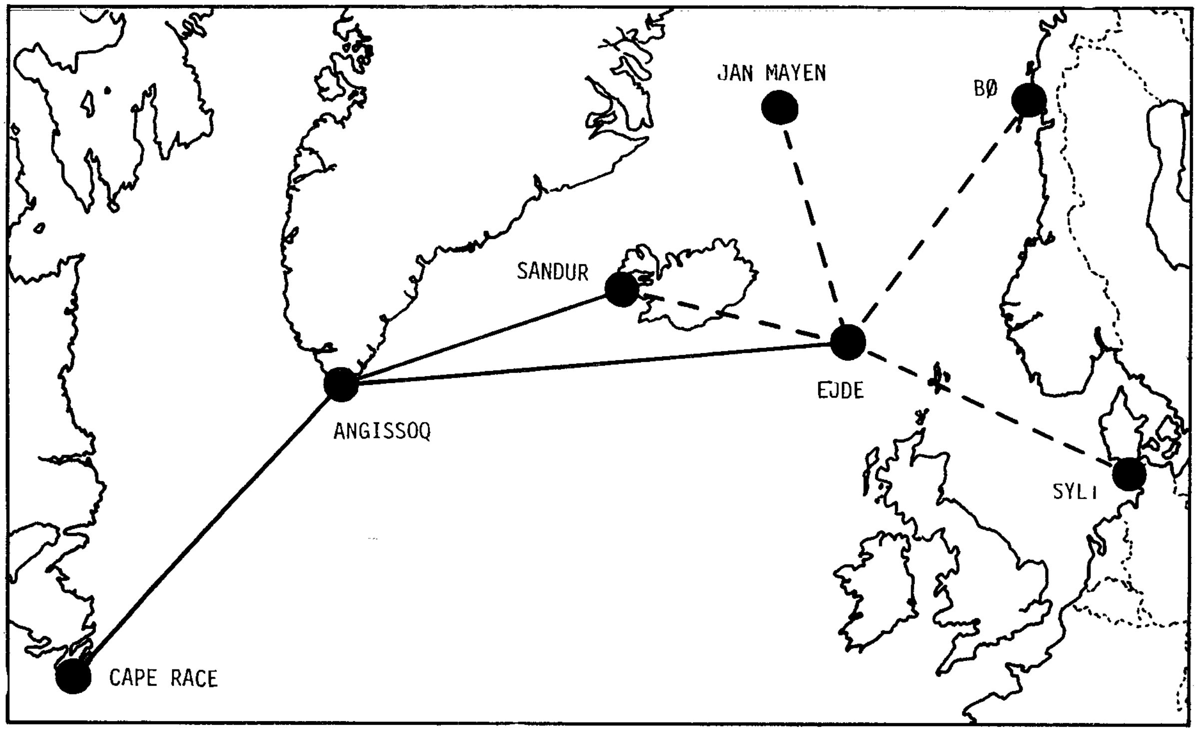

Figure 1: Existing North Atlantic (7930) and Norwegian Sea (7970) Loran-C Chains

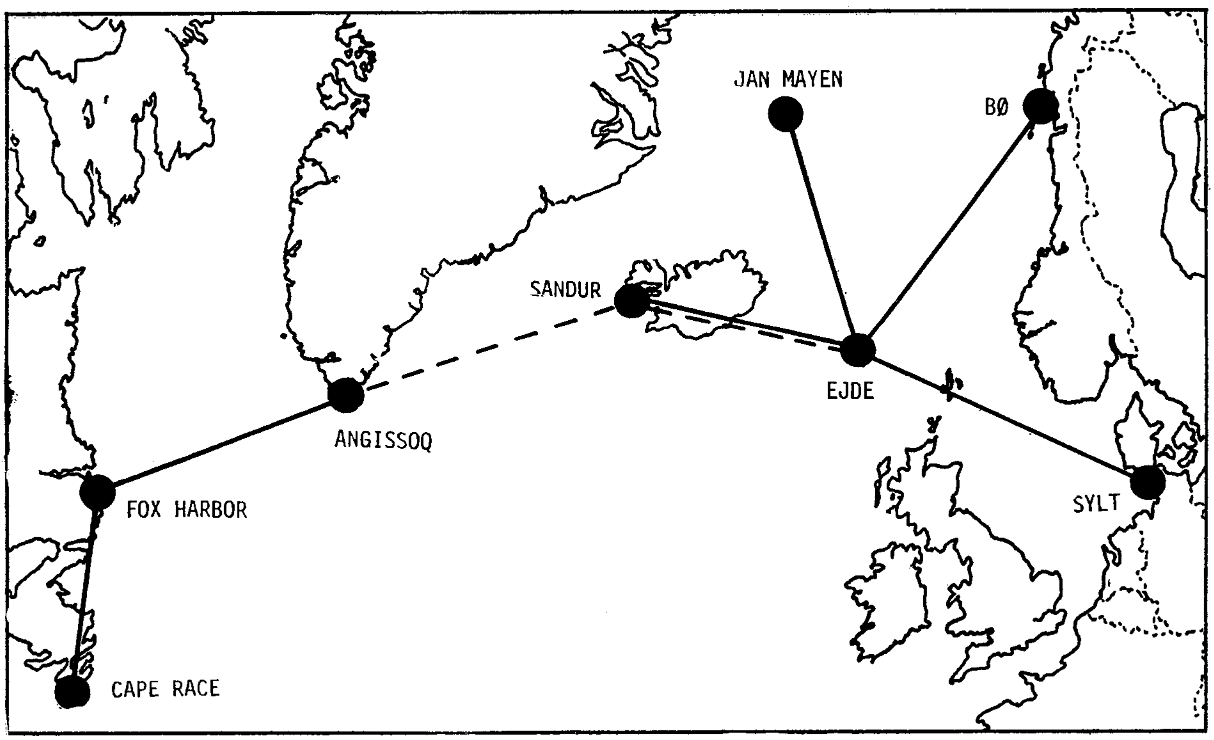

Figure 2: Planned Labrador Sea (7930), North Atlantic (9980) and Norwegian Sea (7970) Loran-C Chains

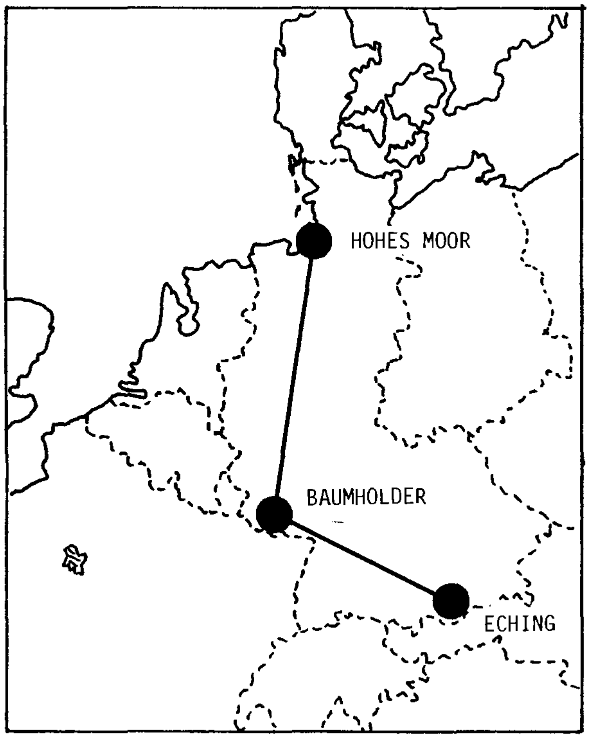

Figure 3: USAFE Loran-D Chain

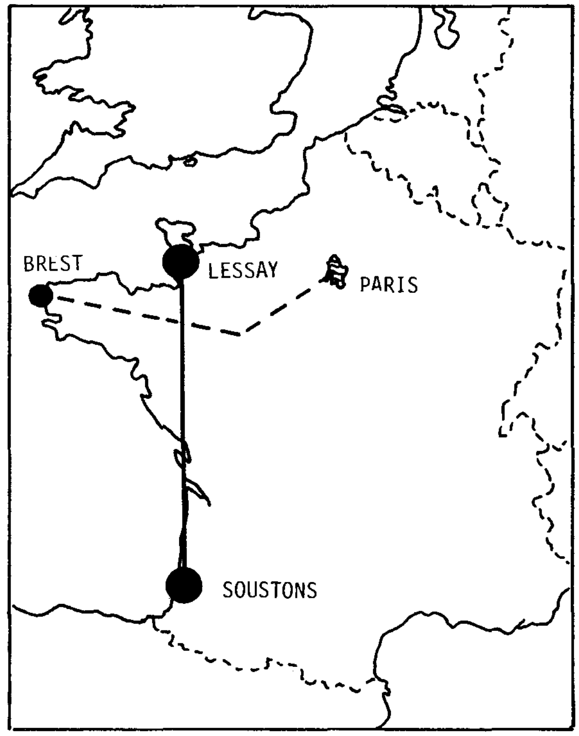

Figure 4: Planned French Loran-C Rho-Rho Chain

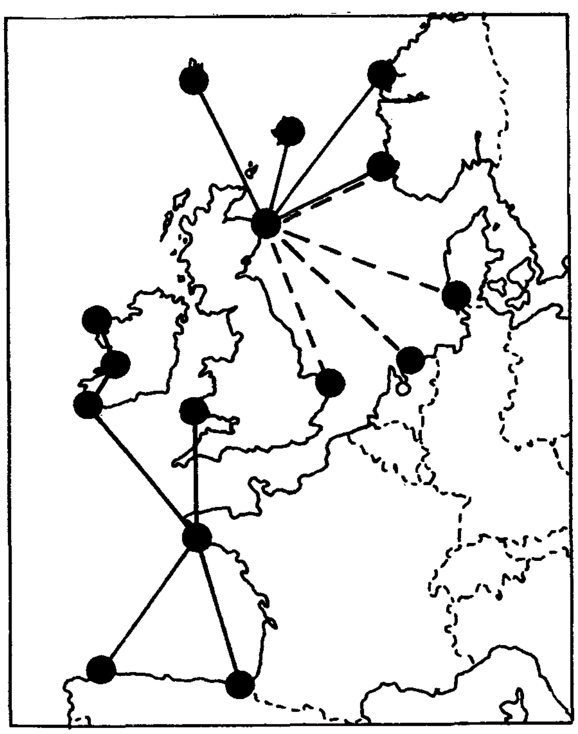

Figure 5: Pulse-8 Chains

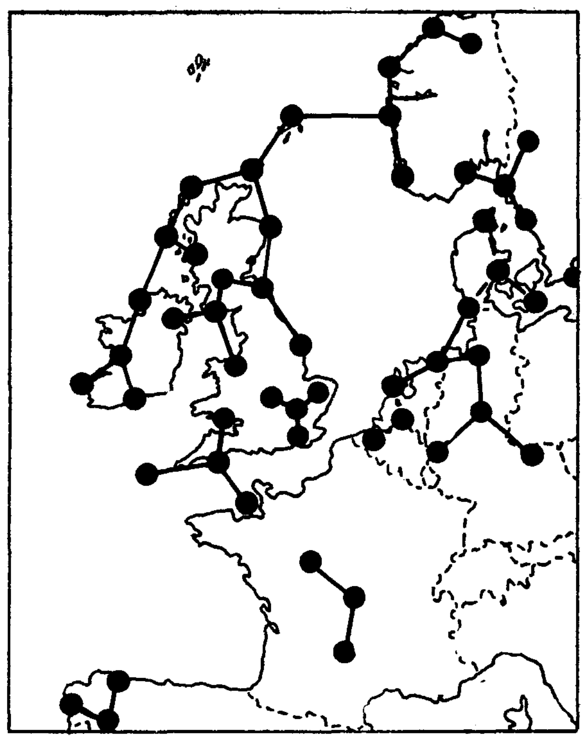

Figure 6: DECCA Chains

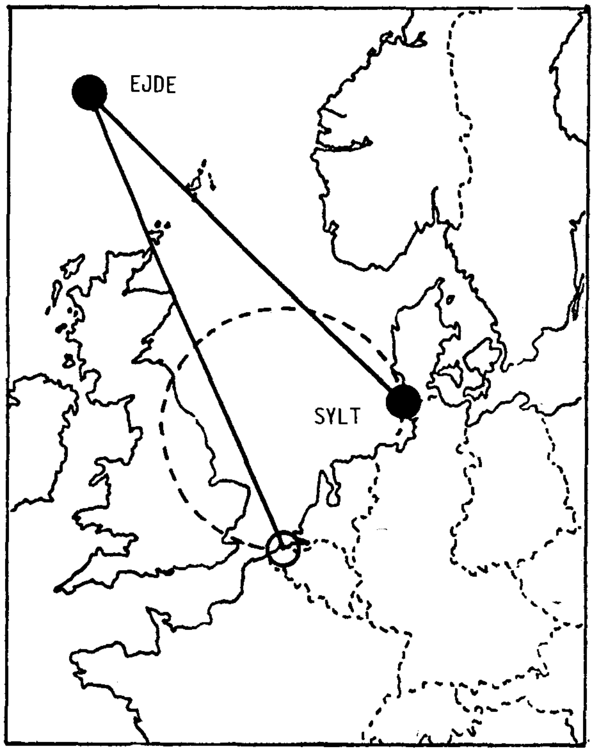

Figure 7: Low-power Belgian station Added to the Norwegian Sea Chain

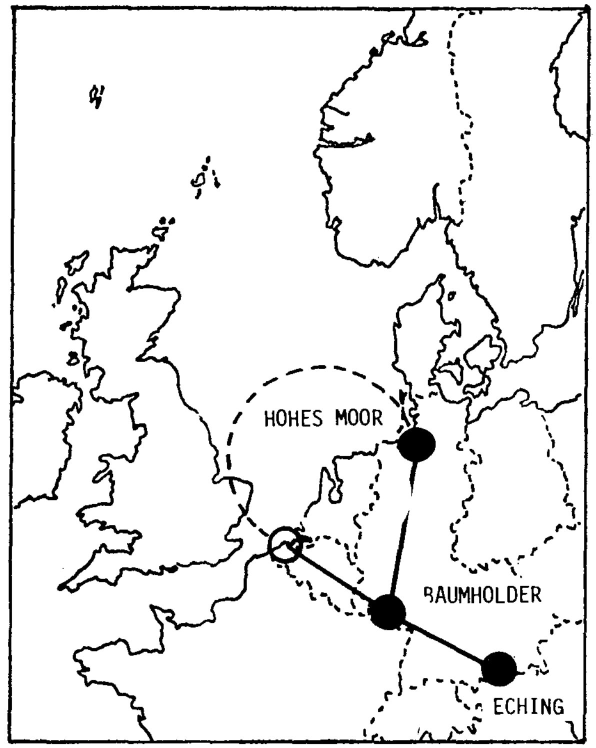

Figure 8: Low-power Belgian station Added to the Loran-D chain

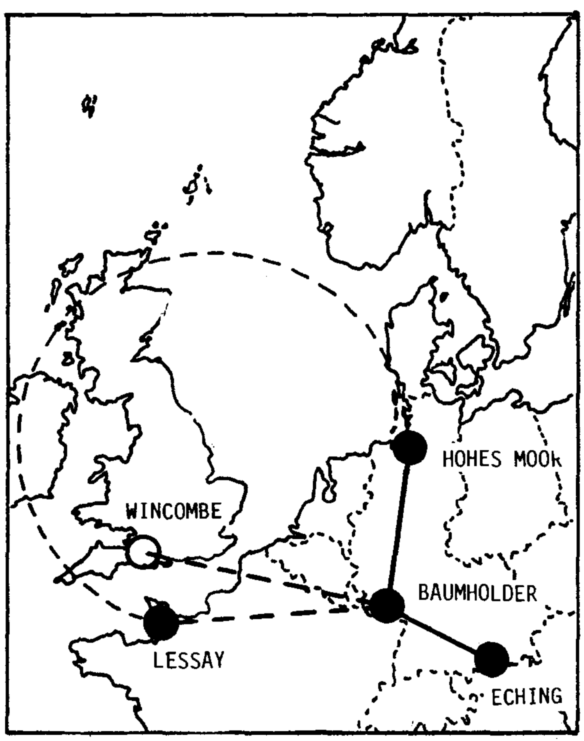

Figure 9: Expanded Loran-D Chain

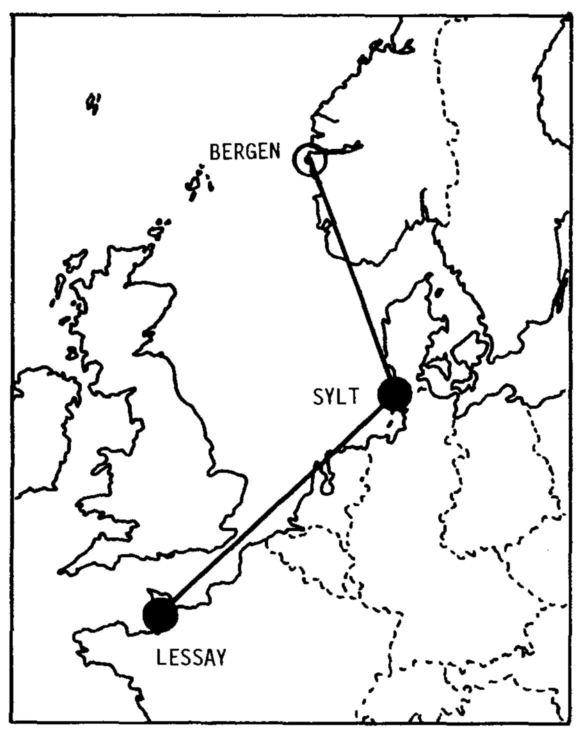

Figure 10: A Possible North Sea Loran-C Chain

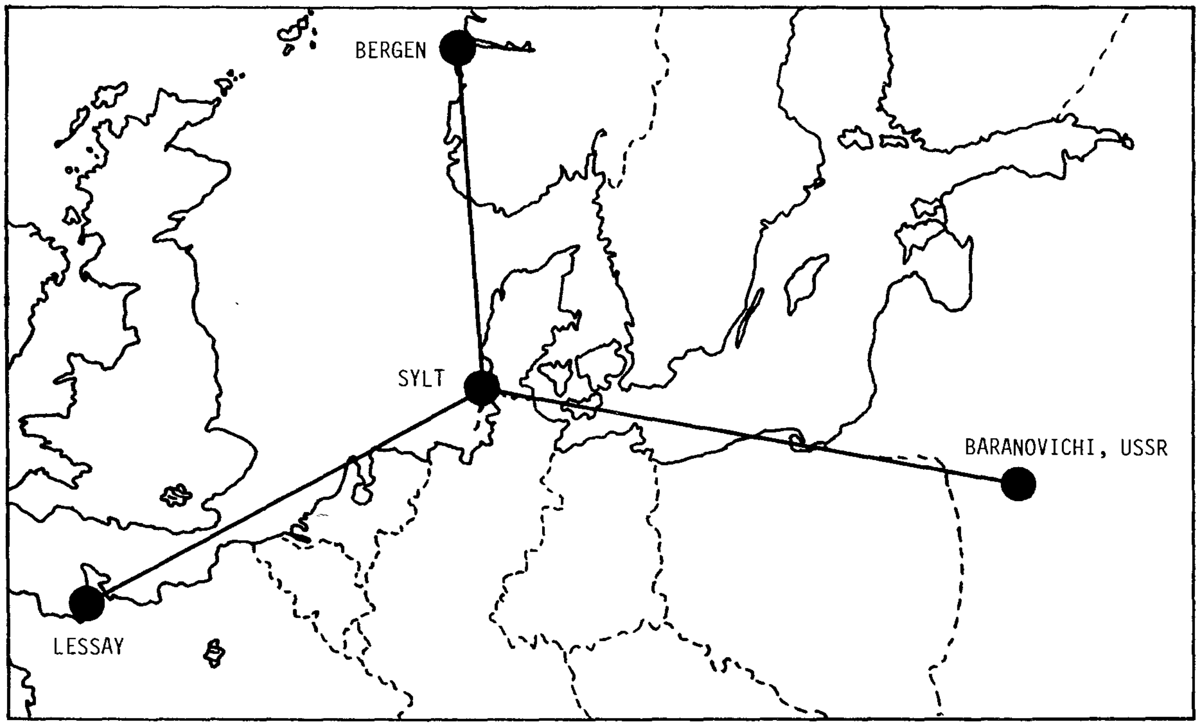

Figure 11: A Potential Loran-C Chain for the North and Baltic Seas

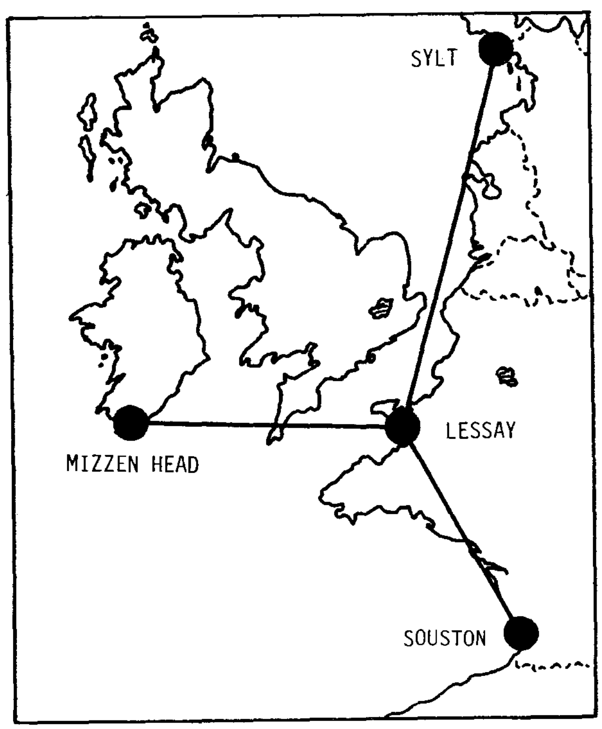

Figure 12: Expansion of the French Chain

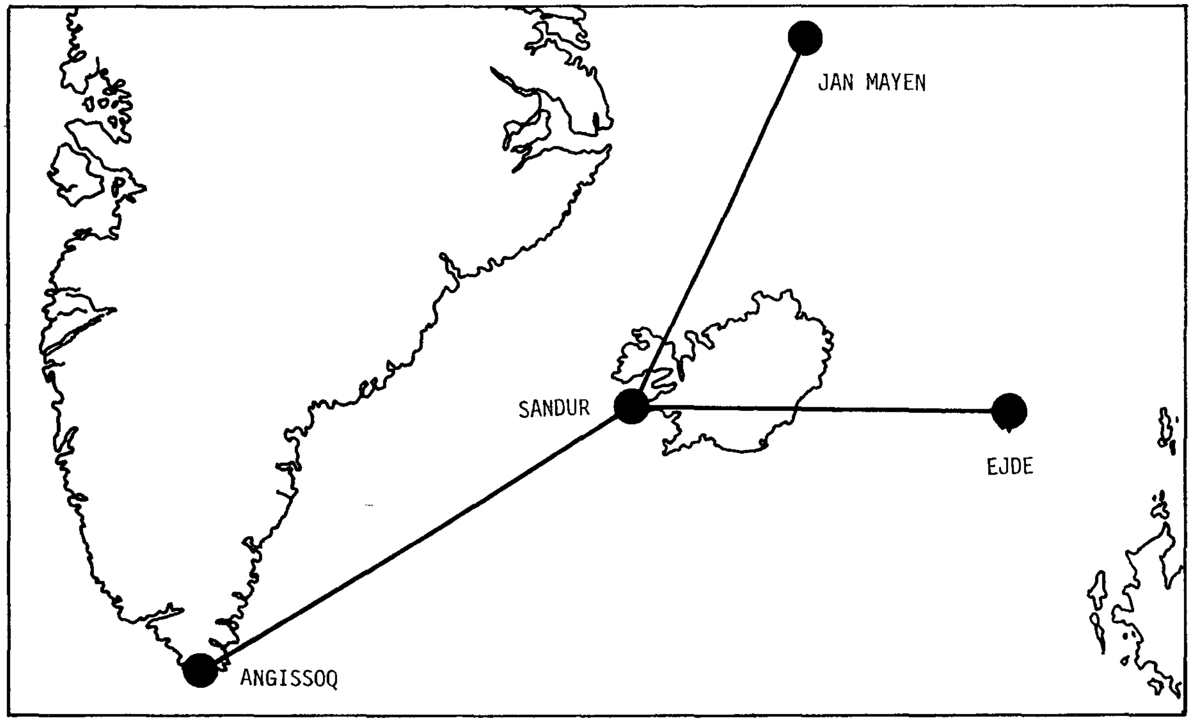

Figure 13: An Improved North Atlantic Chain

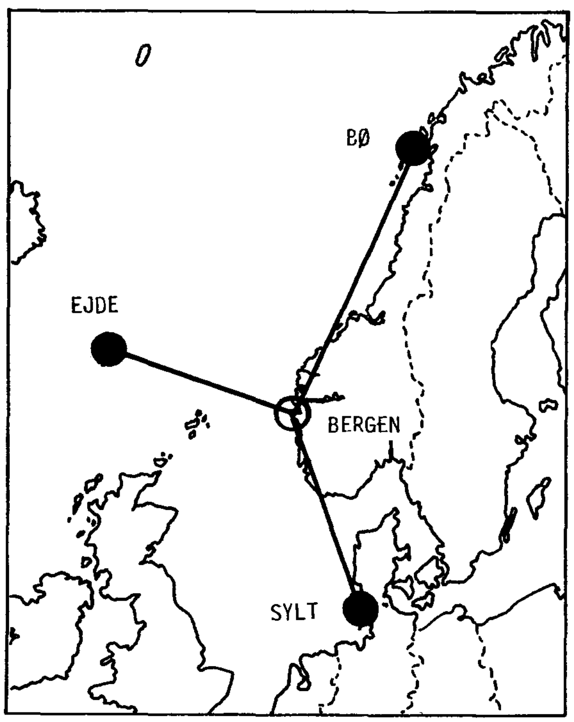

Figure 14: A Plan for Improved Coverage of the Norwegian Coast

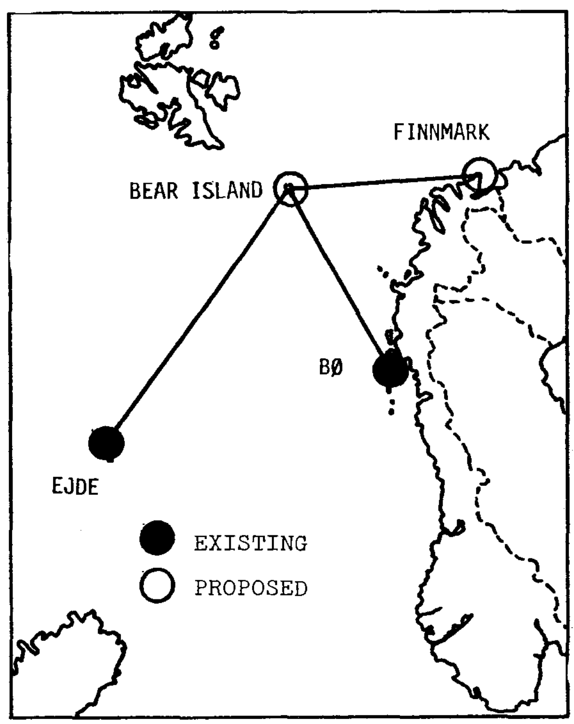

Figure 15: Coverage for Northern Norway

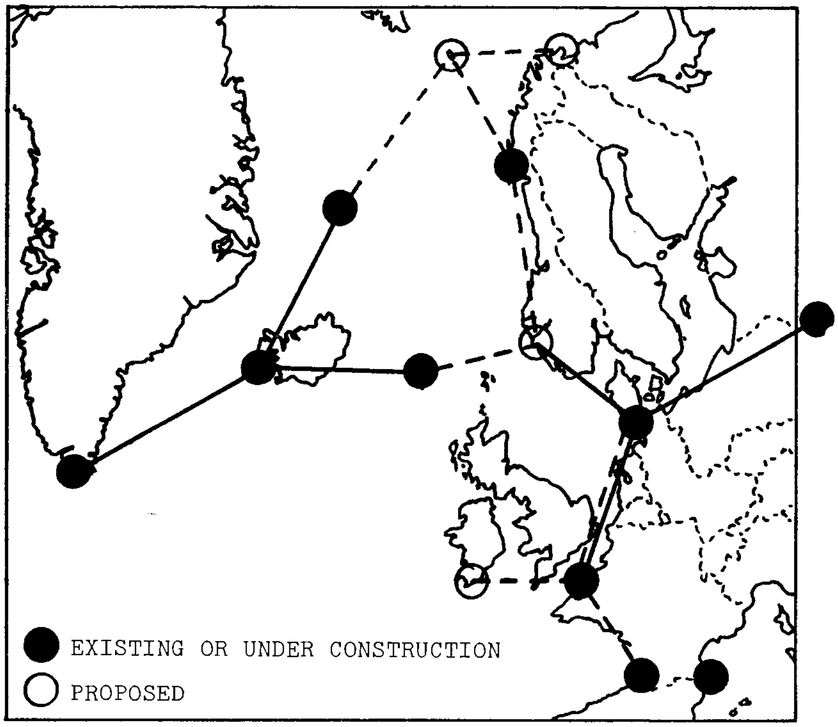

Figure 16: A Plan for Northern European Loran-C Coverage

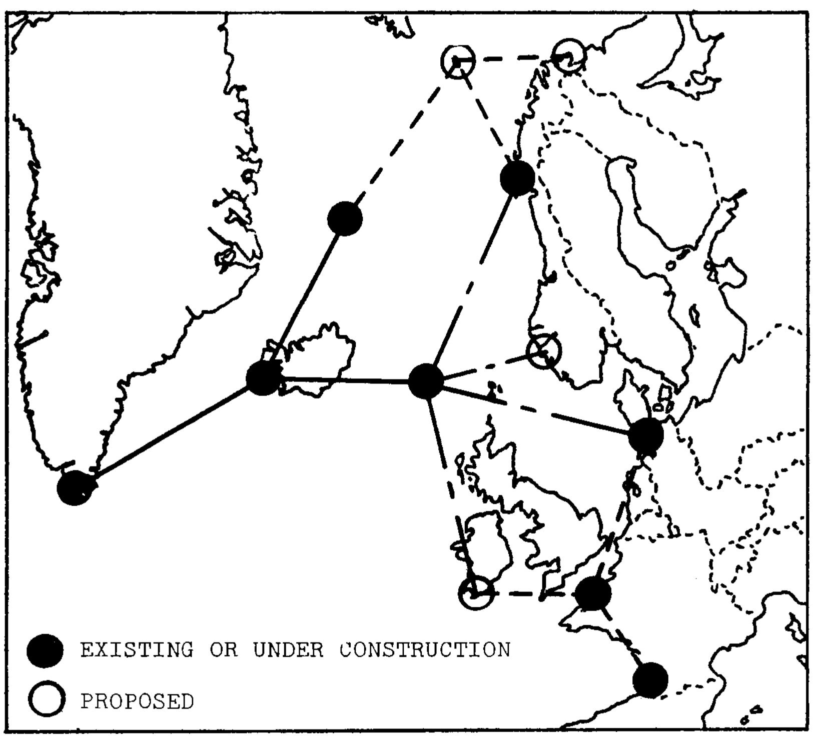

Figure 17: An Alternate Plan for Northern European Loran-C Coverage

A SEMI-EMPIRICAL METHOD FOR LORAN GRID CALIBRATION/PREDICTION

William F. O'Halloran and Krishnan Natarajan
JAYCOR
300 Unicorn Park Drive
Woburn, MA 01801

ABSTRACT

This paper describes a semi-empirical method for calibrating and predicting Loran time differences (TDs). This method uses theoretical results to establish the form of correction polynomials, which are used to model secondary phase corrections. Actual Loran TD measurements are then used to calculate coefficient values for the correction polynomials. The correction polynomials can then be used to both calibrate and predict the Loran TD grid. A Grid Data Management System (GDMS) software package has been developed to implement the semi-empirical model and has been delivered to the Defense Mapping Agency (DMA) to support USAF tactical Loran operations.

The semi-empirical method employs a separate correction polynomial for each transmitter. Each separate correction polynomial is in turn composed of altitude, range, and bearing-dependent correction polynomials. The structure of each correction polynomial is chosen based on theoretical propagation results. A recursive Kalman filter is then used to incorporate actual measurements into the correction polynomials. The initial polynomial coefficients and their uncertainties are also chosen based on theoretical propagation results.

In tests using actual Loran data, the validity of the semi-empirical concept has been demonstrated. Both calibration and prediction results were obtained. The calibration process refers to estimating TDs for a region using measurement data in that region. The prediction process refers to estimating TDs for a region using measurement data from a different geographic region. Calibration accuracies of 230 ft (CEP) have been achieved for a 10,000 square mile area. A prediction accuracy of 440 ft (CEP) was also achieved for a 10,000 square mile area.

BACKGROUND

To support precise tactical air operations using the AN/ARN-101 Loran navigator, stringent navigation accuracy requirements must be met. The Air Force has a need to improve the accuracy of the AN/ARN-101 in denied areas in order to meet these tactical requirements.

The major source of navigation errors in the AN/ARN-101 is warpage of the Loran grid due to propagation errors. Improved Loran accuracy can be obtained by compensating for grid warpage. Traditionally, grid warpage effects have been compensated using one of two methods: theoretical prediction techniques or purely empirical techniques. This paper examines the successful application of a semi-empirical hybrid technique for grid prediction which combines the best features of the traditional theoretical prediction and empirical methods. Using this methodology, JAYCOR has developed a Loran Grid Data Management System (GDMS) for use with the AN/ARN-101. GDMS has been successfully validated using existing data from Eglin AFB (Southeast U.S. Loran-C Chain) and South Korea (Commando Lion Chain). This software, which has been delivered to the Defense Mapping Agency, generates synthetic input measurements for the existing WARP program providing a powerful tool for the Air Force to predict accurate Loran grids into denied areas.

BASIS FOR SEMI-EMPIRICAL MODEL

Theoretical Loran prediction models are based on solving the fundamental equations for propagation of the 100 kHz ground wave signal. To obtain accurate predictions requires a significant amount of geological and topographical terrain data in the vicinity of the propagation paths. The data required are extensive and often difficult to obtain, particularly for denied areas. Prediction of the Loran propagation errors at a given geographic point requires the solution of a complex integral equation subject to the appropriate ground impedance and topographic boundary conditions. The software to accomplish this task is sophisticated and is computationally expensive and time consuming. Furthermore, the theoretical prediction results can often be significantly in error if sufficiently precise input data are not available.

At the other extreme of prediction methods are the purely empirical techniques. This method requires collection of a large amount of Loran time difference (TD) data over the region of interest. Empirical methods involve adjusting the Loran grid to fit the data in order to minimize the statistics of the residual errors, without regard to the underlying propagation phenomena. While this approach can work well in minimizing errors within the data collection region, the results cannot be used to accurately predict TDs outside the existing data set. The empirical approach is therefore not well suited to meeting the Air Force need of predicting TDs into denied areas.

The semi-empirical approach, which has been incorporated into the GDMS, overcomes the major drawbacks of both methods described above. Based on known characteristics of Loran ground wave propagation, a simplified polynomial grid warpage model is postulated which captures the major underlying propagation anomaly effects over the entire chain coverage area. This model is initialized with nominal a-priori parameters with associated uncertainty bounds which depend on the gross features of the propagation paths of interest. A limited number of real-world observations are then used to calibrate the coefficients of the model. Finally, the calibrated model is used to predict TDs in other regions of interest (e.g., denied areas). The major advantages of this semi-empirical approach can be summarized as follows:

- Limited number of measurements necessary
- Takes advantage of knowledge of Loran propagation
- Ability to accurately predict TDs in areas outside measurement region
- Accuracy superior to theoretical or empirical methods alone
- Not computationally cumbersome
- Requires straightforward software (simple Kalman filter)

The next section describes the GDMS model in more detail.

SEMI-EMPIRICAL MODEL DESCRIPTION

Consider a Loran time difference (TD) as measured by the receiver between the master station (M) and a secondary (S):

$$TD = \left(T_S - T_M\right) + CD + BL \qquad (1)$$

where

T_S = Transmission time from Secondary to user

T_M = Transmission time from Master to user

CD = Coding Delay

BL = Baseline length between Master and Secondary

Due to propagation uncertainties, the actual transmission time, T, for each station will in general be different from the nominal transmission time, $\tilde{T}$:

$$T = \tilde{T} + \psi \qquad (2)$$

where $\tilde{T}$ is computed based on an a-priori smooth, homogeneous earth model, and ψ is the secondary phase factor.

The semi-empirical model provides an estimate of ψ based on a polynomial fit to the theoretical Loran propagation behavior. Define $\hat{\psi}$ as the estimate of ψ. The semi-empirical model has the form:

$$\hat{\psi} = A(h,d) + C(d) + F(d,b) \tag{3}$$

where

$A(h,d)$ = Altitude correction polynomial

$C(d)$ = Distance correction polynomial

$F(d,h)$ = Bearing correction polynomial

h = altitude

d = range from transmitter to receiver

b = bearing difference from a reference point to the receiver location

The basic forms of these polynomials can be constructed from known propagation theory results. Figure 1, taken from Reference 1, illustrates typical curves of secondary phase correction versus distance for a specific value of ground impedance and a range of values in vertical lapse rate. Figure 2, taken from Reference 2, illustrates the form of the altitude effect at a given distance and a range of conductivities. Note that the shapes of these curves are easily fit by polynomial forms. This fact and the fact that a polynomial model is extremely simple are the primary reasons why polynomial forms were selected as the basis of the semi-empirical model.

Based on these curves and other theoretical results, the polynomials in Equation 3 have been chose to have the forms:

$$A(h,d) = \left(A_0 + \frac{A_1}{d}\right)h \tag{4}$$

$$C(d) = \frac{C_0}{d} + C_1 + C_2 d + C_3 d^2 \tag{5}$$

$$F(d,b) = \left(F_0 b + F_1 b^2\right)d \tag{6}$$

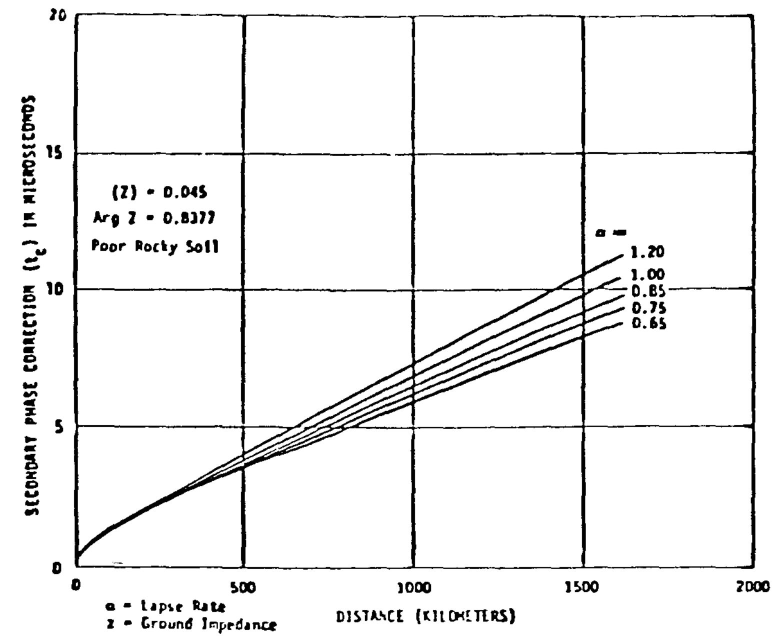

Figure 1. Secondary Phase Correction vs. Distance

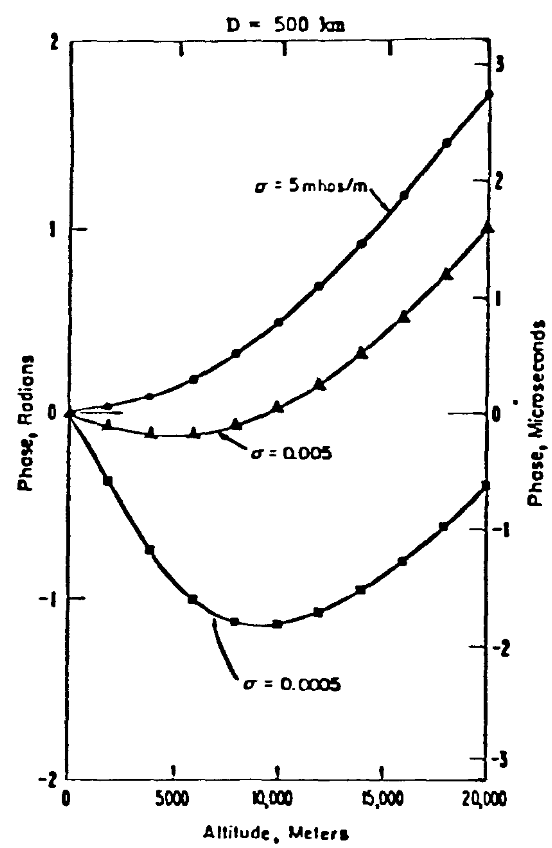

Figure 2. Phase Correction As A Function Of Altitude

This model provides for eight coefficients to be specified for each station. Thus, for a given three-station Loran triad, a total of 24 model coefficients may be estimated.

The GDMS program employs a recursive Kalman filter formulation for estimating the coefficients of the semi-empirical model. Since the coefficients are modeled as unknown constants, the Kalman filter is quite straightforward to implement. The flexibility of the recursive formulation facilitates incorporation of additional data, if available, to refine previous coefficient estimates.

The state vector is given by

$$\underline{x} = \begin{bmatrix} \underline{x}_M \\ --- \\ \underline{x}_1 \\ --- \\ \underline{x}_2 \end{bmatrix} \tag{7}$$

where $\underline{x}_M$ represents the vector of eight coefficients for the master station, and $\underline{x}_1$, $\underline{x}_2$ represent the eight coefficients for secondaries 1 and 2, respectively. Since the coefficients are constant, the dynamics are represented simply by

$$\dot{\underline{x}} = \underline{0} \tag{8}$$

Measurement data at selected survey points within the calibration region are used to provide estimates of the model coefficients. At each survey point, two TD measurements, z, are obtained based on the difference between the measured and computed TDs:

$$z = TD - \widetilde{TD} \tag{9}$$

where TD is the measured value and $\widetilde{TD}$ is computed based on the a-priori smooth, homogeneous earth model. Each measurement is a linear combination of the state of polynomial coefficients and can be expressed in the form

$$z = H\underline{x} + v \tag{10}$$

where v is measurement noise. The model assumes a fixed measurement noise standard deviation of 0.1 μsec. For TD_1, H has the form

$$H_1 = \left[-H_M \,\vdots\, H_1 \,\vdots\, 0 \right] \tag{11}$$

where H_M and H_1 are the partial measurement matrices for the master station and secondary 1, respectively. At the same location, the measurement matrix for the TD_2 error is correspondingly given by

$$H_2 = \left[-H_M \,\vdots\, 0 \,\vdots\, H_2 \right] \tag{12}$$

To complete the specification of the model, it is necessary to provide the filter with initial state estimates and an initial covariance matrix representing the uncertainties in the initial estimates. This is a crucial aspect of the semi-empirical method, since it determines the degree of weighting between initial estimated values and the measurement data. Experience with the semi-empirical model has shown that improved prediction performance can be obtained by providing educated initial coefficient and covariance estimates based on the overall characteristics of the calibration and prediction regions of interest.

The GDMS program incorporates a semi-automatic model initialization module based on default values and user prompts. For each transmitter, the user may input information on path type (e.g., sea water, good soil, poor soil), path mix, and geometry (e.g., no near-field data). The program then assigns initial coefficient estimates and uncertainties based on theoretical propagation results and past experience.

RESULTS

The utility of the GDMS model was validated using existing data from Eglin AFB. Two sets of data were available, as illustrated in Figure 3. Each data set consisted of TD/Latitude-Longitude pairs on a 5 nm spaced grid. The total data set included about 500 points.

To establish a baseline for the uncorrected Loran geodetic accuracy, all of the data points in Area II shown in Figure 3 were evaluated using the nominal smooth, homogeneous earth model. The errors between the computed Loran latitude/longitude and the reference values were calculated. Histograms of radial error were then computed and converted into a cumulative error profile. The circular error probable (CEP) was taken to be the 50th percentile of the cumulative radial error curve. The resulting CEP

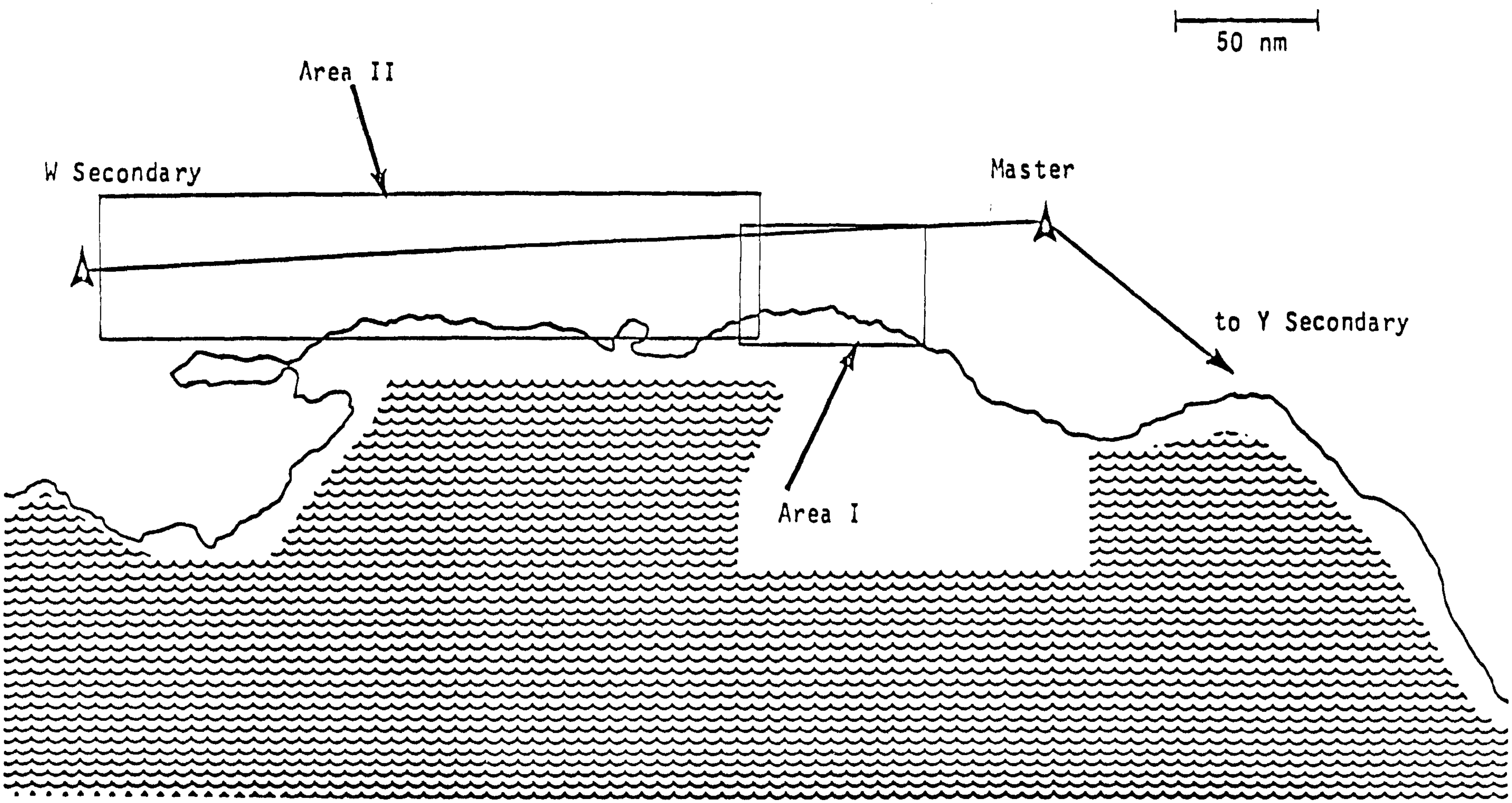

Figure 3. Eglin Air Force Base Test Area

for the uncorrected Loran solutions for this case was determined to be 1627 ft.

Calibration tests were then carried out using the data from Area II. Here, all the data points were input to the GDMS model to determine the coefficients of the semi-empirical secondary phase polynomial model. The calibration accuracy represents the consistency of the resulting calibrated model when used to predict results within the same area used to calibrate the model. Using the calibrated model to predict latitude/longitude at all the data points within Area II resulted in a CEP of 228 ft. This result represents the lower bound on achievable GDMS performance within this 10,000 square mile area.

The most interesting question to answer is how well the GDMS can be used to predict to evaluation areas outside the calibration data set. For this case, approximately 100 uniformly distributed data points in the western quarter of Area II were used as the calibration data set. This area is approximately 50 nm square. The evaluation data set consisted of the remaining data points in the eastern three quarters of Area II as well as all the data points in Area I. The resulting CEP computed for this case was 436 ft. It is interesting to note that some of the points in the evaluation data set were separated by up to 200 nm from some of the points in the calibration data set, thus verifying the ability of the GDMS model to accurately predict into denied areas.

Table 1 summarizes the performance results discussed above. These results are representative of the use of the GDMS semi-empirical model for both calibration and prediction. Sensitivity analyses have also been conducted which show GDMS performance to have minimal sensitivity to the number of calibration points used. Results comparable to those in Table 1 have obtained with as few as 20 calibration points. It is important, however, to provide a reasonable good geographic distribution of calibration points to enhance the observability of the individual coefficients in the polynomial model.

Table 1

Summary of GDMS Test Results

Case No.	Calibration Data Set	Evaluation Data Set	CEP (ft)
1	None	All of Area II	1627
2	All of Area II	All of Area II	228
3	Western Quarter of Area II	All of Area I plus Eastern Three Quarters of Area II	436

CONCLUSIONS

The semi-empirical Loran prediction method has been successfully implemented into a Grid Data Management System (GDMS) software package to be used by the Air Force in improving the accuracy of the tactical AN/ARN-101 Loran navigation systems. Extensive testing using available TD/Lat-Lon pairs of data points has successfully validated the semi-empirical polynomial model approach to within Air Force accuracy objectives. These results have demonstrated that accurate prediction into denied areas in possible using a limited amount of calibration data, provided that the data have sufficient geographic distribution. The GDMS software is an easy-to-use, event-driven package that currently resides on DMA's Honeywell computer. This software will provide predicted synthetic input measurements for the existing AN/ARN-101 WARP program to enhance tactical Loran accuracy in denied areas.

REFERENCES

1. Brown, G., Et Al, Loran Warpage Coefficient Generation Program (Program WARP) Analyst's Manual, U.S. Air Force, ESD, ESD-TR-81-116 (II), March 1981.

2. Johler, J.R., "Loran Radio Navigation Over Irregular, Inhomogeneous Ground With Effective Ground Impedance Maps", Department of Commerce, Office of Telecommunications, OT/TRER 22, November 1971.

CONVENTION SCENE AND AWARDS

A RELAXED HOSPITALITY CHAIRMAN, LLOYD HIGGINBOTHAM

GENERAL CHAIRMAN DAVE CARTER AND TECHNICAL CHAIRMAN DAVE AMOS

FAMILIAR FACES AT THE ANNUAL BANQUET

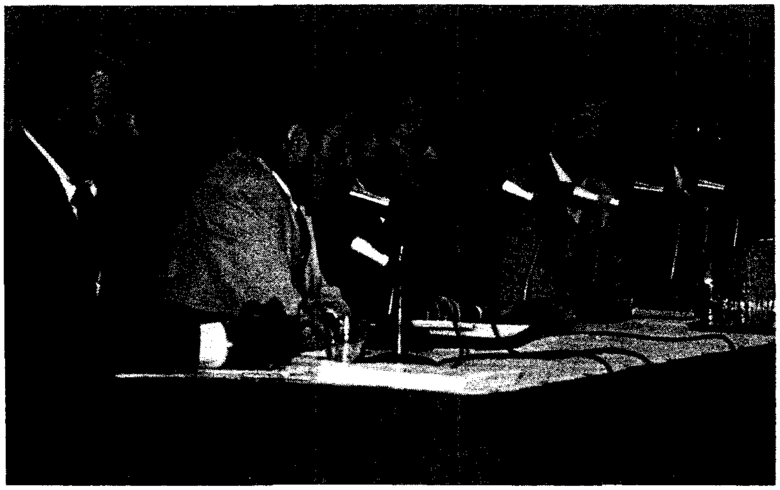

PANEL MEMBERS TOM NOLAN, CAPT. CHARLES DORRIAN (CHAIRMAN), CAPT. TERRY MONTONYE, ED DANFORD, AND CAPT. CRAIG REEDER, MASTER, EXXON GALVESTON

ED McGANN TRIED THE TWIST. MO DEAN SUPPLIES CRITICAL APPRAISAL.

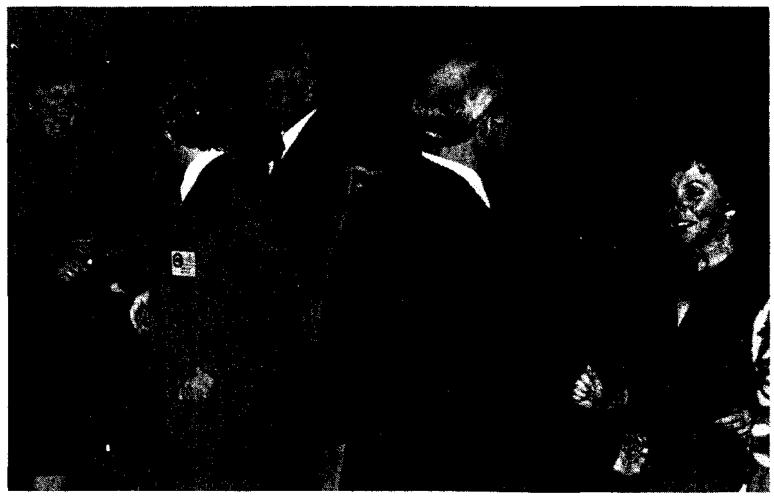

WALT DEAN RECEIVES THE SERVICE AWARD.

THE MEDAL OF MERIT WAS PRESENTED TO
J. RALPH JOHLER BY BOB FRANK.

ED McGANN RECEIVED THE PRESIDENT'S AWARD,
HERE PRESENTED BY PRESIDENT BARNEY
AMBROSENO.

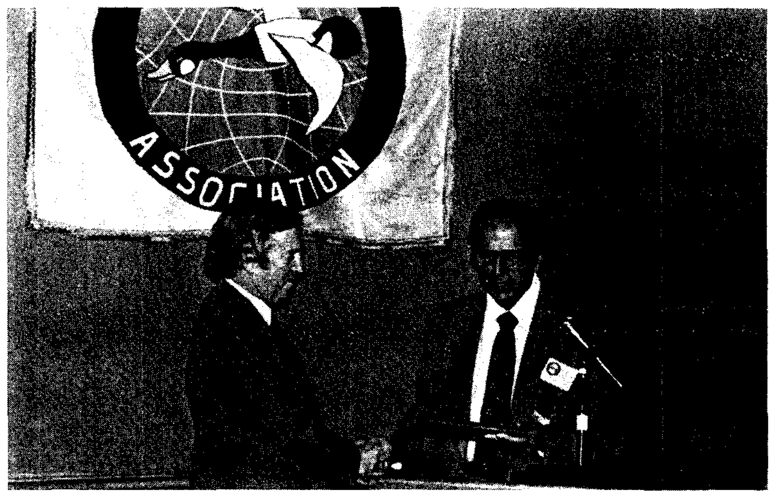

JOHN ANTHONY AND ANDY SEDLOCK (NOT PRESENT) RECEIVED THE BEST PAPER AWARD FROM
THE '81 CONVENTION.

DAVE CARTER OPENED THE CONVENTION ON AN UPBEAT NOTE.

REGISTRATIONS BY LINDA

AN ATTENTIVE AUDIENCE SPARKED THE TECHNICAL SESSIONS.

TOASTMASTER LLOYD AT THE LUNCHEON

JACK FUECHSEL INTRODUCED OUR SPEAKER. . . .

RADM DICK BAUMAN, CHIEF OF THE OFFICE OF NAVIGATION, USCG

DAVE WILTSHIRE ENTERTAINED US AT THE BANQUET.

THE END — MY SENTIMENTS EXACTLY

REGISTERED ATTENDANCE

WILD GOOSE ASSOCIATION 11th ANNUAL TECHNICAL SYMPOSIUM

WASHINGTON, D.C.

OCTOBER 13-15, 1982

JOHN J. ANTHONY
USCG G-DST-1
2100 Second Street S.W.
Washington, D.C. 20593

DOUGLAS S. TAGGART
U.S. COAST GUARD
Avery Point
Groton, CT

CARTER P. PFAELZER
MIT
334 C Newton Street
Brookline, MA 02167

JOSEPH LOVECCHIO
DOT/TSC
Wendall Square
Cambridge, MA

LEON DePALMA
TASC
One Jacob Way
Reading, Mass. 01867

GENE ROBINSON
TEXAS INSTRUMENTS INC.
P.O. BOX 405, MA 3439
Lewisville, TX 75067

GARDNER K. HUSSEY
HAZELTINE CORP.
Cuba Hill Road
Greenlawn, NY 11740

BRUCE FRANCIS
ADVANCED NAVIGATION INC.
621 Lofstrand Lane
Rockville, MD 20850

CHARLES BALTZER
ADVANCED NAVIGATION INC.
621 Lofstard Lane
Rockville, MD 20850

BILL DeGEORGE
ITT AVIONICS
500 Washington, Ave.
Nutley, NY 07110

THOMAS A. KING
BOWDITCH NAVIGATION SYSTEMS
40 PLEASANT STREET
PORTSMOUTH, NY 03801

W.H. HAYES
USCG
ECCEN
Wildwood, NJ 08260

JAMES McCULLOUGH
WOODS HOLE OCEANOGRAPHIC INST.
Woods Hole, MA 02543

DANIEL BLITZ
SANDERS ASSOCIATES
P.O. Box 868
NASHUA, NH 03061

MAJOR WILLIAM L. POLHEMUS
USAF/PAI
Box 5
Cambridge, VT

HATCHER E. CHALKLEY
TEXAS INSTRUMENTS INC.
P.O. Box 405 MS 3439
Lewisville, TX 75067

HAROLD T. SHERMAN
ITT AVIONICS
13239 Nickleson Dr.
Dale City, VA 22193

WILLIAM J. BECKER
TRACOR, INC.
7714 Signal Hill Road
Manassas, VA 22111

MARK LAWRENCE
ADVANCED NAVIGATION INC.
621 Lofstrand Lane
Rockville, MD 20850

LLOYD HIGGINBOTHAM
CONSULTANT
4 Townsend Road
Acton, MA 01720

JESSE PIPKIN
NAVIGATION TECHNOLOGY
12207 Brookglen Drive
Saratoga, CA 95070

ROBERT McKEOWN
ITT AVIONICS DIV.
500 Washington Ave.
Nutley N.J.

VERNON L. JOHNSON
ITT AVIONICS
500 Washington Ave.
Nutley, N.J.

EIRIK JAN TORBERGSEN
Saudi Ports Authority
Riyadh Saudi Arabia

GARRY PERCHIK
ITT AVIONICS
500 Washington Ave.
Nutley, N.J.

PETER H. DANA
1101 Walnut Street
Georgetown, TX 8762

DR. MARTIN MANDELBERG
COAST GUARD R&D CENTER
Avery Point
Groton, CT

JACK L. WALLACE
NATIONAL OCEAN SURVEY (C35x3)
6001 Executive Blve.
Rockville, MD 20852

CAPT ROBERT S. WESTER
USAF
Eglin AFB, FL 32542

GARY GRAHAM
TEXAS A&M UNNIVERSITY
Route 2, Armory
Angleton, TX 77515

BOB SCHELLHASE
U.S. COAST GUARD
9415 Victoria Dr.
Upper Marlboro, MD 20772

EDWIN O. DANFORD
DMAHTC
6500 Broaks Lane
Brookmount, Washington, D.C.

GERFILD F. SAGE
NAVIGATION TECH INC.
2327 Double "O' Mine
Cool, CA 95614

ERIC SCHENING
TRANSPORT CANADA
Telecom/Electronics
Brig transport Canada Bldg,
Ottawa, Ontorio Kiaon?

ROBERT M. BOWLES
U.S. GEOLOGIC SURVEY
P.O. Box 465
Falmouth, MA. 02541

ROCKY T. FUJINO
KODEN ELECTRONICS CO. LTD.
2-10-45, Kamiosaki
Shinagawa-Ku, Tokyo, JAPAN

DAVID H. AMOS
U.S. COAST GUARD
ESD/OCN-1
Hanscom AFB, MA 01731

R. BRENT BURBANK
KING RADIO CO.
400 N. Rogers Road
Olathe, KS 66061

ROBERT E. VOIGT
USAF
ESD/OL-AF
Eglin AFB, FL 32542

CAPT JOHN C. UITHOL
U.S. COAST GUARD
2100 2nd Street S.W.
Washington, D.C.

STEPHEN C. HUNG
U.S. DOT/St. Lawrence Seaway
Development Corp.
800 Independence Ave. S.W.
Washington, D.C. 20591

DANIEL ANDRUSIAK
U.S. COAST GUARD
9083 Andromeda Drive
Burke, VA 22015

CAPT. W. KOHL
U.S. COAST GUARD
4313 Southwood Drive
Alexandria, VA 22309

LCDR ROBERT WEAVER
USCG EECEN
Wildwood, NJ 08260

DAN SLAGLE
U.S. COAST GUARD
4341 Granby Road
Woodbridge, VA 22193

R.H. ORR
U.S. COAST GUARD
14463 Silverdale Drive
Dale City, VA 22193

LT LEE GAZLAY
U.S. COAST GUARD
2100 2nd Street S.W.
Washington, D.C. 20593

GREGORY D. ZIEMER
U.S. COAST GUARD
2100 2nd Street S.W.
Washington, D.C. 20593

ROBERT H. ERIKSON
FAA TECH CENTER
Altantic City Airport, NY 08405

FRANK CASSIDY
EPSCO, INC
67 Everett Street
South Natick, MA 01760

WILLIAM O'HALLORAN
JAYCOR
300 Unicorn Park Drive
Woburn, MA 01801

HERBERT L. BROWN
INTERNAV INC.
66 Cummings Park
Woburn, MA 01801

LARRY D. KING
SYSTEMS CONTROL TECHNOLOGY, INC.
2326 South Congress Ave. Suite 2A
West Palm Beach, FL 33406

DAVID C. SCULL
DOT/RSPA
2112 Wittington Boulevard
Alexandria, VA 22308

R.E. BURKE, JR.,
U.S. COAST GUARD
USCG EECEN
Wildwood, NJ 08260

R.J. WENZEL
USCG
2701 Park Center Drive B-1004
Alexandria, VA 22302

BILL THRALL
USCG
3413 Austin Court
Alexandria, VA 22310

MIKE SELAVKA
U.S. COAST GUARD
USCG HEADQUARTERS (G-NRN-3)
2100 2nd Street S.W.
Washington, D.C. 20593

T.M. DROWN
U.S. COAST GUARD
2100 2nd Street S.W.
Washington, D.C. 20593

RALPH GEORGE
GEORGE ASSOCIATES, INC.
2340 Montgomery Street

LTJG JOHN A BUDDE
U.S. COAST GUARD
HEADQUARTERS (GNRN-3)
2100 2nd Street S.W.
Washington D.C. 20953

JAMES D. KELLY
TASC
1 Jacob Way
Reading, MA 01867

DOUGLAS H. ALSIP
U.S. COAST GUARD
EECEN
Wildwood, NJ 08260

CAPT. JOHN C. FUECHSEL
NATIONAL OCEAN INDUSTRIES ASSOC
1050 17th Street N.W.Suite 700 .
Washington, D.C. 20036

JOSEPH A. WALSH
MARAD
4942 Herkimer Street
Annandale, VA 22003

E.J. HIRD
NAVIGATION SYSTEM, INC.
8841 Monard Drive
Silver Spring, MD 20910

B.J. WATKINS
NAVIGATION SYSTEMS, INC.
8841 Monard Drive
Silver Spring, MD 20910

STEVE A. ROTH
II MORROW, INC.
Box 13549
Salem, OR 97303

J.N. NEWMAN
MIT
Room-5324, MIT
Cambridge, MA 02139

WOODY WORDSWORTH
AUSTRON INC.
1800 Old Meadow Road
McLean, VA 22102

JOHN H. OSTRANDER
NAVAL RESEARCH LABORATORY
4140 Offut Drive
Suitland, MD 20746

RONALD G. ROLL
APL/JHU
3804 Kelsey Street
Silver Spring, MD 20906

ALLEN L. COMSTOCK
TELEDYN HASTINGS - RAYDIST
Box 1275
Hampton, VA 23661

LEO FEHLNER
APL/JHU
118 Quaint Acres Drive
Silver Spring, MD 20904

CARL S. ANDREN
NAVIGATION SYSTEMS, INC.
8841 Monard Drive
Silver Spring, MD 20910

STAN PIASECKI
NAVIGATION SYSTEMS, INC.
8841 Monard Drive
Silver Spring 20910

ROBERT D. BRONSON
II MORROW, INC.
Box 13549
Salem, OR 97309

TED ACHILLES
MORROW ELECTRONICS, INC.
BOx 7078
Salem, OR 97303

LCDR GARY R. WESTLING
USCG ACADEMY
C/O SUPERINTENDENT (DE)
New, London, CT 06320

"DOC" EWEN
EWEN KNIGHT CORP.
60 Beaver Rd.
Weston, MA 02193

CAPT. W.H. HAYES, JR., USCG
EECEN WILDWOOD, NY
Commanding Officer
USCG EECEN
Wildwood, NJ 08260

JAMES F. HARRISON
JHU/APPLIED PHYSICS LABORATORY
Room 14-208
John Hopkins Road
Laurel, MD 20707

ROBERT L. FRANK
CONSULTANT
30795 River Crossing
Birmingham, MI 48010

LT KENNETH DYKSTRA
U.S. COAST GUARD
DEPT. OF APPLIED SCIENCE & ENG
USCG ACADEMY
New London, CT 06300

ROGER W. HASSARD
U.S. COAST GUARD
USCG Activities Europe
Box 50
FPO New York 09510

JOHN M. BEUKERS
BEUKERS LABORATORIES, INC
Flowerfield Building #7
St. James, New York 11780

CARTER P. PFAELZER
M.I.T.
334-C Newton Street
Brookline, MA 02167

BAHAR UTTAM
JAYCOR
205 South Whiting Street
Alexandria, VA 22304

JOHN D. ILLGEN
KAMAN-TEMPO
P.O. Drawer QQ
816 State Street
Santa Barbara, CA 93102

EDWARD L. McGANN
MEGAPULSE, INC.
8 Preston Court
Bedford, MA 01730

RICHARD J. HARRISON
DATAMARINE INTERNATIONAL, INC.
53 Portside Drive
Pocasset, MA 02559

CALVIN CULVER
MICROLOGIC
20801 Dearborn Street
Chatsworth, CA 91311

MARTIN A. LETTS
USCG ELECTRONIC ENGINEERING CENTER
Wildwood, N.J. 08260

BERNARD CANU
SERVICE TECHNIQUES DES
CONSTRUCTIONS ET AMES NAVALES
C/O MEGAPULSE INC.
8 Preston Court
Bedford, MA 01730

MR. RENE VANINA
MEGAPULSE, INC.
Suite 532, Bowen Bldg.
815 15th Street, N.W.
Washington, D.C. 20005

CDR J.O. Alexander
U.S. COAST GUARD, 11th CGD
50 Granada Avenue
Long Beach, CA 90803

WILLIAM BURGIN
SI-TEX-MARINE ELECTRONICS
P.O. Box 6700
1400 Roosevelt Boulevard
Clearwater, FL. 33518

FREDERICK H. RAAB
GREEN MOUNTAIN RADIO RESEARCH
240 Stanford Road
Burlington, VT 05401

WILLIAM M. FLANDERS
FLANDERS ASSOCIATES INC.
5 Abbot Bridge Drive
Andover, MA 01810

DAVID GRAY
CANADIAN HYDROGRAPHIC SERVICE
615 Booth Street
Ottawa, Canada K1A 0E6

BARNEY AMBROSENO
EPSCO
411 Providence Highway
West Wood, MA 02090

KEITH R. BRUHL
SABBATICAL SEVENTH
3110 Faber Drive
Falls Church, VA 22044

LT DAVE BEARD
U.S. COAST GUARD
EECEN
Wildwood, NJ 08260

WALTER N. DEAN
MORROW ELECTRONICS
Box 7078
Salem OR 97303

COLIN C. WEEKS
WIMPOL INC.
Box 219218
Houston, TX 77218

VERNON I. WEIHE
CONSULTANT
4133 N. 33rd Road
Arlington, VA 22207

ITT - AVIONICS
19 Dogwood Road
Boonton, NJ 07005

WILLIAM J. PETERS III
APL/JHU
4713 Eddystone Street
Annandale, VA 22003

DAVE CLEMENTS
USCG PACIFIC AREA
GOVERNMENT ISLAND
Alameda, CA 94501

LESTER BRODEUR
SANDERS ASSOCIATES INC.
Nashua, N.H.

RONALD S. WARREN
TASC
1 Jacob Way
Reading, MA 01867

A.W. MARCHAL
OFFSHORE NAVIGATION
5728 Jefferson HWY
New Orleans, LA

THOMAS JERARDI
APL/JHU
4713 Eddystone Street
Annandale, VA 22003

Mr. VOISARD
SERCEL
BP64 44471 Carquefou Cedex
France

WILLIAM SCHORR
USCG
Apt 112-A2
Governors Island, NY 10004

ROBERT F. DUGAN
KEUFFEL & ESSER Co.
20 Whippany Road
MORRISTOWN N.J. 07960

E. RUSSELL VASS
U.S. COAST GUARD
2nd & "V" Street S.W.
Washington, D.C. 20593

LARRY HOGLE
ARINC RESEARCH
2551 Riva Road
Annapolis, MD 21401